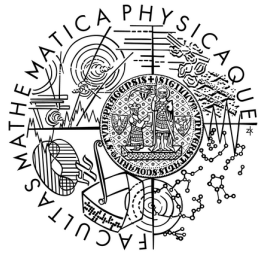

MATEMATICKO-FYZIKÁLNÍ
FAKULTA
Univerzita Karlova

DISERTAČNÍ PRÁCE

Tomáš Husek

Některé aspekty QCD při nízkých energiích v éře přesných měření

Ústav částicové a jaderné fyziky

Vedoucí disertační práce:	doc. RNDr. Karol Kampf, Ph.D.
Studijní program:	Fyzika
Studijní obor:	Subjaderná fyzika

Praha 2017

FACULTY
OF MATHEMATICS
AND PHYSICS
Charles University

DOCTORAL THESIS

Tomáš Husek

Some aspects of low-energy QCD at the precision frontier

Institute of Particle and Nuclear Physics

Supervisor of the doctoral thesis: doc. RNDr. Karol Kampf, Ph.D.
Study programme: Physics
Study branch: Subnuclear Physics

Prague 2017

Prohlašuji, že jsem tuto disertační práci vypracoval samostatně a výhradně s použitím citovaných pramenů, literatury a dalších odborných zdrojů.

Beru na vědomí, že se na moji práci vztahují práva a povinnosti vyplývající ze zákona č. 121/2000 Sb., autorského zákona v platném znění, zejména skutečnost, že Univerzita Karlova má právo na uzavření licenční smlouvy o užití této práce jako školního díla podle §60 odst. 1 autorského zákona.

I declare that I carried out this doctoral thesis independently, and only with the cited sources, literature and other professional sources.

I understand that my work relates to the rights and obligations under the Act No. 121/2000 Coll., the Copyright Act, as amended, in particular the fact that the Charles University has the right to conclude a license agreement on the use of this work as a school work pursuant to Section 60 paragraph 1 of the Copyright Act.

V Praze dne / In Prague, date ..... 2017 Podpis autora / Signature

.....

Název práce: Některé aspekty QCD při nízkých energiích v éře přesných měření
Autor: Tomáš Husek
Katedra/Ústav: Ústav částicové a jaderné fyziky
Vedoucí disertační práce: doc. RNDr. Karol Kampf, Ph.D.

Abstrakt: Tato disertační práce se zabývá aspekty QCD při nízkých energiích, které souvisejí s elektromagnetickými rozpady nejlehčích pseudoskalárních mesonů. Výpočty radiačních korekcí pro rozpady neutrálního pionu (Dalizův rozpad a vzácný rozpad na elektron-pozitronový pár) a nový model pro form faktor elmag. přechodu pionu jsou diskutovány v článcích, ze kterých tato práce vychází. S tím související efektivní přístupy jako např. chirální poruchová teorie či limita velkého N_c jsou představeny v úvodních kapitolách. Také se zde zabýváme komplikacemi, které nastávají při výpočtu radiačních korekcí k Dalitzově rozpadu $\eta^{(\prime)}$ mesonů. V práci jsou rovněž představeny detaily spolupráce s experimenty, které začlenily uvedené publikované výpočty radiačních korekcí do svých simulací. V neposlední řadě jsou pak ukázány některé techniky výpočtů smyčkových integrálů.

Klíčová slova: chirální poruchová teorie, limita velkého N_c, radiační korekce, form faktor elmag. přechodu pionu

Title: Some aspects of low-energy QCD at the precision frontier
Author: Tomáš Husek
Department/Institute: Institute of Particle and Nuclear Physics
Supervisor of the doctoral thesis: doc. RNDr. Karol Kampf, Ph.D.

Abstract: This thesis concentrates on some low-energy aspects of QCD, namely on those which are connected to the electromagnetic decays of lightest neutral pseudoscalar mesons. Calculations of radiative corrections to neutral pion decays (the Dalitz decay and the rare decay) and a novel model for the pion electromagnetic transition form factor are subjects discussed in the attached papers, which this work is based on. The associated theoretical aspects including Chiral Perturbation Theory or the large-N_c limit are introduced. We also discuss the complications which arise when the calculations of radiative corrections for $\eta^{(\prime)}$ Dalitz decays are performed. Some details about the collaboration with experiments which incorporate the calculation of the published corrections are provided. Last but not least, some techniques related to loop integrals are shown.

Keywords: Chiral Perturbation Theory, large-N_c limit, radiative corrections, pion electromagnetic transition form factor

Poděkování

Nelze začít jinak než poděkováním mému vedoucímu, Karlu Kampfovi, za jeho stálou trpělivost, podporu a mnohé rady, a za to, že jeho dveře byly, i doslova, vždy otevřené. Dále pak děkuji Jiřímu Novotnému za mnohé odborné konzultace, které byly za dobu mých studií potřeba, a za detailní připomínky zejména k první kapitole. Mé díky také patří Martinu Zdráhalovi za vstřícnou pomoc při řešení problémů všeho druhu a za pečlivé přečtení některých částí této práce.

Během svého doktorského studia jsem (kumulativně) strávil příznačných bezmála devět měsíců na Uppsala University ve Švédsku. Rád bych tak poděkoval Stefanu Leupoldovi za mnohé dlouhé rozpravy, jež se během mých pobytů uskutečnily, a společně s jeho ženou Sabrinou pak za vřelé přijetí na dobu kratší i delší a za vytvoření rodinné atmosféry v jejich domě, kdykoliv jsem potřeboval překlenovací azyl. V podobném duchu bych rád poděkoval Emilie Passemar za laskavé přijetí při mé dvouměsíční studijní návštěvě Indiana University Bloomington v Indianě, USA, za její podporu a pomoc s věcmi, které byly potřeba.

Mé díky však patří nejen již vystudovaným doktorům a profesorům, nýbrž také mým souputníkům, studentům, at' už v Praze, Uppsale, či Bloomingtonu. Všichni různým dílem přispěli k tom, že mé studium nebylo jen a pouze o studiu.

V neposlední řadě bych chtěl poděkovat svým nejbližším, že měli pochopení pro to, že jsem trávil tak mnoho času prací, místo abych byl s nimi. Nakonec pak děkuji a omlouvám se všem, které jsem sice jmenovitě neuvedl, ale mé upřímné a vřelé díky si zaslouží.

Acknowledgments

There is no other way to begin but to thank to my supervisor Karol Kampf for his continual patience, support and advising and for that his door were always open, also literally. Afterwards, I would like to thank Jiří Novotný for numerous technical conversations needed during my studies and for detailed remarks namely about the first chapter. My thanks go also to Martin Zdráhal for his responsive help in solving problems of all kind and for careful reading of parts of this manuscript.

During my doctoral studies I spent (cumulatively) almost nine months at Uppsala University, Sweden. I would like to thank Stefan Leupold for numerous long discussions which took place during my stays and that together with his wife Sabrina they welcomed me warmly into their house whenever it was necessary — for times short as well as a little bit longer. On a similar note, I would like to thank Emilie Passemar, who was very kind to me during my two months' visit of Indiana University Bloomington, Indiana, USA, for her support and help with things of various kind.

However, my thanks go not only to professors and other distinct colleges, but also to students in Prague, Uppsala and Bloomington. All of them contributed to the fact that my studies were not only about studying itself.

Last but not least, I would like to thank the people closest to me, mainly for their understanding that I spent so much time working instead of being with them. Finally, I thank and apologize to those whom I did not name explicitly though they deserve my sincere thanks too.

"Sera parsimonia in fundo est."
— L. A. Seneca

Moral letters to Lucilius
Letter I: On saving time

To my parents

Contents

Introduction

Contemporary particle physics is very well explained by the so-called Standard Model (SM). This immensely elegant and successful quantum field theory based on the $\mathrm{SU(3)_c} \times \mathrm{SU(2)_L} \times \mathrm{U(1)_Y}$ gauge symmetry group describes the dynamics of the strong interaction as well as of the unified electromagnetic and weak interactions. Despite the fact that the SM is being verified every day using various experimental set-ups, there are several phenomena which cannot be explained within its framework. For instance, the SM does not incorporate neutrino masses and cannot therefore explain neutrino (flavor) oscillations. It also does not provide any viable candidate for dark matter particles or fails to describe the baryon asymmetry to its full extent. Moreover, the fourth known fundamental interaction of nature — the gravitational interaction — is also not included in the SM. Hence, the SM is not a complete theory of fundamental interactions and it is tempting to search beyond its reach.

Looking for effects of new physics and eventually choosing the most nature-compatible one among the beyond-Standard Model scenarios is certainly one of the major contemporary goals of particle physics. In general, there are three frontiers which are being explored: the cosmic, the energy, and the intensity (also called precision) frontier. The content of this thesis contributes to the last one — i.e. to the precision frontier of the Standard Model. A discovery and quantification of new phenomena at this frontier is a very complicated task: it goes along with having our present knowledge under control. Indeed, to draw reasonable conclusions and extract information about eventual new physics from experimental data the theory needs to keep pace with these findings. Due to the fact that experimental devices and techniques are getting more and more precise, theorists should provide sufficiently low uncertainties together with their predictions. Only in this way an eventual discrepancy can be clearly and correctly revealed. New physics has therefore no meaning without the 'old one' being fully explored. Unfortunately, as an example, the low-energy sector of strong interactions remains a significant challenge which is being addressed using multiple different approaches — e.g. Chiral Perturbation Theory or Lattice QCD — and techniques — e.g. dispersion relations, large-N_c limit or operator-product expansion.

The presented doctoral thesis is based on three papers which were published during last couple of years; for detailed references see [1-3] in List of Publications which follows this opening chapter. Instead of being repetitive and doubling the information in the published works, this thesis rather provides an introduction and describes some aspects which are complementary to the attached papers. Let us now briefly present the content of these papers.

Paper I studies radiative corrections in the process $\pi^0 \to e^+e^-$. This decay is usually referred to as the *rare* decay of a neutral pion: the decay is loop- and

helicity-suppressed with the branching ratio $\simeq 6 \times 10^{-8}$. Due to such a significant suppression, it might be possible that this process is sensitive to new physics. The precise measurement of its branching ratio was performed by the KTeV experiment at Fermilab. After it had been published [1] and a subsequent comparison with the Standard Model-based theoretical prediction had been made [2], the resulting $3.3\,\sigma$ discrepancy drew attention of the community. The associated excitement was later on moderated by Ref. [3]. There, the two-loop virtual radiative corrections in the sector of Quantum Electrodynamics (QED) were properly treated and an inconsistency with the previously used approximative results [4, 5] was shown. A proper inclusion of these new corrections to the SM prediction led to a significant decrease of the discrepancy in question down to a level of $2\,\sigma$. Not only is such a discrepancy inconclusive, but it would have been probably decreased even more if the experimental analysis had been redone using new results; for related discussion see Section III.5 of Paper III. Paper I then studies some last missing pieces in the jigsaw. Namely, it is dedicated to the bremsstrahlung correction which is calculated beyond the soft-photon approximation. This serves as a complementary work to Ref. [3] where only soft-photon bremsstrahlung was used to cancel infrared divergences. It has been found that soft-photon limit is a good approximation for the kinematical region used by the KTeV experiment. Moreover, Paper I shows that if the effective approach for the pion transition form factor is used (a local form factor plus a counter term), it requires no significant improvements with respect to higher-order corrections in the Chiral Perturbation Theory expansion.

Paper II is devoted to the Dalitz decay of a neutral pion and describes the next-to-leading order radiative corrections in the QED sector. The Dalitz decay — i.e. the process $\pi^0 \to e^+e^-\gamma$ — is the second most prominent decay of a neutral pion. The work on this project was driven by experimental needs of the NA48/NA62 collaboration at CERN [6]. A reference point for this paper was a classical work [7]. Our aim was to recalculate the radiative corrections presented in [7] without any simplifications so the resulting expressions might be used also for cases in which the mass of final-state leptons is not negligible anymore. This situation arises for the $\eta^{(\prime)} \to \mu^+\mu^-\gamma$ decays. Moreover, the one-loop one-photon-irreducible contribution — which was considered to be negligible at the time [7] was published — was included in our approach. This correction is significant especially when the invariant mass of the final-state lepton pair becomes large. Paper II also includes a detailed description of the computational methods. As an outcome of this work, the `C++` code was prepared and included into the NA48/NA62 analysis software. Likewise, later on also the A2 collaboration at Mainz made use of this code [8].

In Paper III, an improved model for the pion electromagnetic transition form factor $\mathcal{F}_{\pi^0\gamma^*\gamma^*}(p^2, q^2)$ was proposed. In terms of uncertainty treatment and fulfillment of conditions from various inputs, this model provides an eligible alternative to other form-factor models available on the market and used by the community so far. The main motivation for such an investigation was driven by the remaining discrepancy in the rare pion decay. Within a family of large-N_c motivated resonance-saturation models for the pseudoscalar-vector-vector (PVV) correlator in the chiral limit, an ansatz taking into account two multiplets in both vector and pseudoscalar channels was considered; this is where its name — two-

hadron saturation (THS) — comes from. To minimize the number of unknown parameters, high- as well as low-energy theoretical constraints were applied: the operator-product expansion (OPE) at the leading order [9], the Brodsky–Lepage constraint [10] and a matching at the photon point (i.e. for $\mathcal{F}_{\pi^0\gamma^*\gamma^*}(0,0)$) to the chiral anomaly. In the end, a form factor that has only one free dimensionless parameter κ arises. The value of this parameter was determined from a fit to the measurements of the ω-π transition form factor $\mathcal{F}_{\pi^0\omega\gamma^*}$ [11]. By construction, the THS approach satisfies all the theoretical LO constraints given by QCD. It is phenomenologically very successful and for a wide range of quantities it gives reliable predictions which are consistent with the experimental data. It might be also compared with other models, like vector-meson dominance (VMD) — a simple dipole ansatz which violates OPE — or lowest-meson dominance (LMD) [9] — which takes into account only one meson multiplet in each channel and, consequently, it strongly violates the Brodsky–Lepage limit. It is worth noting that in the singly off-shell regime, the THS form factor does not depend on κ: one thus has a full predictive power for associated quantities like the form-factor slope a_π measured for instance from the Dalitz decay.

The thesis is structured as follows. In Chapter 1 we provide an introduction to the framework of effective field theories and apply it to Quantum Chromodynamics in the low-energy domain. Chiral Perturbation Theory then arises as a result of this approach and the related Lagrangian is presented. This effective field theory which describes interactions of the lightest mesons is used in Paper I and partly also in the other two papers. In Chapter 2 we touch a limit of QCD, in which the number of colors is large or eventually sent to infinity. We discuss the main phenomenological implications of this limit for the real world. The main results of this approach for correlators of quark bilinears appear as a guiding principle in Paper III. In Chapter 3 we discuss IR divergences in QED and an important role of bremsstrahlung corrections. The calculation of some basic one-loop corrections used in Paper II and results in terms of scalar one-loop integrals are presented. An application of radiative corrections which were calculated in Paper I and Paper II in the experiment is shown. Finally, in Chapter 4 we go beyond Paper II (and the therein described process $\pi^0 \to e^+e^-\gamma$) and discuss the differences which arise when the radiative corrections for the $\eta^{(\prime)} \to \ell^+\ell^-\gamma$ processes are tackled. This represents a core of a paper in preparation. We conclude with Summary followed by five appendices devoted to more technical issues.

List of Publications

Significant publications

[1] T. Husek and S. Leupold,
"Two-hadron saturation for the pseudoscalar-vector-vector correlator and phenomenological applications,"
Eur. Phys. J. **C75** no. 12, (2015) 586, arXiv:1507.00478 [hep-ph].

[2] T. Husek, K. Kampf, and J. Novotný,
"Radiative corrections to the Dalitz decay $\pi^0 \to e^+e^-\gamma$ revisited,"
Phys. Rev. **D92** no. 5, (2015) 054027, arXiv:1504.06178 [hep-ph].

[3] T. Husek, K. Kampf, and J. Novotný,
"Rare decay $\pi^0 \to e^+e^-$: on corrections beyond the leading order,"
Eur. Phys. J. **C74** no. 8, (2014) 3010, arXiv:1405.6927 [hep-ph].

Conference proceedings

[4] T. Husek,
"Decays of neutral pions: Electromagnetic transition form factor and radiative corrections,"
XIIth Quark Confinement and the Hadron Spectrum,
EPJ Web Conf. **137** (2017) 05006.

[5] T. Husek,
"Electromagnetic transition form factor and radiative corrections in decays of neutral pions,"
MESON 2016 - 14th International Workshop on Meson Production, Properties and Interaction,
EPJ Web Conf. **130** (2016) 04002.

[6] T. Husek, K. Kampf, and J. Novotný,
"Corrections beyond the leading order in $\pi^0 \to e^+e^-$ process,"
Quark Confinement and the Hadron Spectrum XI
AIP Conf. Proc. **1701** (2016) 040008.

[7] S. Giovannella, A. Kupsc, and P. Masjuan, eds.,
"*MesonNet 2014 International Workshop. Mini-proceedings*". 2014.
arXiv:1412.5451 [nucl-ex].

[8] K. Kampf, A. Kupsc, and P. Masjuan, eds.,
"*MesonNet 2013 International Workshop. Mini-proceedings*". 2013.
arXiv:1308.2575 [hep-ph].

Collaboration publications

[9] **NA62** Collaboration, E. Cortina Gil *et al.*,
"The Beam and detector of the NA62 experiment at CERN,"
JINST **12** no. 05, (2017) P05025, `arXiv:1703.08501 [physics.ins-det]`.

Bachelor project significant publications

[10] **OSQAR** Collaboration, P. Pugnat *et al.*,
"Search for weakly interacting sub-eV particles with the OSQAR laser-based experiment: results and perspectives,"
Eur. Phys. J. **C74** no. 8, (2014) 3027, `arXiv:1306.0443 [hep-ex]`.

[11] M. Šulc *et al.*,
"Axion search by laser-based experiment OSQAR,"
Nucl. Instrum. Meth. **A718**, (2013) 530–532.

Publications in active preparation

[12] T. Husek, K. Kampf, S. Leupold and J. Novotný,
"Radiative corrections to the Dalitz decays $\eta^{(\prime)} \to \ell^+\ell^-\gamma$."

[13] T. Husek and S. Leupold,
"Radiative corrections for the decay $\Sigma^0 \to \Lambda e^+e^-$."

Conventions, definitions, notation

Units

Throughout this work we use the rationalized (Lorentz–Heaviside) natural units (NU) where $\hbar = c = 1$. In order to get numerical results in the SI units (seconds, meters), one has two choices. It is either necessary to restore the constants $\hbar$ and c using dimensional analysis of relevant equations or simply convert the numerical results using for instance the following unit relations:

$$1\,\mathrm{MeV}^{-1} \overset{\mathrm{NU}}{=} \hbar\,\mathrm{MeV}^{-1} \overset{\mathrm{SI}}{\simeq} 6.58 \times 10^{-22}\,\mathrm{s}\,, \tag{1}$$

$$1\,\mathrm{MeV}^{-1} \overset{\mathrm{NU}}{=} \hbar c\,\mathrm{MeV}^{-1} \overset{\mathrm{SI}}{\simeq} 197\,\mathrm{fm}\,. \tag{2}$$

Due to the fact that the electric charge is dimensionless in the natural units and hence we might write

$$1 \overset{\mathrm{NU}}{=} \sqrt{\hbar c \varepsilon_0} \overset{\mathrm{SI}}{\simeq} 5.29 \times 10^{-19}\,\mathrm{C}\,, \tag{3}$$

one indeed obtains the unit charge e in the SI units through

$$e \overset{\mathrm{NU}}{=} \sqrt{4\pi\alpha} \overset{\mathrm{NU}}{=} \sqrt{4\pi\alpha\hbar c\varepsilon_0} \overset{\mathrm{SI}}{\simeq} 1.602 \times 10^{-19}\,\mathrm{C}\,. \tag{4}$$

Metric

For the metric of the flat 4-dimensional spacetime we use the convention

$$g_{\mu\nu} = \mathrm{diag}(1, -1, -1, -1) = g^{\mu\nu}\,, \qquad g_{\mu\nu}g^{\mu\nu} = g_\mu{}^\mu = 4\,. \tag{5}$$

Consequently, the scalar product can be written as

$$k \cdot l = g_{\mu\nu}k^\mu l^\nu = k_0 l_0 - \vec{k} \cdot \vec{l}\,. \tag{6}$$

Dirac γ-matrices

The Dirac γ-matrices, which satisfy the anticommutation relations

$$\{\gamma^\mu, \gamma^\nu\} = 2g^{\mu\nu}\mathbb{1}\,, \quad \{\gamma^\mu, \gamma^\nu\} \equiv \gamma^\mu\gamma^\nu + \gamma^\nu\gamma^\mu\,, \tag{7}$$

generate a matrix representation of a Clifford algebra. In the standard Dirac representation, they can be written in the form

$$\gamma^0 = \begin{pmatrix} \mathbb{1} & 0 \\ 0 & -\mathbb{1} \end{pmatrix}, \qquad \gamma^i = \begin{pmatrix} 0 & \sigma^i \\ -\sigma^i & 0 \end{pmatrix}, \tag{8}$$

where $i = 1, \ldots 3$ and σ^i are the Pauli matrices

$$\sigma^1 = \begin{pmatrix} 0 & 1 \\ 1 & 0 \end{pmatrix}, \qquad \sigma^2 = \begin{pmatrix} 0 & -i \\ i & 0 \end{pmatrix}, \qquad \sigma^3 = \begin{pmatrix} 1 & 0 \\ 0 & -1 \end{pmatrix}. \tag{9}$$

We also use the usual *slash* symbol $\not{p} \equiv p_\mu \gamma^\mu$ for an arbitrary four-vector p^μ contracted with the γ-matrices. The γ_5-matrix which is hermitian and anticommutes with all four γ-matrices γ^μ is defined as

$$\gamma_5 \equiv i\gamma^0\gamma^1\gamma^2\gamma^3 \,. \tag{10}$$

It is connected with the totally antisymmetric Levi-Civita pseudo-tensor, which is fixed by

$$\varepsilon_{0123} = 1 \,, \quad \varepsilon^{0123} = -1 \,, \tag{11}$$

through

$$\gamma_5 = \frac{i}{4!}\varepsilon_{\mu\nu\rho\sigma}\gamma^\mu\gamma^\nu\gamma^\rho\gamma^\sigma \,. \tag{12}$$

The Pauli matrices (9) are traceless and hermitian and hence they can generate a unitary matrix representation of the SU(2) group. A simple generalization for the SU(3) case is governed by the Gell-Mann matrices λ^a defined as

$$\begin{aligned}
\lambda^1 &= \begin{pmatrix} 0 & 1 & 0 \\ 1 & 0 & 0 \\ 0 & 0 & 0 \end{pmatrix}, \qquad \lambda^2 = \begin{pmatrix} 0 & -i & 0 \\ i & 0 & 0 \\ 0 & 0 & 0 \end{pmatrix}, \qquad \lambda^3 = \begin{pmatrix} 1 & 0 & 0 \\ 0 & -1 & 0 \\ 0 & 0 & 0 \end{pmatrix}, \\
\lambda^4 &= \begin{pmatrix} 0 & 0 & 1 \\ 0 & 0 & 0 \\ 1 & 0 & 0 \end{pmatrix}, \qquad \lambda^5 = \begin{pmatrix} 0 & 0 & -i \\ 0 & 0 & 0 \\ i & 0 & 0 \end{pmatrix}, \\
\lambda^6 &= \begin{pmatrix} 0 & 0 & 0 \\ 0 & 0 & 1 \\ 0 & 1 & 0 \end{pmatrix}, \qquad \lambda^7 = \begin{pmatrix} 0 & 0 & 0 \\ 0 & 0 & -i \\ 0 & i & 0 \end{pmatrix}, \qquad \lambda^8 = \frac{1}{\sqrt{3}} \begin{pmatrix} 1 & 0 & 0 \\ 0 & 1 & 0 \\ 0 & 0 & -2 \end{pmatrix}.
\end{aligned} \tag{13}$$

Note that for $i = 1, \ldots 3$, $\lambda^i = \mathrm{diag}(\sigma^i, 0)$. The Gell-Mann matrices also satisfy $\mathrm{Tr}[\lambda^a \lambda^b] = 2\delta^{ab}$.

Field strength tensor

For the electromagnetic four-potential we have

$$A^\mu \equiv \left(\phi, \vec{A}\right) \,, \qquad A_\mu = g_{\mu\nu}A^\nu = \left(\phi, -\vec{A}\right) \,. \tag{14}$$

We define the electromagnetic field tensor as an exterior derivative of the 1-form A

$$F_{\mu\nu} \equiv \partial_\mu A_\nu - \partial_\nu A_\mu \tag{15}$$

and its dual tensor as

$$\tilde{F}_{\mu\nu} \equiv \frac{1}{2}\varepsilon_{\mu\nu\alpha\beta}F^{\alpha\beta} = \varepsilon_{\mu\nu\alpha\beta}\,\partial^\alpha A^\beta \,. \tag{16}$$

Considering the electric and magnetic fields, which are obtained from the components of the four-potential A^μ through

$$\vec{E} = -\frac{\partial \vec{A}}{\partial t} - \vec{\nabla}\phi\,, \qquad \vec{B} = \vec{\nabla} \times \vec{A}\,, \tag{17}$$

we can write the explicit form of the field strength tensor:

$$F_{\mu\nu} = \begin{pmatrix} 0 & E_x & E_y & E_z \\ -E_x & 0 & -B_z & B_y \\ -E_y & B_z & 0 & -B_x \\ -E_z & -B_y & B_x & 0 \end{pmatrix}. \tag{18}$$

Epsilon usage

Finally, we use ϵ in the meaning of an infinitesimally small number — for instance as in the case of $[l^2 - m^2 + i\epsilon]$ in a Feynman propagator. It serves to specify on which side of the branch cut in the complex plane one should evaluate a multivalued function, e.g. $\log(-1 - i\epsilon) = -i\pi$. In case it is omitted, its presence is tacitly assumed and it is restored whenever necessary. By 'log' we denote the principal value of the logarithm: $\operatorname{Im} \log z \in [-\pi, \pi]$.

In the dimensional regularization, we use ε defined through $2\varepsilon = 4 - n$ where n is an analytically continued (non-integer) number of spacetime dimensions in the vicinity of 4.

Chapter 1

Chiral Perturbation Theory

Quantum Chromodynamics (QCD) — the quantum field theory which governs the strong interaction and hence the dynamics of quarks and gluons — turns out to be difficult to solve directly in the low energy domain. In this region, the strong coupling α_s becomes large and consequently the perturbation series for related S-matrix elements cease to converge. This is due to the feature called confinement which has its origin in the Yang–Mills nature of QCD. On the other hand, this is exactly the region which we will explore in this work and where the decays of pseudoscalar mesons belong. Looking for ways how to circumvent this unfortunate technical difficulties is essential. One of the solutions lies in using the framework of effective field theories (EFTs).

1.1 Effective field theories

To build an EFT, one first needs to identify the energy domain and relevant dynamical degrees of freedom, the quantum fields of which constitute the building blocks of the Lagrangian describing the specified problem. Our aim now is to write down a local quantum field theory (QFT), which allows us to calculate (among other things) the widths of specific decays of the lightest pseudoscalar mesons. After the particle content of the theory is settled, one needs to transfer the symmetries from the fundamental theory (QCD) in order to actually build the relevant pieces of the Lagrangian. Typically, the hypothesis due to Weinberg [12] states that in order to get a desired S-matrix consistent with the fundamental principles of QFT, one has to write down a Lagrangian containing all possible terms which are compatible with the symmetries of the fundamental theory and contain the right degrees of freedom. After applying these guidelines one in principle ends up with a Lagrangian containing infinite number of terms. On top of that, every such a term comes with a coefficient called a low-energy constant (LEC). These constants are a priori not known; values of these constants may be obtained from experiment or by the matching procedure when the given EFT is compared with the related fundamental theory. Having the infinite number of terms and associated unknown parameters is definitely not a practical outcome of the discussed framework of EFTs. The leading principle which solves this peculiarity and tells us which terms are more important than others is called a power-counting scheme.

1.2 Chiral symmetry

In the following, we will discuss a specific example of EFT, Chiral Perturbation Theory (χPT), which is the low-energy EFT for QCD describing interactions of the lightest mesons. The QCD Lagrangian can be written as

$$\mathcal{L}_{\mathrm{QCD}} = -\frac{1}{4} G^a_{\mu\nu} G^{a\mu\nu} + \bar{q}_i (i \not{D}_{ij} - \mathcal{M}\, \delta_{ij}) q_j \,. \tag{1.1}$$

Above, $G^a_{\mu\nu}$ represent the gluon strength tensors

$$G^a_{\mu\nu} = \partial_\mu \mathcal{A}^a_\nu - \partial_\nu \mathcal{A}^a_\mu + g f^{abc} \mathcal{A}^b_\mu \mathcal{A}^c_\nu \,, \tag{1.2}$$

with $\mathcal{A}^a_\mu$ being the gluon gauge fields in the adjoint representation of SU(3), $a = 1, \ldots 8$, g being a strong coupling constant and f^{abc} being the SU(3) structure constants, $q_i = (u_i, d_i, \ldots, t_i)^{\mathsf{T}}$ stands for a vector (in the flavor space) of quark quantum fields with a specific color i, $D_{\mu,ij} = \delta_{ij}\partial_\mu - igT^a \mathcal{A}^a_{\mu,ij}$ is the covariant derivative and finally $\mathcal{M}$ is the diagonal quark-mass matrix. Strictly speaking, the gauge symmetry allows in (1.1) an additional term — the well-known theta-term:

$$\mathcal{L}_\theta = \theta \frac{g^2}{64\pi^2} G^a_{\mu\nu} \tilde{G}^{a\mu\nu} \,. \tag{1.3}$$

This term violates explicitly P and CP symmetry and would give rise — even though being a total divergence — to the electric dipole moment of a neutron; see e.g. [13] and references therein. However, from the experiments it is apparent that the strong interaction is — compared to the weak interaction — P/CP-conserving and that the electric dipole moment of a neutron is very tiny. This fact suggests that θ would need to be very small. Since there was no clear reason for this to be the case, the resulting fine-tuning problem in strong interactions is called the "strong CP problem". One of the solutions was proposed by R. Peccei and H. Quinn [14, 15], the result of which is a prediction of a new particle called axion, a pseudoscalar pseudo-Nambu–Goldstone boson of the spontaneously broken new U(1) global symmetry named after its authors.

Let us now turn back to the aspects of χPT. The name *chiral* refers to properties of the QCD Lagrangian in the limit of vanishing masses of quarks — i.e. for $\mathcal{M} = 0$. In reality, it is reasonable to apply this limit only for the case of the lightest quarks and build an EFT for vanishing masses of quarks u (up) and d (down), eventually also for the quark s (strange). This is connected to the fact that the current-quark masses of the u-, d- and also of the s-quark are negligible compared to other relevant scales in the hadronic sector:

$$m_u \simeq m_d \ll m_s \lesssim \Lambda_{\mathrm{QCD}} \ll \Lambda_{\mathrm{H}} \simeq \Lambda_{\chi\mathrm{PT}} = 4\pi F_\pi \simeq 1\,\mathrm{GeV} \lesssim m_c < m_b < m_t \,; \tag{1.4}$$

see Table 1.1 for the approximate masses of quarks. The renormalization-scheme-dependent scale $\Lambda^{\overline{\mathrm{MS}}}_{\mathrm{QCD}} \simeq 250\,\mathrm{MeV}$ represents a characteristic scale where the perturbative QCD breaks down. The hadronic scale Λ_{H} then corresponds to the mass scale of the lightest hadrons which are not Nambu–Goldstone bosons and it is close to the chiral symmetry breaking scale $\Lambda_{\chi\mathrm{PT}}$. The criterion stated above is valid also for the s-quark, although it is not so conclusive as in the case of the u- and d-quark. This leads to the fact that the resulting EFT is converging faster

flavor	m_f [MeV]	flavor	m_f [GeV]
u (up)	2.2(6)	c (charm)	1.3
d (down)	4.7(5)	b (bottom)	4.2
s (strange)	96(8)	t (top)	173(1)

Table 1.1: Approximate masses of quarks [16]. On the left we have the light quarks, the current-quark masses of which (in the $\overline{\text{MS}}$ scheme at 2 GeV) can be assumed to be vanishing: the SU(2) or SU(3) chiral symmetry of the QCD Lagrangian is then restored. On the right we see the heavy quarks, the dynamical effects of which are hidden in the LECs of χPT.

for pions than for kaons and other mesons which contain the strange quark as a valence quark.

In the following, we will therefore restrict ourselves to the case of three-flavor QCD. The leading principle for building the low-energy EFT for QCD is the observation that the QCD Lagrangian in the massless case

$$\mathcal{L}_{\text{QCD}}^{m=0} = -\frac{1}{4} G_{\mu\nu}^a G^{a\mu\nu} + i\bar{q}_{\text{L}} \not{D} q_{\text{L}} + i\bar{q}_{\text{R}} \not{D} q_{\text{R}} \tag{1.5}$$

separates the left-handed and the right-handed parts of the quarks fields defined as

$$q_{\text{L,R}} \equiv \frac{1}{2}(1 \mp \gamma_5) q\,, \quad q = (u, d, s)^{\mathsf{T}}\,. \tag{1.6}$$

This restores the so-called chiral symmetry, which is only approximate in the real world due to nonvanishing quark masses and the associated term

$$\mathcal{L}_{\text{QCD}}^{\text{mass}} = -(\bar{q}_{\text{L}} \mathcal{M}\, q_{\text{R}} + \bar{q}_{\text{R}} \mathcal{M}\, q_{\text{L}})\,. \tag{1.7}$$

Note that from now on we suppress the color indices, since we are about to describe hadrons — gauge invariant objects which must be colorless. The Lagrangian (1.5) is invariant under the *extended* chiral symmetry group $\text{U}(3)_{\text{L}} \times \text{U}(3)_{\text{R}}$. For a moment we will focus on its subgroup $\text{SU}(3)_{\text{L}} \times \text{SU}(3)_{\text{R}}$, which is also the symmetry of the Lagrangian (1.5) at the quantum level and which we call the chiral symmetry group. If $q_{\text{L,R}}$ is transformed in the flavor space according to the prescription $q_{\text{L,R}} \to U_{\text{L,R}}\, q_{\text{L,R}}$, the Lagrangian stays invariant for any $U_{\text{L,R}} \in \text{SU}(3)_{\text{L,R}}$ — the group of 3×3 unitary matrices with a unit determinant. In general, $U_{\text{L}} \neq U_{\text{R}}$ — the left-handed and right-handed worlds are separated. A special unitary matrix group can be represented through exponentiation as $U_{\text{L,R}} = \exp(i\alpha_{\text{L,R}}^a T^a)$, where T^a are hermitian generators. In the case of the SU(3) group, $T^a = \lambda^a/2$, where λ^a with $a = 1, \ldots 8$ are the Gell-Mann matrices. Due to the Noether's theorem, every (global) continuous symmetry of a Lagrangian is related to a conservation law. In the case of the chiral symmetry group, the conserved currents are $j_{\text{L,R}}^{a\mu} = \bar{q}_{\text{L,R}} \gamma^\mu T^a q_{\text{L,R}}$. The related conserved charges are then calculated through $Q_{\text{L,R}}^a = \int \text{d}^3\vec{x}\, j_{\text{L,R}}^{a0}$.

Let us briefly mention that there are two interesting special cases for the choice of $U_{\text{L,R}}$. First, consider an element $U_{\text{L}} = U_{\text{R}} = U_{\text{V}}$ of the vector subgroup $\text{SU}(3)_{\text{V}}$. The conserved current is now $V^{a\mu} = j_{\text{L}}^{a\mu} + j_{\text{R}}^{a\mu} = \bar{q}\gamma^\mu T^a q$. Moreover, the mass term (1.7) is invariant under this subgroup for a specific choice of $\mathcal{M}$: if we assume quarks have the same mass $\tilde{m}$, then $\mathcal{M} = \tilde{m}\mathbb{1}$. As a consequence, the whole subgroup $\text{SU}(3)_{\text{V}}$ is a symmetry of the Lagrangian (1.1) even in the $\mathcal{M} \neq 0$

case. The vector subgroup $\mathrm{SU}(3)_\mathrm{V}$ is then responsible for the fact that hadrons are organized into flavour multiplets of approximately degenerate rest mass. The fact that the degeneracy is not exact in the realistic hadron spectrum is given by the fact that the masses of quarks significantly differ. In the more realistic case of $\mathcal{M} = \mathrm{diag}(\hat{m}\mathbb{1}_2, m_s)$, where $\hat{m}$ is the average mass of the u- and d-quarks, the mass term (1.7) is invariant under symmetry transformations given by $\tilde{U}_\mathrm{V} = \mathrm{diag}(\mathrm{U}_\mathrm{V}^{(2)}, e^{i\theta_s})$ with $\mathrm{U}_\mathrm{V}^{(2)} \in \mathrm{SU}(2)_\mathrm{V}$. Hence, one obtains the isospin and strangeness conservation laws. Note that in this case, $\tilde{U}_\mathrm{V} \in \mathrm{U}(3)_\mathrm{V}$ since its determinant is not equal to one. For the real case in which $\mathcal{M} = \mathrm{diag}(m_u, m_d, m_s)$, one gets the flavor conservation in QCD. The orthogonal case to the choice $U_\mathrm{L} = U_\mathrm{R} = U_\mathrm{V}$ is $U_\mathrm{L} = U_\mathrm{R}^\dagger = U_\mathrm{A}$. The associated conserved currents are then $A^{a\mu} = j_\mathrm{R}^{a\mu} - j_\mathrm{L}^{a\mu} = \bar{q}\gamma^\mu\gamma_5 T^a q$.

Let us now go back to the extended chiral group $\mathrm{U}(3)_\mathrm{L} \times \mathrm{U}(3)_\mathrm{R}$. It can be decomposed in the following way:

$$\mathrm{U}(3)_\mathrm{L} \times \mathrm{U}(3)_\mathrm{R} = \mathrm{SU}(3)_\mathrm{V} \times \mathrm{SU}(3)_\mathrm{A} \times \mathrm{U}(1)_\mathrm{B} \times \mathrm{U}(1)_\mathrm{A}\,. \tag{1.8}$$

Such a decomposition is necessary since the subgroups of the whole extended chiral symmetry group are realized in different ways in the particle spectrum. In general, a symmetry of a Lagrangian is realized à la Wigner–Weyl in such a case, in which the resulting vacuum $|0\rangle$ has the same symmetry: i.e. it holds $Q|0\rangle = 0$ with Q being the associated conserved charge. The traces of such a symmetry are visible in the particle spectrum. This is the case of the vector subgroup $\mathrm{SU}(3)_\mathrm{V}$ described above, which sorts the hadrons into multiplets characterized by similar mass. More generally, a theorem by Vafa and Witten [17] states that in the vector-like gauge theories (e.g. QCD with $\theta = 0$) the vector global symmetries cannot be spontaneously broken. The axial-vector part $\mathrm{SU}(3)_\mathrm{A}$ is, on the other hand, spontaneously broken: more precisely, a theorem by 't Hooft [18] states that the axial symmetries are necessarily broken in the presence of confinement and three massless flavors. In this situation we talk about the Nambu–Goldstone [19, 20] realization of the symmetry. The Lagrangian is invariant under such a symmetry, but the ground state — the vacuum — lacks this symmetry: $Q|0\rangle \neq 0$. According to the Goldstone theorem, for every broken generator of the global symmetry group there appears a massless excitation in the spectrum. In the case of the $\mathrm{SU}(N_\mathrm{f})$ group there are $N_\mathrm{f}^2 - 1$ generators and thus for $N_\mathrm{f} = 3$ there are eight broken generators and consequently eight massless Goldstone bosons. Since it is axial-vector group which is broken, we should obtain an octet of massless pseudoscalars. However, this would work in the world with massless quarks. Due to the fact that quarks have a small mass and the chiral symmetry is thus explicitly broken, we are left with the octet of lowest-lying pseudoscalar mesons: pions, kaons and eta. These mesons represent the pseudo-Nambu–Goldstone bosons of the spontaneously broken generators of the $\mathrm{SU}(3)_\mathrm{A}$ part of the chiral symmetry group and should then be significantly light compared to other hadrons of QCD. In other words, there should be a mass gap, which is indeed visible for instance in the case of the SU(2) subgroup: the lightest mesons — pions with $m_\pi \simeq 140\,\mathrm{MeV}$ — are much lighter than vector-meson resonances ρ and ω with $M_\rho \simeq M_\omega \simeq 780\,\mathrm{MeV}$, the quark content of which is given also by the light quarks u and d.

Let us now briefly mention that in (1.8) the $\mathrm{U}(1)_\mathrm{B}$ subgroup corresponds to the baryon number conservation. Finally, $\mathrm{U}(1)_\mathrm{A}$ corresponds to a current which is not

conserved on the quantum level and an anomalous term appears. The divergence of the singlet axial-vector current is given by

$$\partial_\mu A^\mu = 2i\bar{q}\gamma_5\mathcal{M}q + \frac{3g^2}{16\pi^2}\tilde{G}^a_{\mu\nu}G^{a\mu\nu} \tag{1.9}$$

and hence does not vanish in the chiral limit in which $\mathcal{M} \to 0$. However, if in addition the limit of the large number of colors (see Chapter 2 for details) is imposed, the singlet axial-vector current is conserved and the associated pseudoscalar meson η' becomes massless [21].

1.3 Effective Lagrangian for low-energy QCD

As we have already discussed, an EFT Lagrangian contains in general an infinite number of terms and one needs to postulate which of these monomials are more important than others. Such a mechanism is a necessary ingredient of an EFT and is called a power-counting scheme. In χPT — being a low-energy EFT for lowest-lying pseudoscalar mesons which arise as pseudo-Nambu–Goldstone bosons of spontaneously broken (nonlinearly realized) $\mathrm{SU(3)_A}$ — amplitudes (in the chiral limit) are proportional to four-momenta of pseudoscalars and thus vanish in the limit of zero four-momenta. This is due to the soft-Goldstone-boson theorem, which is also referred to as the Adler's zero [22]. Consequently, an expansion in powers of momenta seems to be a natural choice. The powers of these momenta correspond to the number of derivatives of pseudoscalar fields in the Lagrangian. The most important term in the χPT Lagrangian is then the one with the least number of derivatives. Pseudoscalar Goldstone bosons can interact only through their derivatives — this is related to the generalized shift symmetry — and the Lorentz-invariant Lagrangian needs therefore to be even in the number of such fields.

Moreover, we would like to include corrections to vanishing quark masses into the Lagrangian. First, we need to estimate the quark-mass (chiral) counting. The squared masses of pseudoscalar mesons are linear in quark masses: for instance $M_\pi^2 = B_0(m_u + m_d)$, where B_0 is related to the scalar singlet quark condensate $\langle 0|\bar{q}q|0\rangle$. Since a square of the four-momentum of a pseudoscalar is normalized as $p^2 = M_P^2$, the quark masses have the same counting as two derivatives: $m_q \sim \mathcal{O}(q^2)$.

Let us now finally get to the χPT Lagrangian. According to what was written above, the χPT Lagrangian can be written as a series of even-order chiral Lagrangians:

$$\mathcal{L}_{\chi\mathrm{PT}} = \mathcal{L}_2 + \mathcal{L}_4 + \mathcal{L}_6 + \dots \tag{1.10}$$

Applying the Callan–Coleman–Wess–Zumino construction [23] for our case, the lowest-order Lagrangian of order two is then explicitly written as

$$\mathcal{L}_2 = \frac{F_0^2}{4}\,\mathrm{Tr}\Big[D_\mu U (D^\mu U)^\dagger\Big] + \frac{F_0^2}{4}\,\mathrm{Tr}\Big[\chi U^\dagger + U\chi^\dagger\Big]\,. \tag{1.11}$$

Above, the pseudoscalar fields enter the Lagrangian e.g. via the exponential parametrization $U = \exp(i\phi/F_0)$ with the pseudoscalar Goldstone-boson octet

matrix

$$\phi = \phi^a \lambda^a = \sqrt{2} \begin{pmatrix} \frac{1}{\sqrt{2}}\pi^0 + \frac{1}{\sqrt{6}}\eta^8 & -\pi^+ & -K^+ \\ \pi^- & -\frac{1}{\sqrt{2}}\pi^0 + \frac{1}{\sqrt{6}}\eta^8 & -K^0 \\ K^- & -\overline{K^0} & -\sqrt{\frac{2}{3}}\eta^8 \end{pmatrix}. \tag{1.12}$$

The field $\chi = 2B_0(s + ip)$, which carries scalar (s) and pseudoscalar (p) external densities, can be used to include quark mass corrections in a chiral-invariant way — by letting $s = \mathcal{M}$ and $p = 0$. The covariant derivative D_μ is defined via vector (v_μ) and axial-vector (a_μ) external currents as

$$D_\mu U = \partial_\mu U - i[v_\mu, U] + i\{a_\mu, U\}\,. \tag{1.13}$$

Lagrangian (1.11) contains two LECs: F_0 which is related to the pion decay constant $F_\pi \simeq 92\,\mathrm{MeV}$ and B_0 related to the scalar singlet quark condensate.

Let us mention that the higher-order terms are naturally more complicated and contain much more parameters: schematically, for instance $\mathcal{L}_4 = \sum_{i=1}^{10} L_i O_4^i$ [24] or $\mathcal{L}_6 = \sum_{i=1}^{90} C_i O_6^i$. To determine a chiral order ω of a Feynman diagram, it is useful to use the (Weinberg's) formula (in four dimensions) [12, 25]

$$\omega = 2 + 2N_\mathrm{L} + \sum_{k=2}^{\infty} (2k-2) N_{2k}\,, \tag{1.14}$$

where N_L is the number of independent loops in the diagram and N_{2k} is the number of vertices of chiral order $2k$ — those which come from $\mathcal{L}_{2k}$.

Lagrangian (1.11) only describes processes with an even number of Goldstone bosons. To describe for instance the neutral pion decays or the $KK \to 3\pi$ scattering, the odd-sector of the χPT needs to be established. At the leading order it is given by the chiral anomaly and is already of the chiral order four ($\mathcal{O}(q^4)$) at which it is fully reconstructed: the anomaly has no higher-order corrections [26]. The odd-sector chiral Lagrangian of order $\mathcal{O}(q^6)$ was constructed in [27, 28]. The chiral anomaly is transferred to χPT via Wess–Zumino–Witten (WZW) construction [29, 30]. For instance, the two-photon decay of a neutral pion is described by the following Lagrangian:

$$\mathcal{L}^{\pi^0\gamma\gamma}_\mathrm{WZW} = -\frac{e^2 N_c}{48\pi^2 F_\pi} \pi^0 F_{\mu\nu} \tilde{F}^{\mu\nu}\,. \tag{1.15}$$

Here, N_c is the number of colors — the strong-force charges. We see that in the terms of WZW type, the pion field is not coupled through a derivative. The related shift symmetry is, however, indeed realized, but only on the level of the action itself.

Finally — e.g. in the calculation of the branching ratio of the pion rare decay $\pi^0 \to e^+e^-$ — it is useful to introduce a local counter-term (c.t.) Lagrangian [31]

$$\begin{aligned} \mathcal{L}_\mathrm{c.t.} = {} & \frac{3i\alpha^2}{32\pi^2} \left(\bar{l}\gamma^\mu\gamma_5 l\right) \\ & \times \left\{ \chi_1 \,\mathrm{Tr}\Big[Q^2 U^\dagger \partial_\mu U - Q^2 \partial_\mu U^\dagger U\Big] + \chi_2 \,\mathrm{Tr}\Big[Q U^\dagger Q \partial_\mu U - Q \partial_\mu U^\dagger Q U\Big] \right\}, \end{aligned} \tag{1.16}$$

where $Q \equiv \mathrm{diag}(2/3, -1/3, -1/3)$ is the quark-charge matrix. The combination $\chi \equiv -(\chi_1 + \chi_2)/4$ of the two LECs above has a UV-divergent and convergent part.

The UV-divergent part exactly cancels the UV divergence in the leading-order diagram for the $\pi^0 \to e^+e^-$ process, where the WZW term was used as the local $\pi^0 \to \gamma^*\gamma^*$ transition form factor. The convergent part $\chi^{(r)}(\mu)$ of this coupling is renormalization-scheme-dependent and can be extracted from experiment or calculated within various theoretical models. The parameter $\chi^{(r)}(M_\rho)$ then plays an essential role in all three papers attached to this thesis.

Let us conclude by mentioning the fact that Chiral Perturbation Theory embodies a very successful approach for low-energy QCD; see e.g. [32] for a review of higher-order corrections and their comparison with experiment. The validity of χPT beyond the domain of lowest energies might be extended to the hadronic scale by taking into account models for an explicit inclusion of resonances, which are also found to saturate the LECs of χPT [33], and by the use of dispersive techniques [34]. The latter framework allows for the combining of χPT with the unitarity of S-matrix, analyticity and crossing symmetry of the amplitudes.

Chapter 2

Large-N_C limit of QCD

In this chapter we would like to discuss a theoretical concept, which plays a significant role in Paper III. We already know that hadron physics is described by QCD, the $\mathrm{SU(3)_c}$ gauge quantum field theory of quarks and gluons. Even though the fundamental theory is well established, many phenomena — like confinement — are not well understood. Most importantly, hadronic decay rates, scattering amplitudes or masses of the hadrons themselves are significantly difficult to obtain directly from QCD, although recently there has been a remarkable progress in this field using the numerical techniques of lattice QCD. On the other hand, the complete solution of QCD, which would correspond to writing down the exact S-matrix of the theory, is still far away from being possible to be imagined at all. Nevertheless, the situation is not hopeless and apart from the utilization of the EFT framework — as it was described in preceding Chapter 1 — one can indeed say something about the hadronic spectrum directly from QCD.

In particle physics, calculations of processes with a use of perturbation series in various parameters is bread and butter to a phenomenologist. But a construction of a perturbation series which converges fast enough to provide meaningful results requires the right expansion parameter. Usually, it is a coupling constant which embodies this parameter. But it is exactly due to confinement — the notorious property of QCD connected to the fact that the strong coupling α_s grows with distance — which prevents such a series from converging — at least fast enough — in the low-energy domain of the strong interaction. What is then the right parameter for QCD — especially if we consider the masses of the lightest quarks to be negligible — and is there such a parameter at all?

2.1 Number of colors as expansion parameter

In the works of 't Hooft [35] and Witten [36] it was suggested to make the generalization from three colors of quarks — as is the case for QCD — to N_c colors, and accordingly from the SU(3) to $\mathrm{SU}(N_c)$ gauge group with N_c being large. The motivation is that it might be possible to solve the theory in the large-N_c limit. Subsequently, there is a chance that the phenomenological implications which we find might be qualitatively (or even quantitatively) relevant for the real world where $N_c = 3$. Indeed, such a generalized QCD simplifies as N_c becomes large and possesses a systematic expansion in $1/N_c$. On top of that, the resulting phenomenology resembles the known real world of hadron physics governed by QCD.

The question which immediately arises is whether $1/N_c = 1/3$ is small enough to be a good expansion parameter of a reasonably fast-converging series. Such a question is of an utter importance since if we manage to obtain a result using the large-N_c expansion, we would like to know whether it is relevant (and to which extent) also for the case $N_c = 3$. Lets have a look on how things work in Quantum Electrodynamics (QED). Vertices are just $e\gamma^\mu$ with $e = 0.302$ in the natural units. However, an explicit calculation of higher orders reveals that a typical expansion parameter is $\alpha = e^2/4\pi \simeq 1/137$ or even α/π and that the coefficients in such a series are reasonably small — at least up to some very high order of $\simeq 1/\alpha$: the series we work with are actually not convergent but rather asymptotic. This example shows that if we had no information about the details of the calculation, we would not be able to say anything about the convergence of the series knowing only it is connected to the electric charge e. A similar situation arises in QCD. The parameter $1/N_c = 1/3$ is numerically close to e, but since we have no additional information about the actual calculation of (in principle) infinite number of diagrams contributing to a specific order in the $1/N_c$ expansion, we cannot a priori decide whether $1/N_c = 1/3$ is small enough for the resulting series to converge fast and therefore to provide meaningful results.

Yet, there is something we can say about the convergence of the $1/N_c$ expansion. In some sense, the convergence must be good enough since the phenomenological — qualitative, and to some extent also quantitative — results in the large-N_c limit are close to what we observe in the real world. Moreover, in practice one can observe that when something is qualitatively correct, it usually embodies a good quantitative approximation too. This is what creates a common believe that the large-N_c limit is not a misleading concept and that it can actually provide valuable predictions. Another reason why is the use of the large-N_c expansion a reasonable choice is purely practical: it is the only parameter we know about and thus it better should be a good one.

2.2 Phenomenological implications

In what follows we will restrict ourselves to mesons. What are then the phenomenological implications of the Yang–Mills theory of quarks and gluons at $N_c = \infty$? The most important ones can be sorted into the four following points:

1) mesons (and glue states) are free — stable and non-interacting:
   a) meson decay amplitudes are of order $1/\sqrt{N_c}$,
   b) meson-meson elastic scattering amplitudes are of order $1/N_c$;
2) there is an infinite number of meson states;
3) meson amplitudes are given as a sum of tree diagrams, where not quarks and gluons, but physical mesons are interchanged;
4) Zweig's rule is exact, mesons are pure $q\bar{q}$ states.

Are these observations compatible with the real world? The very remarkable feature of the large-N_c limit is that the answer to the previous question is: *Yes!* We shall now discuss the respective items one by one.

At first, we state that mesons are free. However, in the real world we observe that mesons interact and decay. The first impression might therefore be that this statement is just wrong. Despite this, lets have a closer look on the phenomenology of the QCD mesons. The width of e.g. the ω or ϕ mesons is pretty small compared to their masses, and hence they are called narrow resonances: they exhibit as narrow peaks in the spectra of invariant masses of the decay products. For completeness, we list some physical values of associated quantities: $M_\omega \simeq 783\,\mathrm{MeV}$, $\Gamma_\omega \simeq 8\,\mathrm{MeV}$ and $M_\phi \simeq 1019\,\mathrm{MeV}$, $\Gamma_\phi \simeq 4\,\mathrm{MeV}$. Similarly, even the ρ meson — in the case of which one usually talks about a broad resonance and for which $M_\rho \simeq 775\,\mathrm{MeV}$ and $\Gamma_\rho \simeq 148\,\mathrm{MeV}$ — is still visible in the spectrum. This is not a trivial observation; it is not obvious at all that this should happen and that resonances shall be visible. In principle, these could be so broad that we would not see them at all. The large-N_c limit predicts — see 1a) above — that the meson decay amplitudes behave like $1/\sqrt{N_c}$, which translates to $1/N_c$ for a decay width. In the most naïve situation, the decay width would correspond to $\Gamma \simeq M/N_c$, where the meson mass M is the most natural mass-dimension-one parameter. And in the realistic case of $N_c = 3$, this just translates into the fact that the meson decay width is zero with an uncertainty of $1/N_c$ in the units given by its mass M. We immediately see that this is fulfilled even for such a broad resonance like ρ: its width is indeed less than one third of its mass. The previous statements must, of course, be taken with a grain of salt since additional numerical coefficients might spoil this trivial illustration. The physical message should though be clear.

Another very successful consequence of the large-N_c limit is point 4). So far, tetraquarks, which would be other candidates for mesons, have not been observed in the real world. Either they are not formed at all or they are just elusive to experiments. In our experience, mesons, as we know them, exhibit such a behavior that they seem to be close to $q\bar{q}$ states. The Zweig's rule then says why some processes are allowed and some are suppressed. The Zweig's rule itself cannot be explained in the whole energy domain using a simple perturbative QCD argument which states that the suppression is due to the necessary exchanges of additional gluons. The vertices associated to these gluons contain the strong coupling α_s and in the regions where α_s is a relatively small parameter, such an argument seems to be reasonable: this reasoning can be used e.g. for the case of the J/Ψ decays. However, the previous statement is no longer true in the problematic energetic region close to the hadronic scale $\Lambda_\mathrm{H} \simeq 1\,\mathrm{GeV}$. A coupling of order one would not lead to the suppression of the higher-order diagrams in the α_s expansion and the difference between the $\omega \to 3\pi$ and $\phi \to 3\pi$ decays would not have been understood. On the other hand, the large-N_c limit can explain the Zweig's rule in an elegant and general way just by investigating the planarity of the associated diagrams.

The fact that there is an infinite number of resonances in the large-N_c world, as stated in point 2), is indeed reflected in the real world — by the very existence of exited states. These, however, don't build an infinite tower. This finiteness of the number of states is due to the fact that confinement becomes less significant at higher energy scales and hence hadrons with higher masses are not built. Finally, using the fact stated in point 3), one can construct amplitudes of processes and/or meson form factors, which predict measurable quantities compatible with

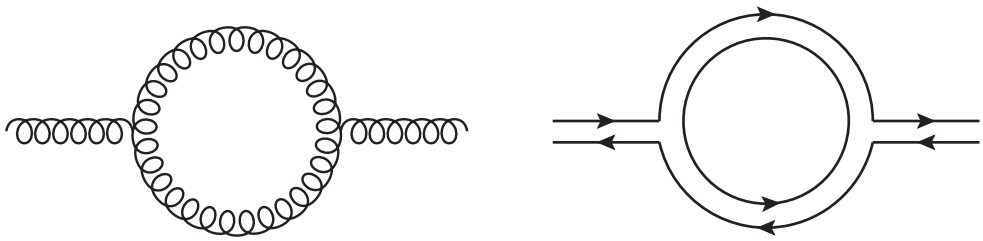

(a) (b)

Figure 2.1: Gluonic one-loop contribution to the gluon propagator. On the left we see the standard Feynman diagram; on the right there is its representation in the 't Hooft double-line representation.

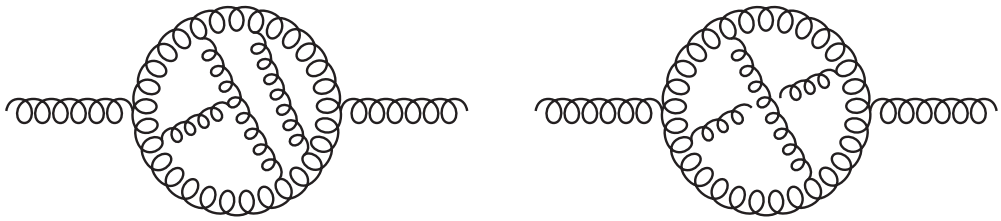

(a) (b)

Figure 2.2: Planar and non-planar gluonic contributions to the gluon propagator. On the left we see an example of a planar diagram; on the right then there is shown a non-planar case.

experiments. In this way one immediately sees the compatibility of the real and large-N_c worlds in question.

2.3 The essence of the large-N_c expansion

In this section we will discuss where the observations enumerated above come from. The main reason lies in the fact that with the large number of colors large (color) combinatoric factors in Feynman diagrams appear. These arise from the difference between quarks and gluons in terms of colors which they carry: quark fields have N_c color components, but gluon fields are $N_c \times N_c$ matrices in the adjoint representation of the SU(N_c) group and thus have $N_c^2 - 1$ components. Moreover, note that in the large-N_c limit $N_c^2 - 1 \simeq N_c^2$. The following arguments are best shown pictorially. To this extent, 't Hooft introduced the double-line notation, in which each propagating gluon is represented by the double line compared to a single-line quark. The double line itself is to stand for a quark-antiquark pair. The associated arrows in the diagrams then show not only the flow of fermionic currents, but also the color charge conservation. Such a way of drawing Feynman diagrams is justified by the fact that gluons have the same SU(N_c) quantum numbers as a $q\bar{q}$ pair. For the following purpose only we will thus treat gluons as they were $q\bar{q}$ pairs.

Lets see how the combinatoric factors appear on a particular example. Imagine the gluonic one-loop contribution to the gluon propagator, which is depicted in Fig. 2.1a. In the double-line notation (see Fig. 2.1b) we can clearly see that even after we fix the color of the outer legs, there is an unconstrained color loop inside the diagram. Such a diagram then contributes with the combinatoric factor N_c.

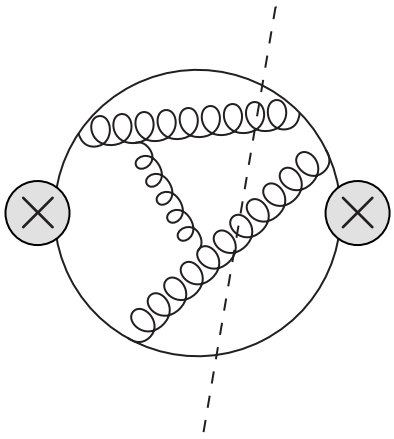

Figure 2.3: An example of a leading-order contribution to the quark bilinear.

On the other hand, if we took the quark one-loop contribution to the gluon propagator, there would be no such unconstrained color loop. Therefore, we can conclude that *internal quark legs are suppressed by the factor* $1/N_c$. The leading diagrams are hence those which contain the minumum number of quark loops.

Regarding the discussed gluon-loop contribution to the gluon propagator, we already know that it comes with the combinatoric factor N_c. We are now in the position to set the dependence of vertices (of a coupling) on N_c. We would like confinement to survive the limit $N_c \to \infty$ and thus the one-loop contribution of the discussed type should not drop as any inverse power of N_c. It is convenient to choose a behavior of vertices in the $1/N_c$ expansion in such a way that they (exactly) cancel the combinatoric factors arising from the loops: hence, we ascribe them the $1/\sqrt{N_c}$ behavior. As a consequence, the gluonic (not necessarily one-loop) contributions to the gluon propagator are of order one in the $1/N_c$ expansion; for an example see Fig. 2.2a. The previous statement is not entirely right though. Imagine the gluonic one-loop contribution (which is of order one) and draw one additional gluon line. If the planarity of the resulting diagram is preserved, such a diagram is of order one: one loop is added and the related combinatoric factor is canceled by the two new vertices. But if the resulting diagram becomes non-planar, the number of (color) loops is decreased; for an example of a non-planar diagram see Fig. 2.2b. This brings us to two substantial observations: the non-planar diagrams are suppressed at least by the factor $1/N_c^2$ and there is an infinite number of planar diagrams at the leading order. Even though we don't know how to sum these infinitely many diagrams, just from the previous observations we can conclude the above stated phenomenological implications.

2.4 Correlators of quark bilinears

In the previous section we discussed the gluon propagator — a two-point function of gluon fields. In the following, we will consider a two-point function of quark bilinears J in the large-N_c limit. Note that the operator $J(x)$ can stand e.g. for a quark scalar density $\bar{q}(x)q(x)$ or for a quark vector current $\bar{q}(x)\gamma^\mu q(x)$. From what is written above one immediately realizes that the leading-order contributions to the matrix element of quark bilinears are planar diagrams with quarks only at the edge; for an example see Fig. 2.3. This implies a very interesting statement about intermediate states. If one draws any leading-order contribution to the quark-

(a)

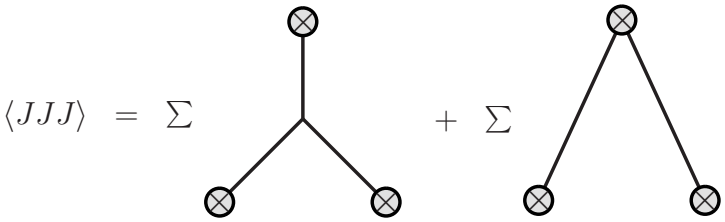

(b)

Figure 2.4: The representation of vacuum expectation values of products of operators J as sums of tree diagrams with one-meson poles. In the upper figure we see the two-point function $\langle JJ \rangle$ and in the lower figure the three-point function $\langle JJJ \rangle$ is depicted.

bilinear matrix element in the double-line notation and cuts the diagram, one can immediately see that color indices which would correspond to related gluon fields are contracted to form just one single meson — not two or for instance a meson and a glue state. In terms of a formula we can then write

$$\langle 0|J(q)J(-q)|0\rangle = \sum_n \frac{|a_n|^2}{q^2 - m_n^2}\,. \tag{2.1}$$

Here, the matrix element a_n of J then corresponds to an amplitude for the creation of the nth meson with a mass m_n from the vacuum: $a_n = \langle 0|J|n\rangle$. From this prescription, where on the right-hand side at the leading order we have written only one-meson states, one can see a few consequences. First, the sum on the right must be infinite, since the high-energy behavior of the left-hand side is known from perturbative QCD and is proportional to the logarithm of q^2: and logarithm cannot be approximated by a finite sum of rational functions. Second, the one-particle poles must be real otherwise the spectral representation of the quark-bilinear correlator would be violated. This is equivalent to claim that these mesons are stable. A diagram corresponding to a two-point function from (2.1) is depicted in Fig. 2.4a. It can be interpreted as follows: It is an infinite sum of tree diagrams in which the quark operator J creates with the amplitude a_n the nth meson from the vacuum, which then propagates with the free-field propagator and is annihilated with another operator J with the amplitude a_n^*.

Accordingly, it can be shown that similar statements hold also for a product of more than two operators. Let us now consider a three-point function $\langle 0|J(p)J(q)J(r)|0\rangle$. It will be again given as an infinite sum — taken over all possible combinations of mesons — of tree diagrams with bare propagators. The contributing diagrams are of two types, which is shown in Fig. 2.4b. In addition to propagators, the first type also contains a local meson-meson-meson vertex, where the mesons — each created by respective quark operator — combine. In the second type of diagrams, two mesons are created from the vacuum by a single operator; these mesons then propagate and subsequently they are absorbed by one quark operator each. The equivalent of equation (2.1) for the three-point

function might be schematically written as follows:

$$\begin{aligned}\langle 0|J(p)J(q)J(r)|0\rangle = &\sum_{k,l,n} \frac{A_{kln}}{(p^2-m_k^2)(q^2-m_l^2)(r^2-m_n^2)} \\ &+ \sum_{k,l} \frac{B_{kl}}{(p^2-m_k^2)(q^2-m_l^2)} + \{p,q,r\}_{\text{cycl.}}\,.\end{aligned} \tag{2.2}$$

Amplitudes A_{kln} and B_{kl} must not have any poles in p, q and r and in order to have a physically acceptable asymptotic behavior, they must be polynomials. Their contribution can be interpreted as vertices.

Imagine now a modeling of a pseudoscalar-vector-vector (PVV) three-point function (correlator), which plays an essential role in the pion rare decay. The large-N_c limit dictates (as in (2.2)) that at the leading order in the $1/N_c$ expansion, the pole structure is given by the physical mesons. After restricting ourselves (from an infinite sum) to two meson multiples per channel only and collecting all the terms into one common denominator, only the polynomial in the numerator needs to be determined: how this is done is described in Paper III together with direct phenomenological implications.

Chapter 3

QED radiative corrections and IR divergences at experiment

This chapter is dedicated to radiative corrections and a related topic of infrared (IR) divergences as they exhibit in the quantum field theory. This topic is immensely broad and in what follows we will concentrate only on some particular examples in QED. After we present some basic calculations which serve as a starting point for Paper II, we discuss an application of the therein presented results in the analysis of the NA62 experiment.

3.1 Photon vacuum polarization in QED

In this section we briefly revise the calculation of the lepton one-loop correction to the photon propagator using the framework of scalar one-loop integrals. The Feynman diagram of this contribution is depicted in Fig. 3.1. The matrix element can be written as

$$-i\Pi_{\mu\nu}(q) = -i^4 e^2 \mu^{4-n} \int \frac{\mathrm{d}^n l}{(2\pi)^n} \frac{\mathrm{Tr}[\gamma_\mu(\not{l} - \not{q} + m)\gamma_\nu(\not{l} + m)]}{[l^2 - m^2 + i\epsilon][(l-q)^2 - m^2 + i\epsilon]}\,, \tag{3.1}$$

where m stands for the lepton mass. The tensor $\Pi_{\mu\nu}$ depends only on one four-vector q^μ. That is why it needs to have the following Lorentz structure:

$$\Pi_{\mu\nu}(q) = q^2 g_{\mu\nu} A(q^2) - q_\mu q_\nu B(q^2)\,. \tag{3.2}$$

After multiplying the expression above with $q^\mu q^\nu$ we find

$$q^\mu q^\nu \Pi_{\mu\nu}(q) = q^4 [A(q^2) - B(q^2)]\,. \tag{3.3}$$

However, with a use of definition (3.1), the left-hand side of the previous equation (after some algebra and using the shift of the integration variable) equals to zero. Consequently, from (3.3) it follows $A(q^2) = B(q^2)$, which means that $\Pi_{\mu\nu}(q)$ is transversal: $q^\mu \Pi_{\mu\nu}(q) = 0$. We can thus rewrite (3.2) into

$$\Pi_{\mu\nu}(q) = (q^2 g_{\mu\nu} - q_\mu q_\nu)\Pi(q^2)\,. \tag{3.4}$$

Since $g^{\mu\nu}\Pi_{\mu\nu}(q) = (n-1)q^2\Pi(q^2)$, we can define $\Pi(q^2)$ directly as

$$\Pi(q^2) = -\frac{ie^2}{q^2}\frac{\mu^{4-n}}{(n-1)} \int \frac{\mathrm{d}^n l}{(2\pi)^n} \frac{\mathrm{Tr}\{(\not{l} - \not{q} + m)[(2-n)\not{l} + nm]\}}{[l^2 - m^2 + i\epsilon][(l-q)^2 - m^2 + i\epsilon]}\,. \tag{3.5}$$

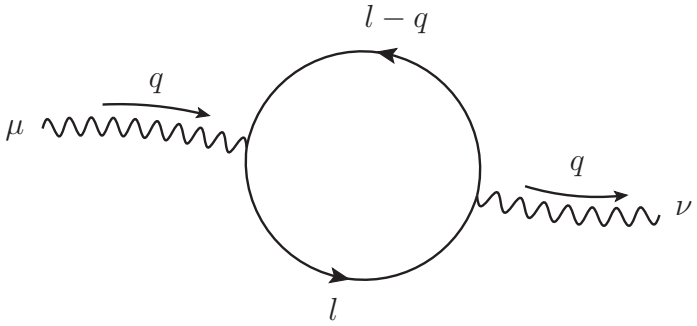

Figure 3.1: One-loop contribution to the QED vacuum polarization.

Note that we have used the n-dimensional versions of the standard contraction identities in the Minkowski space: ${g_\mu}^\mu = n$, $\gamma_\mu\gamma^\mu = n\mathbb{1}$ and $\gamma_\mu \not{a} \gamma^\mu = (2-n)\not{a}$, although on the Dirac space we still have $\mathrm{Tr}[\mathbb{1}] = 4$, i.e. $\mathrm{Tr}[\gamma_\mu\gamma^\mu] = 4n$. The trace in the numerator of the integrand in (3.5) can then be recast simply as $\mathrm{Tr}\{(\not{l} - \not{q} + m)[(2-n)\not{l} + nm]\} = 4(2-n)\, l\cdot(l-q) + 4nm^2$. The subsequent straightforward calculation, using e.g. the technique of the Passarino–Veltman reduction (see Appendix C for details) yields in terms of scalar one-loop integrals

$$\Pi(q^2) = \frac{\alpha}{3\pi}\left\{-\frac{1}{3} + B_0\Big(q^2; m^2, m^2\Big) + \frac{2m^2}{q^2}\left[B_0\Big(q^2; m^2, m^2\Big) - B_0\Big(0; m^2, m^2\Big)\right]\right\}. \tag{3.6}$$

The previous result is UV-divergent since the two-point functions B_0 themselves have this property. Indeed, within the dimensional regularization scheme, they are defined — e.g. in the case of the simplest one — as

$$i\pi^2 B_0\Big(0; m^2, m^2\Big) = (2\pi\mu)^{4-n}\int \frac{\mathrm{d}^n l}{[l^2 - m^2 + i\varepsilon]^2} \tag{3.7}$$

and thus

$$B_0\Big(0; m^2, m^2\Big) = \frac{1}{\varepsilon} - \gamma_\mathrm{E} + \log 4\pi + \log\frac{\mu^2}{m^2}\,. \tag{3.8}$$

Note that we put $\varepsilon = 2 - n/2$ where n is an analytically continued number of spacetime dimensions which serves here as a regulator and γ_E is the Euler–Mascheroni constant. The previous definition embodies a reference point for the used convention; for other definitions and details see Appendix A. The dimensionful parameter μ, which represents a mass scale in the resulting logarithms, can be set to arbitrary values according to the chosen renormalization scheme. The physical observables, however, must not depend on this parameter. Similarly, we calculate (cf. (B.25) in Appendix B)

$$B_0\Big(q^2; m^2, m^2\Big) = B_0\Big(0; m^2, m^2\Big) + 2 + \beta\log(-\gamma)\,, \tag{3.9}$$

where we have used the following useful kinematical functions:

$$\beta \equiv \beta(q^2; m^2) \equiv \sqrt{1 - \frac{4m^2}{q^2}}\,, \qquad \gamma \equiv \gamma(q^2; m^2) \equiv \frac{1-\beta(q^2;m^2)}{1+\beta(q^2;m^2)}\,. \tag{3.10}$$

After the UV divergence of $\Pi(q^2)$ is regulated, we can continue towards the renormalization procedure. In what follows, we will use the on-shell renormalization scheme. Within such a scheme, the renormalized vacuum polarization

function $\overline{\Pi}(q^2)$ is obtained by subtracting the regularized function $\Pi(q^2)$ and its on-shell value

$$\Pi(0) = \lim_{q^2\to 0} \Pi(q^2) = \frac{\alpha}{3\pi}\left\{-\frac{1}{3} + B_0\Big(0; m^2, m^2\Big) + 2m^2 B_0'\Big(0; m^2, m^2\Big)\right\}. \quad (3.11)$$

The on-shell value of the derivative of the $B_0(q^2; m^2, m^2)$ function can be calculated through its definition (3.9)

$$B_0'\Big(q^2; m^2, m^2\Big) \equiv \frac{\partial B_0(q^2; m^2, m^2)}{\partial q^2} = \frac{\partial[\beta \log(-\gamma)]}{\partial q^2} = \frac{1}{q^2}\left[\frac{1-\beta^2}{2\beta}\log(-\gamma) - 1\right] \quad (3.12)$$

via the limiting procedure

$$B_0'\Big(0; m^2, m^2\Big) = \lim_{q^2\to 0} B_0'\Big(q^2; m^2, m^2\Big) = \frac{1}{6m^2}. \quad (3.13)$$

This leads to a very simple result for the on-shell value of the vacuum polarization function:

$$\Pi(0) = \frac{\alpha}{3\pi} B_0\Big(0; m^2, m^2\Big). \quad (3.14)$$

The renormalized vacuum polarization function is then

$$\begin{aligned}\overline{\Pi}(q^2) &= \Pi(q^2) - \Pi(0) \\ &= \frac{\alpha}{3\pi}\left\{-\frac{1}{3} + \left(1 + \frac{2m^2}{q^2}\right)\left[B_0\Big(q^2; m^2, m^2\Big) - B_0\Big(0; m^2, m^2\Big)\right]\right\} \\ &= \frac{\alpha}{\pi}\left\{-\frac{1}{9} + \left(\frac{1}{2} - \frac{\beta^2}{6}\right)[2 + \beta\log(-\gamma)]\right\}.\end{aligned} \quad (3.15)$$

This is consistent with Eq. (II.18) in Paper II.

3.2 Correction to the QED vertex

The matrix element of the QED vertex with on-shell leptons, including all the higher-order corrections, can be in general written in the following form:

$$i\mathcal{M}_\mu^{\bar{\ell}\ell\gamma^*}(p, p') = -ie\bar{u}(p)\Gamma_\mu(p, p')v(p'). \quad (3.16)$$

The vertex function $\Gamma_\mu(p, p')$ can be expressed in terms of the F_1 and F_2 form factors as

$$\Gamma_\mu(p, p') = [F_1(q^2) + F_2(q^2)]\,\gamma_\mu - F_2(q^2)\,\frac{(p-p')_\mu}{2m}, \quad (3.17)$$

where $q = p + p'$. At the leading order (LO) it is simply $\Gamma_\mu^{\mathrm{LO}}(p, p') = \gamma_\mu$, which corresponds to $F_1^{\mathrm{LO}}(q^2) = 1$ and $F_2^{\mathrm{LO}}(q^2) = 0$. At the next-to-leading order (NLO), one Feynman diagram contributes — the one-loop correction to the QED vertex is depicted in Fig. 3.2. The associated matrix element can be written as

$$\Gamma_\mu^{\mathrm{NLO}}(p, p') = -i^5 e^2 \mu^{4-n} \int \frac{\mathrm{d}^n l}{(2\pi)^n} \frac{\gamma_\nu(\not{l} + \not{p} + m)\gamma_\mu(\not{l} - \not{p}' + m)\gamma^\nu}{[l^2 + i\epsilon][(l+p)^2 - m^2 + i\epsilon][(l-p')^2 - m^2 + i\epsilon]}. \quad (3.18)$$

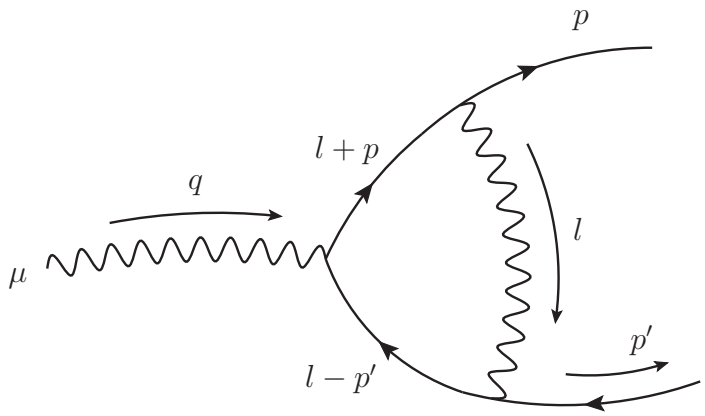

Figure 3.2: One-loop correction to the QED vertex.

The direct calculation with the use of Passarino–Veltman reduction leads to the following expressions for the form factors:

$$F_2^{\mathrm{NLO}}(q^2) = \frac{\alpha}{\pi}\frac{1-\beta^2}{4\beta^2}\left[B_0\Big(q^2;m^2,m^2\Big) - B_0\Big(0;m^2,m^2\Big) - 2\right] \tag{3.19}$$

$$\begin{aligned} F_1^{\mathrm{NLO}}(q^2) + F_2^{\mathrm{NLO}}(q^2) = \frac{\alpha}{\pi}\Bigg\{&-\frac{1}{4}\left[3B_0\Big(q^2;m^2,m^2\Big) - 4B_0\Big(0;m^2,m^2\Big) - 7\right] \\ &-m^2\frac{1+\beta^2}{1-\beta^2}C_0\Big(m^2,m^2,q^2;m^2,\lambda^2,m^2\Big)\Bigg\}. \end{aligned} \tag{3.20}$$

We see that the form factor $F_2(q^2)$ is finite and does not need to be renormalized. On the other hand, the form factor $F_1(q^2)$ contains not only a UV divergence, which needs to be renormalized, but also an IR divergence appearing in the limit when the photon mass regulator λ^2 is send to zero. For completeness, we list the form factor on-shell values:

$$F_2^{\mathrm{NLO}}(0) = \frac{\alpha}{2\pi}, \tag{3.21}$$

$$F_1^{\mathrm{NLO}}(0) = \frac{\alpha}{\pi}\left\{\frac{5}{4} + \frac{1}{4}B_0\Big(0;m^2,m^2\Big) + m^2C_0\Big(m^2,m^2,0;m^2,\lambda^2,m^2\Big)\right\}. \tag{3.22}$$

Note that (3.21) corresponds to the famous Schwinger correction to the anomalous magnetic moment of an electron [37]. To get the renormalized form factor $\overline{F_1^{\mathrm{NLO}}}(q^2) \equiv F_1^{\mathrm{NLO}}(q^2) - F_1^{\mathrm{NLO}}(0)$, we need to subtract (3.19) and (3.22) from (3.20), which yields the following expression:

$$\begin{aligned} \overline{F_1^{\mathrm{NLO}}}(q^2) = \frac{\alpha}{\pi}\Bigg\{&\frac{1}{2\beta^2} - \frac{1+2\beta^2}{4\beta^2}\left[B_0\Big(q^2;m^2,m^2\Big) - B_0\Big(0;m^2,m^2\Big)\right] \\ &-m^2\frac{1+\beta^2}{1-\beta^2}C_0\Big(m^2,m^2,q^2;m^2,\lambda^2,m^2\Big) - m^2C_0\Big(m^2,m^2,0;m^2,\lambda^2,m^2\Big)\Bigg\}. \end{aligned} \tag{3.23}$$

In order to proceed further and get the explicit expressions for the renormalized form factors in terms of elementary functions, we need to know the analytic expressions for the scalar one-loop integrals. These can be indeed calculated using standard techniques. However, the advantage of the present approach lies in the fact that the above results are expressed in terms of integrals which were already

calculated and tabulated. We can thus immediately write results not only for simple integrals like

$$C_0\Big(m^2, m^2, 0; m^2, \lambda^2, m^2\Big) = -\frac{1}{m^2}\log\frac{m}{\lambda}\,, \tag{3.24}$$

but also for the following one (cf. (B.41)):

$$\begin{aligned} &C_0\Big(q^2, m^2, m^2; m^2, m^2, \lambda^2\Big) = \frac{1}{m^2}\frac{1-\beta^2}{2\beta} \\ &\times\left[\mathrm{Li}_2(1-\gamma) - \frac{\pi^2}{4} + \frac{1}{4}\log^2(-\gamma) - i\pi\log(1-\gamma) - \log(-\gamma)\log\frac{m}{\lambda}\right]. \end{aligned} \tag{3.25}$$

In Appendix B we then offer another way how to find the previous result and how to decompose integrals with many different scales and arguments into those containing some vanishing parameters. Having at hand all the necessary analytic formulae, we can finally write the expressions for the form factors $\overline{F_1}(q^2)$ and $F_2(q^2)$ at the NLO:

$$\begin{aligned} \overline{F_1^{\mathrm{NLO}}}(q^2) = \frac{\alpha}{\pi}\Bigg\{&-1 - \frac{1+2\beta^2}{4\beta}\log(-\gamma) + \left[1 + \frac{1+\beta^2}{2\beta}\log(-\gamma)\right]\log\frac{m}{\lambda} \\ &- \frac{1+\beta^2}{2\beta}\left[\mathrm{Li}_2(1-\gamma) + \frac{1}{4}\log^2(-\gamma) - \frac{\pi^2}{4} - i\pi\log(1-\gamma)\right]\Bigg\}, \end{aligned} \tag{3.26}$$

$$F_2^{\mathrm{NLO}}(q^2) = \frac{\alpha}{\pi}\frac{1-\beta^2}{4\beta}\log(-\gamma)\,. \tag{3.27}$$

These are in agreement with expressions (II.22) and (II.23) used in Paper II; for a classical approach see e.g. [38].

3.3 Bremsstrahlung

In the previous section we have considered the one-loop correction to the QED vertex. After the calculation is performed, the matrix element exhibits IR divergence. This originates from the fact that photons are massless. At the first glance, it seems to be a serious problem since one might get rid of the divergence only by introducing a nonzero mass for the photon. However, exactly the same type of divergence is present in the so-called soft-photon bremsstrahlung (BS) contribution to a given process. The matrix element of such a contribution is represented by Feynman diagrams, which arise when — for instance as in our case — the photon line of the one-loop correction to the QED vertex is cut. The square of the sum of resulting diagrams then contains IR divergences. It is important to mention that all the possible crossed diagrams where the bremsstrahlung photon and other external photons are interchanged, need to be taken into account. Only then one can achieve a complete cancellation among the IR divergences. This is a remarkable and quite general result. One question though remains: What is the physical meaning of the bremsstrahlung diagrams and how are they related to the original process we wanted to investigate?

Suppose we are interested in a given process, e.g. the Dalitz decay of a neutral pion $\pi^0 \to e^+e^-\gamma$. At the next-to-leading order (NLO) in the QED expansion,

the one-loop correction to the only QED vertex present contains the IR divergence. We already know that to tame the divergence in question requires taking into account the soft-photon bremsstrahlung contributions. In the case of the $\pi^0 \to e^+e^-\gamma$ process, such a contribution is covered by additional four diagrams: bremsstrahlung photons emitted from electron and positron external legs as well as the crossing with the first photon. However, these diagrams represent a different process, namely $\pi^0 \to e^+e^-\gamma(\gamma)$. The parentheses are used to emphasize the fact that the additional photon is soft or, more generally, that we want to emphasize the relation to the original process $\pi^0 \to e^+e^-\gamma$. The process $\pi^0 \to e^+e^-\gamma(\gamma)$ has a different final state and thus it does not interfere, from a purely theoretical point of view, with the Dalitz decay $\pi^0 \to e^+e^-\gamma$. But for a given experiment, there is a nonzero threshold for the energy/angle of the photon, which could be detected. The tracks of the electrons and positrons might be deflected by the magnetic fields, so the collinear photons can be distinguished from the paths of the leptons. However, the photons which are too soft elude the detection. And in this way the actual finite sensitivity of the detector regulates IR divergences. Taking this fact of inclusive detection of soft photons into account together with the IR-divergent virtual correction allows us to obtain a convergent prediction for requested observables.

3.4 Radiative corrections in experiment

As we mentioned in Introduction, the calculation of radiative corrections for the Dalitz decay of a neutral pion described in Paper II was initiated by needs of the NA48/NA62 experiment at CERN. This experiment serves as a high-intensity kaon beam facility, which can be also viewed as a π^0 factory. The cleanest channel to produce neutral pions is the $K_{2\pi}$ decay $K^\pm \to \pi^\pm\pi^0$. Neutral pions then decay practically instantly (on spot), since their mean free path in the NA62 experiment is a few μm.

After the calculation of the radiative corrections had been finished, a further closer collaboration with the experiment was crucial. In what follows we describe what is needed to be taken into account not only to measure the process $\pi^0 \to e^+e^-\gamma$, but also for the pion rare decay $\pi^0 \to e^+e^-$. Indeed, in the NA62 experiment it is feasible to acquire a statistically significant sample of rare decay events. Such a measurement would definitely contribute to the discrepancy problem triggered by the KTeV measurement.

3.4.1 Event generators for the pion Dalitz decay

The NA62 experiment at CERN and its predecessor, the experiment NA48, collected over years a huge amount of data which could be used to extract the slope parameter a_π of the singly off-shell pion transition form factor

$$\mathcal{F}(q^2) \simeq \mathcal{F}(0)\left(1 + a_\pi \frac{q^2}{M_\pi^2}\right). \tag{3.28}$$

A data sample of $\simeq 10^6$ Dalitz decays acquired during the run in 2007 led to the so far most precise experimental value $a = 0.0368(57)$ [6]. This result already

includes the radiative corrections described in Paper II and a treatment described in the following. Let us mention that the vector-meson dominance (VMD) model predicts $a_\pi^{\mathrm{VMD}} = M_\pi^2/M_\omega^2 \simeq 0.03$.

The effect of the form factor slope on the electron-positron pair invariant mass spectrum is of the same order (and even smaller) that the effect of higher-order corrections: for a successful extraction of the slope from the data it was therefore essential to properly include the NLO corrections to the event simulation software. From historical reasons there were two possible ways how to include the radiative corrections in the NA48/NA62 event simulation. One of them was a universal Monte Carlo generator of QED corrections called PHOTOS which includes the soft-photon bremsstrahlung [39]. The second possibility was represented by the interpolation of tabulated values from the classical work [7], where the bremsstrahlung beyond the soft-photon limit was incorporated. By a direct comparison of the effects of the previous methods on the lepton pair invariant mass spectrum, an inconsistency has been found, the size of which was of the same order as a_π. This was in favor of the second approach: in this approach, an exact bremsstrahlung contribution is calculated.

The Dalitz decay $\pi^0 \to e^+e^-\gamma$, being a three body decay, is described by two independent kinematical variables traditionally named as x and y: x corresponds to the invariant mass of the electron-positron pair and y is related to the angle between one of the leptons and the photon. The bremsstrahlung process $\pi^0 \to e^+e^-\gamma(\gamma)$ associated with the Dalitz decay is described by five independent kinematical variables. Note that in general for $N > 2$, an N-body decay (a process $1 \to N$) of scalar particles in the four-dimensional spacetime is described by $(N+1)(4-1)-10$ independent variables: '+1' stands for the decaying particle, '−1' for the on-shell conditions and '10' for the number of generators of the Poincaré group. As the energy of the bremsstrahlung photon approaches zero, an IR divergence appears which needs to be canceled out with the IR divergence stemming from the virtual corrections. To this extent one needs to integrate the bremsstrahlung contribution over the three kinematical variables associated with the additional photon. Even though only the soft-photon domain is necessary for the IR divergence cancellation, the correction includes the whole kinematically allowed region. This corresponds to the correction to the measured decay width in the case in which one of the photons is systematically ignored. Such a situation is also referred to as a measurement of an inclusive process.

When the extra bremsstrahlung photon is not explicitly simulated and it is only included implicitly through the radiative corrections, this results in a large instability of the slope extraction with respect to the photon candidate selection criteria. The solution laid in the development of two Monte Carlo generators, one of which would generate three- and the second one four-body decays; the latter then includes explicitly an additional bremsstrahlung photon. In order to distinguish the two kinematical situations in which one or another generators apply, an extra cut needs to be introduced. For such a cut it is convenient to be defined in a Lorentz invariant way. A natural way is to use one of the kinematical variables used for the four-body decay description associated with the IR regularization — the normalized invariant mass of the photon pair x_γ for which $\lambda^2 \leq M_\pi^2 x_\gamma$ with λ being the photon-mass regulator. The invariant mass of the diphoton can be expressed in a particular reference system as $M^2 x_\gamma = (k+l)^2 = 2E_k E_l(1-\cos\theta)$,

where k and l are the photon four-momenta. This term can be made small either if the photon energies are small or in case they are emitted in a same direction ($\theta \simeq 0$). Up to some singular situations, after a boost to the lab frame (initial kaons decay in flight) the smallness of x_γ is translated to an ability to distinguish a detection of a single photon from a photon pair in the detector. In this sense it is therefore very natural to introduce a cut on the x_γ variable. Not only we separate cases which contain low-energy photons and are therefore essential for treatment of IR divergences, but also the space separation in the detector is considered.

The event generator algorithm then needs to decide how many three-body and four-body events are simulated. The probability of this distribution is based on the ratio, which needs to be theoretically established and is given by the formula

$$R(x_\gamma^{\mathrm{cut}}) = \frac{\int\limits_{\nu^2}^{1} \mathrm{d}x \int\limits_{0}^{\beta} \mathrm{d}y \, \frac{\mathrm{d}\Gamma^{\mathrm{LO}}(x,y)}{\mathrm{d}x\,\mathrm{d}y} \left[1 + \delta^{\mathrm{virt.}+1\gamma\mathrm{IR}}(x,y) + \int\limits_{0}^{\min(x_\gamma^{\mathrm{cut}}, x_\gamma^{\mathrm{max}})} \mathrm{d}x_\gamma \, \delta^{\mathrm{BS}}(x,y,x_\gamma) \right]}{\int\limits_{\nu^2}^{1} \mathrm{d}x \int\limits_{0}^{\beta} \mathrm{d}y \, \frac{\mathrm{d}\Gamma^{\mathrm{LO}}(x,y)}{\mathrm{d}x\,\mathrm{d}y} \int\limits_{\min(x_\gamma^{\mathrm{cut}}, x_\gamma^{\mathrm{max}})}^{x_\gamma^{\mathrm{max}}} \mathrm{d}x_\gamma \, \delta^{\mathrm{BS}}(x,y,x_\gamma)}, \tag{3.29}$$

where $x_\gamma^{\mathrm{max}} \equiv x_\gamma^{\mathrm{max}}(x,y)$ depends on x and y. In the numerator there stands the integral decay width for the Dalitz decay, where the NLO virtual radiative corrections (see Figs. 4.1a and 4.1b) including the 1γIR contribution (see Figs. 4.1c and 4.1d) were taken into account and where the bremsstrahlung contribution (see Fig. 4.1e) is integrated over the invariant mass of the diphoton up to a cut given by x_γ^{cut}; this part thus corresponds to the three-body decay generator. The associated term connected to the four-body generator stands in the denominator and is given solely by the bremsstrahlung contribution with the diphoton invariant mass above the cut x_γ^{cut}. In this context, the bremsstrahlung contribution also corresponds to the LO decay width for the process $\pi^0 \to e^+e^-\gamma\gamma$. Note that by construction, the numerator as well as the denominator are IR-safe. For the cut $x_\gamma^{\mathrm{cut}} = 0.01$ which was used during the real data analysis one gets $R(0.01) \simeq 17.4$.

A particular value of the parameter x_γ^{cut} does not, of course, affect the dilepton invariant mass distribution. In practice, the choice of its value is a compromise between two factors. From below it is bounded by the fact that the sampling of events according to the distribution based on the BS matrix element squared which diverges for $x_\gamma \to 0$ is getting significantly computer-time-demanding (see below). From above it is the quality of the photon energy reconstruction.

Let us briefly describe how does e.g. the four-body event generator work. First, using a Monte Carlo generator the four-momenta of all the final-state particles (electron, positron and two photons) are generated according to the constant matrix element. From these four-momenta, the invariant kinematical variables are computed. The decays with $x_\gamma < x_\gamma^{\mathrm{cut}}$ are ignored. To sample events which are distributed according to the bremsstrahlung matrix element squared, a technique called rejection sampling is used; the acceptance-rejection method is a type of Monte Carlo method. For a proper normalization, the maximum N of the target distribution needs to be known. The algorithm is then simple: for every event with a particular combination of kinematical variables $\vec{x}$ and a random uniformly distributed number $n \in (0, N)$, only the events with $\overline{|\mathcal{M}_{\mathrm{BS}}(\vec{x})|^2} < n$ are accepted and the rest is rejected.

3.4.2 Event generators for the pion rare decay

In the case of the Dalitz decay, the three- as well as four-body decay event generators were taken into account. For the pion rare decay, there is one particle less in the final state, therefore we shall discuss the two- and three-body generators.

In general, concerning the two-body event generator we actually should not talk about a generator at all since the kinematics of a two-body decay is set by the masses of the involved particles: it is therefore rather a constant. This constant — which depends on a choice of a parameter x_{cut} (described later) — has contributions from all the processes, which have the same initial and final asymptotic states as the decay $\pi^0 \to e^+e^-$ while the soft photons in the final state are allowed; note that for $x \in (x_{\text{cut}}, 1)$ and $x_{\text{cut}} \simeq 1$ the soft photon can be integrated out and what remains is the inclusive two-body decay with radiative corrections included and IR divergences subtracted. For $x \simeq 1$ — since the decay width of the Dalitz decay vanishes as $x \to 1$ — the dominant contribution comes from the $\pi^0 \to e^+e^-$ itself together with the NLO radiative corrections:

$$\Gamma_{\pi^0\to e^+e^-}(x_{\text{cut}}) = \Gamma^{\text{LO}}_{\pi^0\to e^+e^-}\Big[1 + \delta^{\text{virt.}+\text{BS}_{\text{soft}}}(x_{\text{cut}}) + \delta^{\text{BS}_{\text{full}}-\text{BS}_{\text{soft}}}(x_{\text{cut}})\Big] + \mathcal{O}(\alpha^6)\,. \tag{3.30}$$

Above, $\delta^{\text{virt.}+\text{BS}_{\text{soft}}}(x_{\text{cut}})$ contains virtual corrections together with the soft-photon bremsstrahlung to subtract IR divergences and is calculated in [3]. On the other hand, $\delta^{\text{BS}_{\text{full}}-\text{BS}_{\text{soft}}}(x_{\text{cut}})$ contains the correction to the soft-photon approximation used in [3] and is described in Paper I.

Next important process which might contribute to the 2-body 'generator' is the Dalitz decay in the soft-photon regime. This process is suppressed for $x \simeq 1$, but starts to be important very fast when this condition is not satisfied and at some point even the higher-order corrections to this process might exceed the effects of the $\pi^0 \to e^+e^-$ decay. The contribution under discussion can be expressed as

$$\begin{aligned}&\Gamma^{\text{2-body}}_{\pi^0\to e^+e^-\gamma}(x_{\text{cut}})\\ &= \int_{x_{\text{cut}}}^{1}\mathrm{d}x\int_{-\beta}^{\beta}\mathrm{d}y\,\frac{\mathrm{d}\Gamma^{\text{LO}}_{\pi^0\to e^+e^-\gamma}(x,y)}{\mathrm{d}x\,\mathrm{d}y}\Big[1 + \delta^{\text{virt.}+1\gamma\text{IR}}(x,y) + \delta^{\text{BS}}(x,y)\Big] + \mathcal{O}(\alpha^5)\,.\end{aligned} \tag{3.31}$$

If we define the LO decay width of the pion two-photon decay

$$\Gamma^{\text{LO}}_{\pi^0\to\gamma\gamma} = \frac{\alpha^2 M^3}{64\pi^3 F^2} \tag{3.32}$$

and subsequently a common overall factor

$$\rho = \left(\frac{\alpha}{\pi}\right)\Gamma^{\text{LO}}_{\pi^0\to\gamma\gamma} \simeq 1.803\times10^{-8}\,\text{MeV}\,, \tag{3.33}$$

we find numerically (for some chosen cuts) values shown in Tab. 3.1. We see that in agreement with what was written above, for significantly high cut x_{cut} the contribution of the Dalitz decay is negligible. On the other hand, extrapolating to even lower x_{cut} the $\pi^0 \to e^+e^-$ decay would disappear among the higher-order corrections to the Dalitz decay. These are not under control and hence the proper subtraction is not possible; note that $\Gamma^{\text{LO}}_{\pi^0\to e^+e^-\gamma}(x,y) \sim \mathcal{O}(\alpha^3)$ and

$x_{\rm cut}$	0.9	0.95	0.98	0.99	0.995
$\Gamma_{\pi^0\to e^+e^-}(x_{\rm cut})\,[10^{-5}\rho]$	2.62	2.52	2.40	2.31	2.22
$\Gamma^{\text{2-body}}_{\pi^0\to e^+e^-\gamma}(x_{\rm cut})\,[10^{-5}\rho]$	1.53	0.0835	0.00169	7.39×10^{-5}	1.34×10^{-6}

Table 3.1: Contributions to the two-body integral decay width and their dependence on $x_{\rm cut}$. We see that for large x the Dalitz decay is indeed significantly suppressed with respect to the rare decay.

$x_{\rm cut}$	0.95	0.98	0.99	0.995
$\Gamma^{\rm BS}_{\pi^0\to e^+e^-}(0.8, x_{\rm cut})\,[10^{-5}\rho]$	0.168	0.281	0.367	0.454

Table 3.2: The pion rare decay bremsstrahlung contribution to the three-body integral decay width and its dependence on $x_{\rm cut}$.

$\Gamma^{\rm LO}_{\pi^0\to e^+e^-}\sim\mathcal{O}(\alpha^4)$. This is actually the reason why it is so important to consider a cut like $x_{\rm cut}$. It is also clear why the use of $x_{\rm cut}=0.95$ in the KTeV experiment was a reasonable choice. Together with the previous we see that also a contribution from any other relevant process is negligible when $x_{\rm cut}$ is chosen to be high enough. We can conclude that the whole 'generator' will work the best for any reasonably high $x_{\rm cut}$.

For the three-body generator one should use the same generator as for the Dalitz decay together with all the available NLO radiative corrections (including the 1γIR contribution) — the bremsstrahlung should be taken with the cut $x_\gamma^{\rm cut}=1$ — together with the generator for the $\pi^0\to e^+e^-$ bremsstrahlung. The latter is then based on the matrix element squared given by (I.23) in Paper I. This is finite below any $x_{\rm cut}<1$.

As it was in the case of the Dalitz decay, the ratio of the two- and three-body integral decay widths should be provided. The necessary two-body-decay inputs for such a ratio are by definition already prepared as is shown in Tab. 3.1. Concerning the three-body decay generator, we define for the bremsstrahlung contribution to the rare decay integral width (see Figs. 4.1c and 4.1d for associated diagrams)

$$\Gamma^{\rm BS}_{\pi^0\to e^+e^-}(x_{\rm div},x_{\rm cut})=\int_{x_{\rm div}}^{x_{\rm cut}}{\rm d}x\int_{-\beta}^{\beta}{\rm d}y\,\frac{{\rm d}\Gamma^{\rm BS}_{\pi^0\to e^+e^-}(x,y)}{{\rm d}x\,{\rm d}y}\,, \tag{3.34}$$

where $x_{\rm div}$ refers to an additional cut which defines the region interesting for the rare decay measurement. It is chosen in such a way that for $x<x_{\rm div}$ the Dalitz decay becomes overwhelming compared to the rare decay. The numerical values (for $x_{\rm div}=0.8$) are listed in Tab. 3.2. The contribution of the Dalitz decay to the same quantity is

$$\begin{aligned}&\Gamma^{\text{3-body}}_{\pi^0\to e^+e^-\gamma}(x_{\rm div},x_{\rm cut})\\&=\int_{x_{\rm div}}^{x_{\rm cut}}{\rm d}x\int_{-\beta}^{\beta}{\rm d}y\,\frac{{\rm d}\Gamma^{\rm LO}_{\pi^0\to e^+e^-\gamma}(x,y)}{{\rm d}x\,{\rm d}y}\left[1+\delta^{\text{virt.}+1\gamma\rm IR}(x,y)+\delta^{\rm BS}(x,y)\right].\end{aligned} \tag{3.35}$$

Dependance of the numerical values for $\Gamma^{\text{3-body}}_{\pi^0\to e^+e^-\gamma}(x_{\rm div},x_{\rm cut})$ on reasonably high $x_{\rm cut}$ is negligible: $\Gamma^{\text{3-body}}_{\pi^0\to e^+e^-\gamma}(0.8,x_{\rm cut}>0.95)\simeq 28.7\times10^{-5}\,\rho$. The desired two- to

three-body decay ratio $R_{2/3}$ is then defined as

$$R_{2/3}(x_{\rm div}, x_{\rm cut}) = \frac{\Gamma_{\pi^0\to e^+e^-}(x_{\rm cut}) + \Gamma^{\text{2-body}}_{\pi^0\to e^+e^-\gamma}(x_{\rm cut})}{\Gamma^{\rm BS}_{\pi^0\to e^+e^-}(x_{\rm div}, x_{\rm cut}) + \Gamma^{\text{3-body}}_{\pi^0\to e^+e^-\gamma}(x_{\rm div}, x_{\rm cut})}\,. \tag{3.36}$$

For reasonably high $x_{\rm cut}$ the numerator can be approximated by the rare decay contribution $\Gamma_{\pi^0\to e^+e^-}(x_{\rm cut})$; see Tab. 3.1. As an example we provide a numerical value of $R_{2/3}(0.8, 0.95) \simeq 0.091$. Considering these cuts, the denominator of (3.36) is basically given by $\Gamma^{\text{3-body}}_{\pi^0\to e^+e^-\gamma}(0.8, 0.95)$; see Tab. 3.2.

As we have already stated above, the region below the value $x_{\rm div}$ is not interesting for the $\pi \to e^+e^-$ decay measurement. For completeness let us recall that in this region the event generator should be solely given by the Dalitz process with all the available NLO radiative correction and should come together with the four-body generator. This case was described in the previous section. Let us mention that for $x_\gamma^{\rm cut} = 1$ we get a result which is basically independent on $x_{\rm div}$ within the considered region: $\Gamma^{\text{3-body}}_{\pi^0\to e^+e^-\gamma}(\nu^2, x_{\rm div} > 0.8) = 5.154\,\rho$.

Finally, note that all the results were calculated within the THS model for the pion transition form factor; for details see Paper III. The numerical results are therefore slightly model dependent: on a particular choice of the model, $\Gamma^{\rm LO}_{\pi^0\to e^+e^-}$ then depends the most.

Chapter 4

Radiative corrections to the $\eta^{(\prime)} \to \ell^+\ell^-\gamma$ decays

In Paper II, there one can find a detailed description of the calculation of radiative corrections to the Dalitz decay of a neutral pion, i.e. to the process $\pi^0 \to e^+e^-\gamma$. In this chapter we would like to discuss subtleties, snags and difficulties which one encounters and needs to deal with when facing the Dalitz decays of $\eta^{(\prime)}$ mesons and associated NLO radiative corrections. The main differences compared to the pion case stem from the following facts. First, it is the higher rest mass, which in the case of η is above the production of a muon pair and in the case of η' even above the lowest lying resonances ρ and ω, the former of which is a broad $\pi\pi$ resonance. This is connected to the fact that the form factor slope parameter is not negligible as it was in the pion case and a particular model of the form factor is needed to be taken into account. To model such a form factor one needs to incorporate the strange-flavor content of $\eta^{(\prime)}$ mesons and the η-η' mixing. In the following we will comment on the mentioned facts in a more detailed way.

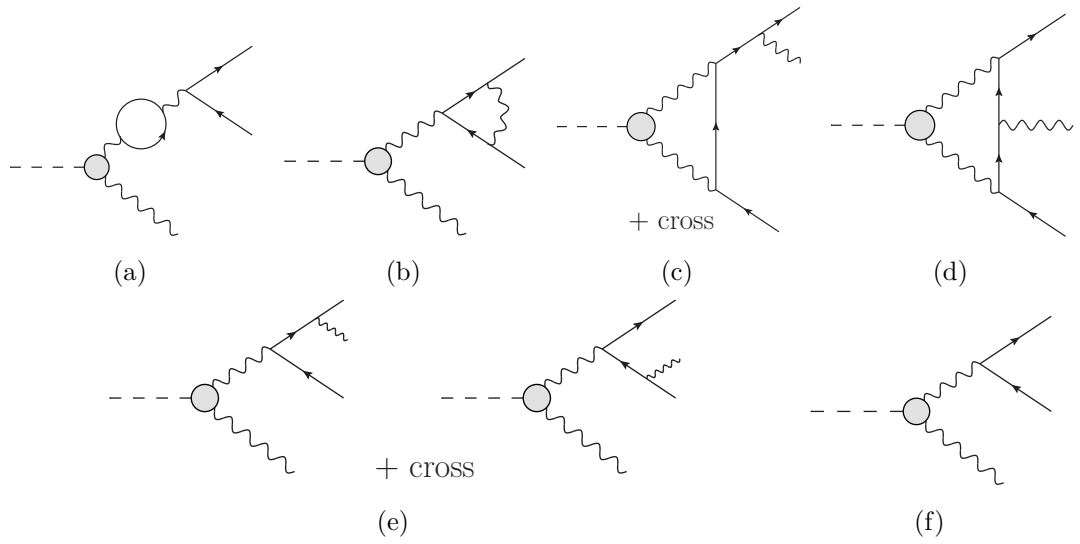

Figure 4.1: NLO QED radiative corrections to the Dalitz decay $P \to \ell^+\ell^-\gamma$: a) vacuum polarization insertion, b) correction to the QED vertex, c) & d) one-loop one-photon-irreducible contributions, e) bremsstrahlung. For completeness, the LO diagram is depicted in figure f). Note that 'cross' in figure (c) corresponds to such a diagram where the photon is emitted from the outgoing positron line. Needless to say, 'cross' in figure (e) stands for the diagrams with outgoing photons interchanged.

Note that naïve radiative corrections for the $\eta \to e^+e^-\gamma$ process were already published [40] soon after the work [7]: compared to [7], the numerical results presented in [40] correspond to the case in which only the numerical value of the physical mass of the decaying pseudoscalar was changed.

4.1 Virtual radiative corrections

What we call the virtual corrections is a contribution to the radiative corrections which is obtained from the interference terms of the LO diagram shown in Fig. 4.1f and diagrams in Figs. 4.1a and 4.1b. It is already discussed in Paper II that in the case of $\eta^{(\prime)}$ meson decays not only the electron loop but also the muon loop should be taken into account. All the necessary formulae connected with these contributions are stated in Section II.3 of Paper II and hold also in the current cases. However, we shall point out some interesting details.

The contribution of the vacuum polarization insertion (VPI) — i.e. the contribution of the lepton loops to the photon propagator — to the correction $\delta^{\mathrm{virt}}(x)$ can be expressed as

$$\delta^{\mathrm{virt}}_{\mathrm{VPI}}(x) \equiv 2\,\mathrm{Re}\left\{-\Pi(M_P^2 x)\right\} = -2\sum_{\ell'=e,\mu}\frac{\alpha}{\pi}\left\{\frac{5}{9}+\frac{\nu_{\ell'}^2}{3x}-\frac{2}{3}\left(1+\frac{\nu_{\ell'}^2}{2x}\right)\right\} \times |\beta_{\ell'}|\left[\theta(\beta_{\ell'}^2)\,\mathrm{arctanh}\,\beta_{\ell'}+\theta(-\beta_{\ell'}^2)\arctan\frac{1}{|\beta_{\ell'}|}\right]\right\}. \tag{4.1}$$

Here, $M_P^2 x$ is the invariant mass of the final-state lepton pair and ℓ' stands for the leptons circulating in the loop and consistently with definition (3.10) we have $\beta_\ell \equiv \beta(M_P^2 x; m_\ell^2)$ and $|\beta_{\ell'}| = \sqrt{|\beta_{\ell'}^2|}$. We also define $\nu_\ell = 2m_\ell/M_P$. Let us note that $\beta_{\ell'}$ has nothing to do with the center-of-mass-system (CMS) speed of the final-state leptons as was the case for β. Since β depends on x, which for the given process of a decay to a lepton pair of flavor ℓ satisfies the limit $x \in [\nu_\ell^2, 1]$, we can run into different kinematic regimes, which are nevertheless explicitly covered by formula (4.1); for this purpose the Heaviside step function θ was used. Whenever $\beta_{\ell'}^2 < 0$, i.e. $\beta_{\ell'}$ itself becomes imaginary, no on-shell lepton-antilepton pair can be created in the loop and the diagram in Fig. 4.1a lacks the imaginary part. This happens if the invariant mass of the final-state lepton pair is under the production threshold of the two loop leptons of flavor ℓ': $\nu_\ell^2 \leq x < \nu_{\ell'}^2$. In turn, this condition can be, of course, only realized in the case of the muon loop contribution to the NLO decay widths of the $\pi^0 \to e^+e^-\gamma$ decay and in the process $\eta^{(\prime)} \to e^+e^-\gamma$, where the kinematical condition $\nu_e^2 \leq x < \nu_\mu^2$ is met within a part of the kinematically allowed region.

4.2 One-photon-irreducible virtual radiative correction

Considering the QED and χPT expansion, the LO diagrams contributing to the one-loop one-photon-irreducible (1γIR) correction to the $P \to \ell^+\ell^-\gamma$ process are

shown in Figs. 4.1c and 4.1d. We treat this contribution separately from the virtual correction to emphasize the fact that it was not included in the original approach [7]. Therein, it was considered to be negligible already for the pion case. This statement had been corrected in Ref. [41] many years before the debate about this issue was finally closed.

In this contribution one cannot factorize out the electromagnetic transition form factor. This correction becomes therefore unavoidably model-dependent already at the two-fold differential level and it is necessary to choose a particular model to evaluate the correction numerically. Compared to the previous calculations of the LO diagram and NLO virtual radiative corrections, a doubly off-shell transition form factor $\mathcal{F}_{P\gamma^*\gamma^*}(l^2,(P-l)^2)$ is needed to be used. This form factor enters the loop and the integration over the unconstrained momentum l is then performed. Note that P stands for both the decaying pseudoscalar as well as for its four-momentum.

Let us now proceed further and consider that during the calculation of the 1γIR loop diagrams the following structure inevitably appears:

$$\frac{\mathcal{F}_{P\gamma^*\gamma^*}(l^2,(P-l)^2)}{[l^2+i\epsilon][(P-l)^2+i\epsilon]}\,. \tag{4.2}$$

By construction, the arguments of the form factor coincide with the photon propagators in the loop; l denotes the loop momentum as is usual. In what follows we consider a family of large-N_c motivated rational resonance-saturation models, which are in detail discussed in Paper III. We then realize that due to a use of the partial fraction decomposition one can perform — within the loop integrals appearing during the evaluation of the diagrams — the following substitution:

$$\frac{\mathcal{F}_{P\gamma^*\gamma^*}(p^2,q^2)}{p^2q^2} = -\frac{N_\mathrm{c}}{12\pi^2F_\pi}\sum_i \alpha_i\, h(c_{1,i},c_{2,i},M_{1,i}^2,M_{2,i}^2)\,. \tag{4.3}$$

Note that from now on we will suppress the explicit writing of the "$+i\epsilon$" part. Above,

$$\begin{aligned} &h(c_1,c_2,M_1^2,M_2^2)\\ &\equiv \frac{1}{p^2q^2}+\frac{c_2}{(p^2-M_1^2)(q^2-M_2^2)}-c_1\left[\frac{1}{p^2(q^2-M_1^2)}+\frac{1}{q^2(p^2-M_1^2)}\right]. \end{aligned} \tag{4.4}$$

In this way we come from the matrix element $\mathcal{M}_{1\gamma\mathrm{IR}}$ to $\sum\alpha_i\mathcal{M}^h_{1\gamma\mathrm{IR}}[h_i]$; note that the normalization constant $\mathcal{F}_{\pi^0\gamma^*\gamma^*}(0,0) = -N_\mathrm{c}/(12\pi^2F_\pi)$ from decomposition (4.3) is already included in $\mathcal{M}^h_{1\gamma\mathrm{IR}}[h_i]$ and that we have used a shorthand notation $h_i \equiv h(c_{1,i},c_{2,i},M_{1,i}^2,M_{2,i}^2)$. In order to get results for the whole family of models it is necessary to analytically integrate over the loop momentum just once; this is the main advantage of this approach. At the end one can choose the particular model of the form factor by setting the parameters in the final matrix element appropriately. We can find the above used constants c_1 and c_2 from projecting on the product of the normalized form factor and the photon propagators: for instance in the case $M_{V_1} = M_{V_2}$ we have

$$c_2 = \frac{1}{\mathcal{F}_{\pi^0\gamma^*\gamma^*}(0,0)}\lim_{p^2,q^2\to M_{V_1}^2}\frac{\mathcal{F}_{P\gamma^*\gamma^*}(p^2,q^2)}{p^2q^2}\,(p^2-M_{V_1}^2)(q^2-M_{V_1}^2)\,. \tag{4.5}$$

This little trick is highly convenient when it is necessary to create a universal code for calculating radiative corrections within different models. Let us also note that substitution (4.4) does obviously not conserve the desired property of the doubly off-shell form factors — the symmetry in their arguments. This ansatz though works generally for the rational models mentioned above, which might have a rather complicated structure. The symmetry in question is then always restored in the final result after including all the pieces $\mathcal{M}^h_{1\gamma\mathrm{IR}}[h_i]$. Moreover, we realize that if we define

$$g(M_1^2, M_2^2) \equiv \frac{1}{(p^2 - M_1^2)(q^2 - M_2^2)}\,, \tag{4.6}$$

we can immediately write

$$h(c_1, c_2, M_1^2, M_2^2) = g(0,0) + c_2\, g(M_1^2, M_2^2) - c_1\Big[g(0, M_1^2) + g(M_1^2, 0)\Big]\,. \tag{4.7}$$

This trivial observation simplifies the loop integration even further. Instead of (4.3), we can then write

$$\frac{\mathcal{F}_{P\gamma^*\gamma^*}(p^2, q^2)}{p^2 q^2} = -\frac{N_\mathrm{c}}{12\pi^2 F_\pi} \sum_i \beta_i\, g(M_{1,i}^2, M_{2,i}^2)\,. \tag{4.8}$$

During the calculation of the amplitude it is only necessary to perform the following substitution:

$$\frac{\mathcal{F}_{P\gamma^*\gamma^*}(p^2, q^2)}{p^2 q^2} \to -\frac{N_\mathrm{c}}{12\pi^2 F_\pi}\, g(M_1^2, M_2^2)\,. \tag{4.9}$$

The desired final amplitude for the particular model is then obtained by writing a suitable combination (in spirit of (4.8)) of such amplitudes which are calculated using substitution (4.9). One only needs to insert the correct masses and coefficients into this combination, which goes along the lines of (4.7), (4.5) and (4.4).

Lets discuss the previous procedure on a particular case and consider for a while the eta-meson decays: $P = \eta$. The simplest physically relevant model we can imagine is based on the vector-meson dominance (VMD) scenario, i.e. by an dipole ansatz which assumes that the form factor is saturated by the lowest-lying multiplet of vector mesons. It has the following form:

$$\begin{aligned} e^2 \mathcal{F}^{\mathrm{VMD}}_{\eta\gamma^*\gamma^*}(p^2, q^2) &= -\frac{N_\mathrm{c}}{8\pi^2 F_\pi}\frac{2e^2}{3} \\ &\times \left[\frac{5}{3}\frac{\cos\phi}{f_\ell}\,\frac{M^4_{\omega/\rho}}{(p^2 - M^2_{\omega/\rho})(q^2 - M^2_{\omega/\rho})} - \frac{\sqrt{2}}{3}\frac{\sin\phi}{f_\mathrm{s}}\,\frac{M^4_\phi}{(p^2 - M^2_\phi)(q^2 - M^2_\phi)}\right]. \end{aligned} \tag{4.10}$$

Above, ϕ is the η-η' mixing angle and f_ℓ together with f_s are the associated decay constants in the quark-flavor basis of the quark currents [42, 43]; for further details concerning derivation of this model see Appendix D. It is then clear after counting of the loop momenta powers that such a form factor guarantees a UV convergence of the loop integrals. The matrix element for such a form factor can be schematically written as

$$\mathcal{M}^{\mathrm{VMD}}_{1\gamma\mathrm{IR}} = \frac{5}{3}\frac{\cos\phi}{f_\ell}\mathcal{M}^h_{1\gamma\mathrm{IR}}\Big[h(1,1,M^2_{\omega/\rho}, M^2_{\omega/\rho})\Big] - \frac{\sqrt{2}}{3}\frac{\sin\phi}{f_\mathrm{s}}\mathcal{M}^h_{1\gamma\mathrm{IR}}\Big[h(1,1,M^2_\phi, M^2_\phi)\Big]\,. \tag{4.11}$$

Following the subsequent decomposition (4.7) and using linearity, one then finds

$$\begin{aligned}&\mathcal{M}^h_{1\gamma\mathrm{IR}}\Big[h(1,1,M_\mathcal{V}^2,M_\mathcal{V}^2)\Big]\\&=\mathcal{M}^h_{1\gamma\mathrm{IR}}\Big[g(0,0)\Big]+\mathcal{M}^h_{1\gamma\mathrm{IR}}\Big[g(M_\mathcal{V}^2,M_\mathcal{V}^2)\Big]-\mathcal{M}^h_{1\gamma\mathrm{IR}}\Big[g(0,M_\mathcal{V}^2)\Big]-\mathcal{M}^h_{1\gamma\mathrm{IR}}\Big[g(M_\mathcal{V}^2,0)\Big]\,.\end{aligned}\tag{4.12}$$

As the only building block, one needs to calculate $\mathcal{M}^h_{1\gamma\mathrm{IR}}\Big[g(M_1^2,M_2^2)\Big]$ obtained in terms of substitution (4.9) in the original matrix element. A simple example of the presented approach applied on the $P\to\ell^+\ell^-$ decays is included as Appendix E.

There is also a complementary technique how to cover a whole set of form factors under consideration. Instead of putting the particular form factor into our diagrams, we can use the local Wess–Zumino–Witten (WZW) term. In other words we trade the form factor for the constant given by the chiral anomaly. It is then clear from simple considerations, that the contributions from Fig. 4.1c need a counter terms to compensate UV divergences. The convergent part of such a counter term carries undetermined constant $\chi^{(\mathrm{r})}(\mu)$ renormalized at scale μ, which can effectively mimic the high-energy behavior of the would-be complete form factor. Using a proper matching procedure, it is possible to acquire a numerical value of this constant $\chi^{(\mathrm{r})}(\mu)$ for a given form-factor model. Up to mass corrections we can use an approximate formula to estimate this effective parameter (see Eq. (III.46) in Paper III). The question is, if this procedure can be used also for a box diagram in Fig. 4.1d which is already convergent for the local WZW form factor. It turns out that the corrections are of order m_ℓ^2/M_V^2 and M_P^2/M_V^2. Hence, for the pion case this assumption works well. On the other hand, for $\eta^{(\prime)}$ it does not and one would need to introduce additional effective parameters in a consistent way. This is though not a trivial task and is beyond the scope of this work. Let us also mention that $\chi^{(\mathrm{r})}(\mu)$ enters the corrections being multiplied by ν^2 and its effect is thus negligible for the decays with electrons in the final state.

4.3 Bremsstrahlung

In this section we briefly build on Paper II — which among others refers about the bremsstrahlung correction calculation for the pion case — and show the differences which come into play due to the fact that we are now interested in $\eta^{(\prime)}$ mesons. We also show some techniques how to deal with the obstacles which arise. Concerning the notation, we will restrict ourselves to the one used in previous works.

The diagrams which contribute to the Dalitz decay bremsstrahlung are shown in Fig. 4.1e. Their contribution is (among others) important to cancel IR divergences stemming from the virtual corrections depicted in Fig. 4.1b, which are of the same type as it was discussed in Sec. 3.2. The corresponding invariant matrix element (including cross terms) can be written in the form

$$i\mathcal{M}_{\mathrm{BS}}=\frac{\mathcal{F}\Big((l+p+q)^2\Big)}{(l+p+q)^2+i\epsilon}\,I(k,l)+(k\leftrightarrow l)\,,\tag{4.13}$$

where

$$I(k,l)=\bar{u}(p)I^{\rho\sigma}(k,l)v(q)\epsilon^*_\rho(k)\epsilon^*_\sigma(l)\tag{4.14}$$

with

$$I^{\alpha\beta}(k,l) = -i^5 e^4 \varepsilon^{(l+p+q)(k)\mu\alpha}\left[\gamma^\beta \frac{(\not{l}+\not{p}+m)}{2l\cdot p + i\epsilon}\gamma^\mu - \gamma^\mu \frac{(\not{l}+\not{q}-m)}{2l\cdot q + i\epsilon}\gamma^\beta\right]. \quad (4.15)$$

Here, we use l and k for the photons and p and q for the electron and positron four-momenta, respectively, and $\mathcal{F}(q^2) \equiv \mathcal{F}_{P\gamma^*\gamma^*}(0,q^2)$. Note that we use the shorthand notation for the product of the Levi-Civita tensor and four-momenta in which $\varepsilon^{(k)\cdots} = \varepsilon^{\mu\cdots}k_\mu$. Inasmuch as an additional photon comes into play it is convenient to introduce a new kinematic variable which stands for the normalized invariant mass squared of the two photons

$$x_\gamma = \frac{(k+l)^2}{M_P^2}\,. \quad (4.16)$$

It has the similar meaning as x in the case of the electron-positron pair. The contribution of the bremsstrahlung to the next-to-leading order two-fold differential decay width can be written as

$$\frac{\mathrm{d}^2\Gamma_{\mathrm{BS}}^{\mathrm{NLO}}}{\mathrm{d}x\,\mathrm{d}y} = \frac{(1-x)}{4M_P(2\pi)^8}\frac{\pi^3 M_P^4}{16}\int J\left[\overline{|\mathcal{M}_{\mathrm{BS}}|^2}\right]\mathrm{d}x_\gamma\,. \quad (4.17)$$

The above used operator J is defined for an arbitrary invariant $f(k,l)$ of the momenta k and l as follows:

$$J[f(k,l)] = \frac{1}{2\pi}\int \frac{\mathrm{d}^3k}{k_0}\frac{\mathrm{d}^3l}{l_0} f(k,l)\,\delta^{(4)}(P-p-q-k-l)\,. \quad (4.18)$$

In the case of the pion Dalitz decay, the value of the slope parameter of the form factor is small: $a \simeq 0.03$. Consequently, the form factor $\mathcal{F}((l+p+q)^2)$ which enters (4.13) can be conveniently expanded in the following way:

$$\mathcal{F}\Big((l+p+q)^2\Big) \simeq \mathcal{F}(M_P^2 x)\left[1 + a\,\frac{2l\cdot(p+q)}{M_P^2}\right]. \quad (4.19)$$

For the process $\pi^0 \to e^+e^-\gamma$, $\mathcal{F}((l+p+q)^2)$ can be therefore approximated by $\mathcal{F}(M_P^2 x)$. This squared leads to the direct cancellation with $|\mathcal{F}(M_P^2 x)|^2$ from the leading order and the bremsstrahlung contribution to the radiative corrections becomes effectively independent on the particular model of the pion transition form factor. However, in the case of an η meson, the slope parameter is $a_\eta \simeq 0.5$, which is definitely not negligible anymore. One would need to include higher-order corrections in expansion (4.19), the convergence would be slower and things would become in general more complicated since additional terms would need to be treated. The real obstacles though appear with the η'-meson case. Due to the fact that $a_{\eta'} \simeq 1.4$, expansion (4.19) is not applicable at all. One thus needs to calculate with the full form factor.

Although in such a case the situation is somewhat different compared to the one in which the form factor cancels out, in general it is possible to use a similar framework as in the pion case — at least in the sense of treating the kinematical integrals. Accordingly, one needs to rewrite the bremsstrahlung correction in terms of integrals which are known from the pion case. These need to be somewhat

generalized due to the presence of poles in the form factor. This becomes more important in the η case compared to the pion decay and need to be taken into account explicitly. For the η' case, this procedure then becomes absolutely crucial since in the hadron spectrum the mass of the η' meson lies above the masses of the lightest vector-meson resonances ρ and ω and close to the ϕ-meson mass. The subsequent (numerical) integrations over all the relevant kinematic configurations of the bremsstrahlung photon become significantly nontrivial due to the running over these poles, which are regulated by incorporating physical widths of the resonances. The narrow resonances like ω and ϕ are somewhat straightforward to include. However, the width of the broad ρ resonance is sensitive to the π-π scattering. This can be also taken into account by the use of recent dispersive data [44, 45]. To this extent, it is convenient to use the Källén–Lehmann spectral representation of the Feynamn propagator, which allows for the use of a common spectral density function for all the mentioned resonances. The facts stated above make the bremsstrahlung contribution — especially in the case of the η' meson — significantly sensitive to the form factor model.

In the Källén–Lehmann spectral representation, the form factor has the following form:

$$\frac{\mathcal{F}(q^2)}{\mathcal{F}(0)} \simeq 1 + q^2 \int_{4m_\pi^2}^{\Lambda^2} \frac{\mathcal{A}(s)\,\mathrm{d}s}{q^2 - s + i\epsilon}\,. \tag{4.20}$$

Concerning the integration range, we restrict ourselves only to $(4m_\pi^2, \Lambda^2)$. This is sufficient for our purpose and covers all the important physics. In the lower bound, m_π is the mass of a charged pion $\pi^\pm$ and $4m_\pi^2$ then constitutes the resonant threshold of the ρ meson. The upper bound is governed by the cut-off $\Lambda \simeq 1.05\,\mathrm{GeV}$ chosen in such a way just to cover the peak and width of the ϕ resonance. The spectral function has in the chosen energy range two main contributions distinguished by isospin, $\mathcal{A}(s) = \mathcal{A}_0(s) + \mathcal{A}_1(s)$. The narrow resonances ω and ϕ contribute to the isospin-zero part

$$\mathcal{A}_0(s) = w_\omega \mathcal{A}_\omega(s) + w_\phi \mathcal{A}_\phi(s)\,, \tag{4.21}$$

with the narrow-resonance spectral function

$$\mathcal{A}_\mathcal{V}(s) \equiv \mathcal{A}(s; M_\mathcal{V}, \Gamma_\mathcal{V}) \equiv -\frac{1}{\pi} \frac{M_\mathcal{V}\Gamma_\mathcal{V}}{(s - M_\mathcal{V}^2)^2 + (M_\mathcal{V}\Gamma_\mathcal{V})^2}\,. \tag{4.22}$$

Note that after the integration over s one indeed gets (up to a sign) the resonance propagator:

$$\int_{-\infty}^{\infty} \frac{\mathcal{A}_\mathcal{V}(s)\,\mathrm{d}s}{q^2 - s + i\epsilon} = -\frac{1}{q^2 - M_\mathcal{V}^2 + iM_\mathcal{V}\Gamma_\mathcal{V}}\,. \tag{4.23}$$

Finally, let us mention, that a one-narrow-resonance VMD model for the form factor can be written in terms of (4.20) with $\mathcal{A}(s) = \mathcal{A}_\mathcal{V}(s)$. The isospin-one part is governed by the ρ meson. In order to include an important effect of $\pi\pi$ scattering, we use the dispersive data and the spectral function has the form [44, 45]

$$\mathcal{A}_1(s) = -\frac{\kappa}{96\pi^2 F_\pi^2} \left[1 - \frac{4m_\pi^2}{s}\right]^{3/2} (1 + \alpha s + \beta s^2)(1 + \alpha_V s)|\Omega(s)|^2\,. \tag{4.24}$$

Apart from the constants, it is important to say that $\Omega(s)$ is the Omnès function. For numerical reasons, the spectral function for the broad ρ resonance may be

fitted, since the analytical expression is much faster to integrate compared to the dispersive data interpolation. To this extent, it is necessary to model the resonance peak behavior. The following function copies the dispersive shape of $\mathcal{A}_1$ satisfactorily:

$$\mathcal{A}_1(s) \simeq \left[a_0 + a_1 s + (a_2 s)^2 + (a_3 s)^3\right] \mathcal{A}(s; M_\rho, \Gamma_\rho(s)) \,. \tag{4.25}$$

The energy dependence of the width of the ρ meson — assuming the main contribution comes from the 2π-decay — can be expressed as

$$\Gamma_\rho(s) \equiv \Gamma_\rho \frac{M_\rho}{\sqrt{s}} \left[\frac{s - 4m_\pi^2}{M_\rho^2 - 4m_\pi^2}\right]^{3/2} . \tag{4.26}$$

Let us now show, how the matrix element squared looks like in the spectral representation. For the sake of writing down its structure, we recast (4.13) as

$$i\mathcal{M}_{\mathrm{BS}} = \frac{\mathcal{F}(E)}{E} I_{\mathrm{E}} + \frac{\mathcal{F}(F)}{F} I_{\mathrm{F}} \tag{4.27}$$

where we have used the shorthand notation $E = (l+p+q)^2 + i\epsilon$ and $F = (k+p+q)^2 + i\epsilon$ and defined $I_{\mathrm{E}} \equiv I(k,l)$ and $I_{\mathrm{F}} \equiv I(l,k)$. After inserting representation of the form factor (4.20) we get

$$\frac{i\mathcal{M}_{\mathrm{BS}}}{\mathcal{F}(0)} = \left[\frac{1}{E} + \int_{4m_\pi^2}^{\Lambda^2} \mathrm{d}s\, \mathcal{A}(s) \frac{1}{E - s + i\epsilon}\right] I_{\mathrm{E}} + (E \leftrightarrow F) \,. \tag{4.28}$$

After the operator J is applied on the matrix element squared and summed over all the spins and polarizations $\overline{|\mathcal{M}_{\mathrm{BS}}|^2} \equiv \sum_{\text{sp., pol.}} |\mathcal{M}_{\mathrm{BS}}|^2$, we can actually use the symmetry $k \leftrightarrow l \Leftrightarrow E \leftrightarrow F$ term by term, which results into

$$\begin{aligned} &J\left[\frac{\overline{|\mathcal{M}_{\mathrm{BS}}|^2}}{\mathcal{F}^2(0)}\right] \\ &\quad = 2\,\mathrm{Re}\, J\Bigg\{\left[\frac{1}{|E|^2} + 2\,\frac{1}{E^*}\int \frac{\mathcal{A}(s)\,\mathrm{d}s}{E - s + i\epsilon} + \iint \frac{\mathcal{A}(s)\,\mathrm{d}s}{E - s + i\epsilon}\frac{\mathcal{A}(s')\,\mathrm{d}s'}{E^* - s' - i\epsilon}\right]\overline{|I_{\mathrm{E}}|^2} \\ &\qquad + \left[\frac{1}{EF^*} + 2\,\frac{1}{F^*}\int \frac{\mathcal{A}(s)\,\mathrm{d}s}{E - s + i\epsilon} + \iint \frac{\mathcal{A}(s)\,\mathrm{d}s}{E - s + i\epsilon}\frac{\mathcal{A}(s')\,\mathrm{d}s'}{F^* - s' - i\epsilon}\right]\overline{I_{\mathrm{E}} I_{\mathrm{F}}^*}\Bigg\} . \end{aligned} \tag{4.29}$$

Now we need to perform a few fraction products decompositions. First, we take the simplest case:

$$\frac{1}{E - s + i\epsilon}\frac{1}{E^*} = \frac{1}{s}\left[\frac{1}{E - s + i\epsilon} - \frac{1}{E^*}\right] . \tag{4.30}$$

Note that we write s instead of $s - i\epsilon$ since $s \neq 0$ due to the positive limits of the integration. Similarly,

$$\frac{1}{E - s + i\epsilon}\frac{1}{E^* - s' - i\epsilon} = \frac{1}{s - s' - 2i\epsilon}\left[\frac{1}{E - s + i\epsilon} - \frac{1}{E^* - s' - i\epsilon}\right] . \tag{4.31}$$

Now, we can use the fact that this term is multiplied by two spectral functions $\mathcal{A}(s)$ and $\mathcal{A}(s')$ and integrated symmetrically over s and s'. After we rename

$s \leftrightarrow s'$ in the second term on the right-hand side of (4.31), we realize that due to the symmetric integration we obtain the complex conjugate of the first term. Since we are anyway interested in the real part only, we just get the factor of two. In the following we use the knowledge of the fact that $E + F^* = M_P^2(1 + x - x_\gamma)$ is a significant J-invariant combination of kinematic variables:

$$\frac{1}{E - s + i\epsilon}\frac{1}{F^*} = \frac{1}{(E + F^*) - s + i\epsilon}\left[\frac{1}{E - s + i\epsilon} + \frac{1}{F^*}\right]. \tag{4.32}$$

Note that due to the presence of the J operator, we can substitute $1/F^*$ by $1/E^*$ on the right-hand side of the previous equation. Finally, using Kramers–Kronig relation we find

$$\frac{1}{E - s + i\epsilon}\frac{1}{F^* - s' - i\epsilon} = \text{p. v.}\,\frac{1}{(E + F^*) - s - s'}\left[\frac{1}{E - s + i\epsilon} + \frac{1}{F^* - s' - i\epsilon}\right], \tag{4.33}$$

where p. v. stands for the principal value. Again, using the fact that the integration is symmetric in s and s' and that we can on the right change $F^* \to E^*$, we obtain the sum of a term and its complex conjugate, which results in a factor of two under the real part operator; note that $\overline{I_{\rm E} I_{\rm F}^*}$ has no (nonvanishing) imaginary part since it is related to the tree diagram. Taking into account the previous decompositions and the fact that

$$\text{Re}\iint \text{d}s\,\text{d}s'\frac{\mathcal{A}(s)\mathcal{A}(s')}{s - s' - 2i\epsilon} = i\pi\,\text{Re}\int \text{d}s\mathcal{A}^2(s) = 0\,, \tag{4.34}$$

we can rewrite (4.29) as

$$\begin{aligned} J\left[\frac{\overline{|\mathcal{M}_{\rm BS}|^2}}{\mathcal{F}^2(0)}\right] &= 4\,\text{Re}\,J\Bigg\{\Bigg[\frac{1}{2}\frac{1}{|E|^2} + \int \text{d}s\,\mathcal{A}(s) \\ &\times\left(\frac{1}{E - s + i\epsilon} - \frac{1}{E^*}\right)\left(\frac{1}{s} + \int\frac{\mathcal{A}(s')\,\text{d}s'}{s - s' - 2i\epsilon}\right)\Bigg]\overline{|I_{\rm E}|^2} \\ &+ \left[\frac{1}{(E + F^*)}\frac{1}{E} + \int \text{d}s\,\frac{\mathcal{A}(s)}{(E + F^*) - s + i\epsilon}\left(\frac{1}{E^*} + \frac{1}{E - s + i\epsilon}\right)\right. \\ &+ \left.\iint \text{d}s\,\text{d}s'\,\text{p. v.}\,\frac{\mathcal{A}(s)\mathcal{A}(s')}{(E + F^*) - s - s'}\frac{1}{E - s + i\epsilon}\right]\overline{I_{\rm E} I_{\rm F}^*}\Bigg\}. \end{aligned} \tag{4.35}$$

Note that for numerical purposes it might be reasonable to write

$$\text{p. v.}\,\frac{1}{(E + F^*) - s - s'} = \frac{1}{(E + F^*) - s - s' + i\epsilon'} + i\pi\delta((E + F^*) - s - s') \tag{4.36}$$

with the pole being on the same side of the cut as of the term $1/(E - s + i\epsilon)$. For the sake of integrating out the bremsstrahlung photon it is convenient to define the following three rescaled parts of the matrix element squared:

$$\frac{e^8}{4}\text{Tr}_{\rm E^2} \equiv \frac{\overline{|I_{\rm E}|^2}}{|E|^2}\,, \tag{4.37}$$

$$\frac{e^8}{4}\text{Tr}_{\rm E}(s) \equiv \frac{\overline{|I_{\rm E}|^2}}{E - s + i\epsilon}\,, \tag{4.38}$$

$$\frac{e^8}{4}\text{Tr}_{\rm EF}(s) \equiv \frac{\overline{I_{\rm E} I_{\rm F}^*}}{E - s + i\epsilon}\,. \tag{4.39}$$

One gets the remaining building blocks of (4.35) by performing the limit $s \to 0$, i.e. taking $\mathrm{Tr}_{\mathrm{E}}(0)$ and $\mathrm{Tr}_{\mathrm{EF}}(0)$. The name Tr is chosen to be in agreement with [7]. Note that the original work of Mikaelian and Smith — which in some sense corresponds to $\mathcal{A}(s) = 0$ since the form factor could have been factorized out — is connected with the previous definitions through

$$\overline{|\mathcal{M}_{\mathrm{BS}}^{\mathrm{M\&S}}|^2} = \frac{e^8}{4} \left|\mathcal{F}(M_P^2 x)\right|^2 \mathrm{Tr}^{\mathrm{M\&S}}\,, \tag{4.40}$$

where

$$J\left[\mathrm{Tr}^{\mathrm{M\&S}}\right] = 4J\left[\frac{1}{2}\mathrm{Tr}_{\mathrm{E}^2} + \frac{\mathrm{Tr}_{\mathrm{EF}}(0)}{M_P^2(1+x-x_\gamma)}\right]. \tag{4.41}$$

Finally, note that (4.35) suggests that we need to perform five integrations (three are implicitly hidden in the J operator), the three of which need to be performed numerically.

Summary

In the presented thesis, some basic approaches, methods and technical issues which one encounters in the low-energy domain of QCD in connection with meson decays are shown. Of course, much more could have been written about this topic. Here, we have concentrated on providing an introduction for attached papers, which contain calculations of radiative corrections for the processes like $\pi^0 \to e^+e^-$ and $\pi^0 \to e^+e^-\gamma$ and we discussed some difficulties which arise when the associated processes $\eta^{(\prime)} \to \ell^+\ell^-$ and most importantly $\eta^{(\prime)} \to \ell^+\ell^-\gamma$ are treated. For pion-involved cases of the above stated applications, having at hand a phenomenologically successful model of the pion transition form factor satisfying all the leading-order constrains given by QCD is an important achievement. This considered together with the radiative corrections, all the necessary inputs e.g. for a new measurement of the rare pion decay are at hand in a ready-to-use form. A collaboration with respective experiments is also essential and it is rewarding to know that the presented calculations are of particular interest within specific collaborations such as NA48/NA62 at CERN or A2 in Mainz.

Appendix A

Scalar one-loop integrals

A.1 Definitions

In this section we list the definitions of scalar one-loop integrals. Inspired by [46], the one-point (tadpole) scalar one-loop integral is defined as

$$\begin{aligned} i\pi^2 A_0\Big(m^2\Big) &\equiv (2\pi)^4 \mu^{4-n} \int \frac{\mathrm{d}^n l}{(2\pi)^n} \frac{1}{l^2 - m^2 + i\epsilon} \\ &= (2\pi\mu)^{4-n} \int \frac{\mathrm{d}^n l}{l^2 - m^2 + i\epsilon} \,. \end{aligned} \tag{A.1}$$

This definition is consistent with the FeynCalc package [47, 48] for Wolfram Mathematica and eventually differes from standard notebook loop calculations by the factor "$-16i\pi^2$". The dimensionful parameter μ serves as the mass dimensionality regulator. For the two-point (bubble) scalar integral we have

$$i\pi^2 B_0\Big(p^2; m_1^2, m_2^2\Big) \equiv (2\pi\mu)^{4-n} \int \frac{\mathrm{d}^n l}{[l^2 - m_1^2 + i\epsilon][(l-p)^2 - m_2^2 + i\epsilon]} \,. \tag{A.2}$$

Using the Feynman parametrization we can rewrite definition (A.2) as

$$i\pi^2 B_0\Big(p^2; m_1^2, m_2^2\Big) = (2\pi\mu)^{4-n} \int_0^1 \mathrm{d}x \int \frac{\mathrm{d}^n l}{\left[l^2 - C + i\epsilon\right]^2} \,, \tag{A.3}$$

where

$$C = p^2x^2 - (p^2 - m_1^2 + m_2^2)x + m_2^2 \quad \text{or} \quad C = p^2x^2 - (p^2 - m_2^2 + m_1^2)x + m_1^2 \,. \tag{A.4}$$

From the previous relations it immediately follows that the two-point integral is invariant under the exchange of the internal masses:

$$B_0\Big(p^2; m_1^2, m_2^2\Big) = B_0\Big(p^2; m_2^2, m_1^2\Big) \,. \tag{A.5}$$

Let us note that the advantage of the used convention lies in the fact that in the expressions for B_0 functions — which are dimensionless — the divergent part comes out directly with no additional factor and thus e.g.

$$B_0\Big(0; m^2, m^2\Big) = \frac{1}{\varepsilon} - \gamma_\mathrm{E} + \log 4\pi + \log \frac{\mu^2}{m^2} \,. \tag{A.6}$$

For the three-point (triangle) scalar one-loop integral we have

$$\begin{aligned} &i\pi^2 C_0\Big(p_1^2, p_2^2, (p_1+p_2)^2; m_1^2, m_2^2, m_3^2\Big) \\ &\equiv \int \frac{\mathrm{d}^n l}{[l^2 - m_1^2 + i\epsilon][(l-p_1)^2 - m_2^2 + i\epsilon][(l-p_1-p_2)^2 - m_3^2 + i\epsilon]}\,. \end{aligned} \tag{A.7}$$

Note that there was no need to introduce $(2\pi\mu)^{4-n}$ in this definition since C_0 — as well as D_0, the definition of which will follow — are UV-convergent by power counting of the loop momenta and thus terms proportional to $4-n = 2\varepsilon$ disappear after performing the limit $\varepsilon \to 0$: there is just no $1/\varepsilon$ to make these terms survive. The C_0 function has a few important symmetries, such as simultaneous rotation in the first and second triplet of the arguments:

$$\begin{aligned} &C_0\Big(p_1^2, p_2^2, (p_1+p_2)^2; m_1^2, m_2^2, m_3^2\Big) \\ &= C_0\Big(p_2^2, (p_1+p_2)^2, p_1^2; m_2^2, m_3^2, m_1^2\Big) \\ &= C_0\Big((p_1+p_2)^2, p_1^2, p_2^2; m_3^2, m_1^2, m_2^2\Big)\,, \end{aligned} \tag{A.8}$$

or a transposition of the arguments such as

$$C_0\Big(p_1^2, p_2^2, (p_1+p_2)^2; m_1^2, m_2^2, m_3^2\Big) = C_0\Big(p_1^2, (p_1+p_2)^2, p_2^2; m_2^2, m_1^2, m_3^2\Big)\,. \tag{A.9}$$

Needless to say, there are other symmetries which just arise from all possible combinations of these elementary operations.

We conclude the definitions of the scalar one-loop integrals with the four-point (box) function defined as

$$\begin{aligned} &i\pi^2 D_0\Big(p_1^2, p_2^2, p_3^2, (p_1+p_2+p_3)^2; (p_1+p_2)^2, (p_2+p_3)^2; m_1^2, m_2^2, m_3^2, m_4^2\Big) \\ &\equiv \int_{\mathbb{R}^n} \frac{\mathrm{d}^n l}{[l^2 - m_1^2 + i\epsilon][(l-q_1)^2 - m_2^2 + i\epsilon][(l-q_2)^2 - m_3^2 + i\epsilon][(l-q_3)^2 - m_4^2 + i\epsilon]}\,, \end{aligned} \tag{A.10}$$

where we have used $q_1 = p_1$, $q_2 = p_1 + p_2$ and $q_3 = p_1 + p_2 + p_3$ analogically to the previous definitions. Regarding the symmetries of the D_0 function, we find that there is again a rotation — simultaneous in the first quadruplet, second doublet and the last quadruplet:

$$\begin{aligned} &D_0\Big(p_1^2, p_2^2, p_3^2, p_4^2; K_1^2, K_2^2; m_1^2, m_2^2, m_3^2, m_4^2\Big) \\ &= D_0\Big(p_4^2, p_1^2, p_2^2, p_3^2; K_2^2, K_1^2; m_4^2, m_1^2, m_2^2, m_3^2\Big) \\ &= D_0\Big(p_3^2, p_4^2, p_1^2, p_2^2; K_1^2, K_2^2; m_3^2, m_4^2, m_1^2, m_2^2\Big) \end{aligned} \tag{A.11}$$

and so on. After some further investigation one finds another symmetry such as

$$\begin{aligned} &D_0\Big(p_1^2, p_2^2, p_3^2, p_4^2; K_1^2, K_2^2; m_1^2, m_2^2, m_3^2, m_4^2\Big) \\ &= D_0\Big(K_1^2, p_1^2, K_2^2, p_3^2; p_2^2, p_4^2; m_3^2, m_1^2, m_2^2, m_4^2\Big)\,. \end{aligned} \tag{A.12}$$

As the last example we list a quite special but useful symmetry:

$$\begin{aligned} &D_0\Big(p_1^2, p_2^2, p_3^2, p_4^2; K_1^2, K_2^2; m_1^2, m_2^2, m_3^2, m_4^2\Big) \\ &= D_0\Big(p_3^2, p_2^2, p_1^2, p_4^2; K_2^2, K_1^2; m_4^2, m_3^2, m_2^2, m_1^2\Big)\,. \end{aligned} \tag{A.13}$$

There is no actual need to define E_0 — the pentagon function — and further on since these can be — due to the properties of the four-dimensional spacetime we work with — rewritten as a liner combination of one-loop integrals with at most four external legs. In particular, a general E_0 function can be written as a combination of five D_0 functions.

Let us mention that within the dimensional regularization approach, it is a common practice to calculate the analytic expressions for the scalar one-loop integrals by using the Feynman parametrization followed by the application of the master formula

$$\int \frac{\mathrm{d}^n l}{(2\pi)^n} \frac{(l^2)^r}{(l^2 - C + i\epsilon)^s} = \frac{i}{(4\pi)^{\frac{n}{2}}} (-1)^{r-s} (C - i\epsilon)^{\frac{n}{2}+r-s} \frac{\Gamma\left(r + \frac{n}{2}\right) \Gamma\left(s - r - \frac{n}{2}\right)}{\Gamma\left(\frac{n}{2}\right) \Gamma(s)}\,, \tag{A.14}$$

which works for $r, s \in \mathbb{N}$.

A.2 Relations between bubbles and tadpoles

In this section we will show some basic relations between A_0 and B_0 scalar one-loop integrals. As we will see, integrals depending on only one scale $m^2 > 0$ can be expressed in terms of the simplest integral $B_0(0; m^2, m^2)$ defined in (A.6), the analytic form of which contains only the notorious divergent part and the obligatory logarithm containing scale μ. A direct use of integral definitions from the last section and standard techniques including formula (A.14) reveals the following relation:

$$A_0\big(m^2\big) = -m^2 B_0\big(0; m^2, m^2\big) \frac{2}{2-n} = m^2 B_0\big(0; m^2, m^2\big)\big[1 + \varepsilon + \mathcal{O}(\varepsilon^2)\big]\,. \tag{A.15}$$

In the case of physical one-loop amplitudes we can safely perform the limit $\varepsilon \to 0$ and obtain

$$A_0\big(m^2\big) = m^2 B_0\big(0; m^2, m^2\big) + m^2\,. \tag{A.16}$$

Similarly, using (A.3) with (A.4) and (A.14) we find

$$B_0\big(0; 0, m^2\big) = B_0\big(0; m^2, m^2\big) \int_0^1 \mathrm{d}x\; x^{\frac{n}{2}-2} = B_0\big(0; m^2, m^2\big) + 1\,, \tag{A.17}$$

and correspondingly,

$$B_0\big(m^2; 0, m^2\big) = B_0\big(0; m^2, m^2\big) \int_0^1 \mathrm{d}x \left(x^2\right)^{\frac{n}{2}-2} = B_0\big(0; m^2, m^2\big) + 2\,. \tag{A.18}$$

Needless to say, in the last equalities we have repeatedly used the limit $\varepsilon \to 0$. Finally, let us remark that putting together (A.16) and (A.17) reveals a simple identity

$$m^2 B_0\big(0; 0, m^2\big) = A_0\big(m^2\big)\,. \tag{A.19}$$

To conclude, let us mention the case of $B_0(m^2; 0, 0)$. This function corresponds to the diagram, the kinematics of which allows to create on-shell particles. Hence, $B_0(m^2; 0, 0)$ needs to contain a nontrivial imaginary part:

$$B_0\big(m^2; 0, 0\big) = \big[B_0\big(0; m^2, m^2\big) + i\pi\big] \int_0^1 \mathrm{d}x\, (x(1-x))^{\frac{n}{2}-2} = B_0\big(0; m^2, m^2\big) + 2 + i\pi\,. \tag{A.20}$$

Appendix B

Decomposition of scalar one-loop integrals

In this appendix we follow a simple trick by 't Hooft and Veltman [46]. While evaluating loop integrals, one always encounters a product of propagators. As a part of such a product, the following term typically appears:

$$\frac{1}{[(l+p)^2-m_1^2][(l+p+q)^2-m_2^2]}\,, \tag{B.1}$$

where the loop momentum is denoted as l. One can multiply the numerator and denominator with

$$(1-\kappa)\Big[(l+p)^2-m_1^2\Big]+\kappa\Big[(l+p+q)^2-m_2^2\Big]\equiv(l+r)^2-M^2 \tag{B.2}$$

to obtain the following identity:

$$\begin{aligned}\frac{1}{[(l+p)^2-m_1^2][(l+p+q)^2-m_2^2]} &= \frac{\kappa}{[(l+r)^2-M^2][(l+r-\kappa q)^2-m_1^2]}\\ &+\frac{1-\kappa}{[(l+r)^2-M^2][(l+r+(1-\kappa)q)^2-m_2^2]}\,.\end{aligned} \tag{B.3}$$

Above, we have defined new four-momentum r and mass M:

$$r=p+\kappa q\,, \tag{B.4}$$

$$M^2=-\kappa(1-\kappa)q^2+\kappa m_2^2+(1-\kappa)m_1^2\,. \tag{B.5}$$

The advantage of decomposition (B.3) lies in the fact that it is possible — for some specific choice of real κ — set either r^2 or M^2 to zero. Any diagram can thus be written as a sum of two diagrams with some internal or external mass set to zero. Loop integrals or scalar one-loop functions which have one vanishing parameter are simpler to calculate. The requirement of κ being a real parameter is given by the fact that all the eventual consequent steps we are used to perform during the evaluation of loop integrals like Feynman parametrization, Wick rotation etc. work unchanged only for real κ.

There are two situations in which some particular parameters appearing in the loop integrals can be zeroed. First, lets focus on the case of $M^2=0$. For later convenience, we define the function (cf. (B.5))

$$M^2(\kappa;a,b,c)\equiv\kappa^2 a-\kappa(a+b-c)+b\,. \tag{B.6}$$

From (B.5) we see that we need to solve the quadratic equation

$$M^2(\kappa; q^2, m_1^2, m_2^2) = 0\,. \tag{B.7}$$

It has real solutions for κ whenever the discriminant satisfies $(q^2 + m_1^2 - m_2^2)^2 - 4m_1^2 q^2 \geq 0$. On can immediately recognize that the discriminant is equal to $\lambda(q^2, m_1^2, m_2^2)$, where $\lambda(a, b, c) \equiv a^2 + b^2 + c^2 - 2ab - 2bc - 2ac$ is the Kälén triangle function. This implies that when the condition $\lambda(q^2, m_1^2, m_2^2) \geq 0$ is fulfilled, one can decompose a related scalar one-loop function into two such functions which both have at least one vanishing internal mass. If we define the following function

$$\kappa_\pm(a, b, c) \equiv \frac{1}{2a}\left[a + b - c \pm \lambda^{\frac{1}{2}}(a, b, c)\right], \tag{B.8}$$

the solutions of quadratic equation (B.7) can be written as

$$\kappa_\pm^{(1)} = \kappa_\pm(q^2, m_1^2, m_2^2)\,. \tag{B.9}$$

Let us note that Eq. (B.7) has real solutions for any space-like q (i.e. for $q^2 < 0$ in the metric we use). On the other hand, for the time-like q, we can set $r^2 = 0$. The second case and the related reasoning looks as follows. The quadratic equation for κ from (B.4) reads

$$r^2 = \kappa^2 q^2 + 2\kappa p \cdot q + p^2 = 0 \tag{B.10}$$

with the condition on the discriminant $(p \cdot q)^2 \geq p^2 q^2$. In the rest frame of the time-like q (or of p accordingly), we have $(p_0\sqrt{q^2})^2 \geq p^2 q^2$. This translates to $p_0^2 \geq p_0^2 - |\vec{p}|^2$ which is always true. In general, the discriminant can be again written in terms of the Källén function and the resulting condition is $\lambda((p+q)^2, p^2, q^2) \geq 0$. If this holds, r^2 can be zeroed for a real κ and consequently, the related diagram can be substituted with a sum of two diagrams, both of which have at least one vanishing external mass. The solutions of quadratic equation (B.10) are

$$\kappa_\pm^{(2)} = \kappa_\pm\left(p^2, q^2, (p+q)^2\right). \tag{B.11}$$

Note that there are situations in which both of the cases are consequently allowed, e.g. in the case of three-point scalar function C_0. This, for instance, results in a term of four scalar one-loop integrals, each of which has two vanishing parameters. In what follows we will discuss some particular examples of the suggested decomposition in case of two-point and three-point scalar one-loop integrals.

B.1 Two-point scalar one-loop integrals

The application of the rules considered above is in the case of the B_0 functions somewhat trivial since the product of the propagators (B.1) can be simplified just by shifting the integration variable:

$$\int \mathrm{d}^4 l\, \frac{1}{[(l+p)^2 - m_1^2][(l+p+q)^2 - m_2^2]} = \int \mathrm{d}^4 l\, \frac{1}{[l^2 - m_1^2][(l+q)^2 - m_2^2]}\,. \tag{B.12}$$

In other words, a general B_0 function always depends only on one external momentum squared and two internal masses. Consequently, one cannot write a general B_0 function as a sum of two B_0s with vanishing external momentum in terms of the previous decomposition. From (B.4) it is obvious that κ would need to be zero, which would result in identity in (B.3). On the other hand, we can easily zero one of the masses; note that B_0 is symmetric under exchange of the internal masses. Whenever $\lambda(q^2, m_1^2, m_2^2) \geq 0$ is satisfied, we can — based on the prescription (B.3) — write

$$\frac{1}{[l^2 - m_1^2][(l+q)^2 - m_2^2]} = \frac{\kappa}{[(l+\kappa q)^2][l^2 - m_1^2]} + \frac{1-\kappa}{[(l+\kappa q)^2][(l+q)^2 - m_2^2]}\,, \tag{B.13}$$

where $\kappa \equiv \kappa_\pm^{(1)} = \kappa_\pm(q^2, m_1^2, m_2^2)$ is the solution to (B.7) so M^2 disappears. Under the integral sign, the second term can be recast due to the possible shift of the variables as

$$\int \mathrm{d}^4 l\, \frac{1-\kappa}{[(l+\kappa q)^2][(l+q)^2 - m_2^2]} = \int \mathrm{d}^4 l\, \frac{1-\kappa}{[(l-(1-\kappa)q)^2][l^2 - m_2^2]}\,. \tag{B.14}$$

In terms of the notation of the scalar one-loop integrals, one then writes for the two possible decompositions of $B_0(q^2; m_1^2, m_2^2)$ (distinguished by different upper scripts $\pm$)

$$B_0^\pm\Big(q^2; m_1^2, m_2^2\Big) = \kappa_\pm\, B_0\Big(\kappa_\pm^2 q^2; 0, m_1^2\Big) + (1-\kappa_\pm)\, B_0\Big((1-\kappa_\pm)^2 q^2; 0, m_2^2\Big)\,, \tag{B.15}$$

with

$$\kappa_\pm = \kappa_\pm(q^2, m_1^2, m_2^2) = \frac{1}{2q^2}\left[q^2 + m_1^2 - m_2^2 \pm \lambda^{\frac{1}{2}}\Big(q^2, m_1^2, m_2^2\Big)\right]. \tag{B.16}$$

Lets now discuss what is the relation between the two choices κ_+ or κ_-. Obviously, $1 - \kappa_\pm(q^2, m_1^2, m_2^2) = \kappa_\mp(q^2, m_2^2, m_1^2)$. Then

$$B_0^+\Big(q^2; m_1^2, m_2^2\Big) = \kappa_+\, B_0\Big(\kappa_+^2 q^2; 0, m_1^2\Big) + (1-\kappa_+)\, B_0\Big((1-\kappa_+)^2 q^2; 0, m_2^2\Big)\,, \tag{B.17}$$

$$\begin{aligned} B_0^-\Big(q^2; m_1^2, m_2^2\Big) &= \kappa_-\, B_0\Big(\kappa_-^2 q^2; 0, m_1^2\Big) + (1-\kappa_-)\, B_0\Big((1-\kappa_-)^2 q^2; 0, m_2^2\Big) \\ &= \Big[(1-\kappa_+)\, B_0\Big((1-\kappa_+)^2 q^2; 0, m_2^2\Big) + \kappa_+\, B_0\Big(\kappa_+^2 q^2; 0, m_1^2\Big)\Big]\Big|_{m_1 \leftrightarrow m_2}\,, \end{aligned} \tag{B.18}$$

which means the second decomposition equals to the first up to the mass exchange $m_1 \leftrightarrow m_2$. The two-point scalar one-loop integral $B_0(q^2; m_1^2, m_2^2)$ is symmetric under such an exchange. We would thus expect, at least in some sense, that the decompositions $B_0^\pm(q^2; m_1^2, m_2^2)$, being the correct decompositions, must also have such a property. Indeed, if we perform the operation $m_1 \leftrightarrow m_2$ on one of the decompositions, we obtain the other one. This, being a different linear combination of different B_0s, is nevertheless still another decomposition of the same original function and hence the symmetry operation under discussion changes only the form but not the numerical result itself. In other words, though it holds $B_0^+(q^2; m_1^2, m_2^2) = B_0^-(q^2; m_1^2, m_2^2)$ — recall that by definition these

are two equivalent decompositions of the very same function — it is nevertheless $B_0^+(q^2;m_1^2,m_2^2) \not\equiv B_0^-(q^2;m_1^2,m_2^2)$, but on the other hand $B_0^+(q^2;m_1^2,m_2^2) \equiv B_0^-(q^2;m_2^2,m_1^2)$. Thus we see that both decompositions are closely related through the symmetry of B_0 which in turn means it does not matter if one uses κ_+ or κ_-.

As an simple example, we provide an explicit analytic formula for function $B_0(q^2;m^2,m^2)$ using previously discussed decomposition. We already know that if the condition $\lambda(q^2,m_1^2,m_2^2) \geq 0$ is satisfied, it holds

$$B_0^{\pm}\Big(q^2;m_1^2,m_2^2\Big) = \kappa_{\pm}\, B_0\Big(\kappa_{\pm}^2 q^2;0,m_1^2\Big) + (1-\kappa_{\pm})\, B_0\Big((1-\kappa_{\pm})^2 q^2;0,m_2^2\Big)\,. \quad \text{(B.19)}$$

The analytic expression for $B_0(q^2;0,m^2)$ is easily obtained using a standard straightforward calculation with the result

$$B_0\Big(q^2;0,m^2\Big) = B_0\Big(0;m^2,m^2\Big) + 2 - \left(1-\frac{m^2}{q^2}\right)\log\left(1-\frac{q^2+i\epsilon}{m^2}\right). \quad \text{(B.20)}$$

Now, we shall calculate $\kappa_{\pm}$ for the special case $B_0(q^2;m^2,m^2)$:

$$\kappa_{\pm}(q^2,m^2,m^2) = \frac{1}{2q^2}\left[q^2 \pm \lambda^{\frac{1}{2}}\Big(q^2,m^2,m^2\Big)\right] = \frac{1}{2}\Big(1 \pm \beta\,\mathrm{sgn}(q^2)\Big)\,. \quad \text{(B.21)}$$

Due to the symmetry reasons we discussed above, in particular the fact that choosing κ_+ and κ_- means exchanging the order of internal masses, we see that both of the two possible decompositions must give the exactly same resulting linear combination, since both internal masses are the same. Consequently, we can forget about the $\mathrm{sgn}(q^2)$ in the above equation and simply write

$$B_0\Big(q^2;m^2,m^2\Big) = \frac{1-\beta}{2}\, B_0\Big(m^2\gamma;0,m^2\Big) + \frac{1+\beta}{2}\, B_0\left(\frac{m^2}{\gamma};0,m^2\right), \quad \text{(B.22)}$$

which results in

$$\begin{aligned} &B_0\Big(q^2;m^2,m^2\Big) \\ &= B_0\Big(0;m^2,m^2\Big) + 2 + \beta\log\left(\frac{2\beta}{1+\beta} - \frac{i\epsilon}{m^2}\right) - \beta\log\left(-\frac{2\beta}{1-\beta} - \frac{i\epsilon}{m^2}\right). \end{aligned} \quad \text{(B.23)}$$

In the region where $\lambda(q^2,m^2,m^2) \geq 0$, β is real and positive. This means that in the above formula we have a difference of logarithms, the imaginary parts of which have the same sign. This fact allows us to combine them in a way we are used to from the domain of real numbers (there is no additional phase):

$$\log\left(\frac{2\beta}{1+\beta} - \frac{i\epsilon}{m^2}\right) - \log\left(-\frac{2\beta}{1-\beta} - \frac{i\epsilon}{m^2}\right) = \log\left(-\gamma + \frac{i\epsilon}{m^2}\frac{\gamma}{\beta}\right), \quad \text{(B.24)}$$

and since $\beta > 0$ we can write

$$B_0\Big(q^2;m^2,m^2\Big) = B_0\Big(0;m^2,m^2\Big) + 2 + \beta\log\left[-\gamma\left(1-\frac{i\epsilon}{m^2}\right)\right]. \quad \text{(B.25)}$$

B.2 Three-point scalar one-loop integrals

In the case of three-point functions we have again two possible decompositions at hand. For a general integral $C_0(q^2, p^2, (p+q)^2; m_2^2, m_1^2, m_0^2)$, if $\lambda(q^2, m_1^2, m_2^2) \geq 0$, we can write it as a sum of two C_0s with at least one internal mass set to zero:

$$\begin{aligned} C_0\Big(q^2, p^2, (p+q)^2; m_2^2, m_1^2, m_0^2\Big) &= \kappa_1\, C_0\Big(p^2, \kappa_1^2 q^2, M_1^2; m_0^2, m_1^2, 0\Big) \\ &+ (1-\kappa_1)\, C_0\Big((p+q)^2, (1-\kappa_1)^2 q^2, M_1^2; m_0^2, m_2^2, 0\Big)\,, \end{aligned} \tag{B.26}$$

where $\kappa_1 \equiv \kappa_-(q^2, m_1^2, m_2^2)$ and $M_1^2 \equiv M^2(\kappa_1; q^2, p^2, (p+q)^2)$. On the other hand, whenever $\lambda((p+q)^2, p^2, q^2) \geq 0$, we are allowed to write

$$\begin{aligned} C_0\Big(q^2, p^2, (p+q)^2; m_2^2, m_1^2, m_0^2\Big) &= \kappa_2\, C_0\Big(p^2, \kappa_2^2 q^2, 0; m_0^2, m_1^2, M_2^2\Big) \\ &+ (1-\kappa_2)\, C_0\Big((p+q)^2, (1-\kappa_2)^2 q^2, 0; m_0^2, m_2^2, M_2^2\Big)\,, \end{aligned} \tag{B.27}$$

where $\kappa_2 \equiv \kappa_-(q^2, p^2, (p+q)^2)$ and $M_2^2 \equiv M^2(\kappa_2; q^2, m_1^2, m_2^2)$.

We see that in case one of the internal masses is zero, we might always — due to the symmetry properties of C_0 — rotate the arguments in such a way that the vanishing mass is on the place of m_0^2 in prescription (B.27). This zero stays intact during the decomposition and one thus ends up with C_0s containing two null parameters. Note that after performing by the symmetry allowed rotations of arguments one does not intermix variables separated by semicolon and thus not spoil the condition $\lambda((p+q)^2, p^2, q^2) \geq 0$. Similarly, if $m_0 = 0$, it survives throughout decomposition (B.26). However, it might not be always possible to rightly position the zero parameter and fulfill $\lambda(q^2, m_1^2, m_2^2) \geq 0$ at the same time.

We shall now discuss the case in which $q^2 = 0$ and $m_1 \neq m_2$. Decomposition (B.26) becomes

$$\begin{aligned} C_0\Big(0, p^2, (p+q)^2; m_2^2, m_1^2, m_0^2\Big) &= \kappa_1'\, C_0\Big(p^2, 0, M_1'^2; m_0^2, m_1^2, 0\Big) \\ &+ (1-\kappa_1')\, C_0\Big((p+q)^2, 0, M_1'^2; m_0^2, m_2^2, 0\Big)\,, \end{aligned} \tag{B.28}$$

with $M_1'^2 \equiv M^2(\kappa_1'; 0, p^2, (p+q)^2)$ and κ_1' being now the solution to the linear equation

$$M^2(\kappa_1'; 0, m_1^2, m_2^2) = -\kappa_1'(m_1^2 - m_2^2) + m_1^2 = 0\,, \tag{B.29}$$

i.e. $\kappa_1' = m_1^2/(m_1^2 - m_2^2)$. Since $\lambda(0, m_1^2, m_2^2) = (m_1^2 - m_2^2)^2 \geq 0$ is always (trivially) fulfilled — remember that it comes from the requirement on the solutions of the quadratic equations to be real and that the equation we solve now is only linear — the validity of (B.28) is just restricted by the requirement $m_1 \neq m_2$.

Similarly, lets discuss the case with $q^2 = 0$ and $p^2 \neq (p+q)^2$, i.e. $p \cdot q \neq 0$, for the second decomposition (B.27), which turns to

$$\begin{aligned} C_0\Big(0, p^2, (p+q)^2; m_2^2, m_1^2, m_0^2\Big) &= \kappa_2'\, C_0\Big(p^2, 0, 0; m_0^2, m_1^2, M_2'^2\Big) \\ &+ (1-\kappa_2')\, C_0\Big((p+q)^2, 0, 0; m_0^2, m_2^2, M_2'^2\Big)\,. \end{aligned} \tag{B.30}$$

Here, $M_2'^2 \equiv M^2(\kappa_2'; 0, m_1^2, m_2^2)$ with κ_2' being the solution to the linear equation $M^2(\kappa_2'; 0, p^2, (p+q)^2) = 0$. Needless to say, the condition $\lambda((p+q)^2, p^2, 0) \geq 0$ is again true in all the cases.

Let us now summarize previous results and assume a general C_0 function with no vanishing parameter. If $\lambda((p+q)^2, p^2, q^2) \geq 0$, we can use (B.27) to zero one external mass. Subsequently, provided there are at least two different internal masses in the resulting C_0 functions, we can, using the appropriate symmetries, rewrite the C_0s in such a way that we can use (B.28) to additionally zero one internal masses. Finally, we are again able to rotate the arguments to get the form of the left hand side of (B.30) and use this decomposition, having one of the zeros on the place of m_0^2. Similarly, if at the very beginning $\lambda(q^2, m_1^2, m_2^2) \geq 0$, we can use a sequence of decompositions (B.26), (B.27) and (B.30), though the second decomposition might not be allowed.

We can now turn to a simple example of $C_0(q^2, m^2, m^2; m^2, m^2, \lambda^2)$, which appears in the calculation of the correction to the QED vertex in Section 3.2 and apply the described decomposition to this case. We first assume that λ^2 stands for the zero mass we would like to preserve and thus it is convenient to put it in the position of m_0^2 as in prescription (B.27). This decomposition serves to set to zero one of the first three arguments. The condition $\lambda(q^2, m^2, m^2) \geq 0$ is always satisfied for on-shell leptons. Next, we need to calculate κ_2 and M_2^2 particularly for case of $C_0(q^2, m^2, m^2; m^2, m^2, \lambda^2)$. The calculation is trivial with the results

$$\kappa_2 = \kappa(q^2, m^2, m^2) = \frac{1-\beta}{2}\,, \tag{B.31}$$

$$M_2^2 = M^2(\kappa_2; q^2, m^2, m^2) = \kappa_2(\kappa_2 - 1)q^2 + m^2 = -\frac{1-\beta^2}{4}q^2 + m^2 = 0\,, \tag{B.32}$$

and since $\kappa_2^2 q^2 = m^2\gamma$ and $(1-\kappa_2)^2 q^2 = m^2/\gamma$, we can finally get the desired decomposition

$$\begin{aligned} &C_0\Big(q^2, m^2, m^2; m^2, m^2, \lambda^2\Big) \\ &= \frac{1}{2}\left[(1-\beta)\, C_0\Big(m^2\gamma, 0, m^2; m^2, 0, \lambda^2\Big) + (1+\beta)\, C_0\left(m^2\frac{1}{\gamma}, 0, m^2; m^2, 0, \lambda^2\right)\right]. \end{aligned} \tag{B.33}$$

Concerning the resulting C_0s, the direct calculation leads, for instance, to the following analytic expression:

$$\begin{aligned} C_0\Big(m^2\gamma, 0, m^2; m^2, 0, \lambda^2\Big) = -\frac{1}{2m^2}\frac{1+\beta}{2\beta}\Bigg[&-\mathrm{Li}_2\left(-\frac{m^2}{\lambda^2}\right) + \log^2\left(-\frac{\lambda^2}{m^2}\frac{1-\beta^2}{4\beta^2}\right) \\ &+2\mathrm{Li}_2\left(\frac{1+\beta}{2\beta} - i\beta\epsilon\right) - \log^2\left(-\frac{\lambda^2}{m^2}\frac{1-\beta}{2\beta}\right)\Bigg]. \end{aligned} \tag{B.34}$$

One then gets $C_0(m^2/\gamma, 0, m^2; m^2, 0, \lambda^2)$ by performing an obvious substitution $\beta \to -\beta$. Above, we have assumed that $\beta > 0$, $\gamma \in (0,1)$ and $\lambda^2 \simeq 0$. The function $\mathrm{Li}_2(z)$ stands for the dilogarithm (also called the Spence's function) defined as

$$\mathrm{Li}_2(z) \equiv -\int_0^z \frac{\ln(1-t)}{t}\,\mathrm{d}t = -\int_0^1 \frac{\ln(1-zt)}{t}\,\mathrm{d}t\,, \quad z \in \mathbb{Z}\,. \tag{B.35}$$

Together,

$$C_0\Big(q^2,m^2,m^2;m^2,m^2,\lambda^2\Big) = -\frac{1}{2m^2}\frac{1-\beta^2}{2\beta} \\ \times\left[\mathrm{Li}_2\left(\frac{1+\beta}{2\beta}-i\beta\epsilon\right)+\frac{1}{2}\log^2\left(\frac{1+\beta}{2\beta}\right)-\frac{1}{2}\log(-\gamma)\log\frac{\lambda^2}{m^2}\right]+\{\beta\to-\beta\}\,. \tag{B.36}$$

Note that during the operation $\beta \to -\beta$, which is meant to be applied on the whole term, one has also $\gamma \to 1/\gamma$. For $z \notin (1,\infty)$, there is a dilogarithm identity

$$\mathrm{Li}_2\left(\frac{1}{1-z}\right)-\mathrm{Li}_2\left(\frac{z}{z-1}\right)=2\,\mathrm{Li}_2\,z+\log(-z)\log(1-z)+\frac{\pi^2}{6}\,. \tag{B.37}$$

Since $(1+\beta)/(2\beta)$ can be written as $1/(1-\gamma)$ and similarly $(1-\beta)/(2\beta)$ as $\gamma/(1-\gamma)$, one can use identity (B.37) to obtain

$$\mathrm{Li}_2\left(\frac{1+\beta}{2\beta}-i\epsilon\right)-\mathrm{Li}_2\left(-\frac{1-\beta}{2\beta}+i\epsilon\right)=2\,\mathrm{Li}_2\,\gamma+\log(-\gamma+i\epsilon)\log(1-\gamma)+\frac{\pi^2}{6}\,. \tag{B.38}$$

Note that "$+i\epsilon$" in the second dilogarithm on the left is expendable since its argument is negative. Finally, let us mention that the squares of the logarithms in (B.36) combine into

$$\frac{1}{2}\log^2\left(\frac{1+\beta}{2\beta}\right)-\frac{1}{2}\log^2\left(-\frac{1-\beta}{2\beta}\right)=\log(-\gamma)\log(1-\gamma)-\frac{1}{2}\log^2(-\gamma)\,. \tag{B.39}$$

A subsequent use of another logarithmic identity

$$\mathrm{Li}_2\,z=-\mathrm{Li}_2(1-z)-\log(z)\log(1-z)+\frac{\pi^2}{6} \tag{B.40}$$

leads to the final result

$$C_0\Big(q^2,m^2,m^2;m^2,m^2,\lambda^2\Big) = \frac{1}{m^2}\frac{1-\beta^2}{2\beta} \\ \times\left[\mathrm{Li}_2(1-\gamma)-\frac{\pi^2}{4}+\frac{1}{4}\log^2(-\gamma)-i\pi\log(1-\gamma)-\log(-\gamma)\log\frac{m}{\lambda}\right]. \tag{B.41}$$

Appendix C

Passarino–Veltman reduction

In this appendix, we describe the basic idea of the well-known Passarino–Veltman — sometimes also called tensorial — reduction of loop integrals. It is a very useful technique which effectively helps to reduce amplitudes containing uncontracted loop momenta to scalar integrals, which are tabulated. Most importantly, this approach is suitable for being implemented in computational tools. We start with useful identities and then show two examples.

C.1 Identities

Loosely inspired by Passarino and Veltman [49], we start with the following formula:

$$\int l^\mu f(l,p)\ \mathrm{d}^n l = \frac{p^\mu}{p^2} \int (l\cdot p) f(l,p)\ \mathrm{d}^n l\,, \tag{C.1}$$

where f is an arbitrary scalar function of loop momentum l and external momentum p in n dimensions, which typically means that it depends on all possible scalar products of l and p: l^2, p^2 and $l\cdot p$. We also allow f to depend on masses: a typical example of f would contain Feynman propagators. It is easy to show the validation of (C.1). To this extent, we define

$$X^\mu(p) \equiv \int l^\mu f(l,p)\ \mathrm{d}^n l\,. \tag{C.2}$$

We immediately see that to comply with the vector character of X^μ it must hold

$$X^\mu(p) = p^\mu X(p)\,, \tag{C.3}$$

since p^μ is the only available tensor which can carry the free index μ. Putting the last two expressions together and multiplying by p_μ we get

$$p^2 X(p) = \int (l\cdot p) f(l,p)\ \mathrm{d}^n l\,. \tag{C.4}$$

After dividing by p^2 and inserting the resulting expression for $X(p)$ into (C.3) we obtain (C.1), which was to prove.

Following the strategy of previous lines we can derive additional expressions which vary in the number of free indices and external momenta. An additional

simple example of the tensorial reduction is for instance the one with two external momenta:

$$\int l^\mu f(l,p,q)\ \mathrm{d}^n l = \frac{(p\cdot q)q^\mu - q^2 p^\mu}{(p\cdot q)^2 - p^2 q^2}\int (l\cdot p) f(l,p,q)\ \mathrm{d}^n l + (p \leftrightarrow q)\,. \tag{C.5}$$

Having in mind the previous example, the proof is obvious. Finally, let us introduce one last example which includes two loop momenta carrying free indices:

$$\begin{aligned}\int l^\mu l^\nu f(l,p)\,\mathrm{d}^n l = \frac{1}{(1-n)p^2}\left[g^{\mu\nu} - \frac{p^\mu p^\nu}{p^2}\right]\int \left[(l\cdot p)^2 - l^2 p^2\right] f(l,p)\ \mathrm{d}^n l \\ + \frac{p^\mu p^\nu}{(p^2)^2}\int (l\cdot p)^2 f(l,p)\ \mathrm{d}^n l\,.\end{aligned} \tag{C.6}$$

Since we will use this formula later, let us show how it is derived too. As in the previous case, we start with the definition:

$$X^{\mu\nu}(p) \equiv \int l^\mu l^\nu f(l,p)\ \mathrm{d}^n l\,. \tag{C.7}$$

It is again apparent that we can write

$$X^{\mu\nu}(p) = g^{\mu\nu}X_2(p) + p^\mu p^\nu X_{11}(p)\,. \tag{C.8}$$

To proceed further, we multiply this expression consecutively by $p^2 g^{\mu\nu}$ and $p^\mu p^\nu$ which leads to

$$n\,p^2 X_2(p) + (p^2)^2 X_{11}(p) = \int l^2\, p^2 f(l,p)\ \mathrm{d}^n l\,, \tag{C.9}$$

$$p^2 X_2(p) + (p^2)^2 X_{11}(p) = \int (l\cdot p)^2 f(l,p)\ \mathrm{d}^n l\,. \tag{C.10}$$

Note that above we have consistently used ${g_\mu}^\mu = n$. Now, we just need to solve this simple system of two linear equations. Subtracting the equations, we find

$$X_2(p) = \frac{1}{(1-n)p^2}\int \left[(l\cdot p)^2 - l^2 p^2\right] f(l,p)\ \mathrm{d}^n l\,, \tag{C.11}$$

and after substituting this result back we reveal

$$X_{11}(p) = \frac{1}{(p^2)^2}\int (l\cdot p)^2 f(l,p)\ \mathrm{d}^n l - \frac{1}{p^2}X_2(p)\,. \tag{C.12}$$

Collecting the previous expressions leads through definition (C.8) to original reduction formula (C.6).

C.2 Examples of tensorial reduction

As an example we first show the simplification of the following term into scalar one-loop integrals:

$$I_1 \equiv (2\pi\mu)^{4-n}\int \mathrm{d}^n l\,\frac{(l\cdot q)^2}{(l^2-m^2)(l+q)^2}\,. \tag{C.13}$$

Needless to say, q is here an external momentum. Note that in this section we will omit writing "$+i\epsilon$" in the propagators; we just tacitly assume it is still there. Since one can conveniently rewrite the scalar product $l \cdot q$ as

$$l \cdot q = \frac{1}{2}\left[(l+q)^2 - (l^2 - m^2) - q^2 - m^2\right], \tag{C.14}$$

we immediately see that we can partly cancel the scalar products containing loop momentum l in the numerator with the Feynman denominators and obtain

$$I_1 = (2\pi\mu)^{4-n} \int \mathrm{d}^n l \; \frac{1}{2}\left[\frac{(l\cdot q)}{l^2 - m^2} - \frac{(l\cdot q)}{(l+q)^2} - \frac{(l\cdot q)(q^2+m^2)}{(l^2-m^2)(l+q)^2}\right]. \tag{C.15}$$

The first term disappears due to the fact that the denominator is symmetric under the loop momentum sign change $l^\mu \to -l^\mu$ while the numerator is antisymmetric. In the second term we use the integration variable shift $l \to l - q$ to see that it again vanishes, partly due to the symmetric integration and partly due to the fact that in the dimensional regularization it holds $A_0(0) = 0$. Using identity (C.14) again in the remaining term one finds

$$I_1 = -(2\pi\mu)^{4-n} \int \mathrm{d}^n l \; \frac{q^2+m^2}{4}\left[\frac{1}{l^2 - m^2} - \frac{1}{(l+q)^2} - \frac{q^2+m^2}{(l^2-m^2)(l+q)^2}\right]. \tag{C.16}$$

The second term in the bracket again disappears and we can write the result in terms of scalar one-loop integrals defined in Appendix A:

$$I_1 = \frac{i\pi^2}{4}(q^2+m^2)\left[(q^2+m^2)B_0\Big(q^2;0,m^2\Big) - A_0\Big(m^2\Big)\right]. \tag{C.17}$$

As the second example we show the tensorial reduction of the term

$$I_2 = (2\pi\mu)^{4-n} \int \mathrm{d}^n l \, \frac{l^\kappa l^\lambda}{(l+q)^2(l-p)^2}\,. \tag{C.18}$$

The free indices κ and λ might be contracted with γ-matrices or other external momenta which can be taken outside of the integral. Naïvely, one could think that this integral depends on two external momenta and thus one needs to use an identity for two external momenta and two free indices, which is quite lengthy. However, one can apply a shift of the loop momentum $l \to l + p$ and obtain

$$I_2 = (2\pi\mu)^{4-n} \int \mathrm{d}^n l \, \frac{(l+p)^\kappa (l+p)^\lambda}{l^2(l+p+q)^2} = (2\pi\mu)^{4-n} \int \mathrm{d}^n l \, \frac{l^\kappa l^\lambda + l^\kappa p^\lambda + l^\lambda p^\kappa + p^\kappa p^\lambda}{l^2(l+r)^2}\,, \tag{C.19}$$

where we have defined $r = p + q$. Hence, we changed the situation in which it seemed we need to deal with two external momenta p and q to only one external momentum r. Consequently, we can make use of identities (C.1) and (C.6) which results into

$$(2\pi\mu)^{4-n} \int \mathrm{d}^n l \, \frac{l^\kappa l^\lambda}{l^2(l+r)^2} = \frac{n r^\kappa r^\lambda - r^2 g^{\kappa\lambda}}{4(n-1)} (2\pi\mu)^{4-n} \int \mathrm{d}^n l \, \frac{1}{l^2(l+r)^2}, \tag{C.20}$$

$$(2\pi\mu)^{4-n} \int \mathrm{d}^n l \, \frac{l^\kappa p^\lambda + l^\lambda p^\kappa}{l^2(l+r)^2} = \frac{r^\kappa p^\lambda + r^\lambda p^\kappa}{r^2} (2\pi\mu)^{4-n} \int \mathrm{d}^n l \, \frac{l\cdot r}{l^2(l+r)^2} \tag{C.21}$$

Altogether, for the integral I_2 we can then write

$$I_2 = \left[\frac{nr^\kappa r^\lambda - r^2 g^{\kappa\lambda}}{4(n-1)} - \frac{1}{2}\left(p^\kappa q^\lambda + p^\lambda q^\kappa\right)\right] i\pi^2 B_0\Big(r^2; 0, 0\Big)\,. \tag{C.22}$$

Now, we just need to perform properly the limit $n \to 4$. Using $2\varepsilon = 4 - n$ we have

$$\frac{n}{n-1} = 1 + \frac{1}{n-1}\,, \tag{C.23}$$

$$\frac{1}{n-1} = \frac{1}{3-2\varepsilon} = \frac{1}{3}\frac{1}{\left(1-\frac{2}{3}\varepsilon\right)} = \frac{1}{3} + \frac{2}{9}\varepsilon + \mathcal{O}(\varepsilon^2)\,. \tag{C.24}$$

Note that it was necessary to expand these terms up to the linear order in ε since B_0 functions are UV-divergent, which is in the dimensional regularization given by the presence of the $1/\varepsilon$ term. The result for I_2 thus finally reads

$$\begin{aligned} I_2 = {} & \frac{1}{18}\left[(p+q)^\kappa (p+q)^\lambda - (p+q)^2 g^{\kappa\lambda}\right] \\ & + \frac{i\pi^2}{12} B_0\Big((p+q)^2; 0, 0\Big)\left[4\left(p^\kappa p^\lambda + q^\lambda q^\kappa\right) - 2\left(p^\kappa q^\lambda + p^\lambda q^\kappa\right) - (p+q)^2 g^{\kappa\lambda}\right]. \end{aligned} \tag{C.25}$$

Appendix D

VMD inspired model for the $\eta^{(\prime)}$ transition form factors

For a phenomenological model of a transition between the $\eta^{(\prime)}$ meson and off-shell photons we need to take into account a strange quark content of $\eta^{(\prime)}$. It is more convenient to work in the quark-flavor basis than in the octet-singlet one. In such a basis, the vector currents related to physical states of ω, ρ^0 and ϕ mesons are identical to the basis currents. Having a standard definition of vector currents and pseudoscalar densities in the octet-singlet basis (now $a = 0, 1, \ldots, 8$)

$$j^a_\mu(x) \equiv \bar{q}(x)\gamma_\mu T^a q(x)\,, \quad j^a(x) \equiv \bar{q}(x) i\gamma_5 T^a q(x)\,, \tag{D.1}$$

we can write for the currents of our interest

$$j^\omega_\mu = \frac{1}{2}\Big[\bar{u}\gamma_\mu u + \bar{d}\gamma_\mu d\Big] = \sqrt{\frac{2}{3}} j^0_\mu + \frac{1}{\sqrt{3}} j^8_\mu \equiv j^{\ell 0}_\mu\,, \tag{D.2}$$

$$j^{\rho^0}_\mu = \frac{1}{2}\Big[\bar{u}\gamma_\mu u - \bar{d}\gamma_\mu d\Big] = j^3_\mu \qquad\qquad \equiv j^{\ell 1}_\mu\,, \tag{D.3}$$

$$j^\phi_\mu = \frac{1}{\sqrt{2}}\Big[\bar{s}\gamma_\mu s\Big] \qquad\quad = \frac{1}{\sqrt{3}} j^0_\mu - \sqrt{\frac{2}{3}} j^8_\mu \equiv j^{\mathrm{s}}_\mu\,. \tag{D.4}$$

Note that for simplicity we have left out the spacetime coordinates x of the currents and quark fields. Above, we see the relations between neutral-meson-related vector currents, appropriate combinations of quark-flavor-diagonal vector currents, their octet-singlet basis decomposition and finally the quark-flavor basis definition. The electromagnetic current reads

$$\frac{1}{e} j^{\mathrm{em}}_\mu = \frac{2}{3}\bar{u}\gamma_\mu u - \frac{1}{3}\bar{d}\gamma_\mu d - \frac{1}{3}\bar{s}\gamma_\mu s = \frac{1}{3} j^{\ell 0}_\mu + j^{\ell 1}_\mu - \frac{\sqrt{2}}{3} j^{\mathrm{s}}_\mu\,. \tag{D.5}$$

In the chiral limit, the PVV correlator $\Pi(r^2; p^2, q^2)$ is defined in the octet-singlet basis by

$$d^{abc}\epsilon_{\mu\nu\alpha\beta} p^\alpha q^\beta \Pi(r^2; p^2, q^2) \equiv \int \mathrm{d}^4x\, \mathrm{d}^4y\, e^{ip\cdot x + iq\cdot y} \langle 0|T[j^a(0) j^b_\mu(x) j^c_\nu(y)]|0\rangle \tag{D.6}$$

with $r = p + q$. In the above formulae we have used $d^{abc} \equiv 2\,\mathrm{Tr}\Big[\{T^a, T^b\}T^c\Big]$. As it is common, we define $T^a \equiv \lambda^a/2$, where λ^a denote the Gell-Mann matrices in the flavor space and d^{abc} are the U(3) symmetric symbols.

If we, for simplicity, schematically rewrite (D.6) as $\mathrm{corr}(j^a, j^b_\mu, j^c_\nu) = d^{abc}\Pi$ then — using linearity and definitions (D.2), (D.3) and (D.4) — we get only three non-trivial combinations of currents in the quark-flavor basis:

$$\mathrm{corr}(j^\ell, j^{\ell 0}_\mu, j^{\ell 0}_\nu) = \Pi^\ell \,, \tag{D.7}$$

$$\mathrm{corr}(j^\ell, j^{\ell 1}_\mu, j^{\ell 1}_\nu) = \Pi^\ell \,, \tag{D.8}$$

$$\mathrm{corr}(j^\mathrm{s}, j^\mathrm{s}_\mu, j^\mathrm{s}_\nu) = \sqrt{2}\,\Pi^\mathrm{s} \,. \tag{D.9}$$

In this way we have found the normalization relation among bases (there is an additional factor $\sqrt{2}$ in the case of the strange correlator). Note that $j^\ell \equiv \frac{i}{2}\big[\bar{u}\gamma_5 u + \bar{d}\gamma_5 d\big]$ and $j^\mathrm{s} \equiv \frac{i}{\sqrt{2}}\big[\bar{s}\gamma_5 s\big]$. In Eqs. (D.7-D.9) we have gone beyond the chiral limit: from now on we will distinguish between the light and strange correlators.

Since the quark content of the $\eta^{(\prime)}$ physical states is not equal to the U(3) isoscalar states, there is a mixing between η and η' mesons. In the quark-flavor basis, this mixing occurs (for $A \in \{\ell, \mathrm{s}\}$) among the states $|\eta^A\rangle$ defined as $\langle 0|j^A|\eta^B\rangle = \delta^{AB}\mathcal{Z}_{\eta^A}$ together with $\langle \eta^A|\eta^B\rangle = \delta^{AB}$. The resulting mixing (in the quark-flavor basis) can be written as

$$|\eta\rangle = \cos\phi\,|\eta^\ell\rangle - \sin\phi\,|\eta^\mathrm{s}\rangle \,, \tag{D.10}$$

$$|\eta'\rangle = \sin\phi\,|\eta^\ell\rangle + \cos\phi\,|\eta^\mathrm{s}\rangle \,. \tag{D.11}$$

Next, we define the correlator $\eta^A VV$ for each basis state (again, $A \in \{\ell, \mathrm{s}\}$):

$$\Pi_{\eta^A VV}(p^2, q^2) \equiv \frac{1}{\mathcal{Z}_{\eta^A}} \lim_{r^2 \to M_\eta^2} (r^2 - M_\eta^2)\Pi^A(r^2; p^2, q^2) \,. \tag{D.12}$$

The factors $\mathcal{Z}_{\eta^A} = \langle 0|j^A|\eta^A\rangle$ are related to the pion case $\mathcal{Z}_\pi = B_0 F_\pi$ by $\mathcal{Z}_{\eta^A} = \mathcal{Z}_\pi f_A$; we have introduced the ratio of the decay constants $f_A \equiv F_A/F_\pi$. For the ηVV correlator we can then finally write

$$\Pi_{\eta VV}(p^2, q^2) = \cos\phi\,\Pi_{\eta^\ell VV} - \sqrt{2}\sin\phi\,\Pi_{\eta^\mathrm{s} VV} \,. \tag{D.13}$$

The $\sqrt{2}$ factor comes from (D.9) and the mixing factors from (D.10).

To avoid difficulties connected with defining the resulting ηVV correlator all the way through (D.12), we will use the vector-meson dominance (VMD) ansatz

$$\Pi^\mathrm{VMD}_{\eta^A VV}(p^2, q^2) = -\frac{N_\mathrm{c}}{8\pi^2 F_A}\frac{M_A^4}{(p^2 - M_A^2)(q^2 - M_A^2)} \,, \tag{D.14}$$

where the light and strange channels are saturated by associated resonances: $M_\ell = M_{\rho^0/\omega}$ and $M_\mathrm{s} = M_\phi$. Using meson-specific factors shown in Tab. D.1, we can finally define the doubly off-shell electromagnetic transition form factor of the $\eta^{(\prime)}$ meson in the quark-flavor basis:

$$\mathcal{F}_{\eta\gamma^*\gamma^*}(p^2, q^2) = \sum_\mathcal{V} \kappa_\mathcal{V}^2(\kappa_{\eta\mathcal{V}} f_{A(\mathcal{V})})\Pi_{\eta^{A(\mathcal{V})}VV}(p^2, q^2) \,. \tag{D.15}$$

For $A(\mathcal{V})$ above we simply substitute $A(\rho^0) = A(\omega) = \ell$ and $A(\phi) = \mathrm{s}$. In the VMD case (inserting ansatz (D.14)) the form factor becomes

$$\begin{aligned} e^2\mathcal{F}^\mathrm{VMD}_{\eta\gamma^*\gamma^*}(p^2, q^2) = -\frac{N_\mathrm{c}}{8\pi^2 F_\pi}\frac{2e^2}{3}\Bigg[&\frac{5}{3}\frac{\cos\phi}{f_\ell}\frac{M^4_{\rho^0/\omega}}{(p^2 - M^2_{\rho^0/\omega})(q^2 - M^2_{\rho^0/\omega})} \\ &- \frac{\sqrt{2}}{3}\frac{\sin\phi}{f_\mathrm{s}}\frac{M_\phi^4}{(p^2 - M_\phi^2)(q^2 - M_\phi^2)}\Bigg] \,. \end{aligned} \tag{D.16}$$

$\mathcal{V}$	ω	ρ^0	ϕ
$\kappa_{\mathcal{V}}$	$e/3$	e	$-e\sqrt{2}/3$
$\kappa_{\eta\mathcal{V}}$	$\cos(\phi)/f_\ell$	$\cos(\phi)/f_\ell$	$-\sqrt{2}\sin(\phi)/f_\mathrm{s}$
$\kappa_{\eta'\mathcal{V}}$	$\sin(\phi)/f_\ell$	$\sin(\phi)/f_\ell$	$\sqrt{2}\cos(\phi)/f_\mathrm{s}$

Table D.1: Overlaps and mixing coefficients used in the $\eta^{(\prime)}$ transition form factor derivation according to formula (D.15). The overlaps $\kappa_{\mathcal{V}}$ of the electromagnetic current j_μ^{em} with the meson-related current $j_\mu^{\mathcal{V}}$ are given by the coefficients in (D.5). The $\sqrt{2}$ factor in $\kappa_{\eta^{(\prime)}\phi}$ comes from (D.9).

To get the η' form factor, it is then only necessary to perform the following substitution:

$$\mathcal{F}^{\mathrm{VMD}}_{\eta'\gamma^*\gamma^*}(p^2,q^2) = \mathcal{F}^{\mathrm{VMD}}_{\eta\gamma^*\gamma^*}(p^2,q^2)\Big|_{\substack{\cos\phi\to\sin\phi\\ \sin\phi\to-\cos\phi}} . \tag{D.17}$$

As a simple aplication, we can have a look on the two-photon decay of a pseudoscalar $P \in \{\pi^0, \eta^{(\prime)}\}$. The decay width of such a process can be expressed as follows:

$$\Gamma^{\mathrm{VMD}}_{P\to\gamma\gamma} = \frac{1}{2}\frac{1}{16\pi M_P}\left(\frac{\alpha}{\pi F_\pi}\right)^2 \frac{M_P^4}{2}\kappa_P^2 . \tag{D.18}$$

Of course, for a neutral pion we would have $\kappa_{\pi^0} = 1$. In the $\eta^{(\prime)}$ case we can write

$$\kappa_{\eta^{(\prime)}} = \frac{3}{2e^2}\sum_{\mathcal{V}} \kappa_{\mathcal{V}}^2 \kappa_{\eta^{(\prime)}\mathcal{V}} , \tag{D.19}$$

which becomes (cf. (D.16) for $p^2 = q^2 = 0$)

$$\kappa_\eta = \frac{5}{3}\frac{\cos\phi}{f_\ell} - \frac{\sqrt{2}}{3}\frac{\sin\phi}{f_\mathrm{s}} \simeq 0.98 , \tag{D.20}$$

$$\kappa_{\eta'} = \frac{5}{3}\frac{\sin\phi}{f_\ell} + \frac{\sqrt{2}}{3}\frac{\cos\phi}{f_\mathrm{s}} \simeq 1.26 . \tag{D.21}$$

Note that e.g. $\kappa_\eta \simeq 0.98$ is consistent with experiment, although it differs significantly from a naïve WZW-based calculation [31] for which $\kappa_\eta = 1/\sqrt{3}$.

Appendix E

Form factors in $P \to \ell^+\ell^-$ decays

In this appendix we apply the approach explained in Section 4.2 to the $P \to \ell^+\ell^-$ decays. We would like to show how the building block for the matrix element looks like in this case and calculate the coefficients for the specific transition form factor models.

On account of the Lorentz symmetry and parity conservation, the on-shell matrix element of the $P \to \ell^+\ell^-$ process can be written in terms of just one pseudoscalar form factor in the following form:

$$i\mathcal{M}_{P\to\ell^+\ell^-} = P_{P\to\ell^+\ell^-}\left[\bar{u}(\vec{q}_1)\gamma_5 v(\vec{q}_2)\right]. \tag{E.1}$$

Subsequently, the decay width reads

$$\Gamma(P \to \ell^+\ell^-) = \frac{2M_P^2|P_{P\to\ell^+\ell^-}|^2}{16\pi M_P}\sqrt{1-\frac{4m_\ell^2}{M_P^2}}\,. \tag{E.2}$$

Taking into account only the leading-order (LO) contribution in the QED expansion, we find for the pseudoscalar form factor

$$P^{\mathrm{LO}}_{P\to\ell^+\ell^-} = \frac{ie^4 m_\ell}{M_P^2}\int\frac{\mathrm{d}^4 l}{(2\pi)^4}\frac{\mathcal{F}_{P\gamma^*\gamma^*}(p^2,q^2)\lambda(M_P^2,p^2,q^2)}{p^2q^2(l^2-m_\ell^2)}\,. \tag{E.3}$$

Here, $p = l - q_1$ and $q = l + q_2$, where q_1 and q_2 are the lepton momenta and λ is the triangle Källén function. For the rational resonance-saturation models, we will use in agreement with substitution (4.3) the following definition:

$$\begin{aligned} P^h_{P\to\ell^+\ell^-}\left[h(c_1,c_2,M_{V_1}^2,M_{V_2}^2)\right] &= \frac{ie^4 m_\ell}{M_P^2}\left(-\frac{N_{\mathrm{c}}}{12\pi^2 F_\pi}\right) \\ &\quad\times\int\frac{\mathrm{d}^4 l}{(2\pi)^4}\frac{h(c_1,c_2,M_{V_1}^2,M_{V_2}^2)\lambda(M_P^2,p^2,q^2)}{(l^2-m_\ell^2)}\,. \end{aligned} \tag{E.4}$$

In the case of the process $\eta \to \mu^+\mu^-$ within the vector-meson dominance (VMD) model, we can write (cf. (D.16))

$$\begin{aligned} &P^{\mathrm{VMD}}_{\eta\to\mu^+\mu^-} \\ &= \left\{\frac{5}{3}\frac{\cos\phi}{f_\ell}P^h_{\eta\to\mu^+\mu^-}\left[h(1,1,M_{\rho/\omega}^2,M_{\rho/\omega}^2)\right] - \frac{\sqrt{2}}{3}\frac{\sin\phi}{f_{\mathrm{s}}}P^h_{\eta\to\mu^+\mu^-}\left[h(1,1,M_\phi^2,M_\phi^2)\right]\right\}. \end{aligned} \tag{E.5}$$

Note that in the pion case we would simply have

$$P^{\mathrm{VMD}}_{\pi^0\to e^+e^-} = P^{h}_{\pi^0\to e^+e^-}\Big[h(1,1,M^2_{\rho/\omega},M^2_{\rho/\omega})\Big]\,. \tag{E.6}$$

After recalling (4.12) we know that the previous expressions might be obtained in terms of linear combinations of the building blocks $P^{h}_{P\to\ell^+\ell^-}\Big[g(M^2_{V_1},M^2_{V_2})\Big]$. Using the dimensional regularization, the dimensional reduction scheme [50, 51] and Passarino–Veltman reduction [49], the explicit result of the necessary loop integration in terms of scalar one-loop integrals reads

$$\begin{aligned}
&P^{h}_{P\to\ell^+\ell^-}\Big[g(M^2_{V_1},M^2_{V_2})\Big] = -\frac{e^4 m_\ell}{16\pi^2}\left(-\frac{N_{\mathrm{c}}}{12\pi^2 F_\pi}\right)\\
&\times\left\{\frac{M^2_{V_1}}{2m^2_\ell}\Big[B_0(0,M^2_{V_1},M^2_{V_1}) - B_0(m^2_\ell,m^2_\ell,M^2_{V_1}) + 1\Big]\right.\\
&+\frac{M^2_{V_1}}{M^2_P}\Big[B_0(m^2_\ell,m^2_\ell,M^2_{V_2}) - B_0(m^2_\ell,m^2_\ell,M^2_{V_1})\Big] - B_0(m^2_\ell,m^2_\ell,M^2_{V_1})\\
&\left.-\frac{1}{2}\Big[1 + B_0(0,m^2_\ell,m^2_\ell) - \tilde{C}_0(m^2_\ell,m^2_\ell,M^2_P,M^2_{V_1},m^2_\ell,M^2_{V_2})\Big]\right\} + \Big\{M^2_{V_1}\leftrightarrow M^2_{V_2}\Big\}\,.
\end{aligned} \tag{E.7}$$

Above, it was convenient to introduce the following combination of the three-point scalar one-loop function C_0 and the Källén triangle function λ:

$$\tilde{C}_0(m^2,m^2,M^2_1,M^2_2,m^2,M^2_3) \equiv \frac{1}{M^2_1}\lambda(M^2_1,M^2_2,M^2_3)\,C_0(m^2,m^2,M^2_1,M^2_2,m^2,M^2_3)\,. \tag{E.8}$$

In what follows, we would like to provide some basic examples of the decomposition of the loop integrals containing various models for transition form factors in the case of the rare decay of a neutral pion. Lets start with some definitions. The VMD ansatz for the electromagnetic transition form factor of a neutral pion takes a simple form

$$\mathcal{F}^{\mathrm{VMD}}_{\pi^0\gamma^*\gamma^*}(p^2,q^2) = -\frac{N_{\mathrm{c}}}{12\pi^2 F_\pi}\frac{M^4_V}{(p^2-M^2_V)(q^2-M^2_V)}\,. \tag{E.9}$$

The lowest-meson dominance (LMD) model [52], where also the lowest-lying pseudoscalar multiplet was taken into account, gives the following result:

$$\mathcal{F}^{\mathrm{LMD}}_{\pi^0\gamma^*\gamma^*}(p^2,q^2) = \mathcal{F}^{\mathrm{VMD}}_{\pi^0\gamma^*\gamma^*}(p^2,q^2)\left[1-\frac{4\pi^2F^2_\pi}{N_{\mathrm{c}}M^4_V}(p^2+q^2)\right]. \tag{E.10}$$

As the last example we introduce the two-hadron saturation (THS) model proposed in Paper III, which for the PVV correlator takes into account two meson multiplets in both vector and pseudoscalar channels:

$$\begin{aligned}
\mathcal{F}^{\mathrm{THS}}_{\pi^0\gamma^*\gamma^*}(p^2,q^2) = -\frac{N_{\mathrm{c}}}{12\pi^2F_\pi}&\left\{1+\frac{\kappa}{2N_{\mathrm{c}}}\frac{p^2q^2}{(4\pi F_\pi)^4} - \frac{4\pi^2F^2_\pi(p^2+q^2)}{N_{\mathrm{c}}M^2_{V_1}M^2_{V_2}}\left[6+\frac{p^2q^2}{M^2_{V_1}M^2_{V_2}}\right]\right\}\\
&\times\frac{M^4_{V_1}M^4_{V_2}}{(p^2-M^2_{V_1})(p^2-M^2_{V_2})(q^2-M^2_{V_1})(q^2-M^2_{V_2})}\,.
\end{aligned} \tag{E.11}$$

In terms of decomposition (4.3) we can write for the amplitudes

$$\mathcal{M}_{1\gamma\mathrm{IR}}^{\mathrm{VMD}} = \mathcal{M}_{1\gamma\mathrm{IR}}^{h}\Big[h(1,1,M_V^2,M_V^2)\Big]\,, \tag{E.12}$$

$$\mathcal{M}_{1\gamma\mathrm{IR}}^{\mathrm{LMD}} = \mathcal{M}_{1\gamma\mathrm{IR}}^{h}\Big[h\Big(c_1^{\mathrm{LMD}},2c_1^{\mathrm{LMD}}-1,M_V^2,M_V^2\Big)\Big]\,, \tag{E.13}$$

$$\begin{aligned}\mathcal{M}_{1\gamma\mathrm{IR}}^{\mathrm{THS}} = {}& \frac{1}{4}\mathcal{M}_{1\gamma\mathrm{IR}}^{h}\Big[h\Big(4c_{1,1}^{\mathrm{THS}},4c_{2,1}^{\mathrm{THS}},M_{V_1}^2,M_{V_2}^2\Big)\Big]\\ &+\frac{1}{4}\mathcal{M}_{1\gamma\mathrm{IR}}^{h}\Big[h\Big(0,4c_{2,2}^{\mathrm{THS}},M_{V_1}^2,M_{V_1}^2\Big)\Big]\\ &+(M_{V_1}^2\leftrightarrow M_{V_2}^2)\,,\end{aligned} \tag{E.14}$$

where the coefficients $c_{1,i}^{\mathrm{model}}$ and $c_{2,i}^{\mathrm{model}}$ have the following form:

$$c_1^{\mathrm{LMD}} = 1-\frac{4\pi^2F_\pi^2}{N_{\mathrm{c}}M_V^2}\,, \tag{E.15}$$

$$c_{1,1}^{\mathrm{THS}} = \frac{M_{V_2}^2}{M_{V_2}^2-M_{V_1}^2}\left(1-\frac{24\pi^2F_\pi^2}{N_{\mathrm{c}}M_{V_2}^2}\right), \tag{E.16}$$

$$c_{2,1}^{\mathrm{THS}} = -\frac{M_{V_1}^2M_{V_2}^2}{(M_{V_2}^2-M_{V_1}^2)^2}\left[1+\frac{\kappa M_{V_1}^2M_{V_2}^2}{2N_{\mathrm{c}}(4\pi F_\pi)^4}-\frac{7(2\pi F_\pi)^2}{N_{\mathrm{c}}M_{V_1}^2}\left(1+\frac{M_{V_1}^2}{M_{V_2}^2}\right)\right], \tag{E.17}$$

$$c_{2,2}^{\mathrm{THS}} = \frac{M_{V_2}^4}{(M_{V_2}^2-M_{V_1}^2)^2}\left[1+\frac{\kappa M_{V_1}^4}{2N_{\mathrm{c}}(4\pi F_\pi)^4}-\frac{(4\pi F_\pi)^2}{2N_{\mathrm{c}}M_{V_2}^2}\left(6+\frac{M_{V_1}^2}{M_{V_2}^2}\right)\right]. \tag{E.18}$$

We can find the above listed constants from projecting on the product of the normalized form factor and the photon propagators: for instance we have

$$c_{2,2}^{\mathrm{THS}} = \frac{1}{\mathcal{F}_{\pi^0\gamma^*\gamma^*}(0,0)}\lim_{p^2,q^2\to M_{V_1}^2}\frac{\mathcal{F}_{\pi^0\gamma^*\gamma^*}^{\mathrm{THS}}(p^2,q^2)}{p^2q^2}\,(p^2-M_{V_1}^2)(q^2-M_{V_1}^2)\,. \tag{E.19}$$

Taking into account decomposition (4.8) into building blocks (E.7), one recovers formulae (A.5-A.7) from Paper III.

Bibliography

[1] **KTeV** Collaboration, E. Abouzaid *et al.*, "Measurement of the rare decay $\pi^0 \to e^+e^-$," *Phys. Rev.* **D75** (2007) 012004, arXiv:hep-ex/0610072.

[2] A. E. Dorokhov and M. A. Ivanov, "Rare decay $\pi^0 \to e^+e^-$: Theory confronts KTeV data," *Phys. Rev.* **D75** (2007) 114007, arXiv:0704.3498.

[3] P. Vasko and J. Novotný, "Two-loop QED radiative corrections to the decay $\pi^0 \to e^+e^-$: The virtual corrections and soft-photon bremsstrahlung," *JHEP* **1110** (2011) 122, arXiv:1106.5956.

[4] Bergström, L., "Radiative corrections to pseudoscalar meson decays," *Z. Phys.* **C20** (1983) 135–140.

[5] A. Dorokhov, E. Kuraev, Y. Bystritskiy, and M. Secansky, "QED radiative corrections to the decay $\pi^0 \to e^+e^-$," *Eur. Phys. J.* **C55** (2008) 193–198, arXiv:0801.2028.

[6] **NA62** Collaboration, C. Lazzeroni *et al.*, "Measurement of the π^0 electromagnetic transition form factor slope," *Phys. Lett.* **B768** (2017) 38–45, arXiv:1612.08162 [hep-ex].

[7] K. Mikaelian and J. Smith, "Radiative corrections to the decay $\pi^0 \to \gamma e^+e^-$," *Phys. Rev.* **D5** (1972) 1763–1773.

[8] **A2** Collaboration, P. Adlarson *et al.*, "Measurement of the $\pi^0 \to e^+e^-\gamma$ Dalitz decay at the Mainz Microtron," *Phys. Rev.* **C95** no. 2, (2017) 025202, arXiv:1611.04739 [hep-ex].

[9] M. Knecht and A. Nyffeler, "Resonance estimates of $\mathcal{O}(p^6)$ low-energy constants and QCD short distance constraints," *Eur. Phys. J.* **C21** (2001) 659–678, arXiv:hep-ph/0106034.

[10] S. J. Brodsky and G. P. Lepage, "Large Angle Two Photon Exclusive Channels in Quantum Chromodynamics," *Phys. Rev.* **D24** (1981) 1808.

[11] **NA60** Collaboration, R. Arnaldi *et al.*, "Study of the electromagnetic transition form-factors in $\eta \to \mu^+\mu^-\gamma$ and $\omega \to \mu^+\mu^-\pi^0$ decays with NA60," *Phys. Lett.* **B677** (2009) 260–266, arXiv:0902.2547.

[12] S. Weinberg, "Phenomenological Lagrangians," *Physica* **A96** (1979) 327.

[13] F. Wilczek, "Problem of Strong P and T Invariance in the Presence of Instantons," *Phys. Rev. Lett.* **40** (1978) 279–282.

[14] R. D. Peccei and H. R. Quinn, "CP Conservation in the Presence of Instantons," *Phys. Rev. Lett.* **38** (1977) 1440–1443.

[15] R. D. Peccei and H. R. Quinn, "Constraints Imposed by CP Conservation in the Presence of Instantons," *Phys. Rev.* **D16** (1977) 1791–1797.

[16] **Particle Data Group** Collaboration, C. Patrignani *et al.*, "Review of Particle Physics," *Chin. Phys.* **C40** no. 10, (2016) 100001.

[17] C. Vafa and E. Witten, "Eigenvalue Inequalities for Fermions in Gauge Theories," *Commun. Math. Phys.* **95** (1984) 257.

[18] G. 't Hooft, C. Itzykson, A. Jaffe, H. Lehmann, P. K. Mitter, I. M. Singer, and R. Stora, "Recent Developments in Gauge Theories. Proceedings, Nato Advanced Study Institute, Cargese, France, August 26 - September 8, 1979," *NATO Sci. Ser. B* **59** (1980) pp.1–438.

[19] Y. Nambu, "Quasiparticles and Gauge Invariance in the Theory of Superconductivity," *Phys. Rev.* **117** (1960) 648–663.

[20] J. Goldstone, "Field Theories with Superconductor Solutions," *Nuovo Cim.* **19** (1961) 154–164.

[21] R. Kaiser and H. Leutwyler, "Large N_c in chiral perturbation theory," *Eur. Phys. J.* **C17** (2000) 623–649, `arXiv:hep-ph/0007101 [hep-ph]`.

[22] S. L. Adler, "Consistency conditions on the strong interactions implied by a partially conserved axial vector current," *Phys. Rev.* **137** (1965) B1022–B1033.

[23] C. G. Callan, Jr., S. R. Coleman, J. Wess, and B. Zumino, "Structure of phenomenological Lagrangians. 2.," *Phys. Rev.* **177** (1969) 2247–2250.

[24] J. Gasser and H. Leutwyler, "Chiral Perturbation Theory to One Loop," *Annals Phys.* **158** (1984) 142.

[25] S. Scherer and M. R. Schindler, "A Primer for Chiral Perturbation Theory," *Lect. Notes Phys.* **830** (2012) pp.1–338.

[26] S. L. Adler and W. A. Bardeen, "Absence of higher order corrections in the anomalous axial vector divergence equation," *Phys. Rev.* **182** (1969) 1517–1536.

[27] H. W. Fearing and S. Scherer, "Extension of the chiral perturbation theory meson Lagrangian to order p^6," *Phys. Rev.* **D53** (1996) 315–348, `arXiv:hep-ph/9408346 [hep-ph]`.

[28] J. Bijnens, L. Girlanda, and P. Talavera, "The Anomalous chiral Lagrangian of order p^6," *Eur. Phys. J.* **C23** (2002) 539–544, `arXiv:hep-ph/0110400 [hep-ph]`.

[29] J. Wess and B. Zumino, "Consequences of anomalous Ward identities," *Phys. Lett.* **B37** (1971) 95.

[30] E. Witten, "Global Aspects of Current Algebra,"
Nucl. Phys. **B223** (1983) 422–432.

[31] M. J. Savage, M. E. Luke, and M. B. Wise, "The rare decays $\pi^0 \to e^+e^-$, $\eta \to e^+e^-$ and $\eta \to \mu^+\mu^-$ in chiral perturbation theory,"
Phys. Lett. **B291** (1992) 481–483, arXiv:hep-ph/9207233.

[32] J. Bijnens, "Chiral perturbation theory beyond one loop,"
Prog. Part. Nucl. Phys. **58** (2007) 521–586,
arXiv:hep-ph/0604043 [hep-ph].

[33] G. Ecker, J. Gasser, A. Pich, and E. de Rafael, "The Role of Resonances in Chiral Perturbation Theory," *Nucl. Phys.* **B321** (1989) 311.

[34] J. Stern, H. Sazdjian, and N. H. Fuchs, "What $\pi - \pi$ scattering tells us about chiral perturbation theory," *Phys. Rev.* **D47** (1993) 3814–3838,
arXiv:hep-ph/9301244 [hep-ph].

[35] G. 't Hooft, "A Two-Dimensional Model for Mesons,"
Nucl. Phys. **B75** (1974) 461–470.

[36] E. Witten, "Baryons in the $1/N$ Expansion,"
Nucl. Phys. **B160** (1979) 57–115.

[37] J. S. Schwinger, "On Quantum electrodynamics and the magnetic moment of the electron," *Phys. Rev.* **73** (1948) 416–417.

[38] G. Kallen, *Quantenelektrodynamik*. New York, Springer, 1972.

[39] P. Golonka and Z. Was, "PHOTOS Monte Carlo: A Precision tool for QED corrections in Z and W decays," *Eur. Phys. J.* **C45** (2006) 97–107,
arXiv:hep-ph/0506026 [hep-ph].

[40] K. O. Mikaelian and J. Smith, "Radiative corrections to the invariant-mass spectrum of a dalitz pair," *Phys. Rev.* **D5** (1972) 2890–2895.

[41] G. B. Tupper, T. R. Grose, and M. A. Samuel, "Two Photon Exchange Effect in Radiative Corrections to $\pi^0 \to \gamma e^- e^+$,"
Phys. Rev. **D28** (1983) 2905.

[42] T. Feldmann, P. Kroll, and B. Stech, "Mixing and decay constants of pseudoscalar mesons: The Sequel," *Phys. Lett.* **B449** (1999) 339–346,
arXiv:hep-ph/9812269 [hep-ph].

[43] R. Escribano and J.-M. Frere, "Study of the η-η' system in the two mixing angle scheme," *JHEP* **06** (2005) 029, arXiv:hep-ph/0501072 [hep-ph].

[44] C. Hanhart, A. Kupść, U. G. Meißner, F. Stollenwerk, and A. Wirzba, "Dispersive analysis for $\eta \to \gamma\gamma^*$," *Eur. Phys. J.* **C73** no. 12, (2013) 2668,
arXiv:1307.5654 [hep-ph]. [Erratum: Eur. Phys. J.C75,no.6,242(2015)].

[45] C. Hanhart, S. Holz, B. Kubis, A. Kupść, A. Wirzba, and C. W. Xiao, "The branching ratio $\omega \to \pi^+\pi^-$ revisited," *Eur. Phys. J.* **C77** no. 2, (2017) 98,
arXiv:1611.09359 [hep-ph].

[46] G. 't Hooft and M. J. G. Veltman, "Scalar One Loop Integrals," *Nucl. Phys.* **B153** (1979) 365–401.

[47] R. Mertig, M. Bohm, and A. Denner, "FEYN CALC: Computer algebraic calculation of Feynman amplitudes," *Comput. Phys. Commun.* **64** (1991) 345–359.

[48] V. Shtabovenko, R. Mertig, and F. Orellana, "New Developments in FeynCalc 9.0," *Comput. Phys. Commun.* **207** (2016) 432–444, `arXiv:1601.01167 [hep-ph]`.

[49] G. Passarino and M. Veltman, "One-loop corrections for e^+e^- annihilation into $\mu^+\mu^-$ in the Weinberg model," *Nucl. Phys.* **B160** (1979) 151–207.

[50] W. Siegel, "Supersymmetric Dimensional Regularization via Dimensional Reduction," *Phys. Lett.* **B84** (1979) 193.

[51] Novotný, J., "Axial anomaly and dimensional regularization: A Review," *Czech. J. Phys.* **44** (1994) 633–661.

[52] M. Knecht, S. Peris, M. Perrottet, and E. de Rafael, "Decay of pseudoscalars into lepton pairs and large-N_C QCD," *Phys. Rev. Lett.* **83** (1999) 5230–5233, `arXiv:hep-ph/9908283`.

List of Tables

List of Figures

List of Abbreviations

χPT	Chiral Perturbation Theory
PVV	pseudoscalar-vector-vector
1γIR	one-photon-irreducible
BS	bremsstrahlung
c.t.	counter term
CMS	center-of-mass system
EFT	effective field theory
IR	infrared
LEC	low-energy constant
LMD	lowest-meson dominance
LO	leading order
NLO	next-to-leading order
NU	natural units
OPE	operator-product expansion
QCD	Quantum Chromodynamics
QED	Quantum Electrodynamics
QFT	quantum field theory
SI	Le Système international d'unités
SM	Standard Model
THS	two-hadron saturation
VMD	vector-meson dominance
WZW	Wess–Zumino–Witten

Paper I

Rare decay $\pi^0 \to e^+e^-$: on corrections beyond the leading order

Tomáš Husek, Karol Kampf and Jiří Novotný

Institute of Particle and Nuclear Physics, Faculty of Mathematics and Physics, Charles University in Prague
V Holešovičkách 2, Praha 8, Czech Republic

(Submitted on May 27, 2014)

Abstract: The preceding experimental and theoretical results on the rare decay $\pi^0 \to e^+e^-$ are briefly summarized. Already computed two-loop QED corrections are reviewed and the bremsstrahlung contribution beyond the soft-photon approximation is analytically calculated. The possible further contribution of QCD loop corrections is estimated using the leading logarithm approximation. The complete result can be used to fit the value of the contact interaction coupling $\chi^{(\mathrm{r})}$ to the recent KTeV experiment with the result $\chi^{(\mathrm{r})}(M_\rho) = 4.5 \pm 1.0$.

Keywords: 13.20.Cz Decays of π mesons, 12.39.Fe Chiral Lagrangians, 12.40.Vv Vector-meson dominance, 13.40.Ks Electromagnetic corrections to strong- and weak-interaction processes

I.1 Motivation

Experimental measurements of the rare decay of a neutral pseudoscalar meson to a lepton pair and its comparison with theoretical predictions offer an interesting way to study low-energy (long-distance) dynamics in the Standard Model (SM) [1, 2, 3]. Systematical theoretical treatment of the process dates back to 1959, when the first prediction of the decay rate was published by Drell [4]. While the possible contributions of the weak sector of the SM are small enough to be neglected, the leading order QED contribution is described by two virtual photon exchange triangle diagram. That is why the double off-shell pion transition form factor $F_{\pi^0\gamma^*\gamma^*}$, which is not known from the first principles, plays essential role.

Because of this one-loop structure for the leading order, the process is very rare and suppressed in the comparison to two photons decay ($\pi^0 \to \gamma\gamma$) by a factor of $2(\alpha m_e/M_{\pi^0})^2$ due to the approximate helicity conservation of the interaction and thus may be sensitive to possible effects of the physics beyond the SM (expected branching ratio from the pure SM calculation is about 10^{-7}).

Recently, this decay has attracted attention of the theorists again in connection with a new precise branching ratio measurement. The KTeV-E799-II experiment at Fermilab [5] has observed $\pi^0 \to e^+e^-$ events (altogether 794 candidates),

where $K_L \to 3\pi^0$ decay was used as a source of neutral pions. The KTeV result is

$$\frac{\Gamma(\pi^0 \to e^+e^-,\, x > 0.95)}{\Gamma(\pi^0 \to e^+e^-\gamma,\, x > 0.232)} = (1.685 \pm 0.064 \pm 0.027) \times 10^{-4}\,. \tag{I.1}$$

Here we have introduced the Dalitz variable

$$x \equiv \frac{(p+q)^2}{M^2} = \frac{(P-k)^2}{M^2} = 1 - \frac{2E_k}{M}\,, \tag{I.2}$$

where p, q and k are four-momenta of electron, positron and photon, respectively, $P = (p + q + k)$ is the four-momentum of neutral pion π^0 with a mass M and E_k is the energy of the real outgoing photon in the pion CMS. The lower bound of the Dalitz variable x is used to suppress the contribution of the Dalitz decay $\pi^0 \to e^+e^-\gamma$, which naturally arises with lower x.

By means of extrapolating the Dalitz branching ratio in (I.1) to the full range of x, the branching ratio of the neutral pion decay into an electron-positron pair was determined to be equal to

$$B(\pi^0 \to e^+e^-(\gamma),\, x > 0.95) = (6.44 \pm 0.25 \pm 0.22) \times 10^{-8}\,. \tag{I.3}$$

Here the first error is from data statistics alone and the second is the total systematic error. For the matter of interest, current PDG average value $(6.46 \pm 0.33) \times 10^{-8}$ [6] is mainly based on this new result.

The KTeV collaboration used the result (I.3) for further calculations. They used the early calculation of Bergström [7] to extrapolate the full radiative tail beyond $x > 0.95$ and to scale the result back up by the overall radiative corrections of 3.4 % to get the lowest order rate (with the final state radiation removed) for $\pi^0 \to e^+e^-$ process. The final result is

$$B^{\text{no-rad}}_{\text{KTeV}}(\pi^0 \to e^+e^-) = (7.48 \pm 0.29 \pm 0.25) \times 10^{-8}\,. \tag{I.4}$$

Subsequent comparison with theoretical predictions of the SM was made in [1, 2] using pion transition form factor data from CELLO [8] and CLEO [9] experiments. Finally, it has been found, that according to SM the result should be

$$B^{\text{no-rad}}_{\text{SM}}(\pi^0 \to e^+e^-) = (6.23 \pm 0.09) \times 10^{-8}\,. \tag{I.5}$$

This can be interpreted as a $3.3\,\sigma$ discrepancy between the theory and the experiment. Of course, the discrepancy initiated further theoretical investigation of its possible sources [10, 11]. Aside from the attempts to find the corresponding mechanism within the physics beyond the SM, also the possible revision of the SM predictions has been taken into account. Many corrections of this kind have been already made, but so far with no such a significant influence on the final result.

I.2 Leading order

According to the Lorentz symmetry the on-shell invariant matrix element of the $\pi^0 \to e^+e^-$ process can be generally written in terms of just one pseudoscalar form factor

$$i\mathcal{M}(\pi^0 \to e^+e^-) = \overline{u}(p,m)\gamma^5 v(q,m) P(p^2, q^2, P^2) \tag{I.6}$$

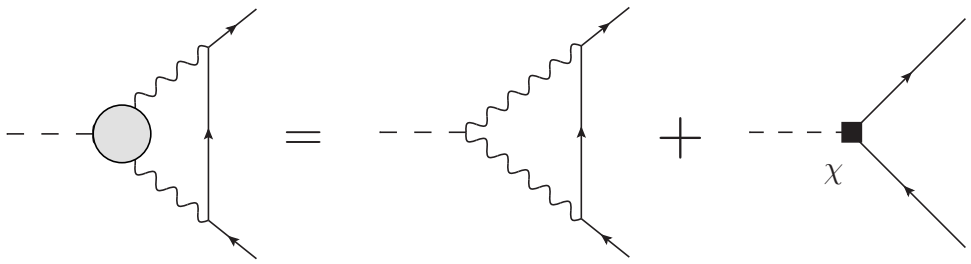

Figure I.1: Leading order contribution in the QED expansion and its representation in terms of the leading order of the chiral perturbation theory.

and, as a consequence, the total decay rate is given by

$$\Gamma(\pi^0 \to e^+e^-) = \frac{M}{8\pi}\sqrt{1-\nu^2}\left|P(m^2,m^2,M^2)\right|^2 , \tag{I.7}$$

where m stands for electron mass and $\nu \equiv 2m/M$. The leading order in the QED expansion is depicted as the left hand side of the graphical equation in the Fig. I.1. Here the shaded blob corresponds to the off-shell pion transition form factor $F_{\pi^0\gamma^*\gamma^*}(l^2,(P-l)^2)$ where l is the loop momentum. This form factor serves as an effective UV cut-off due to its $1/l^2$ asymptotics governed by OPE (see e.g. [12]) and the loop integral over $\mathrm{d}^4 l$ is therefore convergent. It is convenient to pick up explicitly the non-analytic contribution of the two-photon intermediate state (the imaginary part[1] is determined uniquely up to the normalization given by the on-shell value of $F_{\pi^0\gamma^*\gamma^*}(0,0) \equiv F_{\pi^0\gamma\gamma}$) and express the form factor in the following way (cf. [13])

$$\begin{aligned} &P^{\mathrm{LO}}(m^2,m^2,M^2) \\ &= \alpha^2 m F_{\pi^0\gamma\gamma}\frac{1}{\sqrt{1-\nu^2}}\left[\mathrm{Li}_2(z) - \mathrm{Li}_2\left(\frac{1}{z}\right) + i\pi\log(-z)\right] \\ &+ 2\alpha^2 m F_{\pi^0\gamma\gamma}\left\{\frac{3}{2}\log\left(\frac{m^2}{\mu^2}\right) - \frac{5}{2} + \chi\left(\frac{M^2}{\mu^2},\,\frac{m^2}{\mu^2}\right)\right\}. \end{aligned} \tag{I.8}$$

Here, Li_2 is the dilogarithm,

$$z = -\frac{1-\sqrt{1-\nu^2}}{1+\sqrt{1-\nu^2}} \tag{I.9}$$

and μ represents the intrinsic scale connected with the form factor[2] $F_{\pi^0\gamma^*\gamma^*}$. The function $\chi\left(P^2/\mu^2,\, m^2/\mu^2\right)$ represents the remainder which collects the contributions of higher intermediate states and is real and analytic[3] for $P^2/\mu^2 < 1$.

The leading order terms in the chiral expansion of the form factor P^{LO} are depicted as the right hand side of the graphical equation in Fig. I.1. The $\pi^0\gamma\gamma$ vertex in the loop graph is local and corresponds to the leading order term of the

[1] Imaginary part of this contribution is given by Cutkosky rules cutting the two virtual photon lines in the Fig. I.1.

[2] It means the scale at which the loop integral is effectively cut off. The term $\frac{3}{2}\log\left(m^2/\mu^2\right)$ represents the leading dependence of the form factor P on this scale.

[3] Note that the higher intermediate states, which appear when also the blob in the Fig. I.1 is cut, start for $P^2 \sim \mu^2$.

chiral expansion of the form factor $F_{\pi^0\gamma^*\gamma^*}$. Therefore the loop integration is no more UV finite and a counterterm (represented by the tree graph in the Fig. I.1) is necessary. The sum of these two terms can be written in the form (I.8), where the transition form factor $F_{\pi^0\gamma\gamma}$ and the remainder $\chi\left(P^2/\mu^2, m^2/\mu^2\right)$ are replaced by their leading orders in the chiral expansion

$$F^{\mathrm{LO}}_{\pi^0\gamma\gamma} = \frac{1}{4\pi^2 F}\,,\ \chi^{\mathrm{LO}}\left(P^2/\mu^2, m^2/\mu^2\right) = \chi^{(\mathrm{r})}(\mu)\,, \tag{I.10}$$

where $\chi^{(\mathrm{r})}(\mu)$ is the finite part of the above mentioned counterterm renormalized at scale μ. The graphical equation in the Fig. I.1 can be understood as the matching condition for $\chi^{(\mathrm{r})}(\mu)$ at the leading order in the chiral expansion. It enables to determine $\chi^{(\mathrm{r})}(\mu)$ once the form factor $F_{\pi^0\gamma^*\gamma^*}$ is known. The latter can be theoretically modeled e.g. by the lowest meson dominance (LMD) approximation to the large-N_C spectrum of vector meson resonances yielding [13]

$$\chi^{(\mathrm{r})}(M_\rho) = 2.2 \pm 0.9\,, \tag{I.11}$$

where $M_\rho = 770\,\mathrm{MeV}$ is the mass of the ρ meson. For other alternative estimates cf. Tab. I.1 and for the complete discussion see [1].

Model	CLEO+OPE	QCDsr	LMD+V	NχQM
$\chi^{(\mathrm{r})}(M_\rho)$	2.6 ± 0.3	2.8 ± 0.1	2.5	2.4 ± 0.5

Table I.1: Numerical values of $\chi^{(\mathrm{r})}$ in different models according to [1, 3]. The first two columns denoted as CLEO+OPE and QCDsr correspond to various treatments of CLEO data. LMD+V is an improvement of the LMD ansatz and NχQM stands for the nonlocal chiral quark model.

Using the value (I.11) we get for the $\pi^0 \to e^+e^-$ branching ratio numerically

$$B^{\mathrm{LO}}_{\mathrm{SM}}(\pi^0 \to e^+e^-) = (6.1 \pm 0.3) \times 10^{-8}\,. \tag{I.12}$$

I.3 Two-loop virtual radiative corrections

The full two-loop virtual radiative (pure QED) corrections of order $\mathcal{O}(\alpha^3 p^2)$ were calculated in [3]. In this section we will present a short review of the main results.

The relevant contributions to the amplitude are shown in Fig. I.2. There are six two-loop diagrams. Listed sequentially, we have two vertex corrections (a, b), electron self-energy insertion (c), box-type correction (d) and two vacuum polarization insertions (e, f). Of course, for every such diagram a one-loop graph with corresponding counterterm must be added to renormalize the subdivergences. The relevant finite parts of these counterterms can be fixed by the requirement that the parameters m and α coincide with their physical values. After the subdivergences are canceled, the remaining superficial divergences has to be renormalized by another additional tree counter-term with coupling ξ. The finite part $\xi^{(\mathrm{r})}(\mu)$ of this coupling has been estimated in [3] using its running with the renormalization scale as

$$\xi^{(\mathrm{r})}(M_\rho) = 0 \pm 5.5\,. \tag{I.13}$$

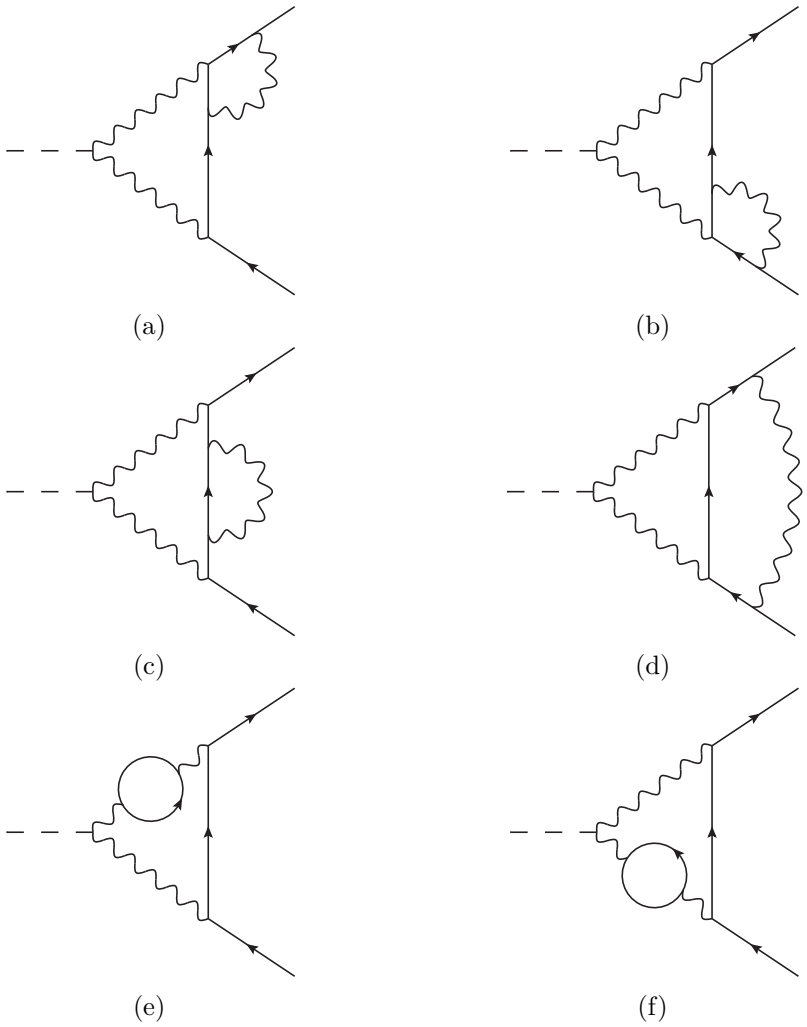

Figure I.2: Two-loop virtual radiative corrections for $\pi^0 \to e^+e^-$ process.

Besides the UV divergences, the graph (d) in the Fig. I.2 is also IR divergent. It is therefore necessary to consider IR-safe decay width of the inclusive process $\pi^0 \to e^+e^-(\gamma)$ with additional real photon in the final state. In [3] the real photon bremsstrahlung has been taken into account using the soft-photon approximation. The final result depends on the experimental upper bound on the soft photon energy which can be expressed in terms of the lower bound $x^{\rm cut}$ on the Dalitz variable x (see (I.2)). The result can be expressed in terms of the correction factor $\delta(x^{\rm cut})$ defined as

$$\begin{aligned} &\Gamma^{\rm NLO}\left(\pi^0 \to e^+e^-(\gamma),\, x > x^{\rm cut}\right) \\ &\equiv \delta\left(x^{\rm cut}\right)\Gamma^{\rm LO}\left(\pi^0 \to e^+e^-\right)\,, \end{aligned} \tag{I.14}$$

where $\Gamma^{\rm LO}$ is the leading order width and $\Gamma^{\rm NLO}$ is the next-to-leading $\mathcal{O}(\alpha^3 p^2)$ correction. The $x^{\rm cut}$ dependent overall correction $\delta(x^{\rm cut})$ has various sources and to emphasize the origin of its constituents, we will use the same symbol decorated with appropriate indices. For the complete QED two-loop correction $\delta^{(2)}$ including soft-photon bremsstrahlung and KTeV cut $x^{\rm cut}$=0.95, in [3] it was obtained

$$\delta^{(2)}(0.95) \equiv \delta^{\rm virt.} + \delta^{\rm BS}_{\rm soft}(0.95) = (-5.8 \pm 0.2)\,\%\,, \tag{I.15}$$

where only the uncertainties of $\chi^{(\mathrm{r})}$ and $\xi^{(\mathrm{r})}$ were taken as the source of the error. This result differs significantly from the previous approximate calculations done by Bergström [7] or Dorokhov et al. [10], where for $\delta^{(2)}\,(0.95)$ we would get $-13.8\,\%$ and $-13.3\,\%$, respectively.

There is a simple interrelation of this partial result of the QED radiative corrections and the branching ratio (I.3) obtained by KTeV experiment (for the details see [3]). We can write the theoretical prediction for the branching ratio measured by KTeV as

$$\begin{aligned} &B(\pi^0 \to e^+e^-(\gamma),\, x > 0.95) \\ &= \frac{\Gamma^{\mathrm{LO}}(\pi^0 \to e^+e^-)}{\Gamma(\pi^0 \to \gamma\gamma)}\, B(\pi^0 \to \gamma\gamma)\left[1 + \delta^{(2)}(0.95) + \Delta^{\mathrm{BS}}(0.95) + \delta^{\mathrm{D}}(0.95)\right], \end{aligned} \tag{I.16}$$

where the only experimental input is the precise branching ratio $B(\pi^0 \to \gamma\gamma) = (98.823 \pm 0.034)\,\%$. In the above formula,

$$\begin{aligned} \delta^{\mathrm{D}}(x^{\mathrm{cut}}) &= \frac{1}{\Gamma^{\mathrm{LO}}(\pi^0 \to e^+e^-)} \int_{x^{\mathrm{cut}}}^{1} \mathrm{d}x \left(\frac{\mathrm{d}\Gamma^{\mathrm{Dalitz}}}{\mathrm{d}x}\right)^{\mathrm{NLO}}_{1\gamma IR} \\ &= \frac{1.75 \times 10^{-15}}{[\Gamma^{\mathrm{LO}}(\pi^0 \to e^+e^-)/\mathrm{MeV}]} \end{aligned} \tag{I.17}$$

corresponds to the unsubtracted fraction of the Dalitz decay background[4] omitted in the KTeV analysis and discussed in [14, 3]. In what follows we will concentrate on the last missing ingredient of the formula (I.16), namely

$$\Delta^{\mathrm{BS}}\left(x^{\mathrm{cut}}\right) \equiv \delta^{\mathrm{BS}}\left(x^{\mathrm{cut}}\right) - \delta^{\mathrm{BS}}_{\mathrm{soft}}\left(x^{\mathrm{cut}}\right), \tag{I.18}$$

which is the difference between the exact bremsstrahlung and its soft photon approximation. This difference has been only roughly estimated in [3] and this estimate has been taken as a source of the error. Our aim is to calculate Δ^{BS} exactly and test the adequacy of the soft photon approximation for the cut $x^{\mathrm{cut}} = 0.95$ used in the KTeV analysis.

I.4 Bremsstrahlung

In this section, we discuss the above mentioned exact bremsstrahlung (BS), i.e. the real radiative correction corresponding to the process $\pi^0 \to e^+e^-(\gamma)$ beyond the soft-photon approximation. As a consequence of the gauge invariance, the invariant amplitude for the BS correction

$$\mathcal{M}_{(\lambda)}(p,q,k) \equiv \epsilon^{*\rho}_{(\lambda)}(k)\mathcal{M}^{\mathrm{BS}}_{\rho}(p,q,k) \tag{I.19}$$

(where k and $\epsilon^{*\rho}_{(\lambda)}(k)$ is the photon momentum and polarization vector, respectively) has to satisfy the Ward identity

$$k^{\rho}\mathcal{M}^{\mathrm{BS}}_{\rho} = 0 \tag{I.20}$$

[4] This fraction comes form the contribution of the interference term of the NLO one-photon-irreducible ($1\gamma IR$) graph with the leading order Dalitz amplitude. See [3] and [14] for more details.

for on-shell k and thus it can be generally expressed in the form [14]

$$\begin{aligned} i\mathcal{M}_{\rho}^{\mathrm{BS}}(p,q,k) = \frac{ie^5}{8\pi^2 F}\Big\{ & P(x,y)\left[(k\cdot p)\,q_\rho - (k\cdot q)\,p_\rho\right]\left[\bar{u}(p,m)\gamma_5 v(q,m)\right] \\ & + A(x,y)\Big[\bar{u}(p,m)\left[\gamma_\rho\,(k\cdot p) - p_\rho(k\cdot\gamma)\right]\gamma_5 v(q,m)\Big] \\ & - A(x,-y)\Big[\bar{u}(p,m)\left[\gamma_\rho\,(k\cdot q) - q_\rho(k\cdot\gamma)\right]\gamma_5 v(q,m)\Big] \\ & + T(x,y)\left[\bar{u}(p,m)\gamma_\rho \not{k}\gamma_5 v(q,m)\right]\Big\} \end{aligned} \tag{I.21}$$

in terms of scalar form factors P, A and T. These are functions of two independent kinematic variables (x,y), defined as

$$\begin{aligned} x = \frac{(p+q)^2}{M^2}\,, \quad y = -\frac{2}{M^2}\left[\frac{k\cdot(p-q)}{1-x}\right] \\ x\in[\nu^2,1]\,, \quad y\in\left[-\sqrt{1-\frac{\nu^2}{x}},\sqrt{1-\frac{\nu^2}{x}}\right]\,. \end{aligned} \tag{I.22}$$

As mentioned above, x is the Dalitz variable (i.e. a normalized square of the total energy of e^+e^- pair in their CMS) and y has the meaning of a rescaled cosine of the angle included by the directions of outgoing photon and positron in the e^+e^- CMS. The modulus squared of the amplitude has the form [14]

$$\begin{aligned} & \overline{|\mathcal{M}^{\mathrm{BS}}(x,y)|^2} \equiv \sum_{\text{polarizations}} \left|\mathcal{M}_{(\lambda)}(p,q,k)\right|^2 = \\ & = \frac{16\pi\alpha^5}{F^2}\frac{M^4(1-x)^2}{8}\Big\{ M^2\left[x(1-y^2)-\nu^2\right]\Big[xM^2\,|P|^2 \\ & + 2\nu M\,\mathrm{Re}\left\{P^*\left[A(x,y)+A(x,-y)\right]\right\} - 4\,\mathrm{Re}\left\{P^*T\right\}\Big] \\ & + 2M^2(x-\nu^2)(1-y)^2\,|A(x,y)|^2 + (y\to -y) \\ & - 8\nu M y(1-y)\,\mathrm{Re}\left\{A(x,y)T^*\right\} + (y\to -y) \\ & - 4\nu^2M^2y^2\,\mathrm{Re}\left\{A(x,y)A(x,-y)^*\right\} + 8(1-y^2)\,|T|^2\Big\} \end{aligned} \tag{I.23}$$

and using the variables x, y the differential decay rate is

$$\mathrm{d}\Gamma^{\mathrm{BS}}(x,y) = \frac{M}{(8\pi)^3}\overline{|\mathcal{M}^{\mathrm{BS}}(x,y)|^2}(1-x)\,\mathrm{d}x\,\mathrm{d}y\,. \tag{I.24}$$

To the amplitude $\mathcal{M}_{(\lambda)}(p,q,k)$ five Feynman diagrams contribute (cf. Fig. I.3). Four of them correspond to the photon emission from the outgoing fermion lines (see Fig. I.3a—I.3d). Naively, one would expect that only these four diagrams are necessary to consider since only they include IR divergences which are needed to cancel the IR divergences stemming from the virtual corrections (see graph (d) in the Fig. I.2 and the corresponding one-loop diagram with counterterm). However, this result would not be complete. The reason is that the Ward identity (I.20)

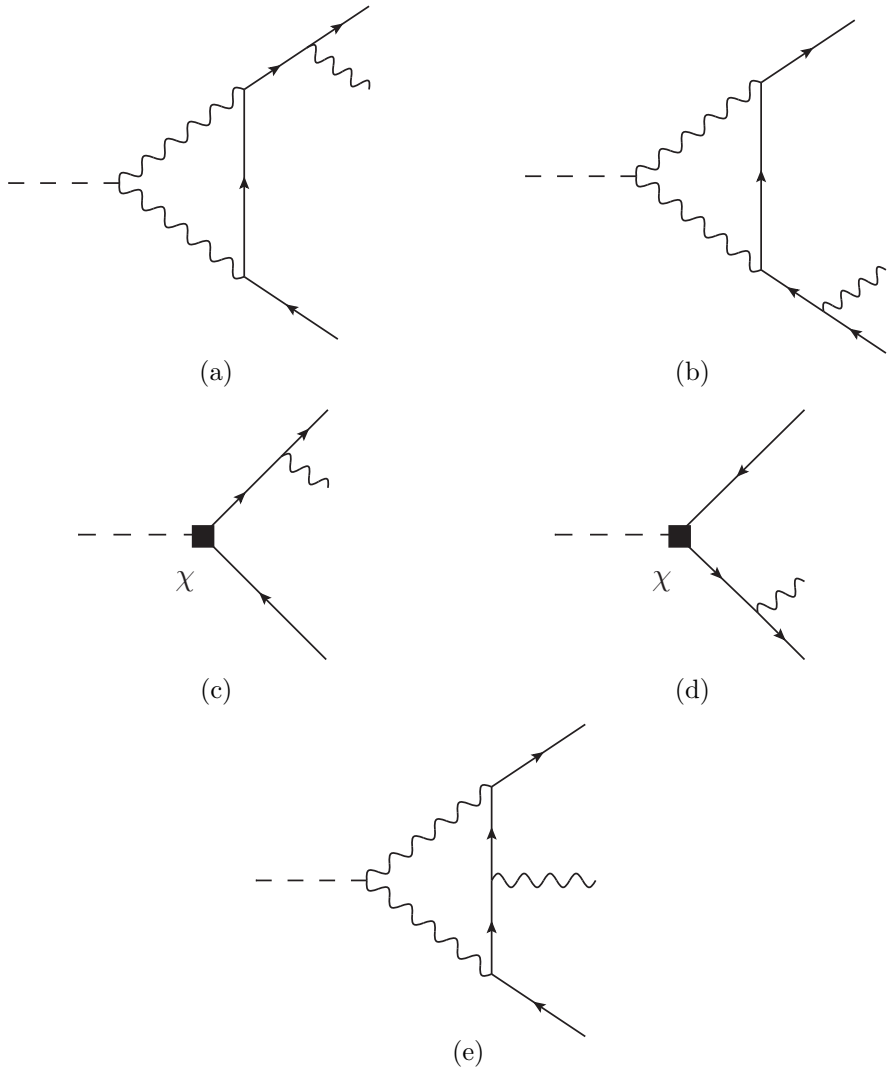

Figure I.3: Bremsstrahlung Feynman diagrams for $\pi^0 \to e^+e^-$ process including counterterms.

would be violated[5]. Thus it is necessary to add the third (box) diagram (Fig. I.3e, photon emitted from the inner fermion line) to fulfill this relation.

In the graphs (I.3a) and (I.3b) the $\pi\gamma\gamma$ vertex stems from the Wess–Zumino–Witten action [15, 16] and the remaining vertices correspond to standard QED Feynman rules. These graphs are UV divergent by power counting and have to be regularized. In what follows, we use the dimensional regularization. In order to bypass the problems with intrinsically four-dimensional objects like γ_5 and the Levi-Civita pseudo-tensor $\varepsilon^{\mu\nu\alpha\beta}$, we use its variant known as Dimensional Reduction[6] (cf. [17]), which keeps the algebra of γ-matrices four-dimensional while the loop tensor integrals are regularized dimensionally and expressed in terms of the scalar one-loop integrals using the Passarino–Veltman reduction [18]. Within this framework we first get rid of the Levi-Civita tensor using the four-dimensional

[5]Note that in the framework of the soft-photon approximation the sum of these four graphs satisfies the Ward identity by itself.

[6]Note however, that in general case the regularization by dimensional reduction might spoil gauge invariance. In the case of our amplitude, we have checked that the gauge invariance is preserved and the regularized amplitude has the general form (I.21).

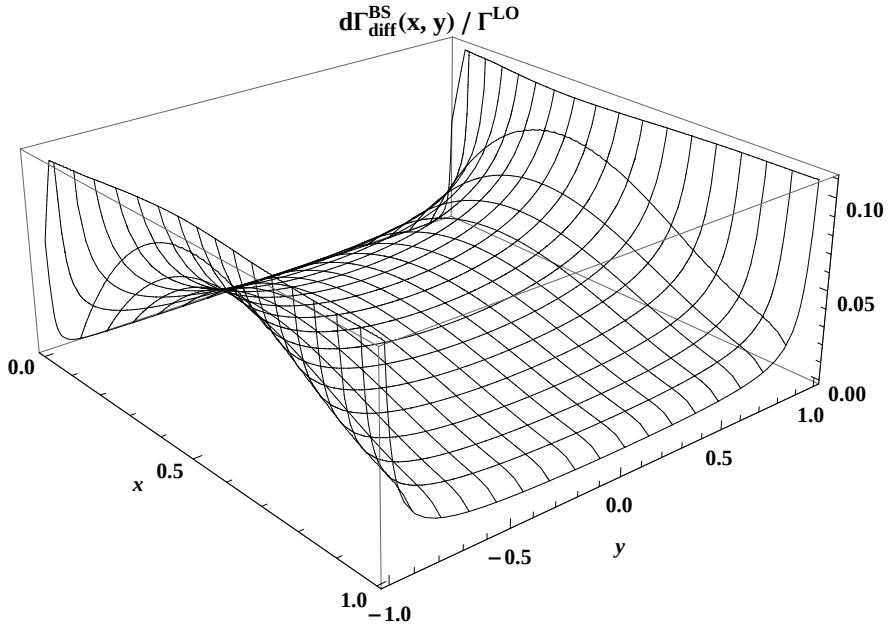

Figure I.4: 3D plot of $\mathrm{d}\Gamma^{\mathrm{BS}}_{\mathrm{diff}}(x,y)$ normalized to the leading order contribution of the $\pi^0 \to e^+e^-$ process.

identities, e.g.

$$\begin{aligned} \varepsilon^{\alpha\beta\mu\nu}\gamma_\mu\gamma_\nu &= i\gamma_5\left[\gamma^\alpha,\gamma^\beta\right] \\ \varepsilon^{\alpha\beta\mu\nu}\gamma_\mu\gamma_\rho\gamma_\nu &= 2i\gamma_5\left(g^\alpha_\rho\gamma^\beta - g^\beta_\rho\gamma^\alpha\right)\,, \end{aligned} \tag{I.25}$$

and then contract the reduced tensor integrals with the γ-matrix structures[7]. The contributions of the box diagram Fig. I.3e turns out to be finite while the triangle diagrams Fig. I.3a and Fig. I.3b contain subdivergences which have to be renormalized by means of the tree graphs with counterterm corresponding to the coupling χ (see Fig. I.3c and I.3d). Summing all the relevant contributions and using the four-dimensional Dirac algebra, we get finally the form factors P, A, and T, the explicit form of which is summarized in I.A.

The differential decay rate $\mathrm{d}\Gamma^{\mathrm{BS}}(x,y)$ (cf. (I.24)) give rise to IR divergences when integrated over the phase space. The divergences originate from the soft-photon region

$$|\mathbf{k}| < \frac{1}{2}M(1-x^{\mathrm{cut}})\,, \tag{I.26}$$

which is defined in terms of the variables (x,y) by means of the cut on the Dalitz variable $x > x^{\mathrm{cut}}$. These divergences are exactly the same as those stemming from an analogous integral of the differential decay rate $\mathrm{d}\Gamma^{\mathrm{BS}}_{\mathrm{soft}}(x,y)$ calculated within the soft-photon approximation. The latter is already included in the two-loop result [3], we therefore present our result for the exact BS as a difference

$$\mathrm{d}\Gamma^{\mathrm{BS}}_{\mathrm{diff}}(x,y) = \mathrm{d}\Gamma^{\mathrm{BS}}(x,y) - \mathrm{d}\Gamma^{\mathrm{BS}}_{\mathrm{soft}}(x,y)\,, \tag{I.27}$$

the integral of which is IR finite. The result for $\mathrm{d}\Gamma^{\mathrm{BS}}_{\mathrm{diff}}(x,y)$ is shown in Fig. I.4 and (integrated over the allowed region of y given by (I.22)) in Fig. I.5. For $\Delta^{\mathrm{BS}}(x^{\mathrm{cut}})$

[7] According to the prescription [17], we take the metric tensors stemming from the Passarino–Veltman reduction effectively as four-dimensional.

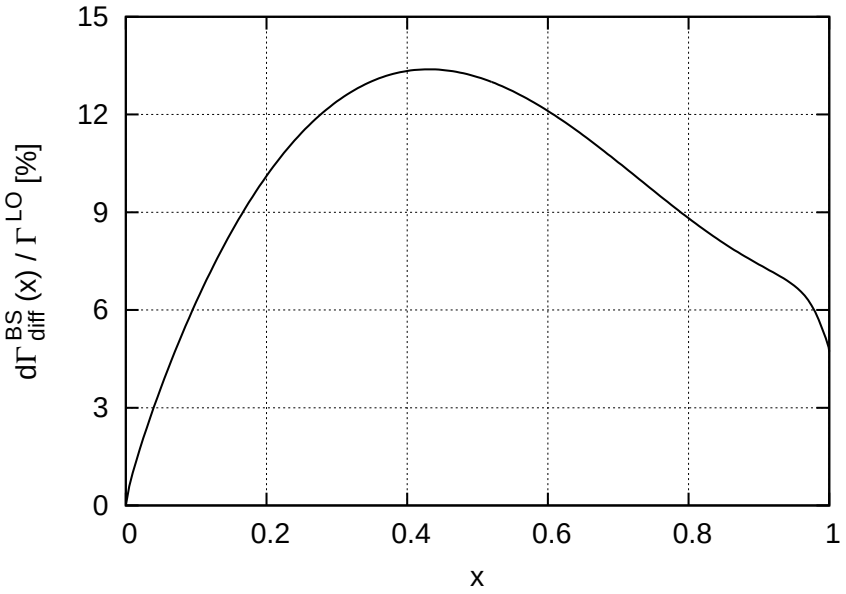

Figure I.5: Plot of $\mathrm{d}\Gamma^{\mathrm{BS}}_{\mathrm{diff}}(x) = \int \mathrm{d}\Gamma^{\mathrm{BS}}_{\mathrm{diff}}(x,y)\,\mathrm{d}y$ normalized to the leading order contribution of the $\pi^0 \to e^+e^-$ process.

we get finally

$$\Delta^{\mathrm{BS}}(x^{\mathrm{cut}}) = 2\int_{x^{\mathrm{cut}}}^{1}\int_{0}^{\sqrt{1-\nu^2/x}} \frac{\mathrm{d}\Gamma^{\mathrm{BS}}_{\mathrm{diff}}(x,y)}{\Gamma^{\mathrm{LO}}\left(\pi^0 \to e^+e^-\right)}\,. \tag{I.28}$$

The dependence of $\Delta^{\mathrm{BS}}(x^{\mathrm{cut}})$ on x^{cut} is shown in Fig. I.6. For $x^{\mathrm{cut}} = 0.95$ and for $\chi^{(\mathrm{r})}$ given by (I.11) we get numerically

$$\Delta^{\mathrm{BS}}(0.95) = (0.30 \pm 0.01)\,\%\,, \tag{I.29}$$

where the error stems from the uncertainty in $\chi^{(\mathrm{r})}(M_\rho)$. In other words, using this cut of Dalitz variable in KTeV experiment, the soft-photon approximation is a very good approach to the exact result. The dependence of $\Delta^{\mathrm{BS}}(0.95)$ on $\chi^{(\mathrm{r})}$ is shown in Fig. I.7.

Now we have all ingredients needed in formula (I.16) under control and we can thus fit the value of the coupling $\chi^{(\mathrm{r})}$ to meet the experiment with the result

$$\chi^{(\mathrm{r})}(M_\rho) = 4.5 \pm 1.0\,. \tag{I.30}$$

The error is dominated by the experimental uncertainty, while the theoretical error corresponding to the estimate (I.13) is negligible. To compare, some previously estimated values, which were considered as relevant, are shown in Tab. I.1.

I.5 Estimate of the theoretical uncertainty of $\chi^{(\mathrm{r})}$

The above determination of $\chi^{(\mathrm{r})}$ represents an effective LO value of this coupling and includes therefore implicitly higher order chiral contributions. The corrections to the LO value of $\chi^{(\mathrm{r})}$ start at the NLO and stem from the two-loop graphs which correspond to a substitution of the one-loop subgraphs (and corresponding counterterms) for the shaded blob on the left hand side of the graphical

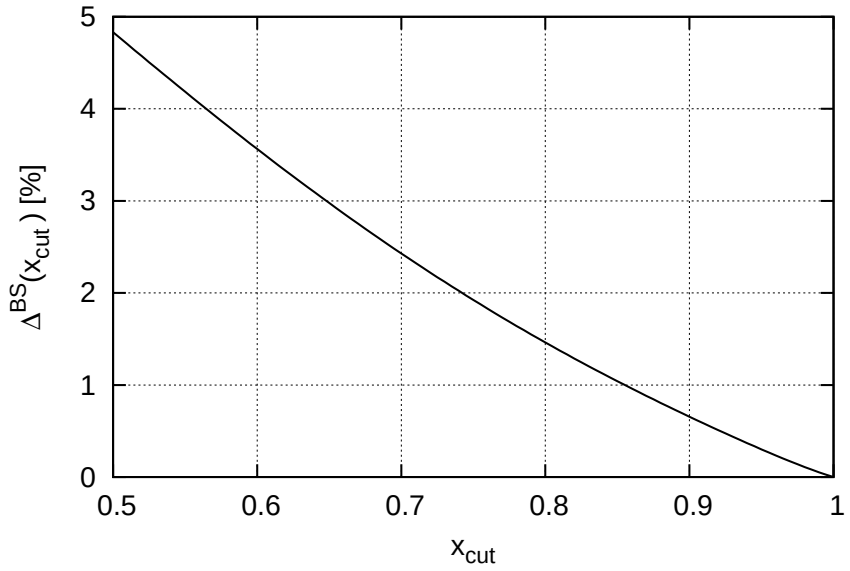

Figure I.6: The dependence of $\Delta^{\rm BS}$ on the cut on the Dalitz variable.

equation depicted in Fig. I.1. The relative size of such corrections is set by the factor $(M/4\pi F)^2 \sim 10^{-2}$ and can be naively treated as negligible, however it can be significantly numerically enhanced by the large double logarithm terms like $\log^2(\mu^2/m^2) \sim 10^2$ for $\mu \sim M_\rho$.

Complete calculation of the NLO corrections is beyond the scope of the present article. In this section, we will only restrict ourselves to the rough estimate based on explicit calculation of the above mentioned leading (double) logarithms, which are expected to represent a numerically relevant part of the full NLO contribution. According to the Weinberg consistency relation [19], this can be achieved by means of evaluation of infinite parts of one-loop graphs only. In what follows, we will adapt this relation to our case.

Let us write the contribution of the above mentioned two-loop graphs as

$$P^{\rm NLO} = P^{\text{2-loop}} + P^{\text{1-loop}}_{\rm CT} + P^{\rm tree}_{\rm CT} + \left(Z^{\text{1-loop}}\right)^{\frac{1}{2}} P^{\rm LO}\,, \tag{I.31}$$

where the first three terms correspond to one-particle irreducible (1PI) contributions (including two-loop graphs, one-loop graphs with counterterms and tree counterterm graphs) and the last term represents the renormalization of the external pion line by means of the one-loop Z-factor. The contributions of the 1PI loop graphs $P^{\text{2-loop}}$ can be written schematically[8] as an expansion in $\varepsilon = 2 - \frac{d}{2}$

$$P^{\text{2-loop}} = \mu^{-4\varepsilon}\left(\frac{\mu^2}{m^2}\right)^{2\varepsilon}\left[\frac{P^{\text{2-loop}}_{-2}}{\varepsilon^2} + \frac{P^{\text{2-loop}}_{-1}}{\varepsilon} + \mathcal{O}(\varepsilon^0)\right]. \tag{I.32}$$

[8]Because we are interested only in the singular parts we ignore the difference between MS, $\overline{MS}$ and $\overline{MS}_\chi$ subtraction schemes in what follows. Such an omission can affect only the finite parts which are irrelevant for the leading log calculation.

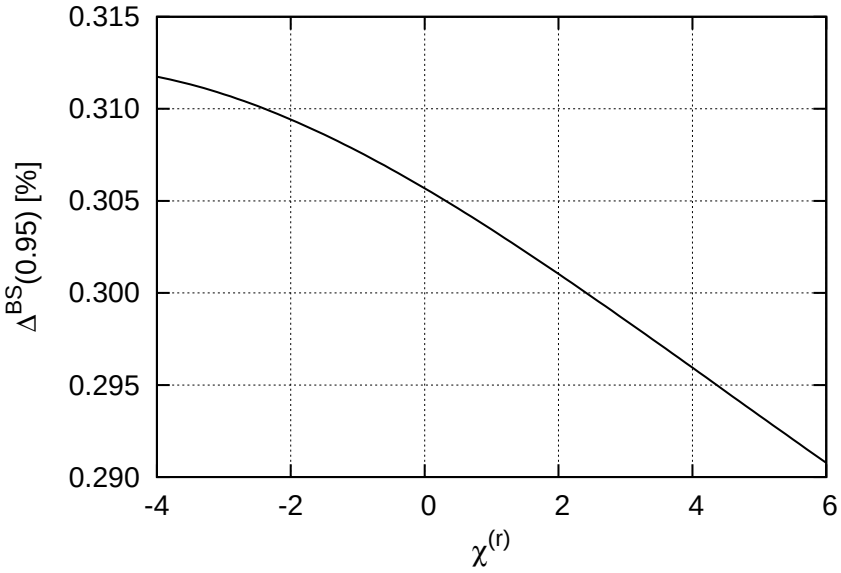

Figure I.7: The dependence of $\Delta^{\rm BS}(0.95)$ on $\chi^{(\rm r)}$. It is apparent, that the dependence is very slight and can be neglected in the calculation of the $\chi^{(\rm r)}$.

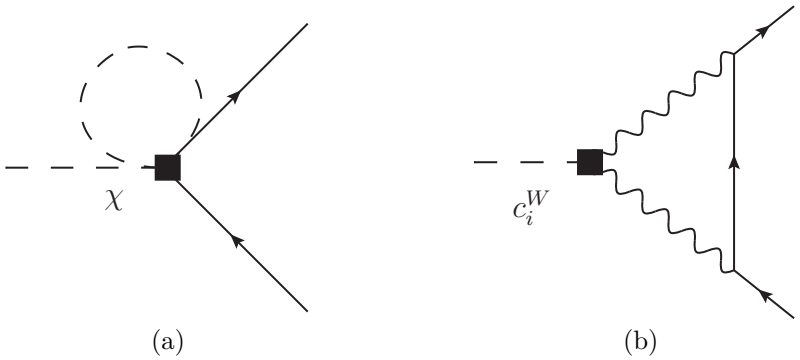

Figure I.8: One-loop diagrams of order α^2/F^3 for $\pi^0 \to e^+e^-$ process.

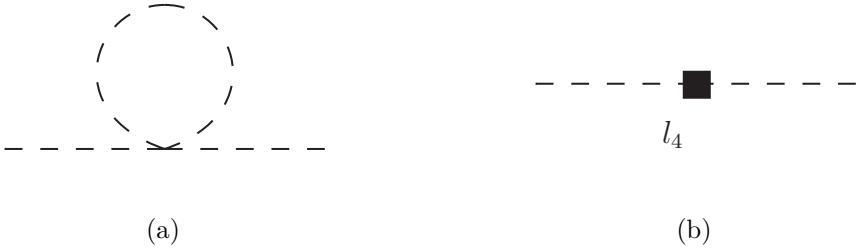

Figure I.9: Z-factor contributions

In the same way, for $P_{\rm CT}^{\text{1-loop}}$ we get (see Fig. I.8)

$$P_{\rm CT}^{\text{1-loop}} = \mu^{-4\varepsilon}\left(\frac{\mu^2}{m^2}\right)^{\varepsilon}\left[\sum_{i=7,11,13}\left(c_i^{W(\rm r)}(\mu) - \frac{\eta_i^W}{32\pi^2\varepsilon}\right)\left(\frac{P_{i,-1}^{\text{1-loop}}}{\varepsilon} + \mathcal{O}(\varepsilon^0)\right) + \left(\chi^{(\rm r)}(\mu) - \frac{\eta_\chi}{32\pi^2\varepsilon}\right)\left(\frac{P_{\chi,-1}^{\text{1-loop}}}{\varepsilon} + \mathcal{O}(\varepsilon^0)\right)\right] \tag{I.33}$$

and the one-loop ingredients of the term $\left(Z^{\text{1-loop}}\right)^{1/2} P^{\rm LO}$ are then in the same

way (see Fig. I.9)

$$\begin{aligned}\left(Z^{\text{1-loop}}\right)^{\frac{1}{2}} &= \mu^{-2\varepsilon}\left[\left(\frac{\mu^2}{m^2}\right)^{\varepsilon}\left(\frac{Z_{-1}^{\frac{1}{2},\text{1-loop}}}{\varepsilon}+\mathcal{O}(\varepsilon^0)\right)+\beta_4\left(l_4^{(\text{r})}(\mu)-\frac{\gamma_4}{32\pi^2\varepsilon}\right)\right]\\ P^{\text{LO}} &= \mu^{-2\varepsilon}\left[\left(\frac{\mu^2}{m^2}\right)^{\varepsilon}\left(\frac{P_{-1}^{\text{LO}}}{\varepsilon}+\mathcal{O}(\varepsilon^0)\right)+\beta_\chi\left(\chi^{(\text{r})}(\mu)-\frac{\eta_\chi}{32\pi^2\varepsilon}\right)\right].\end{aligned} \tag{I.34}$$

Here $l_i^{(\text{r})}(\mu)$, $c_i^{W(\text{r})}(\mu)$ and $\chi^{(\text{r})}(\mu)$ are finite parts of the one-loop counterterms. We use the standard notation for the two-flavour Chiral Perturbation Theory (ChPT) both in the even [20, 21] and in the odd sector [22]. The coefficient β_χ can be obtained from (I.8) and (I.10)

$$\beta_\chi = \frac{1}{2}\left(\frac{\alpha}{\pi}\right)^2\frac{m}{F} \tag{I.35}$$

and β_4 will be discussed below. The Weinberg condition is based on absence of nonlocal divergences of the form $\log(\mu^2)/\varepsilon$. It can be expressed as the following constraint

$$\begin{aligned}0 = 2P_{-2}^{\text{2-loop}} &- \sum_{i=7,11,13}\left(\frac{\eta_i^W P_{i,-1}^{\text{1-loop}}}{32\pi^2}\right)-\frac{\eta_\chi P_{\chi,-1}^{\text{1-loop}}}{32\pi^2}\\ &+2Z_{-1}^{\frac{1}{2},\text{1-loop}}P_{-1}^{\text{LO}}-Z_{-1}^{\frac{1}{2},\text{1-loop}}\frac{\beta_\chi\eta_\chi}{32\pi^2}-\frac{\beta_4\gamma_4 P_{-1}^{\text{LO}}}{32\pi^2}.\end{aligned} \tag{I.36}$$

The contribution of the leading double logs P^{LL} is

$$\begin{aligned}P^{\text{LL}} = \frac{1}{2}\log^2\left(\frac{\mu^2}{m^2}\right)\times&\\ \left[4P_{-2}^{\text{2-loop}}-\sum_{i=7,11,13}\left(\frac{\eta_i^W P_{i,-1}^{\text{1-loop}}}{32\pi^2}\right)-\frac{\eta_\chi P_{\chi,-1}^{\text{1-loop}}}{32\pi^2}\right.&\\ \left.+4Z_{-1}^{\frac{1}{2},\text{1-loop}}P_{-1}^{\text{LO}}-Z_{-1}^{\frac{1}{2},\text{1-loop}}\frac{\beta_\chi\eta_\chi}{32\pi^2}-\frac{\beta_4\gamma_4}{32\pi^2}\right].&\end{aligned} \tag{I.37}$$

Using the constraint (I.36), we get finally

$$\begin{aligned}P^{\text{LL}} = \left(\frac{1}{8\pi}\right)^2\log^2\left(\frac{\mu^2}{m^2}\right)\left[\sum_{i=7,11,13}\left(\eta_i^W P_{i,-1}^{\text{1-loop}}\right)\right.&\\ \left.+\eta_\chi P_{\chi,-1}^{\text{1-loop}}+\beta_\chi\eta_\chi Z_{-1}^{\frac{1}{2},\text{1-loop}}+\beta_4\gamma_4 P_{-1}^{\text{LO}}\right].&\end{aligned} \tag{I.38}$$

Let us now discuss the ingredients of the formula (I.38). The infinite parts of the couplings χ and l_4 are

$$\gamma_4 = 2\,,\ \frac{\eta_\chi}{32\pi^2} = -\frac{3}{2}\,. \tag{I.39}$$

From the finiteness of P^{LO}, it follows

$$P_{-1}^{\text{LO}} = \frac{\beta_\chi\eta_\chi}{32\pi^2} = -\frac{3}{4}\left(\frac{\alpha}{\pi}\right)^2\frac{m}{F}\,. \tag{I.40}$$

For the couplings c_i^W, the infinite parts depend on the form of the l_4 term in the chiral Lagrangian (see (see [23, 24, 25]) for details). For the standard choice

$$\mathcal{L}_4^{\text{std}} = \frac{il_4}{4}\langle u^\mu \chi_{\mu-}\rangle \tag{I.41}$$

we get

$$\eta_7^W = \eta_{11}^W = -\eta_{13}^W = \frac{1}{32\pi^2 F^2} \tag{I.42}$$

(in this case, $\beta_4 = 0$), while for equivalent case, which differs by terms proportional to the LO equation of motion

$$\begin{aligned}\mathcal{L}_4 &= \frac{l_4}{8}\langle u^\mu u_\mu\rangle\langle\chi_+\rangle \\ &= \frac{il_4}{4}\langle u^\mu\chi_{\mu-}\rangle + \frac{il_4}{4}\left\langle \widehat{\chi}_-\left(\nabla_\mu u^\mu - \frac{i}{2}\widehat{\chi}_-\right)\right\rangle ,\end{aligned} \tag{I.43}$$

we get $\beta_4 = -(M/F)^2$ and

$$4\eta_7^W = \eta_{11}^W = -\eta_{13}^W = \frac{1}{32\pi^2 F^2}\,. \tag{I.44}$$

Because both choices have to lead to the same result, we get the following relation

$$\frac{P_{7,-1}^{\text{1-loop}}}{(8\pi F)^2} = -\frac{2}{3}\beta_4\gamma_4 P_{-1}^{\text{LO}} = \left(\frac{\alpha}{\pi}\right)^2 \frac{m}{F}\left(\frac{M}{F}\right)^2 . \tag{I.45}$$

The Z factor is not a physical observable therefore is both sensitive to the field redefinition and in principle infinite. To calculate it we will use the exponential parametrization $U = \exp(i\phi/F)$ (see e.g. [24]):

$$Z_{-1}^{\frac{1}{2},\text{1-loop}} = -\frac{1}{3}\left(\frac{M}{4\pi F}\right)^2 . \tag{I.46}$$

The only missing ingredients are then $P_{11,-1}^{\text{1-loop}}$, $P_{13,-1}^{\text{1-loop}}$ and $P_{\chi,-1}^{\text{1-loop}}$, which correspond to the one-loop graphs depicted in the Fig. I.8. Explicitly, we get

$$P_{\chi,-1}^{\text{1-loop}} = \frac{2}{3}\left(\frac{\alpha}{\pi}\right)^2 \frac{m}{F}\left(\frac{M}{4\pi F}\right)^2 \tag{I.47}$$

$$P_{11,-1}^{\text{1-loop}} = -\frac{1}{4}P_{7,-1}^{\text{1-loop}} \tag{I.48}$$

$$P_{13,-1}^{\text{1-loop}} = -\left(\frac{4\pi}{3}\right)^2\left(\frac{\alpha}{\pi}\right)^2 \frac{m}{F}M^2\left(1-\frac{5}{2}\nu^2\right) . \tag{I.49}$$

Putting all these ingredients together, we find that

$$\sum_{i=7,11}\eta_i^W P_{i,-1}^{\text{1-loop}} + \eta_\chi P_{\chi,-1}^{\text{1-loop}} + \beta_\chi\eta_\chi Z_{-1}^{\frac{1}{2},\text{1-loop}} + \beta_4\gamma_4 P_{-1}^{\text{LO}} = 0 \tag{I.50}$$

and we get finally

$$\begin{aligned}P^{\text{LL}} &= \left(\frac{1}{8\pi}\right)^2 \eta_{13}^W P_{13,-1}^{\text{1-loop}} \log^2\left(\frac{\mu^2}{m^2}\right) \\ &= \frac{1}{72}\left(\frac{\alpha}{\pi}\right)^2 \frac{m}{F}\left(\frac{M}{4\pi F}\right)^2\left(1-\frac{5}{2}\nu^2\right)\log^2\left(\frac{\mu^2}{m^2}\right),\end{aligned} \tag{I.51}$$

which implies the following leading log correction, which has to be subtracted from the experimentally determined coupling (I.30)

$$\begin{aligned}\Delta^{\mathrm{LL}}\chi^{(\mathrm{r})}(\mu) &= \beta_\chi^{-1} P^{\mathrm{LL}} \\ &= \frac{1}{36}\left(\frac{M}{4\pi F}\right)^2 \left(1-\frac{5}{2}\nu^2\right)\log^2\left(\frac{\mu^2}{m^2}\right)\,. \end{aligned} \tag{I.52}$$

Numerically

$$\Delta^{\mathrm{LL}}\chi^{(\mathrm{r})}(M_\rho) = 0.081\,, \tag{I.53}$$

which is well below the uncertainty of $\chi^{(\mathrm{r})}$ in (I.30). This can be taken as an indication of the robustness of our determination of $\chi^{(\mathrm{r})}$ with respect to the NLO chiral corrections.

I.6 Conclusion

In this article we have revisited the decay $\pi^0 \to e^+e^-$. It has attracted a lot of attention since its recent precise measurement by KTeV Collaboration at Fermilab due to the discrepancy with the theoretical predictions. Provided that the measured quantity is in agreement with the future experiments one can attribute the existing discrepancy to the quantum corrections, correct modeling of the double off-shell pion transition form factor $F_{\pi^0\gamma^*\gamma^*}$ and/or possible contribution of the new physics. Our focus here was on the first part, i.e. standard model corrections to the leading order calculation. We have first briefly summarized recent precise theoretical works dealing with the two-loop QED corrections. The missing bremsstrahlung contribution to this process has been calculated. We have shown that the soft-photon approximation is an adequate approach in the region of KTeV experiment. Besides the electromagnetic corrections we have also studied possible stability in the strong sector. It is best modeled using the higher pion-loop contributions for example in the framework of $SU(2)$ ChPT. It is often the case that in the two-flavour ChPT the order of these corrections can be estimated by the size of the chiral logarithms. In fact they represent the potential enhancement of the usual counting. We have explicitly calculated the coefficient of the leading logarithm and due to the large suppression factor 1/72 (see (I.51)) it turns out to be very small. This might be an indication of the fast convergence of the perturbation series which is a situation similar to the chiral corrections of $\pi^0 \to \gamma^{(*)}\gamma^{(*)}$ decay (cf. [25, 26]).

Using the most reliable QCD modeling of the $F_{\pi^0\gamma^*\gamma^*}$ via the lowest-meson dominance approach [13] we agree with the estimate made in [3] of 2σ discrepancy between the theory (including all radiative corrections) and the experiment. Let us remind that this number is significantly smaller than usually quoted difference (3.3σ), however, let us stress that this bigger number was obtained from the rough estimates of the QED radiative corrections and it is thus an indication of the importance of the full two-loop calculation for this process.

On the other hand, still unsatisfactory situation in the first-principle modeling of the three-point vector-vector-pseudoscalar correlator leads to the possibility to use the precise measurement and the full radiative calculation of this process to set the hadronic form factor, represented for this process by the constant χ. The obtained value $\chi^{(\mathrm{r})}(M_\rho) = 4.5 \pm 1.0$ (see (I.30)) is slightly different from

the usual estimations, however, represents the model independent prediction for this quantity, based on the KTeV experiment. It can be further used e.g. in the hadronic light-by-light contribution of the muon $g-2$ (see e.g. [27, 28] for details).

Acknowledgment

This work is supported by Charles University in Prague, project PRVOUK P45, and by Ministry of Education of the Czech Republic, grant LG 13031. T.H. was supported by the grants SVV 260097/2014 and GAUK 700214.

Appendix

I.A Explicit form of the bremsstrahlung form factors

In Section I.4 we have defined the invariant amplitude for the bremsstrahlung correction $\mathcal{M}_\rho^{\mathrm{BS}}$ using the form factors P, A and T. In this appendix we will summarize their explicit form using the standard Passarino–Veltman scalar one-loop integrals B_0, C_0 and D_0. The only divergent function is then B_0. Its explicit form will be given here as a reference point for our notation

$$\begin{aligned} i\pi^2 B_0(0,m^2,m^2) &= (2\pi)^4\mu^{4-d}\int\frac{\mathrm{d}^d l}{(2\pi)^d}\frac{1}{\left[l^2-m^2+i\epsilon\right]^2} \\ &= i\pi^2\Big[\frac{1}{\varepsilon}-\gamma_{\mathrm{E}}+\log 4\pi+\log\left(\frac{\mu^2}{m^2}\right)\Big]\,, \end{aligned} \tag{I.54}$$

where we have introduced $\varepsilon = 2-\frac{d}{2}$. Note that in this regularization scheme the bare counterterm coupling χ is given by [29, 13]

$$\chi = \frac{3}{2}\left(\frac{1}{\varepsilon}-\gamma_{\mathrm{E}}+\log 4\pi\right)+\chi^{(\mathrm{r})}(\mu)\,. \tag{I.55}$$

The bremsstrahlung form-factors are

$$\begin{aligned} -16i\pi^2 P(x,y) &= \frac{2\nu}{M(1-x)^2(1-y^2)} \\ &\times\Bigg\{-\frac{4}{M^2}\Big[3B_0(0,m^2,m^2)-2\chi+5\Big] \\ &+\frac{1}{[x(1-y^2)-\nu^2]}\Bigg[2x(1-x)(1-y^2)(1-y)\,C_0(m^2,0,K_-^2,0,m^2,m^2) \\ &+2(1+y)\Big[x(1-y^2)+x^2(1-y)^2-2\nu^2\Big]\,C_0(m^2,M^2,K_-^2,m^2,0,0) \\ &+\frac{M^2}{2}(1-x)(1-y^2)\Big[x(1-x)(1-y^2)-2\nu^2\Big] \\ &\quad\times D_0(m^2,M^2,m^2,0,K_-^2,K_+^2,m^2,0,0,m^2)\Bigg]\Bigg\} \\ &+(y\to -y)\,, \end{aligned} \tag{I.56}$$

$$
\begin{aligned}
-16i\pi^2 A(x,y) &= -\frac{8}{M^2[2(1-x)(1-y)+\nu^2]} \\
&- \frac{4\nu^2}{M^2(1-x)^2(1-y)^2}\left\{-2+\frac{3(1-x)(1-y)+\nu^2}{2(1-x)(1-y)+\nu^2}\right. \\
&\left.\times\left[B_0(K_-^2,0,m^2)-B_0(0,m^2,m^2)\right]\right\} \\
&- \frac{2\nu^2}{(1-x)(1-y)}\,C_0(m^2,0,K_-^2,0,m^2,m^2) \\
&- \frac{1}{2\left[x(1-y^2)-\nu^2\right]} \\
&\times\left\{-2(1-y)\left[(1-x)(1-y^2)+2\nu^2\right]C_0(m^2,0,K_-^2,0,m^2,m^2)+(y\to -y)\right. \\
&+\left[2(1-y^2)\left[1+x+(1-x)y\right]+\frac{8\nu^2 y}{1-x}\right]C_0(m^2,M^2,K_-^2,m^2,0,0)+(y\to -y) \\
&\left.+M^2(1-y^2)\left[(1-x)^2(1-y^2)+4\nu^2\right]D_0(m^2,M^2,m^2,0,K_-^2,K_+^2,m^2,0,0,m^2)\right\},
\end{aligned}
\tag{I.57}
$$

$$
\begin{aligned}
-16i\pi^2 T(x,y) &= \frac{2\nu}{M(1-x)(1-y)}\left[3B_0(0,m^2,m^2)-2\chi+5\right] \\
&+\frac{2\nu\left[B_0(K_-^2,0,m^2)-B_0(0,m^2,m^2)-1\right]}{M\left[2(1-x)(1-y)+\nu^2\right]} \\
&-\frac{\nu M}{2\left[x(1-y^2)-\nu^2\right]}\left[2(1-y)\left[2x+(1-x)y^2-2\nu^2\right]C_0(m^2,0,K_-^2,0,m^2,m^2)\right. \\
&-\frac{1}{(1-x)(1-y)} \\
&\times\left\{2(1-y)\left[-2x(1-y)+(1-x^2)y^2+(1-x)^2y^3\right]+4\nu^2\left[1-2y(1-y)\right]\right\} \\
&\times C_0(m^2,M^2,K_-^2,m^2,0,0) \\
&-\frac{M^2}{2}\left\{\left(1-y^2\right)\left[2x+(1-x)^2y^2\right]-2\nu^2\left(1-2y^2\right)\right\} \\
&\left.\times D_0(m^2,M^2,m^2,0,K_-^2,K_+^2,m^2,0,0,m^2)\right] \\
&+(y\to -y)\,.
\end{aligned}
\tag{I.58}
$$

In these formulae we have denoted $K_- \equiv k+p$ and $K_+ \equiv k+q$, i.e.

$$
K_\pm^2 = \frac{M^2}{2}(1-x)(1\pm y)+m^2\,. \tag{I.59}
$$

The real parts of all scalar one-loop integrals used in the previous formulae can be found in [14]. We will list the scalar functions here together with the correct imaginary part:

$$
B_0(0,m^2,m^2) = \frac{1}{\varepsilon}-\gamma_{\rm E}+\log 4\pi+\log\left(\frac{\mu^2}{m^2}\right)\,, \tag{I.60}
$$

$$B_0(K_\pm^2,0,m^2) = B_0(0,m^2,m^2) + 2 - \left(1-\frac{m^2}{K_\pm^2}\right)\left[\log\left(\frac{K_\pm^2}{m^2}-1\right) - i\pi\right], \quad \text{(I.61)}$$

$$\begin{aligned} C_0(m^2,0,K_\pm^2,0,m^2,m^2) &= \frac{1}{K_\pm^2-m^2}\left[\frac{\pi^2}{6} - \mathrm{Li}_2\left(\frac{K_\pm^2}{m^2}+i\epsilon\right)\right] \\ &= \frac{(-1)}{K_\pm^2-m^2}\left[\frac{\pi^2}{6} - \mathrm{Li}_2\frac{m^2}{K_\pm^2} - \log\frac{K_\pm^2}{m^2}\left(\frac{1}{2}\log\frac{K_\pm^2}{m^2} - i\pi\right)\right], \end{aligned} \quad \text{(I.62)}$$

$$\begin{aligned} C_0(m^2,M^2,K_\pm^2,m^2,0,0) &= \frac{1}{\sqrt{\lambda}}\left\{2\mathrm{Li}_2(1-a_1) - \mathrm{Li}_2\left(1-\frac{a_1}{a_2}\right) - \mathrm{Li}_2(1-a_1a_2)\right. \\ &\left. + \log(a_2)\left[\log\left(\frac{K_\pm^2-m^2}{M^2}\right) - \frac{1}{2}\log(a_2)\right] - \log(a_1)\left[\log\left(\frac{K_\pm^2-m^2}{m^2}\right) - i\pi\right]\right\}, \end{aligned} \quad \text{(I.63)}$$

where $\lambda = \lambda(m^2,M^2,K_\pm^2) = c^2 - 4m^2M^2$, $c = m^2+M^2-K_\pm^2$,

$$a_1 = \frac{c-2M^2+\sqrt{\lambda}}{c-2M^2-\sqrt{\lambda}}, \quad a_2 = \frac{c(c-\sqrt{\lambda})}{2m^2M^2} - 1\,. \quad \text{(I.64)}$$

Finally, the four-point function presented in the above formula is given by

$$\begin{aligned} &D_0(m^2,M^2,m^2,0,K_-^2,K_+^2,m^2,0,0,m^2) \\ &= \frac{2}{M^2m^2}\frac{y}{(y^2-1)}\left\{\Big(\log[2(a-1)] - i\pi\Big)\log y + \mathrm{Li}_2(1-y) - \mathrm{Li}_2(1-y^{-1})\right\}, \end{aligned} \quad \text{(I.65)}$$

where $y = a + \sqrt{a^2-1}$ and

$$a = 1 + \frac{(K_-^2-m^2)(K_+^2-m^2)}{2M^2m^2} = 1 + \frac{1}{2\nu^2}(1-x)^2(1-y^2)\,. \quad \text{(I.66)}$$

The soft photon approximation ($x \to 1$) needed in the main text is provided by the P form factor with the explicit result

$$\begin{aligned} P_{\rm soft}(x,y) &= \frac{i}{(4\pi)^2}\frac{16\nu}{M^3(1-x)^2(1-y^2)} \\ &\times\Big[2\chi - 5 - 3B_0(0,m^2,m^2) + M^2C_0(m^2,M^2,m^2,m^2,0,0)\Big], \end{aligned} \quad \text{(I.67)}$$

while

$$A_{\rm soft}(x,y) = 0\,, \qquad T_{\rm soft}(x,y) = 0\,. \quad \text{(I.68)}$$

The last term in (I.67) is given by (cf. with (I.8))

$$M^2C_0(m^2,M^2,m^2,m^2,0,0) = \frac{1}{\sqrt{1-\nu^2}}\left[\mathrm{Li}_2(z) - \mathrm{Li}_2\left(\frac{1}{z}\right) + i\pi\log(-z)\right]. \quad \text{(I.69)}$$

Bibliography

[1] A. E. Dorokhov and M. A. Ivanov, "Rare decay $\pi^0 \to e^+e^-$: Theory confronts KTeV data," *Phys. Rev.* **D75** (2007) 114007, arXiv:0704.3498 [hep-ph].

[2] A. Dorokhov, "Rare decay $\pi^0 \to e^+e^-$ as a Test of Standard Model," *Phys. Part. Nucl. Lett.* **7** (2010) 229–234, arXiv:0905.4577 [hep-ph].

[3] P. Vasko and J. Novotny, "Two-loop QED radiative corrections to the decay $\pi^0 \to e^+e^-$: The virtual corrections and soft-photon bremsstrahlung," *JHEP* **1110** (2011) 122, arXiv:1106.5956 [hep-ph].

[4] S. Drell, "Direct decay $\pi^0 \to e^+ + e^-$," *Il Nuovo Cimento Series 10* **11** (1959) 693–697.

[5] **KTeV** Collaboration, E. Abouzaid *et al.*, "Measurement of the rare decay $\pi^0 \to e^+e^-$," *Phys. Rev.* **D75** (2007) 012004, arXiv:hep-ex/0610072 [hep-ex].

[6] **PDG** Collaboration, J. Beringer *et al.*, "Review of Particle Physics," *Phys. Rev.* **D86** (Jul, 2012) 010001.

[7] Bergström, L., "Radiative corrections to pseudoscalar meson decays," *Z. Phys.* **C20** (1983) 135–140.

[8] **CELLO** Collaboration, H. Behrend *et al.*, "A measurement of the π^0, η and η' electromagnetic form factors," *Z. Phys.* **C49** (1991) 401–410.

[9] **CLEO** Collaboration, J. Gronberg *et al.*, "Measurements of the meson-photon transition form factors of light pseudoscalar mesons at large momentum transfer," *Phys. Rev.* **D57** (1998) 33–54, arXiv:hep-ex/9707031 [hep-ex].

[10] A. Dorokhov, E. Kuraev, Y. Bystritskiy, and M. Secansky, "QED radiative corrections to the decay $\pi^0 \to e^+e^-$," *Eur. Phys. J.* **C55** (2008) 193–198, arXiv:0801.2028 [hep-ph].

[11] Y. Kahn, M. Schmitt, and T. M. Tait, "Enhanced rare pion decays from a model of MeV dark matter," *Phys. Rev.* **D78** (2008) 115002, arXiv:0712.0007 [hep-ph].

[12] M. Knecht and A. Nyffeler, "Resonance estimates of $\mathcal{O}(p^6)$ low-energy constants and QCD short distance constraints," *Eur. Phys. J.* **C21** (2001) 659–678, arXiv:hep-ph/0106034 [hep-ph].

[13] M. Knecht, S. Peris, M. Perrottet, and E. de Rafael, "Decay of pseudoscalars into lepton pairs and large-N_C QCD," *Phys. Rev. Lett.* **83** (1999) 5230–5233, arXiv:hep-ph/9908283 [hep-ph].

[14] K. Kampf, M. Knecht, and J. Novotny, "The Dalitz decay $\pi^0 \to e^+e^-\gamma$ revisited," *Eur. Phys. J.* **C46** (2006) 191–217, arXiv:hep-ph/0510021 [hep-ph].

[15] J. Wess and B. Zumino, "Consequences of anomalous Ward identities," *Phys. Lett.* **37B** (1971) 95–97.

[16] E. Witten, "Global Aspects of Current Algebra," *Nucl. Phys.* **B223** (1983) 422–432.

[17] P. Frampton, "Conditions for Renormalizability of Quantum Flavor Dynamics," *Phys. Rev.* **D20** (1979) 3372.

[18] G. Passarino and M. Veltman, "One-loop corrections for e^+e^- annihilation into $\mu^+\mu^-$ in the Weinberg model," *Nucl. Phys.* **B160** (1979) 151–207.

[19] S. Weinberg, "Phenomenological Lagrangians," *Physica* **A96** (1979) 327.

[20] J. Gasser and H. Leutwyler, "Chiral Perturbation Theory to One Loop," *Annals Phys.* **158** (1984) 142.

[21] J. Gasser and H. Leutwyler, "Chiral Perturbation Theory: Expansions in the Mass of the Strange Quark," *Nucl. Phys.* **B250** (1985) 465–516.

[22] J. Bijnens, L. Girlanda, and P. Talavera, "The Anomalous chiral Lagrangian of order p**6," *Eur. Phys. J.* **C23** (2002) 539–544, arXiv:hep-ph/0110400 [hep-ph].

[23] B. Ananthanarayan and B. Moussallam, "Electromagnetic corrections in the anomaly sector," *JHEP* **05** (2002) 052, arXiv:hep-ph/0205232 [hep-ph].

[24] K. Kampf and J. Novotny, "Effective vertex for $\pi^0\gamma\gamma$," *Acta Phys. Slov.* **52** (2002) 265, arXiv:hep-ph/0210074 [hep-ph].

[25] K. Kampf and B. Moussallam, "Chiral expansions of the π^0 lifetime," *Phys. Rev.* **D79** (2009) 076005, arXiv:0901.4688 [hep-ph].

[26] J. Bijnens, K. Kampf, and S. Lanz, "Leading logarithms in the anomalous sector of two-flavour QCD," *Nucl. Phys.* **B860** (2012) 245–266, arXiv:1201.2608 [hep-ph].

[27] M. J. Ramsey-Musolf and M. B. Wise, "Hadronic light by light contribution to muon $g-2$ in chiral perturbation theory," *Phys. Rev. Lett.* **89** (2002) 041601, arXiv:hep-ph/0201297 [hep-ph].

[28] J. P. Miller, E. de Rafael, B. L. Roberts, and D. Stöckinger, "Muon (g-2): Experiment and Theory," *Ann. Rev. Nucl. Part. Sci.* **62** (2012) 237–264.

[29] M. J. Savage, M. E. Luke, and M. B. Wise, "The Rare decays pi0 —> e+ e-, eta —> e+ e- and eta —> mu+ mu- in chiral perturbation theory," *Phys. Lett.* **B291** (1992) 481–483, arXiv:hep-ph/9207233 [hep-ph].

Paper II

Radiative corrections to the Dalitz decay $\pi^0 \to e^+e^-\gamma$ revisited

Tomáš Husek, Karol Kampf and Jiří Novotný

Institute of Particle and Nuclear Physics, Faculty of Mathematics and Physics, Charles University in Prague
V Holešovičkách 2, Praha 8, Czech Republic

(Submitted on April 23/September 8, 2015)

Abstract: We have recalculated the Mikaelian and Smith radiative corrections to the Dalitz decay $\pi^0 \to e^+e^-\gamma$ beyond the soft-photon approximation, i.e. over the whole range of the Dalitz plot and with no restrictions on the radiative photon. In contrast to the previous calculations, we did not neglect the terms of order higher than $\mathcal{O}(m^2)$ and also included the one-photon-irreducible contribution at one-loop level and the virtual muon loop contribution. The results can then be used also for heavier particles in the final state.

Keywords: 13.20.Cz Decays of π mesons, 13.40.Ks Electromagnetic corrections to strong- and weak-interaction processes

II.1 Introduction

Right after the process $\pi^0 \to \gamma\gamma$, the second most important decay channel of a neutral pion is the Dalitz decay $\pi^0 \to e^+e^-\gamma$ with a branching ratio $(1.174 \pm 0.035)\,\%$ [1]. This decay was named after Richard H. Dalitz, who first studied it in Ref. [2]. Experimental data of this process provide information about the semi-off-shell pion transition form factor $\mathcal{F}_{\pi^0\gamma\gamma^*}(Q^2/M^2)$ in the timelike region and in particular its slope parameter a.

Radiative corrections to the total decay rate of the Dalitz decay $\pi^0 \to e^+e^-\gamma$ were first addressed by D. Joseph [3]. The pioneering study of the corrections to the differential decay rate was done by B. E. Lautrup and J. Smith [4] using the soft-photon approximation. This analysis was soon after extended by K. O. Mikaelian and J. Smith [5] by hard-photon corrections to the whole range of the bremsstrahlung photon energy. As one of the main results of their work the table of radiative corrections $\delta(x, y)$ to the leading-order (LO) differential decay rate was presented.

It turned out that such a table would be very useful for the Monte Carlo simulations in experiments covering π^0 decays, e.g. the NA48 experiment at CERN [6]. In practice, for the table of values $\delta(x, y)$, which was published in Ref. [5], an interpolation or extrapolation procedure needs to be used in order to get the radiative correction at any desired point of the Dalitz plot. This might lead to a large uncertainty.

We have therefore recalculated, generalized and extended the results presented in Ref. [5] and prepared the code which can give a value at any kinematical

point (x, y). As we have not neglected the higher-order terms in the electron mass and included also the muon loop contribution to the vacuum polarization insertion correction, our result can be in principle also applied to the other related processes. The decay of an eta meson to a muon pair and a photon, where the masses of the final-state particles are not anymore negligible in comparison to the decaying pseudoscalar, is such an example. On the other hand, when an eta meson and its decays come into play, some peculiarities inevitably appear. We comment on this a little in the present work but postpone the details and the results of the radiative corrections for this case to the paper in preparation. Nevertheless, we try to be as general as possible considering the presented results so one can utilize the formulas without modifications later on.

To proceed even further we have also included the one-loop one-photon-irreducible contribution, which was considered to be negligible in the original paper [5] due to its proportionality to the lepton mass. This statement had been corrected in Ref. [7] many years before the debate about this issue was closed; see e.g. Refs. [8, 9]. We provide here a complete calculation of this contribution making no approximations considering the lepton masses and energy of the photon. We show that this correction is indeed important and changes significantly the values of entries stated in Table I of Ref. [5] especially for a large invariant dilepton mass.

Let us also mention that a systematic treatment of the next-to-leading-order (NLO) corrections to the Dalitz decay of a neutral pion in the framework of chiral perturbation theory with dynamical leptons and photons was studied in Ref. [10]. Here we will also use some results of this work.

It is worth it to notice that throughout the paper we stick to the notation which was used in Ref. [5] using only minor modifications. Even though some of the names may appear to be clumsy, we believe that it would be confusing to do otherwise. Naturally, such an approach is also very convenient for the reader who is familiar with the original work.

Our paper is organized as follows. We recapitulate first some basic facts about the LO differential decay width calculation in Sec. II.2. Then we proceed to the review of the NLO radiative corrections in the QED sector in Secs. II.3, II.4 and II.5. In particular, in Sec. II.3 we discuss the virtual corrections including the muon loop contribution, in Sec. II.4 we introduce the one-photon-irreducible contribution and in Sec. II.5 we describe the bremsstrahlung correction calculation. Some technical details together with extensive results concerning the bremsstrahlung contribution to the NLO correction have been moved to the Appendixes.

II.2 Leading order

First, let us briefly introduce some basic notation. In what follows we denote the four-momenta of the neutral pion (of the mass M), electron (mass m), positron and photon by P, p, q and k, respectively. We also introduce common kinematic variables x and y defined as

$$x = \frac{(p+q)^2}{M^2}\,, \quad y = -\frac{2}{M^2}\frac{P\cdot(p-q)}{(1-x)}\,, \tag{II.1}$$

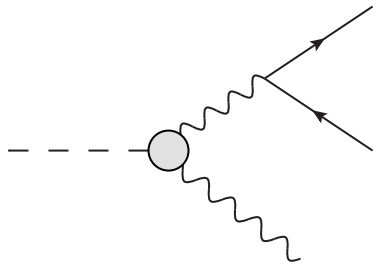

Figure II.1: Leading order diagram of the Dalitz decay $\pi^0 \to e^+e^-\gamma$ in the QED expansion.

where x is a normalized square of the total energy of the e^+e^- pair in their center-of-mass system (CMS), or simply of the electron-positron pair invariant mass. The variable y has then the meaning of the rescaled cosine of the angle between the directions of the outgoing photon and positron in the e^+e^- CMS. If we introduce $\nu = 2m/M$ and

$$\beta = \beta(x) = \sqrt{1 - \frac{\nu^2}{x}}\,, \tag{II.2}$$

we can write the limits on x and y as

$$x \in [\nu^2, 1]\,, \quad y \in [-\beta, \beta]\,. \tag{II.3}$$

The leading-order diagram of the Dalitz decay $\pi^0 \to e^+e^-\gamma$ is shown in Fig. II.1. The shaded blob corresponds to the neutral pion semi-off-shell transition form factor[9]

$$\mathcal{F}\left(\frac{Q^2}{M^2}\right) = \mathcal{F}_{\pi^0\gamma\gamma^*}\left(\frac{Q^2}{M^2}\right) \equiv \mathcal{F}_{\pi^0\gamma\gamma^*}(0)\, f\left(\frac{Q^2}{M^2}\right), \tag{II.4}$$

which is related to the doubly off-shell transition form factor $\mathcal{F}_{\pi^0\gamma^*\gamma^*}(Q_1^2/M^2, Q_2^2/M^2) = \mathcal{F}_{\pi^0\gamma^*\gamma^*}(Q_2^2/M^2, Q_1^2/M^2)$, defined as

$$\int \mathrm{d}^4x\, e^{il\cdot x}\langle 0|T[j^\mu(x)j^\nu(0)]|\pi^0(P)\rangle = -i\varepsilon^{\mu\nu\alpha\beta} l_\alpha P_\beta \mathcal{F}_{\pi^0\gamma^*\gamma^*}\left(l^2/M^2, (P-l)^2/M^2\right), \tag{II.5}$$

by $\mathcal{F}_{\pi^0\gamma\gamma^*}(Q^2/M^2) = \mathcal{F}_{\pi^0\gamma^*\gamma^*}(0, Q^2/M^2)$. In Eq. (II.4), f is a dimensionless function, which can be linearly expanded in the chiral perturbation theory in terms of the slope parameter a as follows

$$f(z) \simeq 1 + az\,. \tag{II.6}$$

In our case it then holds $Q^2 = (P-k)^2 = M^2x$ and for the leading-order matrix element in the QED expansion we can write

$$\begin{aligned} i\mathcal{M}^{\mathrm{LO}}(p,q,k) = \frac{e^3}{M^2x}\mathcal{F}(x)\epsilon^{*\rho}(k) \Big\{ & 2m\left[\bar{u}(p,m)\gamma_\rho \not{k}\gamma_5 v(q,m)\right] \\ & + \Big[\bar{u}(p,m)\left[\gamma_\rho\,(k\cdot p) - p_\rho \not{k}\right]\gamma_5 v(q,m)\Big] \\ & - \Big[\bar{u}(p,m)\left[\gamma_\rho\,(k\cdot q) - q_\rho \not{k}\right]\gamma_5 v(q,m)\Big]\Big\}\,. \end{aligned} \tag{II.7}$$

[9] As it also follows from the definition (II.4), we will use shortly $\mathcal{F}(0) = \mathcal{F}_{\pi^0\gamma\gamma^*}(0)$, which is complementary to the doubly off-shell transition form factor taken at the photon point $\mathcal{F}_{\pi^0\gamma\gamma^*}(0) = \mathcal{F}_{\pi^0\gamma^*\gamma^*}(0,0) \equiv \mathcal{F}_{\pi^0\gamma\gamma}$, which at the LO of the chiral expansion is equal to $\mathcal{F}^{\mathrm{LO}}_{\pi^0\gamma\gamma} = -1/(4\pi^2 F)$.

Summing the modulus squared of the previous result over the fermion spins and photon polarizations and taking into account that, in general, in terms of variables x and y it holds

$$\mathrm{d}\Gamma(x,y) = \frac{M}{(8\pi)^3}\overline{|\mathcal{M}(x,y)|^2}(1-x)\,\mathrm{d}x\,\mathrm{d}y\,, \tag{II.8}$$

the differential decay rate then reads

$$\begin{aligned}\frac{\mathrm{d}^2\Gamma^{\mathrm{LO}}}{\mathrm{d}x\mathrm{d}y} &= \frac{M}{(8\pi)^3}\frac{e^6M^2}{2}|\mathcal{F}(x)|^2\,\frac{(1-x)^3}{x}\left[1+y^2+\frac{\nu^2}{x}\right]\\ &= \left(\frac{\alpha}{\pi}\right)|f(x)|^2\,\Gamma^{\mathrm{LO}}_{\pi^0\to\gamma\gamma}\frac{(1-x)^3}{4x}\left[1+y^2+\frac{\nu^2}{x}\right]\,.\end{aligned} \tag{II.9}$$

Here we have used the LO expression for the decay rate of the neutral pion main decay mode

$$\Gamma^{\mathrm{LO}}_{\pi^0\to\gamma\gamma} = \frac{e^4M^3}{64\pi}|\mathcal{F}(0)|^2\,. \tag{II.10}$$

Integrating (II.9) over y we find

$$\frac{\mathrm{d}\Gamma^{\mathrm{LO}}}{\mathrm{d}x} = \left(\frac{\alpha}{\pi}\right)|f(x)|^2\,\Gamma^{\mathrm{LO}}_{\pi^0\to\gamma\gamma}\frac{8\beta}{3}\frac{(1-x)^3}{4x}\left[1+\frac{\nu^2}{2x}\right]. \tag{II.11}$$

Moving beyond the leading order, it is convenient to introduce the NLO correction δ to the LO differential decay width, which can be in general defined as (in the case of the two-fold differential decay width)

$$\delta(x,y) = \frac{\mathrm{d}^2\Gamma^{\mathrm{NLO}}}{\mathrm{d}x\mathrm{d}y}\Bigg/\frac{\mathrm{d}^2\Gamma^{\mathrm{LO}}}{\mathrm{d}x\mathrm{d}y} \tag{II.12}$$

or (in the one-fold differential case)

$$\delta(x) = \frac{\mathrm{d}\Gamma^{\mathrm{NLO}}}{\mathrm{d}x}\Bigg/\frac{\mathrm{d}\Gamma^{\mathrm{LO}}}{\mathrm{d}x}\,. \tag{II.13}$$

Such a correction can be divided into three parts emphasizing its origin

$$\delta = \delta^{\mathrm{virt}} + \delta^{1\gamma\mathrm{IR}} + \delta^{\mathrm{BS}}\,. \tag{II.14}$$

Here, δ^{virt} stands for the virtual radiative corrections, $\delta^{1\gamma\mathrm{IR}}$ for the one-photon-irreducible contribution, which is treated separately from δ^{virt} in our approach, and δ^{BS} for the bremsstrahlung. Having knowledge of $\delta(x,y)$, we can calculate $\delta(x)$ as a trivial consequence of previous equations using the prescription

$$\delta(x) = \frac{3}{8\beta}\frac{1}{(1+\frac{\nu^2}{2x})}\int_{-\beta}^{\beta}\delta(x,y)\left[1+y^2+\frac{\nu^2}{x}\right]\mathrm{d}y\,. \tag{II.15}$$

In the following sections, we discuss the individual contributions one by one.

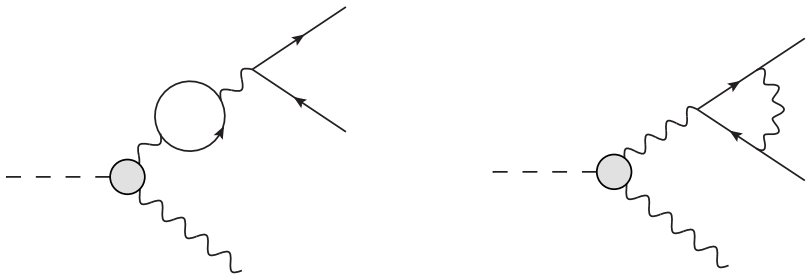

(a) (b)

Figure II.2: Virtual radiative corrections for $\pi^0 \to e^+e^-\gamma$ process: vacuum polarization insertion (a) and correction to the QED vertex (b).

II.3 Virtual radiative corrections

From the interference terms of the LO diagram shown in Fig. II.1 with the one-loop diagrams presented in Fig. II.2, we get NLO virtual radiative corrections which can be written as [5]

$$\delta^{\text{virt}}(x,y) = 2\,\text{Re}\left\{-\Pi(x) + F_1(x) + \frac{2F_2(x)}{1+y^2+\frac{\nu^2}{x}}\right\} \tag{II.16}$$

or (through the formula (II.15)) as

$$\delta^{\text{virt}}(x) = 2\,\text{Re}\left\{-\Pi(x) + F_1(x) + \frac{3F_2(x)}{2\left(1+\frac{\nu^2}{2x}\right)}\right\}. \tag{II.17}$$

For the correction stemming from the vacuum polarization insertion in Fig. II.2(a) we can write

$$\Pi(x) = \Pi_e(x) + \Pi_\mu(x)\,. \tag{II.18}$$

Here we have explicitly written not only the contribution coming from the electron loop as it was done in Ref. [5], but also from the muon loop. This becomes both necessary and convenient when one goes beyond the decay $\pi^0 \to e^+e^-\gamma$, which we discuss throughout this text, and proceeds to the process $\eta \to \mu^+\mu^-\gamma$. In the end, we might then simply do the exchange $m_e \leftrightarrow m_\mu$ (m_e and m_μ stand for the electron and muon mass, respectively) in the expression for the correction δ to vary the final-state lepton masses. Let us remark that independently of the considered processes, the loop with the lightest fermion is of the greatest importance. Thus, taking only the electron loop into account (i.e. leaving the muon part in (II.18)) and performing simply the tempting lepton mass substitution in the whole expression, we would miss out a very important contribution. Obviously, the vacuum polarization insertion defined in a way shown in (II.18) stays after such an operation intact, as desired. The other option would be to treat separately the final-state lepton masses m and the masses of the particles in the vacuum polarization insertion loops m_e and m_μ. This more universal approach was used in the code which comes with the paper. Let us now introduce for the later convenience

$$\gamma = \gamma(x) = \frac{1-\beta(x)}{1+\beta(x)}\,. \tag{II.19}$$

The individual terms used in (II.18) are then defined as

$$\Pi_\ell(x) = \frac{\alpha}{\pi}\left[-\frac{1}{9} + \frac{1}{3}\left(1 + \frac{\nu_\ell^2}{2x}\right)\left(2 + \beta_\ell \log[-\gamma_\ell]\right)\right]. \tag{II.20}$$

In the above formula, ℓ stands for e or μ in the loop and changes the meaning of the so far used electron mass m in the definitions of ν, β and γ to m_e or m_μ. Unlike in Ref. [5] where only the real part of (II.20) above the threshold $x = \nu_\ell^2$ is shown, we quote here the full expression valid in all kinematical regimes. This is necessary to get right the contribution from the charged fermion loop when the transferred momentum is not sufficiently large to produce the real pair, i.e. for $x < \nu_\ell^2$, and lacks therefore the imaginary part. This situation for instance appears (at least for a part of the kinematical region) when the pseudoscalar decays to the electron-positron pair via the muon loop. For the purpose of real algebra used in the code (i.e. to avoid complex logarithms and so on) we can extract the real part of (II.20). For an arbitrary mass of the charged loop fermion we find

$$\mathrm{Re}\left\{\beta_\ell \log[-\gamma_\ell]\right\} = -2|\beta_\ell|\left\{\theta(\beta_\ell^2)\,\mathrm{arctanh}\,\beta_\ell + \theta(-\beta_\ell^2)\arctan\frac{1}{|\beta_\ell|}\right\}. \tag{II.21}$$

In the following, we stick exclusively back to the process $\pi^0 \to e^+e^-\gamma$ and m then denotes the outgoing electron mass as before. Finally, for the electromagnetic form factors $F_1(x)$ and $F_2(x)$ stemming from the QED vertex correction in Fig. II.2(b) we have

$$\begin{aligned} F_1(x) = \frac{\alpha}{\pi}\Bigg\{ & -1 - \frac{1+2\beta^2}{4\beta}\log(-\gamma) \\ & - \frac{1+\beta^2}{2\beta}\left[\mathrm{Li}_2(1-\gamma) + \frac{1}{4}\log^2(-\gamma) - \frac{\pi^2}{4} - i\pi\log(1-\gamma)\right] \\ & + \left[1 + \frac{1+\beta^2}{2\beta}\log(-\gamma)\right]\log\frac{m}{\lambda}\Bigg\} \end{aligned} \tag{II.22}$$

and

$$F_2(x) = \frac{\alpha}{\pi}\frac{\nu^2}{4x\beta}\log(-\gamma). \tag{II.23}$$

In the above formulas, Li_2 stands for the dilogarithm and λ is the infrared cutoff. To extract the real parts from the previous terms (II.22) and (II.23) (in a sense of applying the operator Re), in the kinematically allowed region where $M^2x \geq 4m^2$ we use $\log(-\gamma) = \log(\gamma) + i\pi$, since $0 \leq \gamma \leq 1$. Thus it is straightforward to see that the real parts of $F_1(x)$ and $F_2(x)$ indeed coincide with the form factors stated in Ref. [5] including the Coulomb term proportional to $-\pi^2/2$.

II.4 One-photon-irreducible virtual radiative correction

One-photon-irreducible (1γIR) contributions were extensively studied in Ref. [11] in connection with the bremsstrahlung correction to the $\pi^0 \to e^+e^-$ process. Here we will summarize the most important results which are necessary to proceed

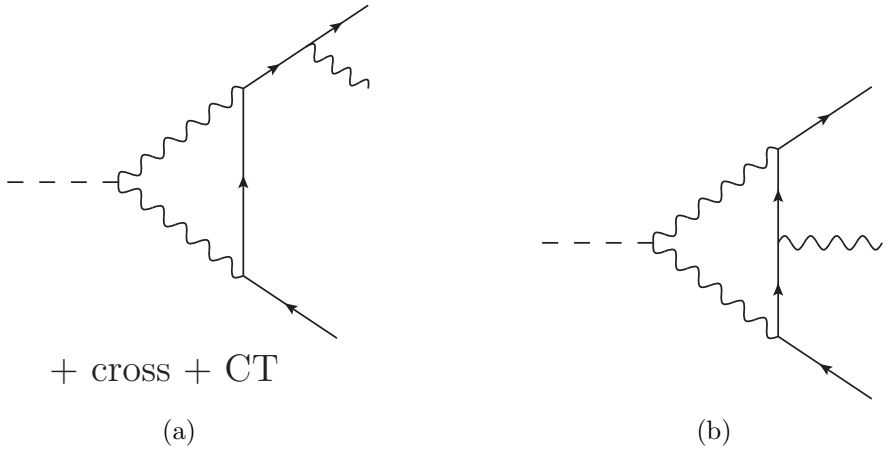

Figure II.3: One-loop one-photon-irreducible contribution LO Feynman diagrams for $\pi^0 \to e^+e^-\gamma$ process considering the QED and χPT expansion: triangle diagrams and related counterterms (a) and box diagram (b). Note that "cross" accounts for a diagram with a photon coming from the outgoing positron line. "CT" then stands for two counterterm diagrams necessary to compensate the UV divergent parts of the related Feynman diagrams.

toward our purpose considering NLO corrections to the decay $\pi^0 \to e^+e^-\gamma$Ä. Let us emphasize that this contribution was not included in the calculations performed in Ref. [5]. On the other hand, it was shown later on in Ref. [7] within the limit $m \to 0$ that there is no point in treating the 1γIR correction as negligible. In the following we show the results of the calculation beyond this massless limit. For the reasons specified in the previous sentences we have devoted to this contribution a separate section, even though it is of course just one additional virtual radiative correction.

Until now we have not considered any particular form of the semi-off-shell form factor $\mathcal{F}(x)$ in our calculations. To get the one-photon-irreducible contribution in a closed form, it is though necessary to choose a concrete form of $\mathcal{F}_{\pi^0\gamma^*\gamma^*}$. Accordingly, we should consider at this moment a general doubly off-shell pion transition form factor $\mathcal{F}_{\pi^0\gamma^*\gamma^*}\left(l^2/M^2, (P-l)^2/M^2\right)$, where l stands for a loop momentum. In Fig. II.3, we can see the LO of the considered contribution in chiral perturbation theory. In such a limit we take the constant $\mathcal{F}^{\mathrm{LO}}_{\pi^0\gamma\gamma} = -1/(4\pi^2 F)$ as the local form factor and it is thus clear due to the power counting that a counterterm is needed. The finite part of such a counterterm renormalized at scale μ is governed by the parameter $\chi^{(\mathrm{r})}(\mu)$, which corresponds to the high-energetic behavior of the complete form factor. This can be theoretically modeled e.g. by the lowest-meson-dominance (LMD) approximation to the large-N_C spectrum of vector-meson resonances yielding the value $\chi^{(\mathrm{r})}(M_\rho) = 2.2 \pm 0.9$ [12], which can be further used for numerical results. The dependance of the correction $\delta^{1\gamma\mathrm{IR}}$ on $\chi^{(\mathrm{r})}$ can be neglected for the values given by relevant models as well as experiments, when a decay with the electrons in the final state is taken into account. We will comment on this in the end of this section. Let us emphasize in a more straightforward way that using "only" the LO expansion of the form factor is compensated by the effective value $\chi^{(\mathrm{r})}$ which differs for particular models. One gets the model corresponding value of $\chi^{(\mathrm{r})}$ for instance from the matching to the full calculation. In this sense one loses no information. On the contrary, the model dependence of any such result can be conveniently altered easily just by changing the value of $\chi^{(\mathrm{r})}$.

The total matrix element covering all the diagrams represented in Fig. II.3 can be written in such a form which manifestly satisfies the Ward identities for the conserved electromagnetic vector current

$$\begin{aligned} i\mathcal{M}_{1\gamma\mathrm{IR}}(p,q,k) &= -\frac{ie^5}{2}\mathcal{F}^{\mathrm{LO}}_{\pi^0\gamma\gamma}\epsilon^{*\rho}(k) \\ &\times\Big\{P(x,y)\left[(k\cdot p)\,q_\rho-(k\cdot q)\,p_\rho\right]\left[\bar u(p,m)\gamma_5 v(q,m)\right] \\ &+A(x,y)\Big[\bar u(p,m)\left[\gamma_\rho\,(k\cdot p)-p_\rho\not{k}\right]\gamma_5 v(q,m)\Big] \\ &-A(x,-y)\Big[\bar u(p,m)\left[\gamma_\rho\,(k\cdot q)-q_\rho\not{k}\right]\gamma_5 v(q,m)\Big] \\ &+T(x,y)\left[\bar u(p,m)\gamma_\rho\not{k}\gamma_5 v(q,m)\right]\Big\}. \end{aligned} \tag{II.24}$$

Here P, A and T are scalar form factors, the explicit form of which can be found in Appendix A of Ref. [11].

To get the NLO one-photon-irreducible part of the correction δ we need to consider the interference term of LO matrix element (II.7) and the 1γIR contribution (II.24) and sum it over the photon polarizations with the result

$$\begin{aligned} \overline{\mathcal{M}^{\mathrm{LO}}_{1\gamma\mathrm{IR}}(x,y)} &\equiv \sum_{\text{polar.}}\Big[\mathcal{M}^{\mathrm{LO}}(p,q,k)\Big]^*\mathcal{M}_{1\gamma\mathrm{IR}}(p,q,k) \\ &= -\frac{ie^8M^3}{8}\frac{(1-x)^2}{x}\mathcal{F}^*(x)\mathcal{F}^{\mathrm{LO}}_{\pi^0\gamma\gamma} \\ &\times\Big\{4\nu T(x,y)+\Big[A(x,y)M[x(1-y)^2-\nu^2]+(y\to -y)\Big]\Big\}. \end{aligned} \tag{II.25}$$

Putting the above formula into (II.8) and (II.12) and normalizing to the LO two-fold differential decay width (II.9) we get finally

$$\begin{aligned} \delta^{1\gamma\mathrm{IR}}(x,y) &= 2\,\mathrm{Re}\left\{\overline{\mathcal{M}^{\mathrm{LO}}_{1\gamma\mathrm{IR}}(x,y)}\right\}\frac{M(1-x)}{(8\pi)^3}\Big/\frac{\mathrm{d}^2\Gamma^{\mathrm{LO}}}{\mathrm{d}x\mathrm{d}y} \\ &= 2\,\mathrm{Re}\left\{-\frac{\alpha}{\pi}\frac{\mathcal{F}^{\mathrm{LO}}(0)}{\mathcal{F}(x)}\frac{i\pi^2M}{\left[1+y^2+\frac{\nu^2}{x}\right]}\right. \\ &\left.\times\Big\{4\nu T(x,y)+\Big[A(x,y)M[x(1-y)^2-\nu^2]+(y\to -y)\Big]\Big\}\right\}. \end{aligned} \tag{II.26}$$

For our purpose we can safely set $\mathcal{F}(x)\simeq\mathcal{F}^{\mathrm{LO}}(0)$ in the previous formula, considering only the leading order of the chiral expansion; see also (II.6) assuming the slope a is small. It should be mentioned, though, that such an approximation is only reasonable for the Dalitz decay of a neutral pion. For the decays of an eta meson, one should be more cautious and use a better treatment of the full form factor.

Similarly, the dependence on the parameter $\chi^{(\mathrm{r})}$ cannot be neglected when ν becomes significant. Indeed, considering the full expression (A.5) from [11] for the form factor $T(x,y)$, one gets for the χ-dependent contribution to $\delta^{1\gamma\mathrm{IR}}(x,y)$ from (II.26)

$$\delta^{1\gamma\mathrm{IR}}_{\chi^{(\mathrm{r})}}(x,y) = -\frac{\alpha}{\pi}\frac{\mathcal{F}^{\mathrm{LO}}(0)}{\mathcal{F}(x)}\frac{4\nu^2\chi^{(\mathrm{r})}(\mu)}{(1-x)(1-y^2)}\frac{1}{\left[1+y^2+\frac{\nu^2}{x}\right]}. \tag{II.27}$$

Thus, e.g. for the decay $\eta \to \mu^+\mu^-\gamma$ the one-photon-irreducible contribution may be considerably model-dependent. This is, however, not the case for the process $\pi^0 \to e^+e^-\gamma$ where the contribution given in (II.27) is suppressed in comparison to the other terms in (II.26).

II.5 Bremsstrahlung

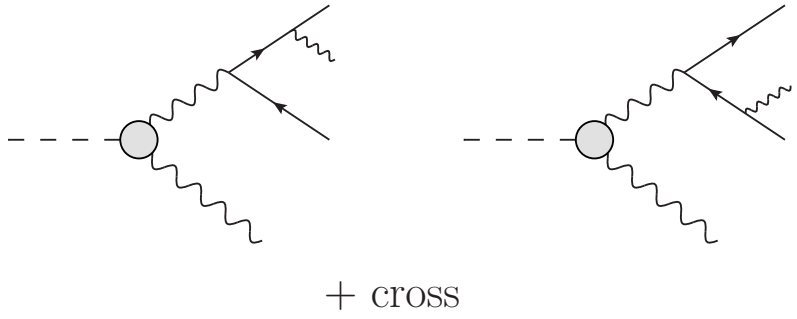

Figure II.4: Bremsstrahlung corrections for $\pi^0 \to e^+e^-\gamma$ process. Needless to say, "cross" stands for the diagrams with outgoing photons interchanged.

In this section we recapitulate the approach used in Ref. [5] for the bremsstrahlung correction calculation. We think it is useful and convenient to rewrite the whole story in a more detailed way so it is transparent and easily understood. As usual, one can then build on that when a few more pieces come into play. In the Appendixes we then provide the results themselves. Note also that especially in this section we restrict ourselves to the original notation used in the work [5].

The diagrams which contribute to the Dalitz decay bremsstrahlung and are thus important to cancel the IR divergences stemming from the virtual corrections discussed in Sec. II.3 are shown in Fig. II.4. The corresponding invariant matrix element (including cross terms) can be written in the form

$$i\mathcal{M}_{\rm BS} = \bar{u}(p)\Big[I^{\rho\sigma}(k,l) + I^{\sigma\rho}(l,k)\Big]v(q)\epsilon^*_\rho(k)\epsilon^*_\sigma(l)\,, \tag{II.28}$$

where[10]

$$\begin{aligned} I^{\alpha\beta}(k,l) = -i^5e^4\mathcal{F}\left(\frac{(l+p+q)^2}{M^2}\right)\frac{\varepsilon^{(l+p+q)(k)\mu\alpha}}{(l+p+q)^2} \\ \times\left[\gamma^\beta\frac{(\not{l}+\not{p}+m)}{2l\cdot p+i\epsilon}\gamma^\mu - \gamma^\mu\frac{(\not{l}+\not{q}-m)}{2l\cdot q+i\epsilon}\gamma^\beta\right]. \end{aligned} \tag{II.29}$$

The form factor $\mathcal{F}((l+p+q)^2/M^2)$ can be expanded (assuming a is small) in the following way

$$\mathcal{F}\left(\frac{(l+p+q)^2}{M^2}\right) \simeq \mathcal{F}(x)\left[1 + a\,\frac{2l\cdot(p+q)}{M^2}\right]. \tag{II.30}$$

[10] We use the shorthand notation for the product of the Levi-Civita tensor and four-momenta in which $\varepsilon^{(k)\cdots} = \varepsilon^{\mu\cdots}k_\mu$.

Thus for the process $\pi^0 \to e^+e^-\gamma$ it can be approximated by $\mathcal{F}(x)$, taking into account only the leading order in the chiral expansion. Let us also introduce Tr for the rescaled matrix element squared and summed over all spins and polarizations of final states by the relation

$$\overline{|\mathcal{M}_{\rm BS}|^2} \equiv \sum_{\text{sp., pol.}} |\mathcal{M}_{\rm BS}|^2 \equiv \frac{e^8}{4}|\mathcal{F}(x)|^2\,\mathrm{Tr}\,. \tag{II.31}$$

Inasmuch as an additional photon comes into play it is convenient to introduce a new kinematic variable which describes the normalized invariant mass squared of the two photons

$$x_\gamma = \frac{(k+l)^2}{M^2}\,. \tag{II.32}$$

It has the similar meaning as x in the case of the electron-positron pair. The limits on x_γ are

$$\frac{\lambda^2}{M^2} \le x_\gamma \le x_\gamma^{\max} \equiv 1 + x - \sqrt{4x + \frac{y^2}{\beta^2}(1-x)^2}\,. \tag{II.33}$$

The contribution of the bremsstrahlung to the next-to-leading order can be described (according to (II.12)) by the correction

$$\delta^{\rm BS}(x,y) = \frac{\mathrm{d}^2\Gamma^{\rm BS}}{\mathrm{d}x\mathrm{d}y}\Big/\frac{\mathrm{d}^2\Gamma^{\rm LO}}{\mathrm{d}x\mathrm{d}y}\,, \tag{II.34}$$

in which in agreement with [5] we can write

$$\begin{aligned}\frac{\mathrm{d}^2\Gamma^{\rm BS}}{\mathrm{d}x\mathrm{d}y} &= \frac{(1-x)}{4M(2\pi)^8}\frac{\pi^3M^4}{16}\int J\Big[\overline{|\mathcal{M}_{\rm BS}|^2}\Big]\mathrm{d}x_\gamma \\ &= \frac{|f(x)|^2}{64}\left(\frac{\alpha}{\pi}\right)^2\Gamma^{\rm LO}_{\pi^0\to\gamma\gamma}(1-x)\int J[\mathrm{Tr}]\,\mathrm{d}x_\gamma\,.\end{aligned} \tag{II.35}$$

The above used operator J is defined for an arbitrary invariant $f(k,l)$ of the momenta k and l as follows

$$J[f(k,l)] = \frac{1}{2\pi}\int\frac{\mathrm{d}^3k}{k_0}\frac{\mathrm{d}^3l}{l_0}f(k,l)\,\delta^{(4)}(P-p-q-k-l)\,. \tag{II.36}$$

Finally, putting the LO differential decay width expression (II.9) and the previous result (II.35) into (II.34) we get

$$\delta^{\rm BS}(x,y) = \frac{1}{64}\left(\frac{\alpha}{\pi}\right)\frac{4x}{(1-x)^2}\frac{\int J[\mathrm{Tr}]\,\mathrm{d}x_\gamma}{\Big[1+y^2+\frac{\nu^2}{x}\Big]}\,. \tag{II.37}$$

In the remaining part of this section we discuss the way the integral $\int J[\mathrm{Tr}]\,\mathrm{d}x_\gamma$ is treated. Most of the explicit formulas are then moved to the Appendixes.

Being on shell ($k^2 = 0 = l^2$) and in the diphoton center-of-mass system where $\vec{P}-\vec{p}-\vec{q} = 0 (= \vec{k}+\vec{l} \equiv \vec{r})$, we find

$$J[f(k,l)] \overset{(\vec{r}=0)}{=} \frac{1}{4\pi}\int \mathrm{d}\Omega\, f(k,\tilde{k}) = \frac{1}{4\pi}\int \mathrm{d}\Omega\, f(\tilde{l},l)\,. \tag{II.38}$$

Here, we have used $\tilde{l}$ to mark the four-momentum l with the opposite momentum direction, i.e. whenever $l = (l_0, \vec{l})$, then $\tilde{l} = (l_0, -\vec{l})$. We can come back to the invariant form in a known way through

$$2l_0 = k_0 + l_0 \overset{(\vec{r}=0)}{=} \sqrt{(k+l)^2} = M\sqrt{x_\gamma} \tag{II.39}$$

or, for example, due to

$$p_0 = \frac{(k_0 + l_0)p_0}{(k_0 + l_0)} \overset{(\vec{r}=0)}{=} \frac{(k+l)\cdot p}{M\sqrt{x_\gamma}}\,. \tag{II.40}$$

If we follow the notation of Ref. [5], we define the propagator denominators in the following way (suppressing $+i\epsilon$ part for now)

$$\begin{gathered} A = l\cdot q\,, \quad B = l\cdot p\,, \quad C = k\cdot q\,, \quad D = k\cdot p\,, \\ E = (p+q+l)^2\,, \quad F = (p+q+k)^2\,. \end{gathered} \tag{II.41}$$

Not only is the whole amplitude invariant under the interchange of the two photons (and thus of k and l in (II.28)), but also the operator J possesses the same symmetry which can be written for an arbitrary function of the propagator denominators (II.41) as

$$J[f(A,B,C,D,E,F)] = J[f(C,D,A,B,F,E)]\,. \tag{II.42}$$

The interchange of p and q (which is also a relevant symmetry in our case) must be compensated on the level of the operator J by changing the y sign, thus

$$J[f(A,B,C,D,E,F)] = J[f(B,A,D,C,E,F)]\Big|_{y\to -y}\,. \tag{II.43}$$

There are also some useful identities which follow from the definitions (II.41) such as

$$E - 2A - 2B = F - 2C - 2D = M^2 x\,, \tag{II.44}$$

$$F + 2A + 2B = E + 2C + 2D = M^2(1 - x_\gamma) \tag{II.45}$$

and

$$A + C = \frac{M^2}{4}\left[(1-x)(1+y) - x_\gamma\right]\,, \tag{II.46}$$

$$B + D = \frac{M^2}{4}\left[(1-x)(1-y) - x_\gamma\right] = (A+C)\Big|_{y\to -y}\,,$$

$$E + F = M^2(1 + x - x_\gamma)\,. \tag{II.47}$$

It is convenient to know the above relations for two reasons. First, we see that we can simply trade one of the above defined variables for the others and thus only two more independent variables in addition to x, y and x_γ (e.g. A and B) are necessary to describe the kinematics of our decay. On the other hand, we realize that some special combinations of the variables $A, \ldots, F$ are invariant with respect to the acting of the operator J (i.e. they depend only on x, y and

x_γ). We can also combine the previous formulas to get some other J-invariant combinations. If we consider, for example, that

$$A = (A + C) - \frac{1}{2}[(E + 2C + 2D) - E - 2D]\,, \tag{II.48}$$

we find

$$\frac{E}{2} - A + D = \frac{M^2}{4}[1 + x - x_\gamma - y(1 - x)]\,. \tag{II.49}$$

Such expressions are useful when we want to reduce the complicated J terms, arising naturally during the calculation of the invariant matrix element squared, to the basic ones which are simple to handle. First, we use the above stated relations to simplify the numerators (e.g. we get rid of A in a term like $A/(DE)$ using the relation (II.49)).[11] Then also the denominators are treated. For example, consider the term $J[1/(ACEF)]$. Then

$$\begin{aligned} \frac{1}{ACEF} &= \frac{1}{(A+C)}\frac{1}{(E+F)}\frac{(A+C)(E+F)}{ACEF} \\ &= \frac{1}{(A+C)(E+F)}\left(\frac{1}{AE} + \frac{1}{AF} + \frac{1}{CE} + \frac{1}{CF}\right)\,. \end{aligned} \tag{II.50}$$

After applying the operator J and using the symmetry (II.42), we find

$$J\left[\frac{1}{ACEF}\right] = \frac{2}{(A+C)(E+F)}\left(J\left[\frac{1}{AE}\right] + J\left[\frac{1}{CE}\right]\right)\,. \tag{II.51}$$

All necessary reductions of this type are summarized in Appendix II.B, except for such terms which one can get using the discussed symmetries (II.42) and (II.43). The computational methods used to calculate the basic terms are introduced in Appendix II.C. For the list of the results for these integrals see Appendix II.D. Here, in comparison to Ref. [5], we include also the new term $J[1/(A^2E^2)]$ which appears due to the fact that $\mathcal{O}(\nu^4)$ terms were not neglected in our approach. The completely reduced rescaled matrix element squared Tr, which represents in terms of $J[\mathrm{Tr}]$ an important ingredient for the bremsstrahlung correction $\delta^{\mathrm{BS}}(x, y)$ (cf. (II.37)), is presented in Appendix II.A. We believe we provide here the results in a more refined way in comparison with Ref. [5].

The last step is the integration over x_γ. There are basic integrals which behave like $1/x_\gamma$ and are divergent when this integration is performed if no x_γ appears in the numerator to compensate it. The essential divergent integrals are $J[1/A^2]$ and $J[1/(AB)]$. The divergent part of integrals like $J[1/(A^2E)]$ and $J[1/(A^2E^2)]$ can then be written in terms of these essential ones. For example, using (II.44) we get

$$\frac{1}{A^2E} = \frac{1}{M^2x}\left(\frac{1}{A^2} - \frac{2}{AE} - \frac{2B}{A^2E}\right)\,. \tag{II.52}$$

Needless to say, there are also $A \to B$ counterparts of the mentioned integrals. This unwelcome behavior can be extracted from the Tr expression to get the convergent part $\mathrm{Tr_C}$, which can be treated numerically, and the divergent part

[11] The combination (II.49) is of course in some minimalistic sense redundant for the considered procedure, since we can always make two-step substitution instead. In such a case, we would trade A for C using (II.46) and then C for E and D using (II.45).

$\mathrm{Tr_D}$, which should be treated analytically. In the former case we can set $\lambda \to 0$ and the lower bound on x_γ is then zero. In the latter case the cutoff λ has to be preserved.

Finally, as expected, the sum of the divergent part of the bremsstrahlung correction $\delta_{\mathrm{D}}^{\mathrm{BS}}(x,y)$, the explicit form of which can be found in (II.63), and the divergent part of virtual correction $\delta^{\mathrm{virt}}(x,y)$, represented in the following formula by the electromagnetic form factor $F_1(x)$, in particular

$$\delta_{\mathrm{D}}^{\mathrm{BS}}(x,y) + 2\,\mathrm{Re}\left\{F_1(x)\right\}, \tag{II.53}$$

is IR finite. In other words, terms proportional to $\log m/\lambda$ cancel each other in the final formula of the correction $\delta(x,y)$.

In the end of this section, let us go back to Eq. (II.30). In cases when the slope a is no longer negligible in comparison to 1, one should consider the entire right-hand side of (II.30) instead of only $\mathcal{F}(x)$ alone. It is then necessary to go beyond the approach used in Ref. [5]. If we square the bremsstrahlung matrix element (II.28), we get for the simple case with $a = 0$ which we have treated so far

$$|\mathcal{M}_{\mathrm{BS}}^{a=0}|^2 = |I_{k,l} + I_{l,k}|^2 = |I_{k,l}|^2 + |I_{l,k}|^2 + 2I_{k,l}^* I_{l,k}\,. \tag{II.54}$$

Here we have denoted

$$I_{k,l} \equiv \bar{u}(p) I_{a=0}^{\rho\sigma}(k,l) v(q) \epsilon_\rho^*(k) \epsilon_\sigma^*(l) \tag{II.55}$$

and likewise for $I_{l,k}$. Using the building blocks of the "no-slope" matrix element modulus squared (II.54) and considering the expansion (II.30) we find the correction for the bremsstrahlung expression

$$\overline{|\mathcal{M}_{\mathrm{BS}}^{a\neq 0}|^2} = [1 + a(1-x-x_\gamma)]\overline{|\mathcal{M}_{\mathrm{BS}}^{a=0}|^2} + a\frac{(E-F)}{M^2}\left(\overline{|I_{k,l}|^2} - \overline{|I_{l,k}|^2}\right). \tag{II.56}$$

If we apply the operator J and take into account the symmetry (II.42), the previous formula can be boiled down to

$$J\left[\overline{|\mathcal{M}_{\mathrm{BS}}^{a\neq 0}|^2} - \overline{|\mathcal{M}_{\mathrm{BS}}^{a=0}|^2}\right] = 2a\left\{(1-x-x_\gamma)\,J\left[\overline{I_{k,l}^* I_{l,k}}\right] + 4\,J\left[\frac{(A+B)}{M^2}\overline{|I_{k,l}|^2}\right]\right\}. \tag{II.57}$$

This expression can be calculated along the same lines as $J[\mathrm{Tr}]$. One then gets a similar expression to $\mathrm{Tr_C}$ in (II.61) including some new integrals. These need to be calculated in addition to the known basic terms. Note that there is no divergent part in (II.57) which needs to be treated separately.

The above correction does not need to be considered in the decay $\pi^0 \to e^+e^-\gamma$ so we do not present the related results in this paper. On the other hand, it becomes important when treating the eta meson decays.

II.6 Results

For the reader's convenience, we put here together the individual pieces (II.16), (II.26) and (II.37) and write the overall NLO correction

$$\begin{aligned}\delta(x,y) &= \delta^{\mathrm{virt}}(x,y) + \delta^{\mathrm{BS}}(x,y) + \delta^{1\gamma\mathrm{IR}}(x,y)\\ &= 2\,\mathrm{Re}\left\{-\Pi(x) + F_1(x) + \frac{2F_2(x)}{1+y^2+\frac{\nu^2}{x}} + \frac{\alpha}{\pi}\frac{1}{64}\frac{4x}{(1-x)^2}\frac{\int J[\mathrm{Tr_C}]\mathrm{d}x_\gamma}{\left[1+y^2+\frac{\nu^2}{x}\right]} + \delta_{\mathrm{D}}^{\mathrm{BS}}(x,y)\right.\\ &\left. - \frac{\alpha}{\pi}\frac{i\pi^2 M}{\left[1+y^2+\frac{\nu^2}{x}\right]}\left\{4\nu T(x,y) + \left[A(x,y)M[x(1-y)^2-\nu^2] + (y\to -y)\right]\right\}\right\}.\end{aligned} \tag{II.58}$$

Here, the convergent part of the rescaled bremsstrahlung invariant matrix element squared (to be integrated over x_γ numerically) $\mathrm{Tr_C}$ is given by (II.61) and the analytically integrated divergent part of the bremsstrahlung correction $\delta_{\mathrm{D}}^{\mathrm{BS}}(x,y)$ is shown in (II.63). Let us recall that the explicit formulas for the scalar form factors A and T can be found in Appendix A of Ref. [11].

Taking the result (II.58) and using the formula (II.15), we get the overall correction to the one-fold differential leading-order decay width, which is shown in Fig. II.5. For comparison, also the sum $\delta^{\mathrm{virt}}(x) + \delta^{\mathrm{BS}}(x)$, which would have corresponded to the correction presented in the original paper [5] if the $\mathcal{O}(\nu^4)$ terms and the muon loop had not been omitted, and one-photon-irreducible contribution $\delta^{1\gamma\mathrm{IR}}$ are shown. We see that in the case of the decay $\pi^0 \to e^+e^-\gamma$ the 1γIR correction is negative for the whole range of values of x and enhances thus the effect of the sum $\delta^{\mathrm{virt}}(x) + \delta^{\mathrm{BS}}(x)$ which is also negative in a wide range of x.

Taking into account all the discussed contributions, a similar table of values of correction $\delta(x,y)$ as it was provided in the original work [5], can be produced at the very same points according to (II.58); see Table II.1. Considering the contributions introduced in this work but left out in Ref. [5], the 1γIR correction is the most important one, especially for large x. The correction of the old Mikaelian and Smith values is significant and greater than 10 % already for $x \simeq 0.5$. This can be visible in Fig. II.5 and also from the difference of the entry values between the Table I in Ref. [5] and Table II.1 in the present work, provided the remaining contributions are not significant. Indeed, the muon loop vacuum polarization insertion contribution, which is independent on y, grows nearly linearly with x from $\delta^{\mathrm{virt}}_{\mu\text{-loop}}(0.01,y) = -0.0005\,\%$ up to $\delta^{\mathrm{virt}}_{\mu\text{-loop}}(0.99,y) = -0.0616\,\%$ and is thus negligible. A similar conclusion holds then also for the $\mathcal{O}(\nu^4)$ contribution, which is most significant for small x with the value $\delta^{\mathrm{BS}}_{\nu^4}(0.01,0) = 0.0035\,\%$.

With our present knowledge, we are now in a position to calculate the correction to the integrated decay width. In this case, the transition form factor $\mathcal{F}(x)$ cannot be scaled out anymore. On the other hand, for relevant examples [13] this model dependence is negligible for the decay $\pi^0 \to e^+e^-\gamma$ and we get $\delta = 8.30 \times 10^{-3}$. This can be rewritten in a common way as

$$\frac{\Gamma^{\mathrm{NLO}}_{\pi^0\to e^+e^-\gamma}}{\Gamma^{\mathrm{LO}}_{\pi^0\to\gamma\gamma}} = 0.986 \times 10^{-4}\,. \tag{II.59}$$

Without the inclusion of the 1γIR contribution, the above number would become 1.03×10^{-4}. The stated values are consistent with the previous results 1.05×10^{-4}

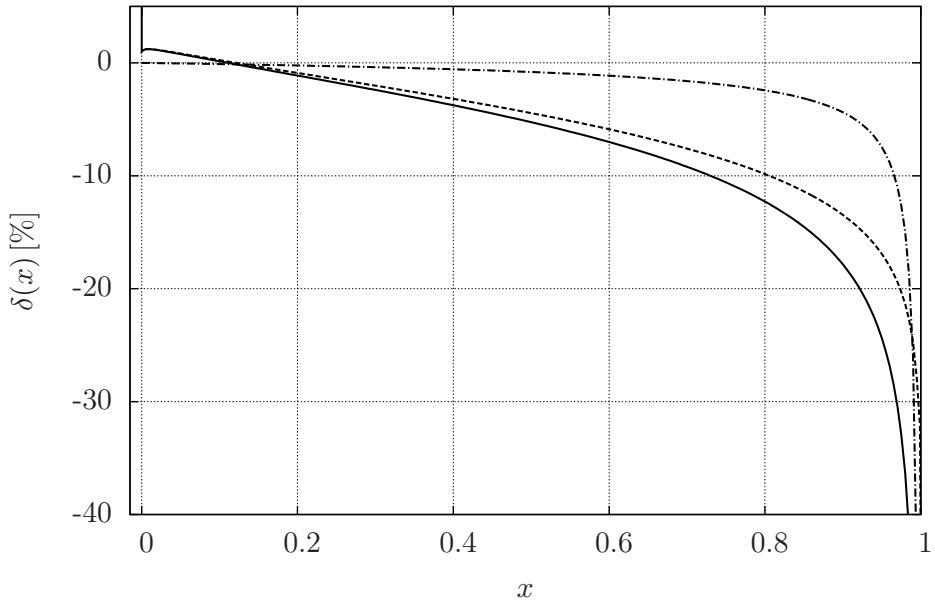

Figure II.5: The overall NLO correction $\delta(x)$ for the decay $\pi^0 \to e^+e^-\gamma$ calculated according to the formula (II.58) (solid line) in comparison to its constituents. The sum $\delta^{\mathrm{virt}}(x) + \delta^{\mathrm{BS}}(x)$ is depicted as a dashed line and the one-photon-irreducible contribution $\delta^{1\gamma\mathrm{IR}}$ is shown as a dash-dot line. The divergent behavior of $\delta(x)$ near $x = \nu^2 \simeq 0$ has the origin in the electromagnetic form factor $F_1(x)$ and is connected to the Coulomb self-interaction of the dilepton at the threshold.

of Joseph [3] and 0.95×10^{-4} of Mikaelin and Smith, who admitted that eventual numerical inaccuracy might be present in their result [5].

II.7 Summary

In the preceding sections we have explored all the relevant NLO radiative corrections to the Dalitz decay of a neutral pion in the QED sector. In the direct comparison to the earlier approach of Mikaelian and Smith [5], we have included into our treatment the one-photon-irreducible contribution. On the top of that, as announced above we have enriched the vacuum polarization insertion correction with the muon loop and have not thrown away the $\mathcal{O}(\nu^4)$ terms. The latter is connected to the calculation of an additional nontrivial integral. On the other hand, we were able to write the results in a more compact form even though more terms needed to be covered. The computational methods as well as some intermediate results are also provided and thus it should be possible for an interested reader to trace back all the steps made.

From the newly included contributions only the 1γIR correction is relevant for the decay $\pi^0 \to e^+e^-\gamma$ and should be introduced in the future analyses. Needless to say, the provided calculation is universal considering the masses of the particles involved. It can thus be also shown via direct calculation that if we change the masses of the particles in such a way that they correspond to the process $\eta \to \mu^+\mu^-\gamma$, all the discussed corrections should be taken into account. In other words, both the muon loop as well as the $\mathcal{O}(\nu^4)$ terms give then a non-negligible contribution to the overall $\delta(x, y)$. That is why these corrections should

Table II.1: The overall NLO correction $\delta(x, y)$ given in percent for a range of values of x and y (i.e. the Dalitz-plot corrections) for the process $\pi^0 \to e^+e^-\gamma$.

x \ y	0.00	0.10	0.20	0.30	0.40	0.50	0.60	0.70	0.80	0.90	0.99
0.01	2.761	2.714	2.599	2.449	2.273	2.061	1.786	1.402	0.803	−0.357	−5.657
0.02	2.756	2.720	2.622	2.480	2.300	2.073	1.774	1.355	0.703	−0.546	−5.859
0.03	2.669	2.639	2.552	2.419	2.242	2.012	1.704	1.267	0.586	−0.716	−6.125
0.04	2.558	2.531	2.452	2.327	2.155	1.925	1.611	1.164	0.464	−0.874	−6.372
0.05	2.437	2.412	2.340	2.221	2.053	1.824	1.509	1.054	0.341	−1.025	−6.601
0.06	2.311	2.288	2.221	2.108	1.944	1.717	1.400	0.940	0.216	−1.172	−6.815
0.07	2.184	2.163	2.099	1.990	1.830	1.605	1.288	0.824	0.092	−1.315	−7.017
0.08	2.056	2.036	1.975	1.870	1.714	1.491	1.173	0.707	−0.033	−1.455	−7.211
0.09	1.928	1.909	1.851	1.749	1.596	1.374	1.057	0.588	−0.157	−1.593	−7.397
0.10	1.801	1.783	1.726	1.628	1.477	1.257	0.940	0.469	−0.281	−1.729	−7.578
0.15	1.170	1.154	1.105	1.016	0.874	0.661	0.345	−0.131	−0.900	−2.394	−8.424
0.20	0.546	0.532	0.486	0.402	0.266	0.057	−0.258	−0.738	−1.520	−3.048	−9.219
0.25	−0.079	−0.092	−0.135	−0.217	−0.350	−0.556	−0.871	−1.355	−2.148	−3.704	−9.995
0.30	−0.713	−0.726	−0.768	−0.847	−0.978	−1.184	−1.499	−1.988	−2.790	−4.372	−10.770
0.35	−1.366	−1.378	−1.419	−1.497	−1.627	−1.833	−2.149	−2.641	−3.454	−5.058	−11.558
0.40	−2.044	−2.056	−2.097	−2.174	−2.304	−2.509	−2.827	−3.324	−4.146	−5.773	−12.370
0.45	−2.759	−2.771	−2.811	−2.887	−3.017	−3.222	−3.543	−4.044	−4.875	−6.525	−13.218
0.50	−3.521	−3.533	−3.572	−3.648	−3.777	−3.983	−4.306	−4.811	−5.653	−7.324	−14.115
0.55	−4.344	−4.356	−4.395	−4.470	−4.599	−4.806	−5.130	−5.640	−6.492	−8.186	−15.076
0.60	−5.249	−5.261	−5.299	−5.373	−5.501	−5.708	−6.034	−6.549	−7.410	−9.128	−16.123
0.65	−6.262	−6.273	−6.310	−6.383	−6.510	−6.717	−7.044	−7.563	−8.435	−10.177	−17.284
0.70	−7.425	−7.435	−7.470	−7.541	−7.666	−7.871	−8.198	−8.721	−9.603	−11.371	−18.602
0.75	−8.802	−8.811	−8.844	−8.910	−9.031	−9.232	−9.558	−10.084	−10.976	−12.772	−20.143
0.80	−10.508	−10.516	−10.544	−10.604	−10.717	−10.912	−11.233	−11.759	−12.659	−14.486	−22.024
0.85	−12.779	−12.784	−12.804	−12.851	−12.949	−13.129	−13.438	−13.958	−14.864	−16.724	−24.468
0.90	−16.207	−16.205	−16.206	−16.225	−16.289	−16.434	−16.712	−17.208	−18.108	−20.003	−28.003
0.95	−23.167	−23.144	−23.084	−23.011	−22.960	−22.982	−23.140	−23.532	−24.360	−26.256	−34.451
0.99	−54.287	−54.068	−53.442	−52.496	−51.351	−50.147	−49.029	−48.155	−47.761	−48.467	−55.831

not be overlooked. If necessary, heavier charged fermions may be also introduced in the loops in the same way the muon loop was added.

We believe that this work is a good starting point for a treatment of some other processes such as the Dalitz decays of η. We have also touched on some particular difficulties that appear and one needs to be careful about. A more detailed review of this matter is beyond the scope of this work and will be discussed separately in the paper in preparation.

Let us also say that after the complete recalculation of the results given in Ref. [5] we have verified the formulas therein. The numerical accuracy of the listed values is also sufficient.

The main message of the present work is the completion of the list of the NLO corrections and refining of the expressions. All the formulas necessary for the calculation of the considered correction are listed in the present paper in a ready-to-use form. For the eventual future practical use of an interested reader, we submit together with this text also (as ancillary files) a `C++` code, which contains all the expressions in a well-arranged way. As a demonstration, the resulting program calculates the correction $\delta(x, y)$.

Acknowledgment

We would like to thank Evgueni Goudzovski for turning our attention to this problem.

This work was supported by Charles University in Prague (Grant No. GAUK 700214), by Ministry of Education of the Czech Republic (Grant No. LG 13031) and by the Czech Science Foundation (Grant No. GAČR 15-18080S).

Appendix

II.A Bremsstrahlung matrix element squared

For the rescaled bremsstrahlung invariant matrix element squared Tr (see (II.31) for the definition) we can write

$$J[\mathrm{Tr}] = J[\mathrm{Tr_C}] + J[\mathrm{Tr_D}]\,. \tag{II.60}$$

The explicit forms of the (from the point of view of the integration over x_γ) convergent part $\mathrm{Tr_C}$ and the divergent part $\mathrm{Tr_D}$ of Tr are shown below[12]. The terms are already reduced (see Appendix II.B for the reduction procedure) to the basic integrals (see Appendix II.D for the explicit expressions) and the symmetries of the operator J (II.42) and (II.43) were used. This means the relation $\mathrm{Tr} = \mathrm{Tr_C} + \mathrm{Tr_D}$ holds only effectively (with operator J applied).

[12]Note that $\{y \to -y\}$ in $\mathrm{Tr_C}$ holds for the entire expression (including terms independent of y).

$$
\begin{aligned}
\mathrm{Tr_C} = {} & 16 - 4M^2\left[(1-x)(3-y) - 3x_\gamma + 3\nu^2 + \frac{2\nu^2(x+x_\gamma)}{(1-x)(1+y)-x_\gamma}\right]\frac{1}{A} \\
& - \frac{\nu^2 M^4}{x}\frac{x_\gamma^2}{A^2} + M^4\left(2+\frac{\nu^2}{x}\right)\frac{x_\gamma^2}{AB} + 16\frac{B}{A} - 4\nu^2M^2\frac{B}{A^2} - 16M^4\frac{1}{E^2} \\
& - \frac{32M^2}{(1+x-x_\gamma)}\frac{1}{E} + \frac{8\nu^2M^4(x-x_\gamma)^2}{(1+x-x_\gamma)[1+x-x_\gamma-y(1-x)]}\left(\frac{1}{AE}-\frac{1}{DE}\right) \\
& + \frac{M^4}{2}\Bigg[(1-x-x_\gamma)^2 - 4xx_\gamma - (1-x)^2y^2 - 2\nu^2(x-3x_\gamma) \\
& + \frac{8\nu^2(x-x_\gamma)^2}{(1+x-x_\gamma)^2 - y^2(1-x)^2}\Bigg]\frac{1}{AD} \\
& - 4M^4\left\{2(1-x)^2(1+y^2) + 2x_\gamma^2 + [(1-x)^2(1-y^2)+x_\gamma^2]\frac{\nu^2}{x} - (1-2x)\frac{\nu^4}{x^2}\right\}\frac{1}{AE} \\
& - 4M^4[(1-x-x_\gamma)^2 + (1-x)^2y^2 + 2\nu^2(1+x_\gamma)]\frac{1}{CE} - 8M^6\left(x+\nu^2-\frac{\nu^4}{2x}\right)\frac{1}{AE^2} \\
& - \nu^2M^6\{1+[(1-x)y-x+x_\gamma]^2 - 2\nu^2\}\left[\frac{1}{A^2E} - \frac{1}{M^2x}\frac{1}{A^2}\right] \\
& - \nu^4M^8\left[\frac{1}{A^2E^2} - \frac{1}{M^4x^2}\frac{1}{A^2}\right] \\
& + \frac{4M^4}{(1+x-x_\gamma)}\left(\frac{1}{AE}+\frac{1}{CE}\right)\Bigg\{(1+y^2)[2-x+x^3-2x_\gamma(1-x)^2] \\
& + 2y[1-x-xy-x_\gamma(1-x^2)] - x_\gamma[6x+xx_\gamma+2(1-x_\gamma)^2] \\
& + 2\nu^2[1+2x+x_\gamma(1+x-x_\gamma)] - \frac{4xx_\gamma(x^2+x_\gamma^2) - 2\nu^2(x+x_\gamma)^2}{[(1-x)(1+y)-x_\gamma]}\Bigg\} \\
& + \{y\to -y\}
\end{aligned}
\tag{II.61}
$$

$$
\mathrm{Tr_D} = M^4(1-x)^2\left(1+y^2+\frac{\nu^2}{x}\right)\left[4\left(1-\frac{\nu^2}{2x}\right)\frac{1}{AB} - \frac{\nu^2}{x}\left(\frac{1}{A^2}+\frac{1}{B^2}\right)\right] \tag{II.62}
$$

The integration over x_γ of $J[\mathrm{Tr_D}]$ has to be done analytically. After substituting the appropriate expressions from (II.130) and (II.131) and putting the result into (II.37), we find for the contribution of the divergent part to the bremsstrahlung correction

$$
\begin{aligned}
\delta_{\mathrm{D}}^{\mathrm{BS}}(x,y) = (-2)\left(\frac{\alpha}{\pi}\right)\Bigg\{ & \left(1+\frac{1+\beta^2}{2\beta}\log\gamma\right)\left[\log\frac{m}{\lambda} + \log\frac{2x_\gamma^{\max}}{(1-x)}\right] \\
& - \frac{1}{2}\log(1-y^2) - \frac{1+\beta^2}{4\beta}K(x,y)\Bigg\},
\end{aligned}
\tag{II.63}
$$

where $K(x,y)$ is given by (II.132). It is apparent that the IR divergent part indeed cancels with its counterpart in the virtual correction $\delta^{\mathrm{virt}}(x,y)$.

II.B Reduction of J terms

In this Appendix we summarize all the necessary reductions of the J terms to the basic integrals, the results of which can be found in Appendix II.D. The following formulas are used to get the matrix element squared in the form shown in Appendix II.A.

$$J\left[\frac{1}{EF}\right] = \frac{2}{(E+F)}\,J\left[\frac{1}{E}\right] = \frac{2}{M^2(1+x-x_\gamma)}\,J\left[\frac{1}{E}\right] \tag{II.64}$$

$$J\left[\frac{A}{EF}\right] = \frac{(A+C)}{(E+F)}\,J\left[\frac{1}{E}\right] = \frac{[(1-x)(1+y)-x_\gamma]}{4(1+x-x_\gamma)}\,J\left[\frac{1}{E}\right] \tag{II.65}$$

$$J\left[\frac{1}{AC}\right] = \frac{2}{(A+C)}\,J\left[\frac{1}{A}\right] = \frac{8}{M^2\,[(1-x)(1+y)-x_\gamma]}\,J\left[\frac{1}{A}\right] \tag{II.66}$$

$$\begin{aligned} J\left[\frac{1}{BD}\right] &= \frac{2}{(B+D)}\,J\left[\frac{1}{B}\right] = \frac{8}{M^2\,[(1-x)(1-y)-x_\gamma]}\,J\left[\frac{1}{A}\right]_{y\to -y} \\ &= J\left[\frac{1}{AC}\right]_{y\to -y} \end{aligned} \tag{II.67}$$

$$\begin{aligned} J\left[\frac{1}{AEF}\right] &= \frac{1}{(E+F)}\left(J\left[\frac{1}{AE}\right] + J\left[\frac{1}{CE}\right]\right) \\ &= \frac{1}{M^2(1+x-x_\gamma)}\left(J\left[\frac{1}{AE}\right] + J\left[\frac{1}{CE}\right]\right) \end{aligned} \tag{II.68}$$

$$\begin{aligned} J\left[\frac{1}{ABE}\right] &= \frac{1}{(E-2A-2B)}\left(J\left[\frac{1}{AB}\right] - 2\,J\left[\frac{1}{AE}\right] - 2\,J\left[\frac{1}{BE}\right]\right) \\ &= \frac{2}{M^2 x}\left(\frac{1}{2}\,J\left[\frac{1}{AB}\right] - J\left[\frac{1}{AE}\right] - J\left[\frac{1}{AE}\right]_{y\to -y}\right) \end{aligned} \tag{II.69}$$

$$\begin{aligned} J\left[\frac{1}{ABE^2}\right] &= \frac{1}{(E-2A-2B)}\left(J\left[\frac{1}{ABE}\right] - 2\,J\left[\frac{1}{AE^2}\right] - 2\,J\left[\frac{1}{BE^2}\right]\right) \\ &= \left\{\frac{2}{M^4x^2}\left(\frac{1}{4}\,J\left[\frac{1}{AB}\right] - J\left[\frac{1}{AE}\right]\right) - \frac{2}{M^2x}\,J\left[\frac{1}{AE^2}\right]\right\} + \{y\to -y\} \end{aligned} \tag{II.70}$$

$$\begin{aligned} J\left[\frac{1}{ACE}\right] &= \frac{1}{(A+C)}\left(J\left[\frac{1}{AE}\right] + J\left[\frac{1}{CE}\right]\right) \\ &= \frac{4}{M^2\,[(1-x)(1+y)-x_\gamma]}\left(J\left[\frac{1}{AE}\right] + J\left[\frac{1}{CE}\right]\right) \end{aligned} \tag{II.71}$$

$$\begin{aligned} J\left[\frac{1}{ADE}\right] &= \frac{1}{(\frac{E}{2}-A+D)}\left(\frac{1}{2}\,J\left[\frac{1}{AD}\right] + J\left[\frac{1}{AE}\right] - J\left[\frac{1}{DE}\right]\right) \\ &= \frac{4}{M^2[1+x-x_\gamma-y(1-x)]}\left(\frac{1}{2}\,J\left[\frac{1}{AD}\right] + J\left[\frac{1}{AE}\right] - J\left[\frac{1}{CE}\right]_{y\to -y}\right) \end{aligned} \tag{II.72}$$

$$J\left[\frac{1}{ACEF}\right] = \frac{2}{(A+C)}\,J\left[\frac{1}{AEF}\right]$$
$$= \frac{8}{M^4(1+x-x_\gamma)\left[(1-x)(1+y)-x_\gamma\right]}\left(J\left[\frac{1}{AE}\right]+J\left[\frac{1}{CE}\right]\right) \tag{II.73}$$

$$J\left[\frac{1}{ADEF}\right] = \frac{1}{(E+F)}\left(J\left[\frac{1}{ADE}\right]+J\left[\frac{1}{BCE}\right]\right)$$
$$= \frac{1}{M^2(1+x-x_\gamma)}\left(J\left[\frac{1}{ADE}\right]+J\left[\frac{1}{ADE}\right]_{y\to -y}\right)$$
$$= \left\{\frac{4}{M^4(1+x-x_\gamma)[1+x-x_\gamma-y(1-x)]}\right.$$
$$\left.\times\left(\frac{1}{2}\,J\left[\frac{1}{AD}\right]+J\left[\frac{1}{AE}\right]-J\left[\frac{1}{CE}\right]_{y\to -y}\right)\right\}+\{y\to -y\} \tag{II.74}$$

II.C Computational methods

In this Appendix we show the approaches we used to evaluate the basic integrals listed in Appendix II.D.

Feynman parametrization

With the help of the Feynman parametrization

$$\frac{1}{A_1^{\alpha_1}\cdots A_n^{\alpha_n}} = \frac{\Gamma(\alpha_1+\cdots+\alpha_n)}{\Gamma(\alpha_1)\cdots\Gamma(\alpha_n)}\int_0^1 du_1\cdots\int_0^1 du_n \frac{\delta(\sum_{k=1}^n u_k-1)u_1^{\alpha_1-1}\cdots u_n^{\alpha_n-1}}{[u_1A_1+\cdots+u_nA_n]^{\sum_{k=1}^n\alpha_k}}\,, \tag{II.75}$$

we can prepare, for example, the following terms for further integration

$$\frac{1}{AE} = \frac{2}{E(2A)} = 2\int_0^1 \mathrm{d}\alpha\,\frac{1}{[(E-2A)\alpha+2A]^2}$$
$$\overset{(II.44)}{=} 2\int_0^1 \mathrm{d}\alpha\,\frac{1}{[2(A+\alpha B)+\alpha M^2x]^2} \equiv 2\int_0^1\frac{\mathrm{d}\alpha}{\eta^2} \tag{II.76}$$

$$\frac{1}{A^2E} = \frac{4}{E(2A)(2A)} = 8\int_0^1\mathrm{d}\alpha\int_0^{1-\alpha}\mathrm{d}\beta\,\frac{1}{[(E-2A)\alpha+2A]^3} = 8\int_0^1\frac{(1-\alpha)\mathrm{d}\alpha}{\eta^3} \tag{II.77}$$

$$\frac{1}{AE^2} = \frac{2}{E^2(2A)} = 4\int_0^1\frac{\alpha\,\mathrm{d}\alpha}{\eta^3} \tag{II.78}$$

$$\frac{1}{A^2E^2} = \frac{4}{E^2(2A)^2} = 24\int_0^1\frac{\alpha(1-\alpha)\,\mathrm{d}\alpha}{\eta^4}\,, \tag{II.79}$$

where we have defined $\eta = 2\,l\cdot(\alpha p+q)+\alpha M^2 x + i\epsilon$. Now, let us calculate the following (simplest) integral

$$\begin{aligned} J\left[\frac{1}{AE}\right] &= 2\,J\left[\int_0^1 \frac{\mathrm{d}\alpha}{\eta^2}\right] = \frac{2}{4\pi}\int \mathrm{d}\Omega \int_0^1 \frac{\mathrm{d}\alpha}{\eta^2} \\ &= \frac{1}{2\pi}\int_0^1 \mathrm{d}\alpha \int \frac{\mathrm{d}\Omega}{\left[2\,l\cdot\underbrace{(\alpha p+q)}_{u}+\underbrace{\alpha M^2 x+i\epsilon}_{2l_0 V}\right]^2} = \frac{1}{4l_0^2}\int_0^1 \mathrm{d}\alpha \int_{-1}^1 \frac{\mathrm{d}z}{(u_0-|\vec{u}|z+V)^2} \\ &= \frac{1}{2l_0^2}\int_0^1 \frac{\mathrm{d}\alpha}{u^2+V^2+2u_0V} = \frac{2}{M^4}\int_0^1 \frac{\mathrm{d}\alpha}{w_2\alpha^2+w_1\alpha+w_0}\,. \end{aligned} \tag{II.80}$$

We have introduced

$$w_2 = x^2 + \frac{4l_0p_0x}{M^2} + \frac{4l_0^2m^2}{M^4} \overset{(\vec{r}=0)}{=} x^2 + \frac{1}{2}x\left[(1-x)(1-y)-x_\gamma\right] + \frac{1}{4}\nu^2 x_\gamma \tag{II.81}$$

$$w_1 = \frac{4l_0^2x}{M^2} + \frac{4l_0q_0x}{M^2} - \frac{8l_0^2m^2}{M^4} \overset{(\vec{r}=0)}{=} xx_\gamma + \frac{1}{2}x\left[(1-x)(1+y)-x_\gamma\right] - \frac{1}{2}\nu^2 x_\gamma \tag{II.82}$$

$$w_0 = \frac{4l_0^2m^2}{M^4} \overset{(\vec{r}=0)}{=} \frac{1}{4}\nu^2 x_\gamma\,. \tag{II.83}$$

The last integral can be evaluated as

$$\begin{aligned} \int_0^1 \frac{\mathrm{d}\alpha}{w_2\alpha^2+w_1\alpha+w_0} &= \frac{1}{\sqrt{w_1^2-4w_0w_2}}\log\left(\frac{2w_0+w_1+\sqrt{w_1^2-4w_0w_2}}{2w_0+w_1-\sqrt{w_1^2-4w_0w_2}}\right) \\ &\equiv \frac{1}{\sqrt{\kappa}}\log\left(\frac{\rho+\sqrt{\kappa}}{\rho-\sqrt{\kappa}}\right)\,. \end{aligned} \tag{II.84}$$

The other integrals which belong to this section can be treated in the following way

$$\frac{1}{AB} = \frac{(-1)}{B(-A)} = -\int_0^1 \mathrm{d}\alpha\,\frac{1}{[(A+B)\alpha-A]^2} \tag{II.85}$$

$$\begin{aligned} \frac{1}{CE} = \frac{(-2)}{E(-2C)} &= -2\int_0^1 \mathrm{d}\alpha\,\frac{1}{[(E+2C)\alpha-2C]^2} \\ &\overset{(II.45)}{=} -2\int_0^1 \mathrm{d}\alpha\,\frac{1}{[2(C+\alpha D)+\alpha M^2(x_\gamma-1)]^2} \end{aligned} \tag{II.86}$$

$$\frac{1}{BC} = \frac{1}{[(A+C)-A]B} = \int_0^1 \mathrm{d}\alpha\,\frac{1}{[(A+B)\alpha-B-\alpha\underbrace{(A+C)}_{(II.46)}]^2}\,. \tag{II.87}$$

Legendre polynomials and functions of the second kind

Finally, two basic integrals can be evaluated by expanding to the Legendre functions. We can write

$$\frac{B}{A} = \frac{l\cdot p}{l\cdot q} = \frac{l_0p_0-|\vec{l}||\vec{p}|\cos\theta_p}{l_0q_0-|\vec{l}||\vec{q}|\cos\theta_q} = \frac{|\vec{p}|}{|\vec{q}|}\cdot\frac{\frac{p_0}{|\vec{p}|}-\cos\theta_p}{\frac{q_0}{|\vec{q}|}-\cos\theta_q} \equiv \frac{|\vec{p}|}{|\vec{q}|}\cdot\frac{a-\cos\theta_p}{b-\cos\theta_q}\,, \tag{II.88}$$

where we have introduced $a = p_0/|\vec{p}|$ and $b = q_0/|\vec{q}|$. Now, consider first two Legendre polynomials and Legendre functions of the second kind, i.e.

$$P_0(x) = 1\,,\ P_1(x) = x\,, \tag{II.89}$$

$$Q_0(x) = \frac{1}{2}\log\frac{x+1}{x-1}\,,\ Q_1(x) = xQ_0(x) - 1\,. \tag{II.90}$$

The numerator in (II.88) can thus be rewritten in terms of the Legendre polynomials and the denominator can be expanded in the following way[13]

$$\frac{a-\cos\theta_p}{b-\cos\theta_q} \equiv \frac{a-\hat{\vec{l}}\cdot\hat{\vec{p}}}{b-\hat{\vec{l}}\cdot\hat{\vec{q}}} = \left[aP_0\Big(\hat{\vec{l}}\cdot\hat{\vec{p}}\Big) - P_1\Big(\hat{\vec{l}}\cdot\hat{\vec{p}}\Big)\right]\sum_m (2m+1)P_m\Big(\hat{\vec{l}}\cdot\hat{\vec{q}}\Big)Q_m(b)\,. \tag{II.91}$$

Since there is a useful integral formula for unit vectors $\vec{n}$ and $\vec{n}_i$

$$\int P_m(\vec{n}\cdot\vec{n}_1)P_{m'}(\vec{n}\cdot\vec{n}_2)\,\mathrm{d}\Omega\,(\vec{n}) = \frac{4\pi}{(2m+1)}\delta_{mm'}P_m(\vec{n}_1\cdot\vec{n}_2)\,, \tag{II.92}$$

the infinite sum in (II.91) reduces in the final result to only two terms

$$\begin{aligned}\frac{|\vec{q}|}{|\vec{p}|}J\left[\frac{B}{A}\right] &= \frac{1}{4\pi}\frac{|\vec{q}|}{|\vec{p}|}\int\frac{B}{A}\,\mathrm{d}\Omega = aQ_0(b)P_0\Big(\hat{\vec{p}}\cdot\hat{\vec{q}}\Big) - Q_1(b)P_1\Big(\hat{\vec{p}}\cdot\hat{\vec{q}}\Big)\\ &= aQ_0(b) - \Big(\hat{\vec{p}}\cdot\hat{\vec{q}}\Big)\,Q_1(b)\,.\end{aligned} \tag{II.93}$$

We can differentiate the previous terms in order to get the last missing piece, since

$$\begin{aligned}\frac{B}{A^2} = \frac{l\cdot p}{(l\cdot q)^2} \equiv \frac{|\vec{p}|}{l_0|\vec{q}|^2}\cdot\frac{a-\cos\theta_p}{(b-\cos\theta_q)^2} &= -\frac{1}{l_0|\vec{q}|}\cdot\frac{\partial}{\partial b}\left[\frac{|\vec{p}|}{|\vec{q}|}\cdot\frac{a-\cos\theta_p}{b-\cos\theta_q}\right]\\ = -\frac{1}{l_0|\vec{q}|}\frac{\partial}{\partial b}\left(\frac{B}{A}\right)\,.\end{aligned} \tag{II.94}$$

Hence

$$J\left[\frac{B}{A^2}\right] = -\frac{1}{l_0|\vec{q}|}\frac{\partial}{\partial b}\left(J\left[\frac{B}{A}\right]\right)\,. \tag{II.95}$$

The results can be written in the form

$$J\left[\frac{B}{A}\right] = \frac{p_0}{|\vec{q}|}\,Q_0\left(\frac{q_0}{|\vec{q}|}\right) + \frac{\frac{1}{2}(M^2x - 2m^2) - p_0q_0}{|\vec{q}|^2}\,Q_1\left(\frac{q_0}{|\vec{q}|}\right) \tag{II.96}$$

$$J\left[\frac{B}{A^2}\right] = -\frac{p_0}{l_0|\vec{q}|^2}\,Q_0'\left(\frac{q_0}{|\vec{q}|}\right) - \frac{\frac{1}{2}(M^2x - 2m^2) - p_0q_0}{l_0|\vec{q}|^3}\,Q_1'\left(\frac{q_0}{|\vec{q}|}\right), \tag{II.97}$$

where

$$Q_0'(x) = \frac{1}{1-x^2}\,,\quad Q_1'(x) = Q_0(x) + xQ_0'(x)\,. \tag{II.98}$$

[13]We use the *hat* sign to stand for the unit vector, i.e. $\hat{\vec{l}} = \vec{l}/|\vec{l}|$.

II.D Basic J terms

In this Appendix we list the results of the basic set of integrals generated by acting of the operator J on the desired combinations of variables A, ..., F in terms of (II.38). First, we define a useful logarithmic function

$$\begin{aligned} L(a,b) &\equiv \frac{1}{\sqrt{a^2-b}} \log\left|\frac{a+\sqrt{a^2-b}}{a-\sqrt{a^2-b}}\right| \\ &\overset{a>0}{=} \frac{1}{\sqrt{a^2-b}} \log\left|-1+\frac{2}{1-\sqrt{1-\frac{b}{a^2}}}\right| \end{aligned} \tag{II.99}$$

and variables, in which the results have the simple forms

$$v_1 = \frac{1}{4}\left[(1-x)(1+y)-x_\gamma\right] \tag{II.100}$$

$$v_2 = \frac{1}{4}\left[(1-x)(1-y)-x_\gamma\right] \tag{II.101}$$

$$v_0 = v_1+v_2+x = \frac{1}{2}(1+x-x_\gamma) \tag{II.102}$$

$$\rho = x x_\gamma + 2x v_1 \tag{II.103}$$

$$\rho' = x x_\gamma - 2(1-x_\gamma) v_1 \tag{II.104}$$

$$\kappa = \rho^2 - \nu^2 x x_\gamma \tag{II.105}$$

$$\omega = -v_0^2 + x + \frac{1}{4}(1-x)^2 y^2 \tag{II.106}$$

$$\xi_0 = \nu^2(v_0-1)+\rho \tag{II.107}$$

$$\xi_1 = \rho(v_0-1)+x x_\gamma \tag{II.108}$$

$$\xi_2 = \frac{\kappa}{2x} - \frac{x_\gamma}{2}\xi_0 \tag{II.109}$$

$$\xi = 1 - \frac{12}{\nu^2 x_\gamma}\left(v_1^2 - \frac{\xi_2^2}{\kappa}\right). \tag{II.110}$$

Using standard integration techniques we find the following integrals

$$J[1] = 1 \tag{II.111}$$

$$J\left[\frac{1}{A}\right] = \frac{2}{M^2} L(2v_1, \nu^2 x_\gamma) \tag{II.112}$$

$$J\left[\frac{1}{A^2}\right] = \frac{16}{M^4 \nu^2 x_\gamma} \tag{II.113}$$

$$J\left[\frac{1}{E}\right] = \frac{1}{2M^2} L(v_0, x) \tag{II.114}$$

$$J\left[\frac{1}{E^2}\right] = \frac{1}{M^4 x}. \tag{II.115}$$

With the help of the Feynman parametrization (for details see Appendix II.C) we are able to calculate

$$J\left[\frac{1}{AB}\right] = \frac{8}{M^4 x_\gamma} L(x, \nu^2 x) \tag{II.116}$$

$$J\left[\frac{1}{AE}\right] = \frac{2}{M^4} L(\rho, \nu^2 x x_\gamma) \tag{II.117}$$

$$J\left[\frac{1}{CE}\right] = \frac{2}{M^4} L(\rho', \nu^2 x x_\gamma) \tag{II.118}$$

$$J\left[\frac{1}{BC}\right] = \frac{8}{M^4} L(\omega, \nu^2 x_\gamma \omega) \tag{II.119}$$

$$J\left[\frac{1}{AE^2}\right] = \frac{4\xi_1}{M^6 \kappa x} + \frac{2\xi_2}{M^2 \kappa} J\left[\frac{1}{AE}\right] \tag{II.120}$$

$$J\left[\frac{1}{A^2 E}\right] = \frac{32\xi_2}{M^6 \nu^2 \kappa x x_\gamma} + \frac{4\xi_1}{M^2 \kappa} J\left[\frac{1}{AE}\right] \tag{II.121}$$

as well as the integral, which did not need to be evaluated in the original work [5] due to the systematic neglecting of the terms of order higher than m^2

$$\begin{aligned} J\left[\frac{1}{A^2 E^2}\right] = {} & \frac{16}{M^8 \kappa} \left(\frac{4v_1^2}{\nu^2 x_\gamma} + \frac{v_0^2}{x} + \xi \right) \\ & - \frac{4}{M^4 \kappa} (4 v_0 v_1 + \rho \xi) J\left[\frac{1}{AE}\right]. \end{aligned} \tag{II.122}$$

Using the expansion to the Legendre polynomials and functions of the second kind (see Appendix II.C), we find

$$J\left[\frac{B}{A}\right] = -\frac{\zeta_1}{\zeta} + \frac{M^2 x_\gamma \zeta_2}{2\zeta} J\left[\frac{1}{A}\right] \tag{II.123}$$

$$J\left[\frac{B}{A^2}\right] = \frac{8\zeta_2}{M^2 \nu^2 \zeta} - \frac{\zeta_1}{\zeta} J\left[\frac{1}{A}\right], \tag{II.124}$$

where we have introduced

$$\zeta_1 = 2 x x_\gamma - \nu^2 x_\gamma - 4 v_1 v_2 \tag{II.125}$$

$$\zeta_2 = 2 x v_1 - \nu^2 (v_0 - x) \tag{II.126}$$

$$\zeta = 4 v_1^2 - \nu^2 x_\gamma \,. \tag{II.127}$$

We can extract the divergent parts of the integrals (II.121) and (II.122) through

$$J\left[\frac{1}{A^2 E}\right] = \frac{1}{M^2 x} J\left[\frac{1}{A^2}\right] - \frac{16\xi_0}{M^6 \nu^2 \kappa} + \frac{4\xi_1}{M^2 \kappa} J\left[\frac{1}{AE}\right] \tag{II.128}$$

$$\begin{aligned} J\left[\frac{1}{A^2 E^2}\right] = {} & \frac{1}{M^4 x^2} J\left[\frac{1}{A^2}\right] - \frac{4}{M^4 \kappa} (4 v_0 v_1 + \rho \xi) J\left[\frac{1}{AE}\right] \\ & + \frac{16}{M^8 \kappa} \left[1 + \frac{1}{x} \left(v_0^2 - 2 - \frac{6\xi_0}{\nu^2} \right) + \frac{2}{\nu^2} \left(4 v_1 + x_\gamma + \frac{3 x_\gamma \xi_0^2}{2\kappa} \right) \right]. \end{aligned} \tag{II.129}$$

The above formulas have a very convenient form and are to be substituted into (II.61).

The divergent integrals alone have to be integrated over x_γ analytically. The calculation is done in detail in Ref. [5] and the results can be written in a simple form

$$\int J\left[\frac{1}{A^2}\right] \mathrm{d}x_\gamma = \frac{16}{\nu^2 M^4} \left[\log \frac{m}{\lambda} + \log \frac{2 x_\gamma^{\max}}{(1-x)(1+y)} \right] \tag{II.130}$$

$$\int J\left[\frac{1}{AB}\right]\mathrm{d}x_\gamma = -\frac{8}{M^4 x\beta}\left[\log\frac{m}{\lambda} + \log\frac{2x_\gamma^{\max}}{(1-x)}\right]\log(\gamma) + \frac{4}{M^4 x\beta}K(x,y)\,, \tag{II.131}$$

where

$$K(x,y) = \left[2\log\left(\frac{y+\beta}{2\beta}\right) + \log\frac{\nu^2}{x}\right]\log(\gamma) - \mathrm{Li}_2\left[\frac{\gamma(y-\beta)}{y+\beta}\right] + \mathrm{Li}_2\left[\frac{y-\beta}{\gamma(y+\beta)}\right]. \tag{II.132}$$

These terms are to be used to evaluate $\int J[\mathrm{Tr_D}]\,\mathrm{d}x_\gamma$.

Bibliography

[1] **Particle Data Group** Collaboration, K. Olive *et al.*, "Review of Particle Physics," *Chin. Phys.* **C38** (2014) 090001.

[2] R. Dalitz, "On an alternative decay process for the neutral π-meson, Letters to the Editor," *Proc. Phys. Soc.* **A64** (1951) 667–669.

[3] D. Joseph, "Electron Pair Creation in $\pi^- + p$ Capture Reactions from Rest," *Nuovo Cimento* **16** (1960) 997.

[4] B. Lautrup and J. Smith, "Radiative corrections to decays with a dalitz pair," *Phys. Rev.* **D3** (1971) 1122–1135.

[5] K. Mikaelian and J. Smith, "Radiative corrections to the decay $\pi^0 \to \gamma e^+ e^-$," *Phys. Rev.* **D5** (1972) 1763–1773.

[6] **NA48/2** Collaboration, J. R. Batley *et al.*, "Search for the dark photon in π^0 decays," *Phys. Lett.* **B746** (2015) 178–185, arXiv:1504.00607 [hep-ex].

[7] G. B. Tupper, T. R. Grose, and M. A. Samuel, "Two Photon Exchange Effect in Radiative Corrections to $\pi^0 \to \gamma e^- e^+$," *Phys. Rev.* **D28** (1983) 2905.

[8] M. Lambin and J. Pestieau, "Comment on Radiative Corrections to the Decay $\pi^0 \to e^+ + e^- + \gamma$," *Phys. Rev.* **D31** (1985) 211–212.

[9] G. Tupper, "On the Two Photon Exchange Contribution to $\pi^0 \to e^+ e^- \gamma$," *Phys. Rev.* **D35** (1987) 1726.

[10] K. Kampf, M. Knecht, and J. Novotný, "The Dalitz decay $\pi^0 \to e^+ e^- \gamma$ revisited," *Eur. Phys. J.* **C46** (2006) 191–217, arXiv:hep-ph/0510021 [hep-ph].

[11] T. Husek, K. Kampf, and J. Novotný, "Rare decay $\pi^0 \to e^+ e^-$: on corrections beyond the leading order," *Eur. Phys. J.* **C74** no. 8, (2014) 3010, arXiv:1405.6927 [hep-ph].

[12] M. Knecht, S. Peris, M. Perrottet, and E. de Rafael, "Decay of pseudoscalars into lepton pairs and large-N_C QCD," *Phys. Rev. Lett.* **83** (1999) 5230–5233, arXiv:hep-ph/9908283 [hep-ph].

[13] T. Husek and S. Leupold, "Two-Hadron Saturation for the Pseudoscalar-Vector-Vector Correlator and Phenomenological Applications," arXiv:1507.00478 [hep-ph].

Paper III

Two-Hadron Saturation for the Pseudoscalar-Vector-Vector Correlator and Phenomenological Applications

Tomáš Husek[†] and Stefan Leupold[‡]

[†]*Institute of Particle and Nuclear Physics, Faculty of Mathematics and Physics, Charles University in Prague*
V Holešovičkách 2, Praha 8, Czech Republic

[‡]*Institutionen för Fysik och Astronomi, Uppsala Universitet*
Box 516, S–75120 Uppsala, Sweden

(Submitted on July 2/August 31, 2015)

Abstract: The pseudoscalar-vector-vector (PVV) correlator is constructed using two meson multiplets in the vector and two in the pseudoscalar channel. The parameters are constrained by the operator product expansion at leading order where two or all three momenta are considered as large. Demanding in addition the Brodsky–Lepage limit one obtains (in the chiral limit) a pion-vector-vector (πVV) correlator with only one free parameter. The singly virtual pion transition form factor $\mathcal{F}_{\pi^0\gamma\gamma^*}$ and the decay width of $\omega \to \pi^0\gamma$ are independent of this parameter and can serve as cross-checks of the results. The free parameter is determined from a fit of the ω-π transition form factor $\mathcal{F}_{\pi^0\omega\gamma^*}$. The resulting πVV correlator is used to calculate the decay widths $\omega \to \pi^0 e^+e^-$ and $\omega \to \pi^0\mu^+\mu^-$ and finally the widths of the rare decay $\pi^0 \to e^+e^-$ and of the Dalitz decay $\pi^0 \to e^+e^-\gamma$. Incorporating radiative QED corrections the calculations of π^0 decays are compared to the KTeV results. We find a deviation of 2 σ or less for the rare pion decay.

Keywords: 13.20.Cz Decays of π mesons, 13.40.Ks Electromagnetic corrections to strong- and weak-interaction processes, 11.30.Rd Chiral symmetry, 12.40.Vv Vector-meson dominance

III.1 Introduction and summary

Two major challenges of contemporary particle physics are the search for beyond-Standard Model physics and a better understanding of the non-perturbative low-energy sector of the strong interaction. Typically both aspects intermix when it comes to high-precision determinations of low-energy quantities and the corresponding Standard Model predictions. If a low-energy observable is potentially influenced by quantum effects from new particles, then it is also influenced by hadronic loop effects. The latter often — if not always — constitute the main uncertainty of the Standard Model prediction. On the other hand, new physics can only be revealed if a significant deviation between experiment and Standard

Model calculation is observed. Of course, this requires small uncertainties for both the experimental and the Standard Model result. Our poor understanding of non-perturbative QCD could provide a serious hurdle for a reliable Standard Model calculation and/or for a reliable uncertainty estimate of such a calculation.

Two quantities of current interest which might indicate some deviation between experiment and the Standard Model are the gyromagnetic ratio of the muon [1, 2] and the rare decay of the neutral pion into electron and positron [3, 4]. An important quantity that enters both observables is the pion transition form factor, i.e. the three-point correlator between a neutral pion and two electromagnetic currents.

Two tasks are carried out in the present work: First, the pion-vector-vector (πVV) correlator is determined by combining high-energy quark-based information with low(er)-energy hadronic information. We follow the general approach proposed in [5] with some refinements. Second, we explore some phenomenological consequences of our correlator and focus in particular on the rare pion decay $\pi^0 \to e^+e^-$. Here we include also QED radiative corrections along the lines of [6, 7].

Two limits of QCD are of particular interest for low-energy hadron physics: The chiral limit where the masses of the two or three lightest quarks are neglected [8, 9, 10, 11, 12] and the limit where the number of quark colors, N_c, is sent to infinity [13, 14]. Concerning the πVV correlator the chiral anomaly fixes the low-energy strength unambiguously in the chiral limit. For a large number of colors there are infinitely many, infinitely narrow, i.e. stable, quark-antiquark states for every combination of quantum numbers. They show up as poles in the n-point correlators of quark currents. In the real world of three colors the hadrons generically turn to unstable resonances because the hadronic interactions do not vanish any more. The poles in the correlators turn to cuts (and poles in other Riemann sheets). The cuts start at the corresponding many-body thresholds. Thus the relevance of the large-N_c limit for the real world is highest, if one considers hadrons which are narrow and/or kinematical regions where there are no (significant) cuts. This is our guiding principle when exploring phenomenological consequences. Concerning form factors there are no cuts in the space-like region.

In the Standard Model the rare decay of the pion into electron and positron is caused by a loop where the pion first turns into a pair of (real or virtual) photons; see Fig. III.4 below. At this vertex the pion transition form factor sneaks in. If the form factor was replaced by a constant, the loop would diverge [15, 16, 17]. In QCD the pion transition form factor is suppressed for large virtualities [18, 19, 20]. This leads to a finite result for the π^0-e^+-e^- amplitude at the one-loop level of the Standard Model calculation. Thus for a quantitative determination of the branching ratio of the considered rare pion decay it is necessary to know where and how fast the pion transition form factor reaches its asymptotic form which in turn depends on the various combinations of virtualities.

These considerations show that one needs information from various QCD regimes: The threshold regime governed by the chiral anomaly, the regime of hadronic resonances, and, finally, the regime of asymptotically high energies dictated by quarks and asymptotic freedom. These regimes are connected in the approach of [5] where the operator product expansion (OPE) for various three-point correlators of quark currents is matched to a hadronic ansatz that satisfies

the chiral constraints for the low-energy limit. This ansatz is furthermore based on a truncation of the infinite tower of stable hadronic states that appears in the limit of a large number of colors.

In principle one can work out arbitrary many orders in the OPE and match to the parameters that emerge with the tower of hadron states. However, the higher orders in the OPE contain unknown quark and gluon condensates of high dimensionality. Thus in practice the model dependence emerges from a selection of the to be matched OPE constraints and from the choice where to truncate the tower of hadron states. Using one hadron multiplet per channel and leading-order OPE constraints has been studied in detail in [5]. This truncation is called "lowest-meson dominance" (LMD). In the present work we will explore the consequences of having two hadron multiplets per channel. In the language of [5] our approach would be called "LMD+V+P". To avoid this clumsy name we decided to introduce the name "two-hadron saturation" (THS).

Concerning our quantity of interest, the πVV correlator and the corresponding pion transition form factor, the starting point on the level of quark currents is the pseudoscalar-vector-vector (PVV) correlator. The consequences of LMD for this quantity have been studied in [5]. An application to the rare pion decay to electron and positron was presented in [17]. Two vector multiplets have also been considered in [5, 21]; see also [4] where this has been used for the rare pion decay. What makes our approach different from previous works is that we explore in detail the consequence of two multiplets in *each* channel and that we fit and/or compare to data on the $\pi^0\omega V$ correlator. In fact, including a second multiplet in the vector channel involves the energy region of about 1.4 GeV [22]. In this region there is also a pseudoscalar multiplet. Thus the extension from LMD to two multiplets for a channel suggests to use two multiplets for *every* channel. Concerning the second aspect, the interrelation to the $\pi^0\omega V$ correlator, we will come back to this issue below, after discussing in more detail the pertinent high-energy constraints.

There is yet one more short-distance limit to be considered. Instead of studying the high-energy limit of correlators of quark currents (OPE), one can also study the high-energy limit of correlators that involve specific asymptotic states like hadrons or photons together with one or several quark currents. In particular the high-energy behavior of the pion-photon-vector correlator has recently gained much attention since the BaBar data [23] seem to contradict the Brodsky–Lepage (B-L) scaling limit [20] while the Belle data [24] seem to support it.

Using THS we are able to satisfy all leading-order OPE constraints for the PVV correlator and in addition the B-L constraint for the pion-photon-vector correlator. While LMD satisfies the same OPE constraints, it violates the B-L constraint as can be easily deduced from the explicit form given in [17]; see also the discussion in [5]. As we will show below, the constraints from the leading order of the OPE, from B-L and from the chiral anomaly together fix the THS approach to the πVV correlator up to one single parameter, which we call κ. If the invariant mass of one of the vector currents in this correlator is set to zero, i.e. for the pion-photon-vector correlator, then κ drops out. In other words we have full predictive power for this correlator. Aiming at the rare pion decay into electron and positron one needs the full information on the πVV correlator for arbitrary invariant masses of the two vector currents. In principle, the parameter

κ would be best determined from data on the πVV correlator with both invariant masses being different from real photons. Unfortunately such data do not exist.

In this situation we turn to the second-best choice. Projecting the πVV correlator on one of the vector mesons that we include in THS yields a 3-point correlator for the pion, the vector meson and a quark current with vector quantum numbers. Given that our approach is based on the large-N_c limit where mesons are approximated by infinitely narrow states, it is suggestive to use a narrow vector meson. Since phenomenologically and in the large-N_c limit the pion decouples from the ϕ meson [25, 26, 27, 14], we are left with the ω meson as the best choice for a vector meson. Consequently we will use data on the ω-π transition form factor [28] to fix our remaining parameter κ.

The πVV correlator obtained in this way from THS shows an awesome behavior: If the virtuality of one vector current becomes large while the other is set to zero (photon case), the asymptotic B-L limit is reached rather fast, resembling essentially strict vector-meson dominance (VMD) [29, 30]. The scale that defines where the approach to the asymptotic limit sets in is basically given by the mass of the ρ/ω meson. On the other hand, if both vector currents have the same large virtuality, the corresponding asymptotic limit is reached very late for the πVV correlator as obtained from THS. This finding points to the relevance of details of hadronic physics above 1 GeV. For this case the πVV correlator from VMD falls off much faster than demanded by QCD, while for LMD the asymptotic limit is reached much earlier than for THS. Since the rare decay $\pi^0 \to e^+e^-$ is sensitive to both high- and low-energy physics, it is interesting to study how this intriguing behavior of the πVV correlator obtained from THS influences the branching ratio of this rare process.

Before going into the details of our findings we shall compare our approach to related ones from the literature. The ω-π transition form factor and related quantities have also been addressed in [31, 32, 33] where the ground-state vector mesons are treated as light degrees of freedom. By construction the approach is restricted to low energies, i.e. high-energy constraints were not considered. Nonetheless, it turns out that the THS result for the ω-π transition form factor is numerically very close to the one from [31].

Conceptually close in spirit to THS is the Lagrangian approach utilized, e.g., in [34, 35] (earlier references can be traced back from these works). Also here hadron resonances in the large-N_c limit are used to interpolate between the low-energy region governed by chiral perturbation theory and the high-energy region governed by the OPE or quark scaling considerations. In [35] a PVV and a corresponding πVV correlator are constructed with one multiplet in the vector channel and two multiplets in the pseudoscalar channel (i.e. the Goldstone bosons and one resonance multiplet). For an extension to two multiplets in the vector channel see [36]. The πVV correlator from [35] satisfies the B-L constraint, but the PVV correlator satisfies only one leading-order OPE constraint, not all of them. As shown in [37] the Lagrangian utilized in [35] is not capable to provide correlators that satisfy all OPE constraints; see also the discussion in [5]. Instead of the other OPE constraints on the PVV correlator a high-energy constraint based on quark counting rules is imposed on the $\pi\rho V$ correlator in [35].

In our work we impose high-energy constraints on the PVV correlator (THS satisfies *all* leading-order OPE constraints) and on the πVV correlator (the B-L

limit), but not on the $\pi\rho V$ or $\pi\omega V$ correlator. Our philosophy is that we take the first multiplets to resemble the corresponding ground-state physical particles but the second multiplets to mimic the effect of the tower of infinitely many excited states. Since we study with PVV an order parameter of chiral symmetry breaking [5] one expects that the second multiplets are close to the physical states that are the first excitations on top of the ground states. However, the weighted average of the whole tower of states might shift the effective mass higher up. In the present work we explore the uncertainty of the THS approximation by changing the masses of the second multiplets from the first to the second physical excitations. Concerning the πVV correlator we expect to obtain reasonable results because the pion might not resolve too many details of the intermediate-energy region. Thus replacing the tower of excited resonances by the respective lowest excitation and demanding high-energy constraints for the πVV correlator might be good enough. In contrast, a $\pi\rho V$ or $\pi\omega V$ correlator resolves more from the intermediate-energy region because the vector meson induces a larger mass scale. (The same would apply to a ρPV correlator.) Therefore to satisfy high-energy constraints in this case we expect that one would need a more detailed modeling than just having THS, i.e. one excitation (plus the ground state) in each channel. It might be worth to explore a three-hadron saturation scenario, but this is beyond the scope of the present work. Therefore we demand constraints on the PVV and πVV correlators, but disregard constraints for three-point correlators of one pseudoscalar meson, one vector meson and one vector quark current. For the same reason we only consider leading, but not subleading high-energy/OPE constraints.

From a formal point of view our approach is close to the successive Padé approximations as utilized, e.g., in [38]. Our correlators are also approximated by rational functions. In our approach, however, the poles of the correlators are related to physical states (in the large-N_c limit). In contrast, in the Padé framework of [38] one determines the rational functions by fits to data. It is not the purpose of this Padé approach to look for the poles of the obtained rational functions. In fact, there are no physical restrictions from outside that would make sure that these poles correspond in any way to physical hadrons. But this is what S-matrix theory suggests (in the large-N_c limit): Anything beyond polynomials should be caused by unitarity, analyticity, crossing symmetry and physical states.

Our work is complementary to the dispersion theoretical approach of [39, 40]; see also [41]. While we cannot expect to reach the accuracy of a dispersive approach concerning low-energy quantities, our framework has the advantage to provide a smooth and physical connection between the low- and high-energy region and between the quark based and hadron based correlators. In practice, dispersive calculations are based on an excellent account of the low-energy region (up to about 1 GeV) and a high-energy completion, i.e. a matching to the high-energy behavior deduced from S-matrix theory, QCD or QCD related approaches; see the discussion in [40] concerning the πVV correlator. As already discussed, for our doubly virtual πVV correlator there are regions in the virtualities where the asymptotic regime is reached only at very high energies. In practice this might imply that a naive matching of a dispersive calculation to the asymptotic regime might miss part of the physics present at intermediate energies. Clearly it is worth to explore the interplay of a dispersive calculation with THS in the future.

The rest of the paper is structured in the following way: In Section III.2

we construct the PVV and πVV correlators subject to high- and low-energy constraints. The results for the πVV correlator are compared to data and to other approaches (LMD and VMD). It is studied how the shape of the correlator changes when varying the remaining free parameter κ in a reasonable range. In addition, a model uncertainty is estimated by varying the mass of the second vector-meson multiplet between the *physical* masses of the first and second excitation.

In Section III.3 the $\pi\omega V$ correlator is constructed. The parameter κ is determined from a fit to the ω-π transition form factor. The widths or branching ratios, respectively, for the corresponding decays $\omega \to \pi^0\gamma$, $\pi^0 e^+e^-$, and $\pi^0\mu^+\mu^-$ are determined for THS (and also for LMD and VMD). Actually the first decay does not depend on κ. We find good agreement between THS and the experimental results.

We address the rare pion decay to electron and positron in Section III.4. Including radiative corrections the branching ratio of this process is calculated and we compare again the THS result to other approaches. For the THS case this branching ratio is sensitive to κ. Direct comparison to the experimental value from KTeV [3] seems to suggest that a discrepancy persists on the level of $2\,\sigma$.

In Section III.5 we study the properties of the singly virtual pion transition form factor in the low-energy region, such as slope and curvature. Note that these quantities do not depend on the parameter κ. For the Dalitz decay $\pi^0 \to e^+e^-\gamma$ we calculate the decay width taking into account next-to-leading order (NLO) radiative corrections. These are evaluated along the lines of [42]. Again we compare THS to other approaches. With the full set of radiative corrections at hand, we take a fresh look on the KTeV result. Considering some radiative corrections that were not accounted for in the analysis suggests that the previously stated discrepancy might be even reduced to $1.5\,\sigma$. The main message here, however, is that the radiative corrections are now theoretically under control [6, 7, 42] and can be used in future data analyses.

In Section III.6 we provide an outlook how THS can be further utilized and how the scheme can be extended. Finally, an appendix is added to provide the pseudoscalar form factors in terms of the loop integrals required for the rare pion decay.

Comparing in detail various approaches throughout the present work reveals that the VMD form factor proves to be phenomenologically very successful in most applications, in spite of the facts that VMD is so simple and partially possesses an improper high-energy behavior. However, the THS form factor, which satisfies all the considered constraints, works very well, too. Still, the mean value of the KTeV result remains a challenge for all approaches, even though the discrepancy has been reduced by a considerable level. We provide a brief discussion on this point in the corresponding sections.

III.2 THS approach to the πVV correlator

Following [5, 37] we introduce the PVV correlator $\Pi(r^2; p^2, q^2)$ by

$$d^{abc}\epsilon_{\mu\nu\alpha\beta}p^\alpha q^\beta \Pi(r^2; p^2, q^2) \equiv \int \mathrm{d}^4x\, \mathrm{d}^4y\, e^{ip\cdot x + iq\cdot y}\langle 0|T[P^a(0)V_\mu^b(x)V_\nu^c(y)]|0\rangle \quad \text{(III.1)}$$

with $r = p + q$. The vector and pseudoscalar current, respectively, are defined by[14]

$$V_\mu^a(x) \equiv \bar{q}(x)\gamma_\mu T^a q(x)\,, \quad P^a(x) \equiv \bar{q}(x) i\gamma_5 T^a q(x)\,. \tag{III.2}$$

In the above formulae we have used

$$\mathrm{Tr}\Big[T^a, T^b\Big] = \frac{1}{2}\delta^{ab}\,, \quad d^{abc} \equiv 2\,\mathrm{Tr}\Big[\{T^a, T^b\}T^c\Big]\,. \tag{III.3}$$

For $a = 1, \ldots, 8$ we have $T^a \equiv \lambda^a/2$ where λ^a denote the Gell-Mann matrices in flavor space. Since we utilize the large-N_c limit we have to deal with flavor nonets, i.e. with U(3) instead of SU(3). The formulae (III.3) provide a natural extension to $a = 0$.

Working in the chiral limit[15] and considering two meson multiplets in the vector and two in the pseudoscalar channel, we propose a correlator of the form

$$\Pi^{\mathrm{THS}}(r^2; p^2, q^2) = \frac{B_0 F^2}{r^2(r^2 - M_P^2)} \frac{P(r^2; p^2, q^2)}{(p^2 - M_{V_1}^2)(p^2 - M_{V_2}^2)(q^2 - M_{V_1}^2)(q^2 - M_{V_2}^2)}\,. \tag{III.4}$$

Here $P(r^2; p^2, q^2)$ is the most general polynomial in its arguments that is symmetric in the second and the third argument. For our purpose, a polynomial of order four is sufficient inasmuch as higher powers of momenta in the numerator are not allowed due to the desired high-energy behavior that we will specify below. Thus we start with a term containing 22 monomials and associated free parameters. Schematically this looks as follows:

$$P(r^2; p^2, q^2) = c_0 p^2 q^2 + c_1[(p^2)^4 + (q^2)^4] + c_2[(p^2)^3 q^2 + (q^2)^3 p^2] + c_3 (r^2)^2 p^2 q^2 + \ldots\,. \tag{III.5}$$

The quantities F and B_0 in (III.4) denote the usual low-energy constants of chiral perturbation theory [11, 12]. We will specify them further when needed. M_P denotes the mass of the second multiplet, i.e. first excitation, in the pseudoscalar channel. The first multiplet (ground state) is, of course, the massless multiplet of Goldstone bosons.

The masses of the lowest two vector-meson multiplets are denoted by M_{V_1} and M_{V_2}. As already spelled out in Section III.1 we use for M_{V_1} the mass of the ground-state vector-meson multiplet (in the chiral limit). We assume that this mass is approximately given by the mass of the ω or ρ meson. For M_{V_2} it is suggestive to use the physical mass of the first excitation in the vector channel. However, we do not use a fixed mass here, but study the impact of a variation of M_{V_2} on our results. In this way we explore the uncertainty caused by the higher-lying excitations that are neglected in THS. In practice we vary M_{V_2} in the range

$$M_{V_2} \in [1400, 1740]\,\mathrm{MeV}, \tag{III.6}$$

which is the interval between the masses of the first and the second physical excitation [22].

Finally we note that the same logic applies to the mass M_P of the second pseudoscalar multiplet. For the PVV correlator one should study the impact of

[14] Our convention is $\gamma_5 = i\gamma^0\gamma^1\gamma^2\gamma^3$.

[15] The chiral limit is only used for the construction of the correlator. Once the form factor is settled, we take the physical pion mass for all the kinematics used for comparing the predictions to experimental data.

a variation of M_P. As we will see below, however, this mass does not show up in the final expression for the πVV correlator.

We now demand that the ansatz (III.4) satisfies all the relevant high- as well as low-energy constraints in order to minimize the number of free parameters introduced in (III.5). Starting with the general correlator (III.4) we apply the following leading-order OPE constraints [5]:

$$\Pi\Big((\lambda r)^2;(\lambda p)^2,(\lambda q)^2\Big) = \frac{1}{2}B_0F^2\frac{1}{\lambda^4}\frac{r^2+p^2+q^2}{r^2p^2q^2} + \mathcal{O}\left(\frac{1}{\lambda^6}\right), \tag{III.7}$$

$$\Pi\Big(r^2;(\lambda p)^2,(r-\lambda p)^2\Big) = B_0F^2\frac{1}{\lambda^2}\frac{1}{r^2p^2} + \mathcal{O}\left(\frac{1}{\lambda^3}\right). \tag{III.8}$$

It turns out that the third OPE constraint [5]

$$\Pi\Big((q+\lambda p)^2;(\lambda p)^2,q^2\Big) = \frac{1}{\lambda^2}\frac{1}{p^2}f(q^2) + \mathcal{O}\left(\frac{1}{\lambda^3}\right), \tag{III.9}$$

is automatically fulfilled by our ansatz. Here f denotes a function (actually a two-point correlator [5]) that depends only on q^2 and not on the other kinematic variables p^2 and $p\cdot q$.

Next, we define the πVV correlator:

$$\mathcal{F}_{\pi VV}(p^2,q^2) \equiv \frac{1}{\mathcal{Z}_\pi}\lim_{r^2\to 0} r^2\Pi(r^2;p^2,q^2)\,, \tag{III.10}$$

where

$$\mathcal{Z}_\pi \equiv \frac{i}{2}\langle 0|(\bar{u}\gamma_5 u - \bar{d}\gamma_5 d)|\pi^0\rangle \tag{III.11}$$

denotes the overlap between the pion field and the pseudoscalar quark current. With the usual conventions from chiral perturbation theory one obtains $\mathcal{Z}_\pi = B_0F$ [11, 12]. For large λ one then finds

$$\begin{aligned}\mathcal{F}_{\pi VV}\Big((\lambda p)^2,(\lambda p)^2\Big) &\simeq \frac{1}{\mathcal{Z}_\pi}\lim_{r^2\to 0} r^2\Pi\Big(r^2;(\lambda p)^2,(r-\lambda p)^2\Big)\\ &\overset{(III.8)}{=} \frac{1}{B_0F}B_0F^2\frac{1}{\lambda^2p^2} + \mathcal{O}\left(\frac{1}{\lambda^3}\right),\end{aligned} \tag{III.12}$$

which means that in agreement with [18, 19, 5] we have

$$\mathcal{F}_{\pi VV}(q^2,q^2) \to \frac{F}{q^2}\,,\ q^2\to-\infty\,. \tag{III.13}$$

Hence, this condition is satisfied automatically on account of the OPE constraints. Actually, for the quantity $\mathcal{F}_{\pi VV}(q^2,q^2)$ also the subleading order in the high-energy expansion is known in terms of a quark-gluon condensate [43]; see also the corresponding discussion in [1]. However, we refrain from incorporating this as an additional constraint. The reason is the same as to why we do not use constraints from transition form factors of hadronic resonance states. One might become too sensitive to the details of the intermediate mass region where we use one hadronic state to describe effectively the whole infinite tower of large-N_c excited states. If

one used three instead of two hadronic states per channel, the subleading high-energy constraints might provide a viable input to pin down the growing number of resonance parameters. But this is clearly beyond the scope of the present work.

Instead of involving subleading orders in the high-energy expansion we apply the B-L constraint [20]

$$\frac{\mathcal{F}_{\pi VV}(0,q^2)}{\mathcal{F}_{\pi VV}(0,0)} \to -\frac{24\pi^2 F^2}{N_c}\frac{1}{q^2}\,,\; q^2 \to -\infty\,. \tag{III.14}$$

We define the pion transition form factor as

$$\mathcal{F}_{\pi^0\gamma^*\gamma^*}(p^2,q^2) = \frac{2}{3}\mathcal{F}_{\pi VV}(p^2,q^2) \tag{III.15}$$

and match at the photon point to the chiral anomaly, i.e. to the Wess–Zumino–Witten term [9, 10],

$$\mathcal{F}_{\pi VV}(0,0) = \frac{3}{2}\mathcal{F}_{\pi^0\gamma^*\gamma^*}(0,0) = -\frac{N_c}{8\pi^2 F}\,. \tag{III.16}$$

Together the constraints (III.7), (III.8), (III.14) and (III.16) provide us with a πVV correlator that appears to have only one free dimensionless parameter κ:

$$\begin{aligned}\mathcal{F}^{\rm THS}_{\pi VV}(p^2,q^2) = &-\frac{N_c}{8\pi^2 F}\frac{M_{V_1}^4 M_{V_2}^4}{(p^2-M_{V_1}^2)(p^2-M_{V_2}^2)(q^2-M_{V_1}^2)(q^2-M_{V_2}^2)}\\ &\times\left\{1+\frac{\kappa}{2N_c}\frac{p^2q^2}{(4\pi F)^4}-\frac{4\pi^2F^2(p^2+q^2)}{N_c M_{V_1}^2 M_{V_2}^2}\left[6+\frac{p^2q^2}{M_{V_1}^2M_{V_2}^2}\right]\right\}.\end{aligned} \tag{III.17}$$

Note that our result is independent of the mass M_P of the first pseudoscalar excitation. This happens due to the fact that at the end of the day we could conveniently rescale the only free parameter left. From the structure of the result (III.17) it can be read off that κ emerges from c_0 in (III.5) on account of

$$c_0 = \frac{\kappa M_P^2 M_{V_1}^4 M_{V_2}^4}{(4\pi F)^6}\,. \tag{III.18}$$

We note in passing that κ scales with N_c^3.

A comparison to the work of [5] is in order here concerning the number of free parameters. We shall compare our THS approach to LMD+V of [5], i.e. to the case of one pseudoscalar and two vector multiplets. We recall that THS = LMD+V+P in the language of [5]. After applying the OPE constraints to THS we are left with 12 free parameters for the PVV correlator. This compares to 7 free parameters for the case of LMD+V. The low-energy constraint (III.16) fixes always one more parameter. Once we focus on the πVV correlator we are left with 4 parameters for THS. For LMD+V one has 3. Demanding that the πVV correlator of (III.14) drops like $1/q^2$ limits the free parameters to 2 for both cases THS and LMD+V. Demanding (III.14) *quantitatively* and not just a scaling with $1/q^2$ yields one free parameter for THS as well as for LMD+V. To summarize, after applying all constraints THS has more parameters for the PVV correlator than LMD+V: 8 in THS versus 4 in LMD+V. But concerning the πVV correlator one ends up with one free parameter in both cases.

According to [4] the πVV correlator should satisfy the inequality

$$|\mathcal{F}_{\pi VV}(q^2, q^2)| < |\mathcal{F}_{\pi VV}(0, q^2)|\,,\ q^2 < 0\,. \tag{III.19}$$

It turns out that the THS expression (III.17) satisfies (III.19) for $-45 \lesssim \kappa \lesssim 30$. We will see below that the values for κ that we obtain from fitting to experimental data lie well within this range.

Before further constraining κ from data it is illuminating to study the qualitative shape of the πVV correlator when κ is varied. In addition, we compare our results to similar approaches from the literature, namely to the VMD correlator [29, 30, 5, 37]

$$\mathcal{F}^{\rm VMD}_{\pi VV}(p^2, q^2) = -\frac{N_c}{8\pi^2 F}\frac{M_{V_1}^4}{(p^2 - M_{V_1}^2)(q^2 - M_{V_1}^2)} \tag{III.20}$$

and to the LMD expression [17, 5]

$$\mathcal{F}^{\rm LMD}_{\pi VV}(p^2, q^2) = \mathcal{F}^{\rm VMD}_{\pi VV}(p^2, q^2)\left[1 - \frac{4\pi^2 F^2(p^2 + q^2)}{N_c M_{V_1}^4}\right]. \tag{III.21}$$

See also [44] for a comparison of various correlators.

First of all, we note that the VMD result grossly violates (III.13) while it is not far off from the B-L constraint (III.14). On the other hand, LMD satisfies (III.13), but does not satisfy (III.14). By construction the THS correlator satisfies all the mentioned constraints, but it is interesting to see how fast or slow the asymptotic limits are reached. This is shown in Fig. III.1. To facilitate a comparison with data we show the pion transition form factor (times the virtuality q^2) instead of the πVV correlator. Note that the relation (III.15) between the pion transition form factor and the πVV correlator only amounts to a rescaling.

In the first panel of Fig. III.1 we display the symmetric doubly virtual pion transition form factor. This plot shows three different *types* of lines and a gray band. We shall first discuss the lines: The dash-dotted LMD line approaches very quickly the asymptotic QCD result given by (III.13). The dashed VMD line falls stronger than what is required by QCD. The full lines labeled by values for κ show the THS result for a mass of M_{V_2} taken in the middle of the interval (III.6). All the full lines will approach the LMD line at very large momenta. One sees, however, that typically the THS lines reach this limit rather late. In particular, for $\kappa \geq 15$ the THS form factor peaks at rather high momentum values and with large magnitude in comparison to VMD and LMD. It reaches the asymptotic limit only very slowly. For the case $\kappa \simeq 9$ we see that the associated line is very close to LMD, but peaks later and approaches the asymptotic limit from above. For $\kappa \simeq 6$ we get the limiting case where THS is monotonically growing. Going further down with κ a wiggle appears, which for $\kappa = 0$ and low virtualities resembles very much the VMD behavior. For negative κ the THS results start to undershoot VMD at low virtualities. Moving to even lower κ values there is always a region where the THS result becomes negative. Intuitively we find it hard to believe that the transition form factor of a ground-state hadron (the pion) would display so many wiggles as suggested by the full lines for small values of κ. Indeed, the determination of κ, which will be carried out in the next section, reveals a κ value of about 21. Thus we find the qualitative situation that the THS result for

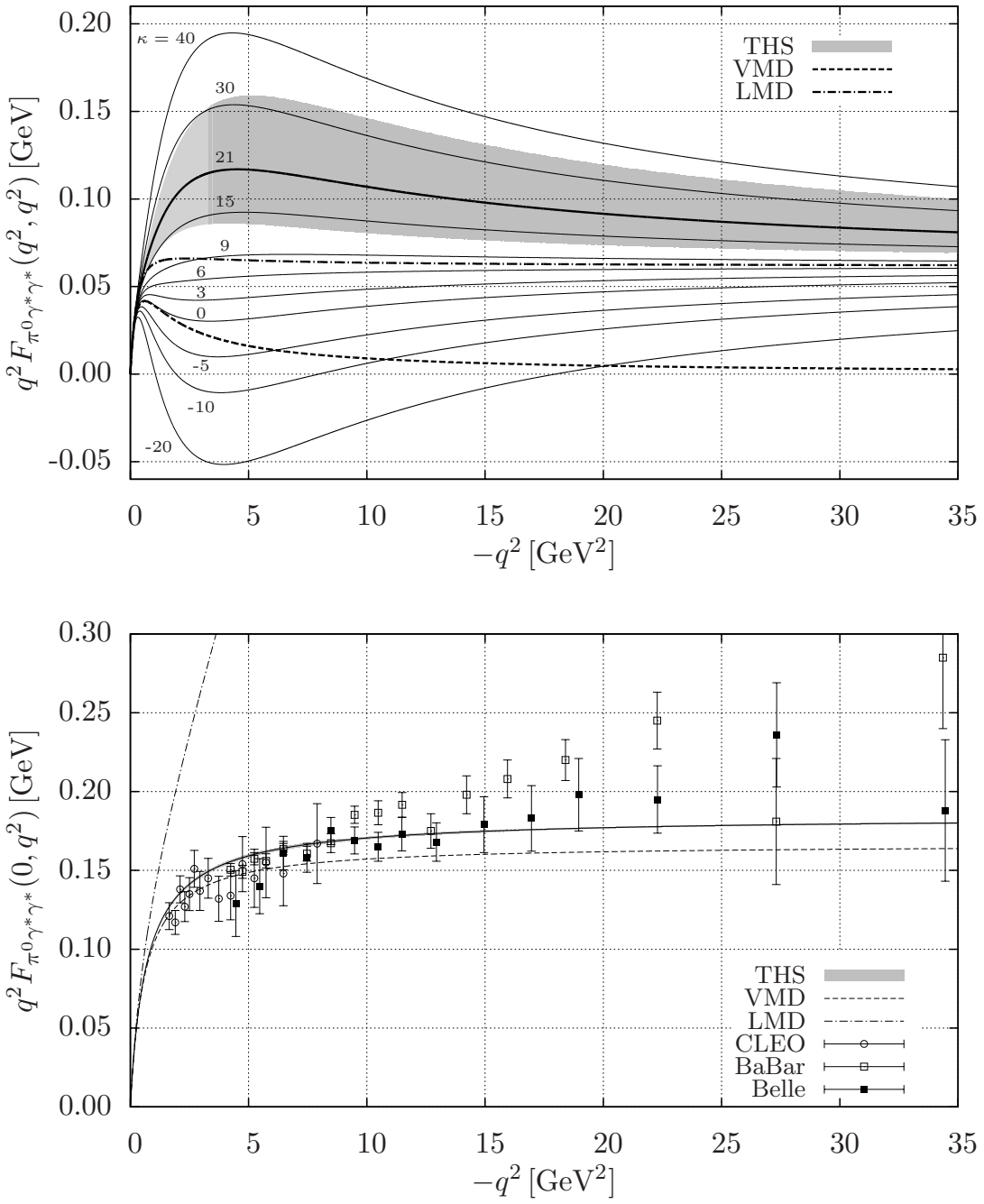

Figure III.1: Symmetric doubly virtual (first panel) and singly virtual (second panel) pion transition form factor as a function of the virtuality in the space-like region. The gray bands constitute the final THS predictions. See the main text for details how the uncertainties are determined. In the second panel the gray band nearly collapses to one full line. The thin full lines in the first panel show what happens if κ is varied in a large range. The corresponding curve that constitutes the center of the gray band has been made bold. The results from VMD and LMD are given by the dashed and dash-dotted lines, respectively. Data are taken from [45, 23, 24].

the pion transition form factor (times the virtuality q^2) overshoots the asymptotic limit, peaks at rather large momenta and approaches the asymptotic limit rather slowly from above.

The gray bands in both panels of Fig. III.1 constitute our final THS predictions for the pion transition form factor. The results from the next section are anticipated where κ is further constrained. To obtain the gray bands all input for our THS pion transition form factor (F, M_{V_1}) is varied within the respective experimentally allowed regions, $\kappa = 21 \pm 3$ as described in the next section, and M_{V_2} is varied within region (III.6). The whole gray band in the first panel shows the qualitative behavior described previously. It also points to a significant quantitative uncertainty of our prediction for the symmetric doubly virtual pion transition form factor. In other words, data on this form factor or in general on any doubly virtual pion transition form factor would be highly welcome to better constrain our approach.

In the second panel of Fig. III.1 we display the singly virtual pion transition form factor. This plot shows two lines, a very narrow gray band and data. We first discuss the gray band, which nearly resembles a full line since its width is so small. Obviously the narrow gray band of the second panel contrasts with the rather broad band of the first panel. However, the singly virtual pion transition form factor is independent of κ as can be easily deduced from (III.17) when putting p^2 to zero. The largest uncertainty comes from a variation of M_{V_2} according to (III.6). Even this variation does not lead to very different results, which causes the curves to nearly collapse to one single line. Thus THS has rather high predictive (or rather *postdictive*) power for the singly virtual pion transition form factor. Another qualitative difference between the gray bands of the first and the second panel is the fact that the THS result for the singly virtual pion transition form factor reaches the asymptotic (B-L) limit rather early. We regard this intriguing behavior of our correlator as one of the highlights of our work: The THS pion transition form factor shows an early (late) onset of the asymptotic behavior for the singly (symmetric doubly) virtual pion transition form factor. It would be extremely interesting to see if this is supported by data in the future.

Finally, we compare the THS result for the singly virtual pion transition form factor to VMD and LMD and to data. The LMD result for $\mathcal{F}_{\pi^0\gamma^*\gamma^*}(0, q^2)$ behaves as a constant for large $|q^2|$. Thus, it cannot even qualitatively explain the data since, of course, it diverges after being multiplied by q^2. This behavior can be seen in the second panel of Fig. III.1 where the LMD result is given by the dash-dotted line. The results for VMD (dashed line) and THS are fairly close. CLEO data [45] are only available for low virtualities ($-q^2 < 8\,\mathrm{GeV}^2$) and prefer VMD to some extent though THS appears to be acceptable as well. The situation turns around for higher virtualities. THS describes the Belle data [24] better than VMD. The early onset of the asymptotic behavior of the THS result for the singly virtual pion transition form factor makes THS essentially identical to the B-L limit. Not surprisingly then, THS agrees well with the Belle data and is at odds with the BaBar data [23] that are not fully compatible with the Belle data. We do not attempt to contribute to a clarification of the differences between Belle and BaBar. In view of these complications we have decided to stick to the B-L constraint (III.14) right from the start.

III.3 Phenomenology of ω decays

Our strategy now is to obtain the parameter κ of the newly proposed πVV correlator (III.17) from the $\pi\omega V$ correlator. Thus we turn to ω data for the reasons specified in Section III.1, namely the lack of doubly virtual data for the pion transition form factor and the fact that the ω meson is fairly long lived to resemble the situation of the large-N_c approximation.

We introduce the overlap between an ω meson and the vector current V, i.e.

$$\mathcal{Z}_\omega \epsilon_\mu(\vec{p},\lambda_\omega) \equiv \frac{1}{2}\langle 0|(\bar{u}\gamma_\mu u + \bar{d}\gamma_\mu d)|\omega(\vec{p},\lambda_\omega)\rangle\,, \tag{III.22}$$

where we assume that the ω meson does not contain hidden strangeness, which is a fairly good approximation to the real world [22]. For later convenience we also define the γ-ω coupling strength

$$F_\omega \equiv \frac{Z_\omega}{M_\omega}\,, \tag{III.23}$$

the modulus of which agrees with F_V as introduced in [46].

With this at hand we can obtain F_ω from the $\omega \to e^+e^-$ decay process. A direct calculation from the Lorentz invariant matrix element

$$i\mathcal{M}_{\omega\to e^+e^-} = \frac{ie\mathcal{Z}_\omega}{3}\bar{u}(\vec{q}_1)(-ie\gamma^\mu)v(\vec{q}_2)\frac{(-i)}{M_\omega^2}\epsilon_\mu(\vec{p},\lambda_\omega)\,, \tag{III.24}$$

yields after averaging and summing over polarizations

$$F_\omega = \left[\frac{4\pi\alpha^2}{27M_\omega}\frac{1}{\Gamma(\omega\to e^+e^-)}\beta_{e\omega}\left(1+\frac{2m_e^2}{M_\omega^2}\right)\right]^{-\frac{1}{2}}, \tag{III.25}$$

where $\beta_{e\omega} = \sqrt{1-4m_e^2/M_\omega^2}$ is the speed of the electron in the rest frame of the decaying ω meson. Taking into account that $m_e^2 \ll M_\omega^2$, we can write

$$F_\omega \simeq \frac{1}{e^2}\sqrt{108\pi M_\omega \Gamma(\omega\to e^+e^-)}\,. \tag{III.26}$$

Using the values $B(\omega\to e^+e^-) = (7.28\pm0.14)\times10^{-5}$ and $\Gamma(\omega) = (8.49\pm0.08)\,\text{MeV}$ [22] we find $\Gamma(\omega\to e^+e^-) = (0.62\pm0.02)\,\text{keV}$. Together with $M_\omega = (782.65\pm0.12)\,\text{MeV}$ we obtain from (III.26) the following value for the coupling strength:

$$F_\omega = (140\pm2)\,\text{MeV}. \tag{III.27}$$

It is convenient to introduce the $\pi^0\omega V$ transition form factor by

$$\mathcal{F}_{\pi^0\omega V}(q^2) = \frac{1}{\mathcal{Z}_\omega}\lim_{p^2\to M_{V_1}^2}(p^2-M_{V_1}^2)\mathcal{F}_{\pi VV}(p^2,q^2)\,. \tag{III.28}$$

This turns out to be the central quantity to determine κ and to address the phenomenologically interesting decays $\omega\to\pi^0\gamma$ and $\omega\to\pi^0\ell^+\ell^-$, where ℓ denotes a lepton.

For the special case when $q^2 = 0$ we find (see also [34] for a similar expression for the case of one vector multiplet)

$$\mathcal{F}^{\text{THS}}_{\pi^0\omega V}(0) = \frac{1}{\mathcal{Z}_\omega}\frac{N_c}{8\pi^2 F}\frac{M_{V_1}^2 M_{V_2}^2}{(M_{V_2}^2 - M_{V_1}^2)}\left[1 - \frac{24\pi^2 F^2}{N_c M_{V_2}^2}\right]. \tag{III.29}$$

Hence the decay width for $\omega \to \pi^0\gamma$ is independent of κ, which provides us with full predictive power for this particular decay and can therefore serve as a cross-check of our formalism. We will come back to this decay after having determined κ from the measured ω-π transition form factor.

In fact, the parameter κ, which constitutes the only unknown parameter of our proposed πVV correlator, can be obtained by a fit to the NA60 data [28] for the normalized transition form factor

$$\hat{\mathcal{F}}_{\pi^0\omega V}(q^2) \equiv \frac{\mathcal{F}_{\pi^0\omega V}(q^2)}{\mathcal{F}_{\pi^0\omega V}(0)} \tag{III.30}$$

in the low-energy time-like region of q^2 with the result

$$\kappa = 21 \pm 3\,. \tag{III.31}$$

The result is displayed in Fig. III.2 as a gray band. The uncertainty comes mainly from the fitting procedure (and so from the error bars of the data) and from the variation of the second-multiplet mass M_{V_2} inside the considered region (III.6). Our fit to the NA60 data has a χ^2 per degree of freedom of 1.5. Apparently we obtain a rather satisfying fit to the NA60 data except for the last two or three data points at the largest values of the dimuon mass. At present, none of the hadron-theory approaches to this ω transition form factor [31, 47, 39, 48, 41] is able to understand these last data points. Recently it has been suggested in [49] using a dispersive calculation and high-energy constraints that these data points might be incompatible with QCD. Clearly it would be highly desirable to obtain additional data for this ω transition form factor, in particular from experiments where the complete final state $\pi^0\ell^+\ell^-$ can be reconstructed and not only the dilepton; see [28] for more details.

In the following we will stick to our result for κ as given in (III.31) and obtained from a fit to the full range of NA60 data since it is the best that one can do in the present situation. However, we briefly discuss two alternatives: If we performed an alternative fit to the NA60 data rejecting the last three data points, we would get $\kappa = 19 \pm 2$, which is fairly compatible with our full fit. The χ^2 per degree of freedom would reduce to 0.8. If we rejected the NA60 data altogether and regarded the dispersive calculation of [39] as the "truth", we would find $\kappa = 13.1 \pm 0.5$. The result of this last fit is also shown in Fig. III.2 as the dark gray band. If we return to the first panel of Fig. III.1 we observe that one obtains the same qualitative features with such values of κ. Nevertheless, we will not use these results further on and will take into account only the result (III.31) of the all-data fit.

As for the pion transition form factor we shall compare our result to similar approaches from the literature. The form factor from [31],

$$\hat{\mathcal{F}}^{\text{TL}}_{\pi^0\omega V}(q^2) = \frac{M_{V_1}^2 + q^2}{M_{V_1}^2 - q^2}\,, \tag{III.32}$$

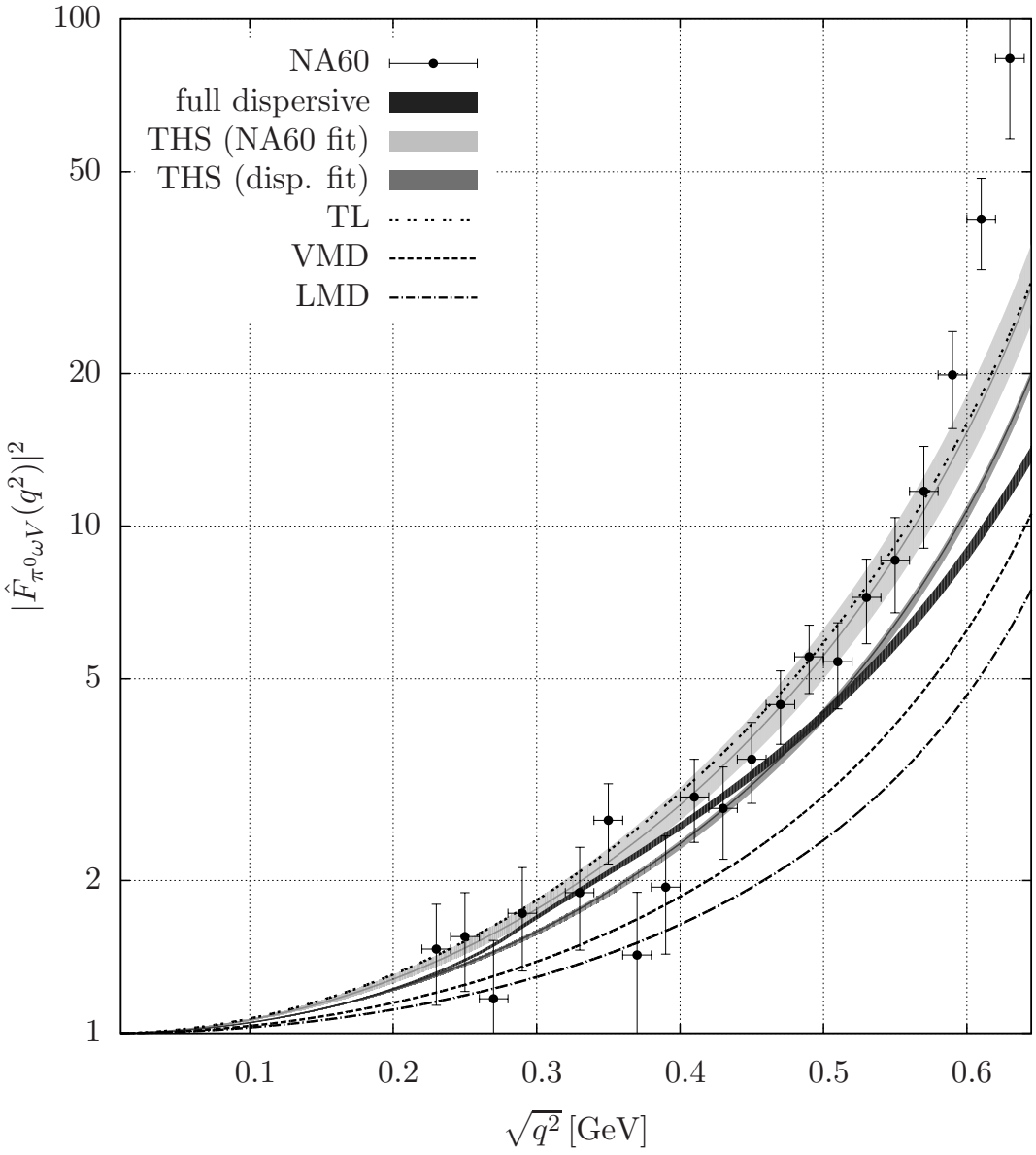

Figure III.2: The normalized ω-π transition form factor as a function of the (time-like) virtuality. Various theoretical calculations are displayed together with NA60 data obtained from the decay $\omega \to \pi^0\mu^+\mu^-$ [28]. See the main text for more details.

labeled by "TL" in Fig. III.2, lies within our uncertainty band in spite of the fact that the derivation is based on a very different approach. The results for VMD and LMD can be obtained from (III.20) and (III.21), respectively, using (III.28) and (III.30). For instance, the VMD expression is

$$\hat{\mathcal{F}}^{\rm VMD}_{\pi^0\omega V}(q^2) = \frac{M_{V_1}^2}{M_{V_1}^2 - q^2}\,. \tag{III.33}$$

As can be seen in Fig. III.2 the results for both VMD and LMD deviate significantly from the data and therefore from our approach. They also deviate from the results of the dispersive calculation of [39], which is shown as the black band in Fig. III.2. As already noted we have performed an alternative fit of our THS expression to the dispersive result — the dark gray band in Fig. III.2. It should be

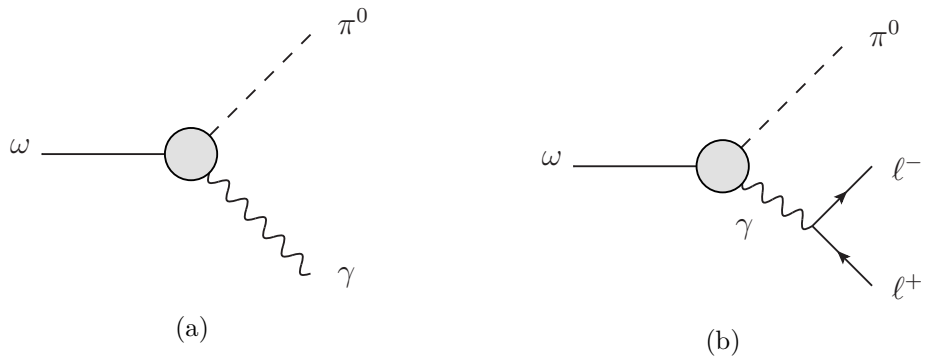

Figure III.3: Feynman diagrams for the $\omega \to \pi^0\gamma$ and $\omega \to \pi^0\ell^+\ell^-$ decays at leading order in QED. The shaded blob corresponds to the $\mathcal{F}_{\pi^0\omega\gamma^{(*)}}(q^2)$ form factor and ℓ denotes e or μ.

noted that our rational function cannot fit the cusp structure in the low-energy region $\sqrt{q^2} \in [0.3, 0.4]$ that emerges in the dispersive calculation from a cross-channel inelasticity; see [39] for a detailed discussion. We repeat our statement that additional data on this transition form factor would be highly welcome.

To further explore the validity of the THS scheme we study selected decay channels of the ω meson. It appears to be convenient to introduce the matrix element

$$\mathcal{M}^{\mu\nu}_{\omega\pi^0}(p,q) = \frac{e}{\mathcal{Z}_\omega \mathcal{Z}_\pi}\left(\frac{2}{3}+\frac{1}{3}\right)\epsilon^{\mu\nu\alpha\beta}p_\alpha q_\beta \lim_{\substack{r^2\to 0\\ p^2\to M_{V_1}^2}} (p^2 - M_{V_1}^2) r^2 \Pi(r^2; p^2, q^2)\,. \quad \text{(III.34)}$$

Using previous definitions (III.10) and (III.28) this can be reduced to

$$\mathcal{M}^{\mu\nu}_{\omega\pi^0}(p,q) = e\mathcal{F}_{\pi^0\omega V}(q^2)\epsilon^{\mu\nu\alpha\beta}p_\alpha q_\beta\,. \quad \text{(III.35)}$$

In (III.34) the factors 2/3 and 1/3 emerge from the respective overlap of the ω meson with the singlet and the 8th component of the octet current, i.e. the factors come from (III.3). These factors actually sum to unity, which is not surprising from a flavor SU(2) point of view where the ω is a pure singlet.

We start with the prediction of the decay width of the $\omega \to \pi^0\gamma$ process, which is depicted in Fig. III.3a. The matrix element

$$\mathcal{M}_{\omega\to\pi^0\gamma} = \mathcal{M}^{\mu\nu}_{\omega\pi^0}(p,q)\epsilon_\mu(\vec{p},\lambda_\omega)\epsilon^*_\nu(\vec{q},\lambda_\gamma)\Big|_{q^2=0} \quad \text{(III.36)}$$

does not depend on κ as already mentioned. This provides us with a pure prediction. After simple manipulations we find

$$\begin{aligned}\Gamma(\omega\to\pi^0\gamma) &= \frac{\alpha M_\omega^3}{24}|\mathcal{F}_{\pi^0\omega V}(0)|^2\left(1-\frac{M_\pi^2}{M_\omega^2}\right)^3 \\ &\simeq \frac{\pi\alpha^3}{162}\frac{\mathcal{Z}_\omega^2|\mathcal{F}_{\pi^0\omega V}(0)|^2}{\Gamma(\omega\to e^+e^-)}\left(1-\frac{M_\pi^2}{M_\omega^2}\right)^3,\end{aligned} \quad \text{(III.37)}$$

where we have used (III.26) to obtain the last expression. Taking $N_c = 3$, $F = (92.22 \pm 0.06)\,\text{MeV}$ [50], $M_\pi = 134.98\,\text{MeV}$, $M_{V_1} = M_\rho = (775.26 \pm 0.25)\,\text{MeV}$ [22] and M_{V_2} in the range (III.6) we obtain the values listed in Tab. III.1. We see that

	VMD	LMD	THS	experiment
$\Gamma(\omega \to \pi^0\gamma)\,[\text{MeV}]$	0.68	0.45	0.63 ± 0.04	0.70 ± 0.03

Table III.1: Decay width of the process $\omega \to \pi^0\gamma$ as obtained from different approaches and from data [22]. We estimate an uncertainty only for our THS case.

THS is within its uncertainties compatible with the experimental data. In this case VMD proves to be phenomenologically successful, too. The value of the LMD approach seems to be off even taking into account the 40% rule-of-thumb uncertainty used in [17].

Moving on to the $\omega \to \pi^0\ell^+\ell^-$ decay, which is depicted in Fig. III.3b, the matrix element can be written in the form

$$\mathcal{M}_{\omega\to\pi^0\ell^+\ell^-} = \mathcal{M}^{\mu\nu}_{\omega\pi^0}(p,q)\epsilon_\mu(\vec{p},\lambda_\omega)\frac{(-i)}{q^2}\bar{u}(\vec{q}_1)(-ie\gamma_\nu)v(\vec{q}_2)\,. \tag{III.38}$$

The decay width can then be expressed as a form-factor-dependent integral over the dilepton invariant mass,

$$\begin{aligned}\Gamma(\omega \to \pi^0\ell^+\ell^-) = \frac{\alpha^2}{72\pi M_\omega^3}\int\limits_{4m_\ell^2}^{(M_\omega-M_\pi)^2} &\frac{|\mathcal{F}_{\pi^0\omega V}(q^2)|^2}{q^2} \\ &\times\sqrt{1-\frac{4m_\ell^2}{q^2}}\left(1+\frac{2m_\ell^2}{q^2}\right)\lambda^{\frac{3}{2}}\left(M_\omega^2,M_\pi^2,q^2\right)\mathrm{d}q^2\,,\end{aligned} \tag{III.39}$$

where λ denotes the Källén triangle function defined as

$$\lambda(a,b,c) \equiv a^2+b^2+c^2-2ab-2ac-2bc\,. \tag{III.40}$$

For THS the result for this decay width depends on the parameter κ. We use the fitted value (III.31) and for the other input quantities the ranges specified after (III.37).

It is common practice to normalize decay widths that involve dileptons to the corresponding decay widths involving photons [30]. This leads to the branching ratios listed in Tab. III.2. Obviously, for the electron case all the results of the

	VMD	LMD	THS	experiment
$\frac{B(\omega\to\pi^0e^+e^-)}{B(\omega\to\pi^0\gamma)}\times 10^3$	9.1	8.9	9.6 ± 0.1	9.3 ± 1.0
$\frac{B(\omega\to\pi^0\mu^+\mu^-)}{B(\omega\to\pi^0\gamma)}\times 10^3$	0.91	0.82	1.33 ± 0.10	1.6 ± 0.5

Table III.2: Branching ratios of the decays $\omega \to \pi^0e^+e^-$ and $\omega \to \pi^0\mu^+\mu^-$ normalized to the branching ratio of the decay $\omega \to \pi^0\gamma$ as obtained from different approaches and from data [22]. We estimate an uncertainty only for our THS case.

considered approaches lie within the experimental uncertainty. For the muon case, however, only the THS result explains the experimental value. This should not come as a surprise given that in Fig. III.2 the LMD and VMD curves lie much lower than the THS band.

III.4 The process $\pi^0 \to e^+e^-$

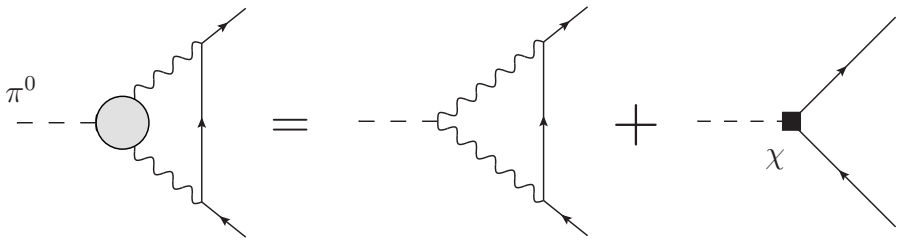

Figure III.4: Leading-order contribution to the $\pi^0 \to e^+e^-$ process in the QED expansion and its representation in terms of the leading order in chiral perturbation theory. The shaded blob corresponds to the doubly virtual pion transition form factor $\mathcal{F}_{\pi^0\gamma^*\gamma^*}(l^2,(r-l)^2)$.

In the following two sections we turn our attention to the decays of the neutral pion. Namely we will discuss the rare decay $\pi^0 \to e^+e^-$, to which this section is devoted, and later on also the Dalitz decay $\pi^0 \to e^+e^-\gamma$.

The decay $\pi^0 \to e^+e^-$ and the radiative corrections connected to this process have been extensively studied in [6, 7]. On the left-hand side of the graphical equation in Fig. III.4 the leading order of the QED expansion of the considered process is depicted. The doubly virtual pion transition form factor $\mathcal{F}_{\pi^0\gamma^*\gamma^*}(l^2,(r-l)^2)$ is represented in the figure as the shaded blob. Here r denotes the pion momentum and l a loop momentum. This transition form factor plays here an essential role, since it serves as an effective ultraviolet (UV) cut-off due to its $1/l^2$ asymptotics governed by the OPE. The loop integral over d^4l is therefore convergent.

On account of Lorentz and parity symmetry the on-shell matrix element of the $\pi^0 \to e^+e^-$ process can be written in terms of just one pseudoscalar form factor in the following form:

$$i\mathcal{M}_{\pi^0\to e^+e^-} = P_{\pi^0\to e^+e^-}\left[\bar{u}(\vec{q}_1)\gamma_5 v(\vec{q}_2)\right] . \tag{III.41}$$

Subsequently, the decay width reads

$$\Gamma(\pi^0 \to e^+e^-) = \frac{2M_\pi^2|P_{\pi^0\to e^+e^-}|^2}{16\pi M_\pi}\sqrt{1-\frac{4m_e^2}{M_\pi^2}} . \tag{III.42}$$

Taking into account only the leading order (LO) in the QED expansion, i.e. the left-hand side of the graphical equation in Fig. III.4, we find (within the dimensional reduction scheme [51, 52])

$$P^{\mathrm{LO}}_{\pi^0\to e^+e^-} = \frac{ie^4m_e}{M_\pi^2}\int\frac{\mathrm{d}^4l}{(2\pi)^4}\frac{\mathcal{F}_{\pi^0\gamma^*\gamma^*}(p^2,q^2)\lambda(M_\pi^2,p^2,q^2)}{p^2q^2(l^2-m_e^2)} . \tag{III.43}$$

Here $p = l - q_1$ and $q = l + q_2$, where q_1 and q_2 are the lepton momenta. Using dimensional regularization and Passarino–Veltman reduction [53] the explicit result of the loop integration in terms of scalar one-loop integrals is given in III.A for various form factors.

On the right-hand side of Fig. III.4 we can see how the previously discussed expression is represented in leading order of chiral perturbation theory [16, 17]. Here, the constant

$$\mathcal{F}_{\pi^0\gamma^*\gamma^*}(0,0) = -\frac{N_c}{12\pi^2F} \tag{III.44}$$

emerging from the chiral anomaly is used instead of the full transition form factor; see (III.16). This leads to a divergent integral [15] and it is thus clear that a counter-term is needed. If the loop is renormalized at scale μ, the finite part of such a counter-term is denoted by $\chi^{(\mathrm{r})}(\mu)$. It corresponds to the high-energy behavior of the complete transition form factor. Therefore, concerning the pion decay, we can characterize each transition form factor by the corresponding value of $\chi^{(\mathrm{r})}(\mu)$.

In fact, using (III.44) instead of the full form factor in (III.43) together with the counter-term Lagrangian from [16, 17] one obtains

$$\begin{aligned} P^{\mathrm{LO}}_{\pi^0\to e^+e^-} &= -2\alpha^2 m_e \mathcal{F}_{\pi^0\gamma^*\gamma^*}(0,0) \\ &\times \left\{ -\frac{5}{2} + \frac{3}{2}\log\left(\frac{m_e^2}{\mu^2}\right) + \chi^{(\mathrm{r})}(\mu) + \frac{1}{2\beta_e}\left[\mathrm{Li}_2(z) - \mathrm{Li}_2\left(\frac{1}{z}\right) + i\pi\log(-z)\right]\right\}. \end{aligned} \tag{III.45}$$

In the above formula Li_2 is the dilogarithm, $\beta_e = \sqrt{1-4m_e^2/M_\pi^2}$, $z = -(1-\beta_e)/(1+\beta_e)$ and μ represents the scale at which the loop integral is effectively cut off; cf. [17]. This effective approach with the constant form factor leading to formula (III.45) can be conveniently used to match with the calculation (III.43) and any full, i.e. momentum-dependent form factor. Thus, for various approaches, the value of the associated effective parameter $\chi^{(\mathrm{r})}(\mu)$ can be extracted. In other words, the left-hand side of (III.45) can be substituted by the expressions for $P^{\mathrm{LO}}_{\pi^0\to e^+e^-}$ stated in III.A and $\chi^{(\mathrm{r})}(\mu)$ is subsequently determined. Following common practice [11, 46, 16, 17] we have chosen $\mu = 770\,\mathrm{MeV} \simeq M_\rho$ to set the renormalization scale.

An approximative way to get the low-energy constant $\chi^{(\mathrm{r})}(\mu)$ up to corrections proportional to m_e/M_π and M_π/μ has been presented in [4]. In our notation this reads

$$\chi^{(\mathrm{r})}(\mu) \simeq \frac{5}{4} + \frac{3}{2}\int_0^\infty \mathrm{d}t\, \log(t)\, \frac{\partial}{\partial t}\frac{\mathcal{F}_{\pi^0\gamma^*\gamma^*}(-t\mu^2,-t\mu^2)}{\mathcal{F}_{\pi^0\gamma^*\gamma^*}(0,0)}\,. \tag{III.46}$$

Using this approach we get very simple formulae for the VMD model

$$\chi^{(\mathrm{r})}_{\mathrm{VMD}}(\mu) \simeq \frac{11}{4} - \frac{3}{2}\log\frac{M_{V_1}^2}{\mu^2} \tag{III.47}$$

as well as for the LMD case (cf. [17])

$$\chi^{(\mathrm{r})}_{\mathrm{LMD}}(\mu) \simeq \frac{11}{4} - \frac{3}{2}\log\frac{M_{V_1}^2}{\mu^2} - \frac{12\pi^2F^2}{N_c M_{V_1}^2}\,. \tag{III.48}$$

For the THS form factor, where the additional mass scale M_{V_2} and the parameter κ come into play, the calculation according to (III.46) yields

$$\begin{aligned} \chi^{(\mathrm{r})}_{\mathrm{THS}}(\mu) \simeq{}& \frac{5}{4} - \frac{3}{2}\log\frac{M_{V_1}^2}{\mu^2} + \frac{3}{2}\frac{M_{V_1}^2 M_{V_2}^2}{(M_{V_2}^2 - M_{V_1}^2)^2} \\ &\times \left\{ \frac{M_{V_2}^2}{M_{V_1}^2} + \frac{M_{V_1}^2}{M_{V_2}^2} - \frac{14}{N_c}(2\pi F)^2\left(\frac{1}{M_{V_1}^2} + \frac{1}{M_{V_2}^2}\right)\right. \\ &- \left[\frac{M_{V_1}^2}{M_{V_2}^2} + \frac{2M_{V_1}^2}{M_{V_2}^2 - M_{V_1}^2} - \frac{7}{N_c}\frac{(4\pi F)^2}{(M_{V_2}^2 - M_{V_1}^2)}\right]\log\frac{M_{V_2}^2}{M_{V_1}^2} \\ &\left. - \frac{\kappa M_{V_1}^2 M_{V_2}^2}{N_c(4\pi F)^4}\left[\frac{M_{V_2}^2 + M_{V_1}^2}{2(M_{V_2}^2 - M_{V_1}^2)}\log\left(\frac{M_{V_2}^2}{M_{V_1}^2}\right) - 1\right]\right\}. \end{aligned} \tag{III.49}$$

The numerical values for the exact as well as for the approximate results are listed in Tab. III.3. In the first row the values gained from the matching of (III.43)

$\chi^{(\mathrm{r})}(\mu = 770\,\mathrm{MeV})$	VMD	LMD	THS
exact result	2.87	2.29	2.2 ± 0.2
approx. from (III.46)	2.72	2.2 ± 0.9	2.0 ± 0.2

Table III.3: Values of the effective parameter $\chi^{(\mathrm{r})}(770\,\mathrm{MeV})$ for various pion transition form factors. In general we provide uncertainty estimates only for THS. The uncertainty for LMD stems from [17].

to (III.45) are listed. The second row contains the results of the approximative formulae (III.47), (III.48) and (III.49). In the LMD case, the value according to (III.48) would be 2.16, but here the listed result has been taken from [17] where also a 40 % uncertainty has been estimated. Needless to say, the used numerical inputs were the same as in the whole text except for one thing. In the case of the pion decays, we use for the ground-state vector-meson multiplet mass M_{V_1} the average of the ρ and ω meson masses, i.e. $M_{V_1} = (779 \pm 4)\,\mathrm{MeV}$.

We can see that the approximative formula (III.46) is indeed reasonable. The numerical values are close to the case of the exact calculation, where electron and pion masses are not neglected. To compare briefly the values for the various approaches, we see in Tab. III.3 that the THS mean value is close to LMD but incompatible with the VMD value. Of course, a meaningful comparison would require an uncertainty estimate for the VMD case, which is not available. Considering the large uncertainty of LMD according to [17], THS and even VMD lie safely within the LMD band. In turn the central value of LMD lies within the THS band.

Finally, we can utilize the above formulae and provide branching ratios to be compared to experiment. The presently most precise measurement was performed by the KTeV collaboration at Fermilab with the result [3]

$$B^{\mathrm{KTeV}}(\pi^0 \to e^+e^-(\gamma)\,,\ x > 0.95) = (6.44 \pm 0.25 \pm 0.22) \times 10^{-8}\,, \qquad \text{(III.50)}$$

where x is the normalized lepton-pair invariant mass, i.e. $x = (q_1 + q_2)^2/M_\pi^2$. This condition can be translated to the photon-energy cut $E_\gamma < M(1 - x_{\mathrm{cut}})/2$ in the rest frame of the decaying pion, with $x_{\mathrm{cut}} = 0.95$. Soon after, the disagreement of (III.50) with a theoretical calculation was found [4].

To predict the quantity (III.50) we proceed as follows. Taking into account NLO QED corrections [6, 7] we can calculate the branching ratio of the inclusive process $\pi^0 \to e^+e^-(\gamma)$, i.e. of a process where we allow bremsstrahlung photons to appear in the final state. Denoting these QED corrections by δ this can be written as

$$B(\pi^0 \to e^+e^-(\gamma)\,,\ x > x_{\mathrm{cut}}) = \frac{\Gamma^{\mathrm{LO}}(\pi^0 \to e^+e^-)[1 + \delta(x_{\mathrm{cut}})]}{\Gamma^{\mathrm{LO}}(\pi^0 \to \gamma\gamma)} \times B(\pi^0 \to \gamma\gamma)\,. \qquad \text{(III.51)}$$

In addition, the width of the pion decay into two photons has the form

$$\Gamma^{\mathrm{LO}}(\pi^0 \to \gamma\gamma) = \frac{1}{2}\frac{1}{16\pi M_\pi}\frac{e^4 M_\pi^4}{2}|\mathcal{F}_{\pi^0\gamma^*\gamma^*}(0,0)|^2 \qquad \text{(III.52)}$$

and $B(\pi^0 \to \gamma\gamma) = (98.823 \pm 0.034)\,\%$ [22]. The calculation of the two-loop virtual radiative corrections together with the bremsstrahlung correction in the soft-photon approximation gives the result $\delta(0.95) = (-5.8 \pm 0.2)\,\%$. It has been shown in [7] that the soft-photon approximation is a valid approach for the value x_{cut}=0.95 used by the KTeV experiment. Note that this value of the correction δ was obtained in [6] in a model-independent way using $\chi^{(\text{r})}(770\,\text{MeV}) = 2.2 \pm 0.9$. However, this result for δ depends negligibly on the range of considered values of $\chi^{(\text{r})}$ shown in Tab. III.3. Hence we consider the result for δ to be valid for our case.

With this NLO QED input we find the values shown in Tab. III.4. Here we

	VMD	LMD	THS	KTeV
$B(\pi^0 \to e^+e^-(\gamma)\,,\ x > 0.95)$	5.96	5.8(3)	5.76(7)	6.44(33)

Table III.4: Branching ratio of the inclusive process $\pi^0 \to e^+e^-(\gamma)$ at NLO of QED for various models for the pion transition form factor. The listed values are to be multiplied by a factor 10^{-8}. The KTeV value is based on the result stated in [3].

see that the central value in the THS case is, of course, compatible with the LMD central value, since the same holds for the values $\chi^{(\text{r})}(\mu)$; see Tab. III.3. The uncertainty of the LMD approach according to [17] makes it compatible with the KTeV result on the level of $1\,\sigma$. Considering VMD, where we do not have an estimate of the theoretical uncertainty, we are then $1.5\,\sigma$ away from the experimental value. Finally, the THS approach is $2\,\sigma$ off. As compared to LMD this is related to the fact that the estimate for our theoretical uncertainty is on the level of only 1 % concerning this particular branching ratio. We recall that this estimate is merely based on two sources: first, the fit for κ, which might be improved in the future by data on the doubly virtual pion transition form factor; second, a large variation in M_{V_2}. By this variation we estimate the uncertainty imposed by a truncation of the infinite tower of resonances. Strictly speaking our model intrinsic uncertainty estimate does not account for the two initial assumptions: the chiral and the large-N_c limit. We expect that to some extent we have accounted for the uncertainties of the large-N_c approximation by focusing on kinematical situations where the (large-N_c suppressed) widths of the resonances do not matter so much *and* by varying the mass of the second vector-meson multiplet in a relatively large range. The uncertainties caused by the chiral limit should be on the order of M_π^2/Λ_χ^2 where Λ_χ denotes the scale of chiral symmetry breaking. Within chiral perturbation theory one uses the scale where new degrees of freedom come into play or where the loops become as important as the tree-level contributions. Roughly this implies $\Lambda_\chi \lesssim M_\rho, 4\pi F$, i.e. an uncertainty of about 3 %. Adding errors in squares this is clearly negligible as compared to the 10 % uncertainty documented in Tab. III.3 for THS. Based on these considerations we regard our uncertainty estimate in Tab. III.4 as reasonable — assuming that our determination of κ from the ω-π transition is correct.

Consequently, if the (central value of the) KTeV result will be confirmed by future experiments and measured with higher precision such that the discrepancy would reach several σ's, then the following two scenarios are conceivable: Either there are some aspects of the THS approach which are not well-suited for the

rare decay $\pi^0 \to e^+e^-$, or it should be seriously considered that physics beyond the Standard Model influences the rare pion decay to a significant extent. However, under the present circumstances we consider the current discrepancy to be inconclusive. We will come back to this discrepancy in the next section.

III.5 Singly virtual pion transition form factor and the Dalitz decay $\pi^0 \to e^+e^-\gamma$

With particular models at hand, we can also explore the properties of the singly virtual pion transition form factor $\mathcal{F}_{\pi^0\gamma^*\gamma^*}(0,q^2)$. A slope a_π and a curvature b_π of the form factor are defined in terms of the Taylor expansion in the invariant mass of the vector current [40]

$$\frac{\mathcal{F}_{\pi^0\gamma^*\gamma^*}(0,q^2)}{\mathcal{F}_{\pi^0\gamma^*\gamma^*}(0,0)} \simeq 1 + a_\pi \frac{q^2}{M_\pi^2} + b_\pi \left(\frac{q^2}{M_\pi^2}\right)^2 . \tag{III.53}$$

By means of the first and second derivative it is straightforward to find the following expressions for the simplest form factors

$$a_\pi^{\mathrm{VMD}} = \frac{M_\pi^2}{M_{V_1}^2} , \quad b_\pi^{\mathrm{VMD}} = \frac{M_\pi^2}{M_{V_1}^2}\, a_\pi^{\mathrm{VMD}} , \tag{III.54}$$

$$a_\pi^{\mathrm{LMD}} = \frac{M_\pi^2}{M_{V_1}^2}\left[1 - \frac{4\pi^2 F^2}{N_c M_{V_1}^2}\right] , \quad b_\pi^{\mathrm{LMD}} = \frac{M_\pi^2}{M_{V_1}^2}\, a_\pi^{\mathrm{LMD}} \tag{III.55}$$

as well as for the THS form factor with its two vector-multiplet mass scales

$$\begin{aligned} a_\pi^{\mathrm{THS}} &= \frac{M_\pi^2}{M_{V_1}^2}\left[1 + \frac{M_{V_1}^2}{M_{V_2}^2} - \frac{24\pi^2 F^2}{N_c M_{V_2}^2}\right] , \\ b_\pi^{\mathrm{THS}} &= \left[\frac{M_\pi^2}{M_{V_1}^2} + \frac{M_\pi^2}{M_{V_2}^2}\right] a_\pi^{\mathrm{THS}} - \frac{M_\pi^4}{M_{V_1}^2 M_{V_2}^2} . \end{aligned} \tag{III.56}$$

Numerical results are shown in Tab. III.5. We see that THS is compatible with

	VMD	LMD	THS	dispers. [40]	exp. [22]
slope a_π	30.0	24.5	29.2(4)	30.7(6)	32(4)
curvature b_π	0.90	0.74	0.87(2)	1.10(2)	–

Table III.5: Slope and curvature of the singly virtual pion transition form factor evaluated for various approaches. The listed values are to be multiplied by a factor of 10^{-3}.

the experimental value and that it is numerically consistent with VMD. Similar to some previous cases, the value predicted by LMD is unsatisfying. Nevertheless, none of the models (VMD, LMD, THS) fully agrees with the results of the dispersive calculation [40]. The latter is capable of producing very reliable results at low energies. We note in passing that the apparent agreement of VMD with the dispersive result for the slope is somewhat accidental. Actually the discrepancy grows, if the ϕ meson is included in the analysis [40].

The disagreement between THS and the dispersive results brings us back to the discussion of the uncertainties inherent to THS and to our attempt to quantify these uncertainties in a reasonable way. Of course, for a given model one can only estimate the model intrinsic uncertainties, which in turn inherit a model dependence. Our numerical values for the uncertainty estimates of the THS results emerge dominantly from the uncertainty in the determination of the parameter κ and from a variation in M_{V_2}. In contrast to most of the results previously presented, the singly virtual pion transition form factor does not depend on the parameter κ. This can be most easily seen from (III.56), but also from (III.15), (III.17). In addition, the dependence on M_{V_2} is minor for the low-energy quantities determined in (III.56). In fact, in (III.56) the mass M_{V_2} essentially shows up in the numerically small combination $\Delta M^2/M_{V_2}^2$ with $\Delta M^2 \equiv M_{V_1}^2 - 24\pi^2 F^2/N_c$. The smallness of ΔM^2 might be seen as an incarnation of the KSFR relations; see, e.g., [54] and references therein. In turn, this implies that our model intrinsic uncertainty determination might underestimate the real uncertainty if the dependence of our results on M_{V_2} and/or κ is accidentally small. While this is the case for the singly virtual pion transition form factor, it is certainly not true for the doubly virtual one; see also Fig. III.1 with the broad uncertainty band in the first panel and the corresponding nearly invisible spread in the second panel. Obviously, one has to take our uncertainty estimates with a grain of salt.

As a closure of the phenomenological part of this work, we inspect the theoretical predictions for the decay width of the Dalitz decay $\pi^0 \to e^+e^-\gamma$. The leading-order QED contribution is depicted in Fig. III.5a. Our aim is also to address the

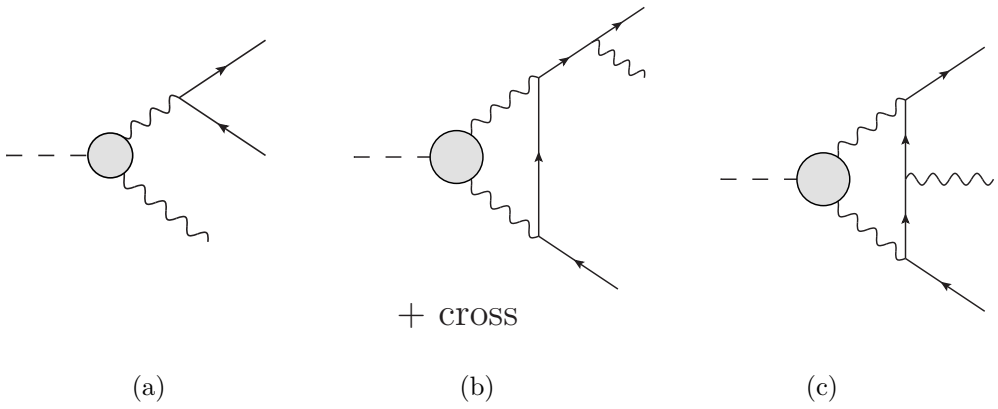

Figure III.5: Leading order diagram of the Dalitz decay $\pi^0 \to e^+e^-\gamma$ in the QED expansion (a) and the one-photon irreducible contributions to the NLO virtual radiative correction (b) and (c). Note that "cross" in (b) accounts for a diagram with a photon emitted from the outgoing positron line. Diagrams (b) and (c) also serve as a bremsstrahlung contribution to the $\pi^0 \to e^+e^-$ decay.

NLO radiative corrections. For this purpose we use the approach documented in [42], which has recently reviewed and extended the classical work of [55]. Hence, together with the bremsstrahlung beyond the soft-photon approximation we use in the following calculations the virtual radiative corrections including also the one-photon irreducible (1γIR) contribution. The diagrams connected with the latter part are schematically shown in Fig. III.5b and III.5c. The mentioned correction then emerges when one considers the interference term with the LO diagram in Fig. III.5a.

	WZW	VMD	LMD	THS
NLO correction $\delta_{\rm D}$	8.338	8.299	8.307	8.3008(3)
$\frac{\Gamma(\pi^0\to e^+e^-\gamma(\gamma))}{\Gamma^{\rm LO}(\pi^0\to\gamma\gamma)}$	11.9503	11.9735	11.9692	11.9729(4)
$\frac{\Gamma(\pi^0\to e^+e^-\gamma(\gamma)\,,\,x>0.2319)}{\Gamma(\pi^0\to e^+e^-\gamma(\gamma))}$	31.03	31.63	31.52	31.61(1)

Table III.6: Theoretical prediction for the Dalitz decay branching ratios at NLO of QED with and without a cut as evaluated for various approaches. "WZW" describes the case where the pion transition form factor is replaced by its low-energy limit. The listed values are to be multiplied by a factor of 10^{-3}.

The decay width of the Dalitz decay at NLO can be written in the following form

$$\Gamma(\pi^0\to e^+e^-\gamma(\gamma)\,,\;x>x_{\rm cut}) = [1+\delta_D(x>x_{\rm cut})]\,\Gamma^{\rm LO}(\pi^0\to e^+e^-\gamma\,,\;x>x_{\rm cut})\,, \tag{III.57}$$

where we have denoted the sum of all the NLO radiative corrections to the integrated decay width as δ_D and where

$$\begin{aligned}&\Gamma^{\rm LO}(\pi^0\to e^+e^-\gamma\,,\;x>x_{\rm cut})\\ &=\left(\frac{\alpha}{\pi}\right)\Gamma^{\rm LO}(\pi^0\to\gamma\gamma)\int_{x_{\rm cut}}^1{\rm d}x\left|\frac{\mathcal{F}_{\pi^0\gamma^*\gamma^*}(0,xM_\pi^2)}{\mathcal{F}_{\pi^0\gamma^*\gamma^*}(0,0)}\right|^2\frac{8\beta_e(x)}{3}\frac{(1-x)^3}{4x}\left(1+\frac{2m_e^2}{xM_\pi^2}\right).\end{aligned} \tag{III.58}$$

In the above formula we have introduced $\beta_e(x)=\sqrt{1-4m_e^2/(xM_\pi^2)}$. Note that contrary to the last section $x_{\rm cut}$ cannot be interpreted as a cut on a single photon energy, since the additional bremsstrahlung photon appears. There are also no restrictions on the energy of the bremsstrahlung photon in this decay width.

The numerical results for the considered approaches are compared in Tab. III.6. In the first row the NLO correction is presented. Naively one might get from the definitions (III.57) and (III.58) the impression that the pion transition form factor does not enter δ_D. This is, however, not the case. The NLO correction involves, of course, the four-body phase-space integrations and the pion transition form factor cannot be scaled out. This is due to the integration over the x variable, which is tacitly performed also on the left-hand side of (III.57). On the other hand, taking into account the correction to the differential decay width, we would get an expression independent of the form factor. This statement then holds only when leaving out the 1γIR part, where the form-factor-dependent loop integration is performed. Nonetheless, concerning model uncertainties, it is encouraging that numerically the NLO correction is to a very large extent independent of the used pion transition form factor. Using the respective value of the NLO correction, the second row in Tab. III.6 shows the corresponding branching ratio if no cut on additional photons is applied, i.e. the branching ratio of the Dalitz decay for the whole kinematic region $x\in[4m_e^2/M_\pi^2,1]$. The results of this row should be compared to the experimental value $\frac{B(\pi^0\to e^+e^-\gamma)}{B(\pi^0\to\gamma\gamma)}=(11.88\pm0.35)\times10^{-3}$, which has been calculated using inputs from [22]. The agreement with the values of the second row in Tab. III.6 is very satisfying.

In the previous section we have stated the value (III.50) as the outcome of the KTeV analysis. However, what KTeV has determined at first place is[16]

$$\left.\frac{\Gamma(\pi^0 \to e^+e^-(\gamma)\,,\ x > 0.95)}{\Gamma(\pi^0 \to e^+e^-\gamma(\gamma)\,,\ x > 0.2319)}\right|_{\rm KTeV} = (1.685 \pm 0.064 \pm 0.027) \times 10^{-4}\,. \quad \text{(III.59)}$$

We note in passing that for the quantity displayed in the last row of Tab. III.6 the corresponding value used by KTeV to obtain finally the result (III.50) is 3.19 % [3]. This value is close but not equal to any of the results in the last row of Tab. III.6.

Having the radiative corrections determined from theory suggests to calculate directly the ratio (III.59) instead of the derived quantity (III.50) and to compare the calculation to the experimental result. However, the result (III.59) is not a direct measurement either, but is, of course, based on an interplay of measurements, Monte Carlo simulations, acceptance corrections, etc. [3, 56]. By the time the KTeV measurements were analyzed not all QED radiative corrections were available. To evaluate the decay width of the Dalitz decay the radiative corrections from [55] have been used. In particular the 1γIR contributions have not been included in [55]. In addition, in the Monte Carlo generator of KTeV the radiative corrections for the e^+e^- decay have been adopted from [57]; see [56]. However, in [57] some approximations have been used that have been proven to be misleading after the exact calculation has been performed [6]. Therefore it would be somewhat misleading to compare a theory result with all radiative corrections included to an experimental result where only part of these corrections have been taken into account. On the other hand, it might be illuminating to provide a rough estimate of the impact of these differences. Before presenting such an estimate we would like to repeat the take-home message from the first section: All NLO QED radiative corrections are now available [6, 7, 42] and can be taken into account in future analyses of data on the pion decays $\pi^0 \to e^+e^-$ and $\pi^0 \to e^+e^-\gamma$.

In spite of the fact that not all radiative corrections have been taken into account in the analysis that led to the result (III.59) we do not feel legitimated to modify this experimental result. Instead we will calculate the ratio of (III.59) within THS[17], but assign an uncertainty to it, which is related to the neglect of the 1γIR contributions.[18] It should be stressed, however, that this is not an entirely valid approach either. After all, as soon as one can calculate the NLO QED radiative corrections, they do not constitute an uncertainty of a result but rather a well-defined shift of the result. Nonetheless, we proceed in the described way to obtain a rough estimate of the uncertainty caused by neglecting part of the radiative corrections.

The quantity of our interest can be generally expressed and expanded as

$$\frac{A \pm \sigma(A)}{B \pm \sigma(B)} \simeq \frac{A}{B}\left[1 \pm \frac{\sigma(A)}{A} \mp \frac{\sigma(B)}{B}\right]\,. \quad \text{(III.60)}$$

[16]Note that we use here the more precise value $x_{\rm cut} = 0.2319$ from [56] in contrast to 0.232 as stated in [3]. This value for $x_{\rm cut}$ corresponds to $(65\,{\rm MeV}/M_\pi)^2$.

[17]According to Tab. III.6 the results from the other approaches are comparable.

[18]The modification induced by using [57] in the Monte Carlo generator is even harder to assess. Therefore we concentrate solely on the 1γIR contributions.

In our case we have $A = \Gamma(\pi^0 \to e^+e^-(\gamma)\,,\ x > 0.95)$ and $B = \Gamma(\pi^0 \to e^+e^-\gamma(\gamma)\,,\ x > 0.2319)$, which we calculate up to NLO using the complete set of corrections. The uncertainties are then given by the 1γIR contributions to the NLO virtual radiative corrections, i.e. by the interference of the diagrams shown in Fig. III.5. Hence

$$\begin{aligned}\frac{\sigma(A)}{A} &= \frac{\left|\Gamma^{\rm NLO}_{1\gamma{\rm IR}}(\pi^0 \to e^+e^-\gamma\,,\ x > 0.95)\right|}{\Gamma(\pi^0 \to e^+e^-(\gamma)\,,\ x > 0.95)} \\ &= \frac{\left|\delta^{1\gamma{\rm IR}}_{\rm D}(x > 0.95)\right|}{[1+\delta(0.95)]}\frac{\Gamma^{\rm LO}(\pi^0 \to e^+e^-\gamma\,,\ x > 0.95)}{\Gamma^{\rm LO}(\pi^0 \to e^+e^-)}\,,\end{aligned} \tag{III.61}$$

which numerically yields $\sigma(A)/A \simeq 0.4\,\%$. For the second term we get

$$\begin{aligned}\frac{\sigma(B)}{B} &= \frac{\left|\Gamma^{\rm NLO}_{1\gamma{\rm IR}}(\pi^0 \to e^+e^-\gamma\,,\ x > 0.2319)\right|}{\Gamma(\pi^0 \to e^+e^-\gamma(\gamma)\,,\ x > 0.2319)} \\ &= \frac{\left|\delta^{1\gamma{\rm IR}}_{\rm D}(x > 0.2319)\right|}{[1+\delta_D(x > 0.2319)]}\,,\end{aligned} \tag{III.62}$$

for which we find $\sigma(B)/B \simeq 0.5\,\%$. We can thus conclude that the total uncertainty would be at the level of $1\,\%$. For completeness we list the values that we have used to get the above stated numbers. The input for (III.61) is $\delta^{1\gamma{\rm IR}}_{\rm D}(x > 0.95) = -8.93(1)\,\%$ for the 1γIR contribution to the NLO virtual radiative correction for the decay width of the Dalitz decay. For the ratio of the LO decay widths of the Dalitz decay with $x > 0.95$ and the $\pi^0 \to e^+e^-$ process we have $\frac{\Gamma^{\rm LO}(\pi^0\to e^+e^-\gamma\,,\,x>0.95)}{\Gamma^{\rm LO}(\pi^0\to e^+e^-)} = 4.31(5)\,\%$. In (III.62) we have utilized for the overall NLO correction to the Dalitz decay $\delta_{\rm D}(x > 0.2319) = -3.189(2)\,\%$ and finally $\delta^{1\gamma{\rm IR}}_{\rm D}(x > 0.2319) = -0.5038(3)\,\%$. In general, we can see that the radiative corrections are getting more important with higher values of $x_{\rm cut}$. Taking values from Tab. III.4 and Tab. III.6 and the previously estimated relative uncertainty of $1\,\%$ (we state this separately) we find

$$\left.\frac{\Gamma(\pi^0 \to e^+e^-(\gamma)\,,\ x > 0.95)}{\Gamma(\pi^0 \to e^+e^-\gamma(\gamma)\,,\ x > 0.2319)}\right|_{\rm theo+uncert.} = (1.54 \pm 0.02 \pm 0.02) \times 10^{-4}\,. \tag{III.63}$$

This result is to be compared with the KTeV value (III.59), yielding a discrepancy of approximately $1.5\,\sigma$. We stress one more time that the result (III.63) should be read with caution.

III.6 Outlook

Several directions are conceivable how the THS scheme might be extended or combined with other approaches. Most straightforward would be to extend THS to other correlators; see also [5]. Eventually one might get cross correlations and in that way more information, e.g., by fitting to additional sets of data.

In the present work we have merely used the PVV correlator as an intermediate step to obtain the πVV correlator. Of course, the PVV correlator is also interesting in its own right. For instance, as it has been worked out in [5], the

low-energy expansion of this correlator determines some of the low-energy constants of the chiral Lagrangian at order p^6 in the anomalous sector [58], i.e. the corrections to the Wess–Zumino–Witten Lagrangian. Having determined some of the parameters of the PVV correlator within THS by demanding high-energy constraints one could provide estimates and/or cross-correlations for these low-energy constants following the procedure outlined in [5].

As already spelled out in Section III.1 we refrained from using high-energy constraints for quantities like the $\pi\omega V$ correlator since the vector meson might probe already too many details of the intermediate-energy region (above 1 GeV) where we have approximated the tower of infinitely many states by one effective state per channel. Extending the scheme from THS to three hadrons per channel, albeit introducing more parameters in the first place, might allow to use quark-scaling relations along the lines of [18, 19, 20] for $\pi\omega V$ and similar correlators which in turn could help to keep the number of free parameters manageable. In the same spirit one can use subleading orders in the high-energy expansion in terms of QCD condensates [43].

In the present work we have used the chiral limit to construct the PVV correlator. In line with this approximation we have focused on the πVV and $\pi\omega V$ correlator where no strange quarks are involved. For a reasonable extension from the pion to the whole pseudoscalar multiplet (a nonet in the large-N_c limit) one has to go beyond the chiral limit. The prospect of such an endeavor would be the possibility to tackle the transition form factors of the η and η' mesons and their rare decays into electron and positron or muon and anti-muon. The simplest way to go beyond the chiral limit would be to utilize a pertinent Lagrangian. In extensions of chiral perturbation theory [8, 11, 12] one frequently uses a Lagrangian where the vector mesons are represented by antisymmetric tensor fields [11, 46, 37, 31, 32, 33, 35, 36]. As discussed in [5] a given resonance Lagrangian of formal chiral order p^6 might not be capable of satisfying all desired OPE constraints. Indeed, as shown in [37] this problem appears at least if only one vector-meson multiplet is used for the PVV correlator. Concerning the vector instead of the antisymmetric tensor representation the same negative result has been reported in [5]. It might appear that the first-order approach suggested in [59] offers more flexibility here. Alternatively or in addition one might consider the inclusion of resonance terms of chiral order p^8. The following consideration might demonstrate that one can expect to create additional terms that would not spoil the OPE right away: If one normalizes the PVV correlator to the corresponding chiral-anomaly expression, a p^6 resonance Lagrangian would produce "corrections" that schematically are given by

$$\mathcal{L}_{p^6,R} \quad \to \quad \frac{Q^2}{(Q^2+M_R^2)^n} \quad \text{with} \quad n \leq 3\,. \tag{III.64}$$

We have replaced all resonance masses by M_R and all momenta by Q. This is sufficient to discuss the high- and low-energy limits. The factor of Q^2 in the numerator of (III.64) emerges from the fact that the resonance Lagrangian is assumed to be of chiral order p^6 while the chiral anomaly is of order p^4. The limitation $n \leq 3$ comes from the fact that a three-point correlator is considered. At high energies a single term with $n = 1$ definitely spoils the OPE. Coupling constants between various contributions must be adjusted such that cancellations appear. Of course,

this is the reason why the OPE is capable to tell something about the resonance parameters. A resonance Lagrangian of chiral order p^8 produces terms with the schematic structure

$$\mathcal{L}_{p^8,R} \quad \to \quad \frac{Q^4}{(Q^2+M_R^2)^n} \quad \text{with} \quad n \leq 3\,. \tag{III.65}$$

Here the terms with $n = 1, 2$ spoil the OPE and must cancel. The terms with $n = 3$, however, produce structures that could be compatible with the OPE but are structurally different from the ones in (III.64). Thus the inclusion of resonance terms of chiral order p^8 might help to obtain an agreement between a Lagrangian approach and the OPE. Needless to say that the systematic construction of a p^8 Lagrangian would be extremely tedious; see [37] and references therein. In practice, according to [21], leading-order OPE constraints[19] together with a singly virtual pion transition form factor that vanishes at large momenta can be achieved by a resonance Lagrangian with two vector-meson multiplets in the antisymmetric tensor representation. Note, however, that the concrete B-L limit (III.14) has not been used in [21]. Nonetheless, the results of [21] suggest that THS can be reproduced from a resonance Lagrangian of order p^6 in the chiral counting.

While leaving the chiral limit might be systematized by a Lagrangian approach, our second basic assumption, the large-N_c limit is much harder to remedy. On purpose we stuck to narrow states (π, ω) and to the space-like or low-energy time-like region where the effects of inelasticities are minor. Nonetheless this induces uncertainties, which are hard to assess on a quantitative level. At low energies an excellent way to deal with inelasticities is to use them in ones favor by a dispersive setup [39, 40, 49]. A powerful framework emerges when combined with chiral low-energy constraints, QCD high-energy constraints, and precise data on the scattering amplitudes that come into play via the inelasticities. In practice the scheme becomes intractable at intermediate energies (roughly above 1 GeV) where more and more many-particle channels open up. Even if one studies low-energy quantities one might need some information from the intermediate-energy regime if the QCD high-energy limit is reached very late. This is exactly what we saw for the THS result of the πVV correlator. This suggests to study the impact of the THS results on a dispersive calculation by using THS in the intermediate- and high-energy space-like regime where its results should be most trustworthy.

In the present work we have determined the πVV correlator with a focus on the rare pion decay into electron and positron. In turn this decay might offer some window to observe low-energy traces of physics beyond the Standard Model. However, the πVV correlator is also interesting because it contains information about the intrinsic structure of the pion. Hence it could be illuminating to figure out what the THS result implies for the pion distribution function [18, 19, 20, 60].

Acknowledgment

T.H. would like to thank for the hospitality of Uppsala University and to all his colleagues there who made a very friendly atmosphere. We also acknowledge

[19] Note that "chiral order" refers to the low-energy expansion, while "leading-order OPE" refers to the high-energy expansion.

valuable discussions with our colleagues K. Kampf and J. Novotný from Prague. We are indebted to M. Knecht for bringing [43] to our attention.

The present work was supported by the Charles University grants GAUK 700214 and SVV 260219/2015, by the Czech Science Foundation grant GAČR 15-18080S and by the project "Study of Strongly Interacting Matter" (HadronPhysics3, Grant Agreement No. 283286) under the 7th Framework Program of the EU.

Appendix

III.A Explicit form factor formulae

In Section III.4 we have defined the invariant amplitude for the process $\pi^0 \to e^+e^-$ using the expression $P^{\mathrm{LO}}_{\pi^0\to e^+e^-}$. In this appendix we summarize its explicit form for various approaches that lead to a rational function for the pion transition form factor. We make use of the standard Passarino–Veltman [53] scalar one-loop integrals B_0 and C_0. The only UV divergent function is then B_0. Its explicit form will be given here as a reference point for the used notation:

$$\begin{aligned} i\pi^2 B_0(0,m^2,m^2) &\equiv (2\pi)^4\mu^{4-d}\int \frac{\mathrm{d}^d l}{(2\pi)^d}\frac{1}{\left[l^2-m^2+i\epsilon\right]^2} \\ &= i\pi^2\left[\frac{1}{\varepsilon}-\gamma_E+\log 4\pi+\log\left(\frac{\mu^2}{m^2}\right)\right], \end{aligned} \tag{III.66}$$

where we have introduced $\varepsilon = 2-\frac{d}{2}$. Note that differences of B_0 functions are finite. It will then be manifest from the form in which the results are presented, that the divergent parts cancel yielding a finite amplitude as desired. It is also convenient to introduce the following combination of the three-point scalar one-loop function C_0 and the Källén triangle function λ:

$$C_0'(m_e^2,m_e^2,m_1^2,m_2^2,m_e^2,m_3^2) \equiv \frac{1}{m_1^2}\lambda(m_1^2,m_2^2,m_3^2)\, C_0(m_e^2,m_e^2,m_1^2,m_2^2,m_e^2,m_3^2)\,. \tag{III.67}$$

For instance, we present two C_0' functions that are used further in this appendix:

$$C_0'(m_e^2,m_e^2,M_\pi^2,0,m_e^2,M_{V_1}^2) = \frac{1}{M_\pi^2}(M_{V_1}^2-M_\pi^2)^2\, C_0(m_e^2,m_e^2,M_\pi^2,0,m_e^2,M_{V_1}^2)\,, \tag{III.68}$$

$$C_0'(m_e^2,m_e^2,M_\pi^2,M_{V_1}^2,m_e^2,M_{V_1}^2) = -(4M_{V_1}^2-M_\pi^2)\, C_0(m_e^2,m_e^2,M_\pi^2,M_{V_1}^2,m_e^2,M_{V_1}^2)\,. \tag{III.69}$$

Now we can finally list the results for $P_{\pi^0\to e^+e^-}$ as obtained from the various approaches to the pion transition form factor:

$$
\begin{aligned}
P^{\rm VMD}_{\pi^0\to e^+e^-} &= -\frac{e^4 m_e}{16\pi^2}\left(-\frac{N_c}{12\pi^2 F}\right)\\
&\times\left\{\frac{2M_{V_1}^2}{M_\pi^2}\Big[B_0(m_e^2,m_e^2,M_{V_1}^2)-B_0(0,m_e^2,m_e^2)-2\Big]+C_0'(m_e^2,m_e^2,M_\pi^2,0,m_e^2,0)\right.\\
&\left.-\,2\,C_0'(m_e^2,m_e^2,M_\pi^2,0,m_e^2,M_{V_1}^2)+C_0'(m_e^2,m_e^2,M_\pi^2,M_{V_1}^2,m_e^2,M_{V_1}^2)\right\},
\end{aligned}
\tag{III.70}
$$

$$
\begin{aligned}
P^{\rm LMD}_{\pi^0\to e^+e^-} &= P^{\rm VMD}_{\pi^0\to e^+e^-}-\frac{e^4 m_e}{16\pi^2}\left(-\frac{N_c}{12\pi^2 F}\right)\left(\frac{8\pi^2F^2}{N_c M_{V_1}^2}\right)\\
&\times\left\{\frac{M_{V_1}^2}{2m_e^2}\Big[B_0(m_e^2,m_e^2,M_{V_1}^2)-B_0(0,M_{V_1}^2,M_{V_1}^2)-1\Big]\right.\\
&-\left(\frac{M_{V_1}^2}{M_\pi^2}-1\right)\Big[B_0(m_e^2,m_e^2,M_{V_1}^2)-B_0(0,m_e^2,m_e^2)-2\Big]\\
&\left.+\,C_0'(m_e^2,m_e^2,M_\pi^2,0,m_e^2,M_{V_1}^2)-C_0'(m_e^2,m_e^2,M_\pi^2,M_{V_1}^2,m_e^2,M_{V_1}^2)\right\},
\end{aligned}
\tag{III.71}
$$

$$
\begin{aligned}
P^{\rm THS}_{\pi^0\to e^+e^-} &= -\frac{e^4 m_e}{16\pi^2}\left(-\frac{N_c}{12\pi^2 F}\right)\left\{-\frac{(2\pi F)^2}{N_c}\left\{\frac{1}{m_e^2}+\frac{24}{M_\pi^2}\right.\right.\\
&+\left[\frac{M_{V_1}^2}{(M_{V_2}^2-M_{V_1}^2)}\left(\frac{1}{m_e^2}\Big[B_0(m_e^2,m_e^2,M_{V_1}^2)-B_0(0,M_{V_1}^2,M_{V_1}^2)\Big]\right.\right.\\
&\left.\left.+\,\frac{2}{M_\pi^2}\Big[7\,B_0(m_e^2,m_e^2,M_{V_2}^2)-B_0(m_e^2,m_e^2,M_{V_1}^2)-6\,B_0(0,m_e^2,m_e^2)\Big]\right)\right]\\
&+\Big[M_{V_1}\leftrightarrow M_{V_2}\Big]\\
&\left.-\,\frac{2}{M_{V_2}^2-M_{V_1}^2}\left(1+\frac{2\kappa M_{V_1}^4 M_{V_2}^4}{(4\pi F)^6 M_\pi^2}\right)\Big[B_0(m_e^2,m_e^2,M_{V_2}^2)-B_0(m_e^2,m_e^2,M_{V_1}^2)\Big]\right\}\\
&+C_0'(m_e^2,m_e^2,M_\pi^2,0,m_e^2,0)\\
&-\left\{\frac{M_{V_2}^2}{M_{V_2}^2-M_{V_1}^2}\left(2-\frac{3}{N_c}\frac{(4\pi F)^2}{M_{V_2}^2}\right)C_0'(m_e^2,m_e^2,M_\pi^2,0,m_e^2,M_{V_1}^2)\right.\\
&-\frac{M_{V_2}^4}{2(M_{V_2}^2-M_{V_1}^2)^2}\left[2+\frac{\kappa M_{V_1}^4}{N_c(4\pi F)^4}-\frac{(4\pi F)^2}{N_c M_{V_2}^2}\left(6+\frac{M_{V_1}^2}{M_{V_2}^2}\right)\right]\\
&\left.\times\,C_0'(m_e^2,m_e^2,M_\pi^2,M_{V_1}^2,m_e^2,M_{V_1}^2)\right\}-\Big\{M_{V_1}\leftrightarrow M_{V_2}\Big\}\\
&-\frac{M_{V_1}^2M_{V_2}^2}{(M_{V_2}^2-M_{V_1}^2)^2}\left[2+\frac{\kappa M_{V_1}^2M_{V_2}^2}{N_c(4\pi F)^4}-\frac{14}{N_c}(2\pi F)^2\left(\frac{1}{M_{V_1}^2}+\frac{1}{M_{V_2}^2}\right)\right]\\
&\left.\times\,C_0'(m_e^2,m_e^2,M_\pi^2,M_{V_1}^2,m_e^2,M_{V_2}^2)\right\}.
\end{aligned}
\tag{III.72}
$$

Bibliography

[1] F. Jegerlehner and A. Nyffeler, "The Muon $g-2$,"
Phys. Rept. **477** (2009) 1–110, arXiv:0902.3360.

[2] E. Czerwinski *et al.*, "MesonNet Workshop on Meson Transition Form Factors," arXiv:1207.6556.

[3] **KTeV** Collaboration, E. Abouzaid *et al.*, "Measurement of the rare decay $\pi^0 \to e^+e^-$," *Phys. Rev.* **D75** (2007) 012004, arXiv:hep-ex/0610072.

[4] A. E. Dorokhov and M. A. Ivanov, "Rare decay $\pi^0 \to e^+e^-$: Theory confronts KTeV data," *Phys. Rev.* **D75** (2007) 114007, arXiv:0704.3498.

[5] M. Knecht and A. Nyffeler, "Resonance estimates of $\mathcal{O}(p^6)$ low-energy constants and QCD short distance constraints,"
Eur. Phys. J. **C21** (2001) 659–678, arXiv:hep-ph/0106034.

[6] P. Vasko and J. Novotný, "Two-loop QED radiative corrections to the decay $\pi^0 \to e^+e^-$: The virtual corrections and soft-photon bremsstrahlung,"
JHEP **1110** (2011) 122, arXiv:1106.5956.

[7] T. Husek, K. Kampf, and J. Novotný, "Rare decay $\pi^0 \to e^+e^-$: on corrections beyond the leading order,"
Eur. Phys. J. **C74** no. 8, (2014) 3010, arXiv:1405.6927.

[8] S. Weinberg, "Phenomenological Lagrangians," *Physica* **A96** (1979) 327.

[9] J. Wess and B. Zumino, "Consequences of anomalous Ward identities,"
Phys. Lett. **B37** (1971) 95.

[10] E. Witten, "Global Aspects of Current Algebra,"
Nucl. Phys. **B223** (1983) 422–432.

[11] J. Gasser and H. Leutwyler, "Chiral Perturbation Theory to One Loop,"
Annals Phys. **158** (1984) 142.

[12] J. Gasser and H. Leutwyler, "Chiral Perturbation Theory: Expansions in the Mass of the Strange Quark," *Nucl. Phys.* **B250** (1985) 465.

[13] G. 't Hooft, "A planar diagram theory for strong interactions,"
Nucl. Phys. **B72** (1974) 461.

[14] E. Witten, "Baryons in the 1/n expansion," *Nucl. Phys.* **B160** (1979) 57.

[15] S. Drell, "Direct decay $\pi^0 \to e^+ + e^-$,"
Il Nuovo Cimento Series 10 **11** (1959) 693–697.

[16] M. J. Savage, M. E. Luke, and M. B. Wise, "The rare decays $\pi^0 \to e^+e^-$, $\eta \to e^+e^-$ and $\eta \to \mu^+\mu^-$ in chiral perturbation theory,"
Phys. Lett. **B291** (1992) 481–483, arXiv:hep-ph/9207233.

[17] M. Knecht, S. Peris, M. Perrottet, and E. de Rafael, "Decay of pseudoscalars into lepton pairs and large-N_C QCD,"
Phys. Rev. Lett. **83** (1999) 5230–5233, arXiv:hep-ph/9908283.

[18] G. P. Lepage and S. J. Brodsky, "Exclusive Processes in Quantum Chromodynamics: Evolution Equations for Hadronic Wave Functions and the Form-Factors of Mesons," *Phys. Lett.* **B87** (1979) 359–365.

[19] G. P. Lepage and S. J. Brodsky, "Exclusive Processes in Perturbative Quantum Chromodynamics," *Phys. Rev.* **D22** (1980) 2157.

[20] S. J. Brodsky and G. P. Lepage, "Large Angle Two Photon Exclusive Channels in Quantum Chromodynamics," *Phys. Rev.* **D24** (1981) 1808.

[21] V. Mateu and J. Portoles, "Form-factors in radiative pion decay,"
Eur. Phys. J. **C52** (2007) 325–338, arXiv:0706.1039 [hep-ph].

[22] **Particle Data Group** Collaboration, K. Olive *et al.*, "Review of Particle Physics," *Chin. Phys.* **C38** (2014) 090001.

[23] **BaBar** Collaboration, B. Aubert *et al.*, "Measurement of the $\gamma\gamma^* \to \pi^0$ transition form factor," *Phys. Rev.* **D80** (2009) 052002, arXiv:0905.4778.

[24] **Belle** Collaboration, S. Uehara *et al.*, "Measurement of $\gamma\gamma^* \to \pi^0$ transition form factor at Belle," *Phys. Rev.* **D86** (2012) 092007, arXiv:1205.3249.

[25] S. Okubo, "Phi meson and unitary symmetry model,"
Phys. Lett. **5** (1963) 165–168.

[26] J. Iizuka, "Systematics and phenomenology of meson family,"
Prog. Theor. Phys. Suppl. **37** (1966) 21–34.

[27] G. Zweig, "An $SU(3)$ model for strong interaction symmetry and its breaking," *CERN-TH-401* (1964) .

[28] **NA60** Collaboration, R. Arnaldi *et al.*, "Study of the electromagnetic transition form-factors in $\eta \to \mu^+\mu^-\gamma$ and $\omega \to \mu^+\mu^-\pi^0$ decays with NA60," *Phys. Lett.* **B677** (2009) 260–266, arXiv:0902.2547.

[29] J. J. Sakurai, *Currents and Mesons*. University of Chicago Press, Chicago, 1969.

[30] L. Landsberg, "Electromagnetic Decays of Light Mesons,"
Phys. Rept. **128** (1985) 301–376.

[31] C. Terschlüsen and S. Leupold, "Electromagnetic transition form factors of light vector mesons," *Phys. Lett.* **B691** (2010) 191–201, arXiv:1003.1030.

[32] C. Terschlüsen, S. Leupold, and M. Lutz, "Electromagnetic Transitions in an Effective Chiral Lagrangian with the η' and Light Vector Mesons," *Eur. Phys. J.* **A48** (2012) 190, arXiv:1204.4125.

[33] C. Terschlüsen, B. Strandberg, S. Leupold, and F. Eichstädt, "Reactions with pions and vector mesons in the sector of odd intrinsic parity," *Eur. Phys. J.* **A49** (2013) 116, arXiv:1305.1181.

[34] P. D. Ruiz-Femenia, A. Pich, and J. Portoles, "Odd intrinsic parity processes within the resonance effective theory of QCD," *JHEP* **07** (2003) 003, arXiv:hep-ph/0306157 [hep-ph].

[35] P. Roig and J. J. Sanz-Cillero, "Consistent high-energy constraints in the anomalous QCD sector," *Phys. Lett.* **B733** (2014) 158–163, arXiv:1312.6206.

[36] P. Roig, A. Guevara, and G. López Castro, "$VV'P$ form factors in resonance chiral theory and the $\pi - \eta - \eta'$ light-by-light contribution to the muon $g-2$," *Phys. Rev.* **D89** no. 7, (2014) 073016, arXiv:1401.4099.

[37] K. Kampf and J. Novotný, "Resonance saturation in the odd-intrinsic parity sector of low-energy QCD," *Phys. Rev.* **D84** (2011) 014036, arXiv:1104.3137.

[38] P. Masjuan and P. Sanchez-Puertas, "Phenomenology of bivariate approximants: the $\pi^0 \to e^+e^-$ case and its impact on the electron and muon $g-2$," arXiv:1504.07001.

[39] S. P. Schneider, B. Kubis, and F. Niecknig, "The $\omega \to \pi^0\gamma^*$ and $\phi \to \pi^0\gamma^*$ transition form factors in dispersion theory," *Phys. Rev.* **D86** (2012) 054013, arXiv:1206.3098.

[40] M. Hoferichter, B. Kubis, S. Leupold, F. Niecknig, and S. P. Schneider, "Dispersive analysis of the pion transition form factor," *Eur. Phys. J.* **C74** no. 11, (2014) 3180, arXiv:1410.4691.

[41] I. V. Danilkin, C. Fernández-Ramírez, P. Guo, V. Mathieu, D. Schott, M. Shi, and A. P. Szczepaniak, "Dispersive analysis of $\omega/\phi \to 3\pi, \pi\gamma^*$," *Phys. Rev.* **D91** no. 9, (2015) 094029, arXiv:1409.7708 [hep-ph].

[42] T. Husek, K. Kampf, and J. Novotný, "Radiative corrections to the Dalitz decay $\pi^0 \to e^+e^-\gamma$ revisited," arXiv:1504.06178 [hep-ph].

[43] V. A. Novikov, M. A. Shifman, A. I. Vainshtein, M. B. Voloshin, and V. I. Zakharov, "Use and Misuse of QCD Sum Rules, Factorization and Related Topics," *Nucl. Phys.* **B237** (1984) 525.

[44] J. Bijnens and F. Persson, "Effects of different form-factors in meson-photon-photon transitions and the muon anomalous magnetic moment," arXiv:hep-ph/0106130 [hep-ph].

[45] **CLEO** Collaboration, J. Gronberg *et al.*, "Measurements of the meson-photon transition form factors of light pseudoscalar mesons at large momentum transfer," *Phys. Rev.* **D57** (1998) 33–54, arXiv:hep-ex/9707031.

[46] G. Ecker, J. Gasser, A. Pich, and E. de Rafael, "The Role of Resonances in Chiral Perturbation Theory," *Nucl. Phys.* **B321** (1989) 311.

[47] S. Ivashyn, "Vector to pseudoscalar meson radiative transitions in chiral theory with resonances," *Prob. Atomic Sci. Technol.* **2012N1** (2012) 179–182, arXiv:1111.1291.

[48] Y.-H. Chen, Z.-H. Guo, and H.-Q. Zheng, "Radiative transition processes of light vector resonances in a chiral framework," *Phys. Rev.* **D90** no. 3, (2014) 034013, arXiv:1311.3366.

[49] B. Ananthanarayan, I. Caprini, and B. Kubis, "Constraints on the $\omega\pi$ form factor from analyticity and unitarity," *Eur. Phys. J.* **C74** no. 12, (2014) 3209, arXiv:1410.6276.

[50] K. Kampf, "ChPT calculations of pion formfactors," *Nucl. Phys. Proc. Suppl.* **234** (2013) 299–302, arXiv:1209.2902.

[51] W. Siegel, "Supersymmetric Dimensional Regularization via Dimensional Reduction," *Phys. Lett.* **B84** (1979) 193.

[52] J. Novotný, "Axial anomaly and dimensional regularization: A Review," *Czech. J. Phys.* **44** (1994) 633–661.

[53] G. Passarino and M. Veltman, "One-loop corrections for e^+e^- annihilation into $\mu^+\mu^-$ in the Weinberg model," *Nucl. Phys.* **B160** (1979) 151–207.

[54] S. Leupold, "Rho meson properties from combining QCD based models," *Nucl. Phys.* **A743** (2004) 283–302, arXiv:hep-ph/0303020 [hep-ph].

[55] K. Mikaelian and J. Smith, "Radiative corrections to the decay $\pi^0 \to \gamma e^+ e^-$," *Phys. Rev.* **D5** (1972) 1763–1773.

[56] R. Niclasen, *Measuring the Branching Ratio of the Rare Decay $\pi^0 \to e^+e^-$*. PhD thesis, University of Colorado, Feb., 2006.

[57] Bergström, L., "Radiative corrections to pseudoscalar meson decays," *Z. Phys.* **C20** (1983) 135–140.

[58] T. Ebertshäuser, H. Fearing, and S. Scherer, "The Anomalous chiral perturbation theory meson Lagrangian to order p^6 revisited," *Phys. Rev.* **D65** (2002) 054033, arXiv:hep-ph/0110261 [hep-ph].

[59] K. Kampf, J. Novotný, and J. Trnka, "On different lagrangian formalisms for vector resonances within chiral perturbation theory," *Eur. Phys. J.* **C50** (2007) 385–403, arXiv:hep-ph/0608051.

[60] I. Cloët, L. Chang, C. Roberts, S. Schmidt, and P. Tandy, "Pion distribution amplitude from lattice-QCD,"
Phys. Rev. Lett. **111** (2013) 092001, arXiv:1306.2645.